Transition metal imido complexes: synthesis and applications to polymerisation catalysis

Coles, Martyn Paul

Transition Metal Imido Complexes : Synthesis and Applications to Polymerisation Catalysis

by

Martyn Paul Coles, B.Sc. (Dunelm), G.R.S.C.

University of Durham

A thesis submitted in part fulfilment of the requirements for the degree of Doctor of Philosophy at the University of Durham.

December 1995.

STATEMENT OF COPYRIGHT

DECLARATION

The work described in this thesis was carried out in the Department of Chemistry of the University of Durham between October 1992 and September 1995. All the work is my own, unless stated to the contrary, and it has not been submitted previously for a degree at this or any other University.

For my family and friends.

"In other studies you go as far as others have gone before you, and there is nothing more to know; but in a scientific pursuit there is continual food for discovery and wonder."

- Mary Shelley, Frankenstein.

ACKNOWLEDGEMENTS

This thesis would not be in your hands now without the help and encouragement of a number of people over the past three years. Primarily, my sincere thanks to Prof. Vernon Gibson who, not content with just planting the seed of inspiration within his students, tends and nurtures it until it reaches fruition. His support and enthusiasm have made working in his research group an honour and a pleasure.

I am also indebted to Dr Ian Little (BP Chemicals, Sunbury) for his advice and to Prof. Ken Wade for his interest in recent months. Prof. W. Clegg and Dr M.R.J. Elsegood are gratefully acknowledged for the structural determinations presented in this work and Mr G.M. Forrest and the IRC must also be thanked for help in polymer analysis. Financial support from EPSRC (formally SERC) and BP Chemicals Ltd. are acknowledged.

The technical staff at Durham are often taken for granted, but without their help and expertise, none of this work would have been possible. Special mention has to be made to Alan Kenwright and Julia Say who provide an outstanding NMR service. The glassblowers Ray and Gordon are truly 'the salt of the earth' (and aren't too bad at making up NMR tubes at short notice either!). Jarka and Bob are thanked for the entertaining elemental analysis and Lara for the rapid mass spec. service. I would also like to mention Jean and Hazel who have always had a smile and a kind word for me.

To all members of the lab past and present I must add my thanks for keeping me (almost) sane. 'Whistling' Matt Jolly, Brenda, 'Dancing' Phil Dyer, Ollie (?), Gaz, Raz (safe man), Rich, Carl, Ulrich, Matt (Impressive) Giles and Brian (Whato) Kimbers. Thanks for all the good times. To my contemporaries Mike and Leela I wish every success for the future. I look forward to meeting up in years to come and reminiscing about the Durham days over a pint (or two). Ed must receive special mention for dragging me (kicking and screaming) to Klute on many occasions and I would like to also thank Chris for being the brother I never had over the past two years.

Finally, I would like to thank my family for their love and support (moral and financial) and lastly special (smashing) thanks to Lesley for sticking by me through the good and the not quite so good.

ABSTRACT

Transition Metal Imido Complexes: Synthesis and Applications to Polymerisation Catalysis.

This thesis describes studies into Group 5 and Group 6 transition metal imido complexes, with particular emphasis on the development of complexes which can be applied to catalytic processes.

Chapter 1 highlights the electronic and structural aspects of the imido and alkylidene ligands. The isolobal analogy between Group 4 bent metallocene, Group 5 half-sandwich imido and Group 6 bis(imido) metal fragments is outlined. In addition, Ziegler-Natta type α-olefin polymerisation and Ring Opening Metathesis Polymerisation (ROMP) are briefly reviewed.

Chapter 2 describes initial screening of half-sandwich vanadium imido and chromium bis(ᵗbutylimido) dichloride complexes as catalyst precursors. Synthesis of the chromium bis(imido) dialkyl complex $Cr(N^tBu)_2(CH_2Ph)_2$ (**1**) is described, its conversion to a cationic alkyl species is probed and the polymerisation activity associated with the resultant compound is addressed. Finally this chapter details the synthesis and characterisation of a range of bis(adamantylimido) chromium complexes.

Chapter 3 presents a synthetic entry point into the bis(arylimido) chemistry of chromium. The complex $Cr(NAr)_2(NH^tBu)Cl$ (**12**) is described (Ar = 2,6-^{i}Pr$_2$C$_6$H$_3$) and its conversion to the dichloride complex $Cr(NAr)_2Cl_2$ (**14**) is examined. **14** forms the stable monoadduct with pyridine, the X-ray crystallographic study of which reveals a distorted square based pyramidal geometry about the chromium atom. The inclusion of the arylimido ligand at the metal centre allows stabilisation of the chromium bis-phosphine complexes $Cr(NAr)_2(PMe_3)_2$ (**18**) and $Cr(NAr)_2(PMe_2Ph)_2$ (**19**). The reactivity of **18** towards unsaturated hydrocarbon substrates is briefly investigated.

Chapter 4 focuses on the organometallic chemistry of the [$Cr(NAr)_2$] moiety. A range of dialkyl derivatives are isolated and the molecular structures of a selection are solved. The generation of the nascent species [$Cr(NAr)_2(=CHCMe_3)$] is investigated and the conversion of $Cr(NAr)_2(CH_2CMe_3)_2$ (**24**) to $Cr(NAr)_2(CHDCMe_3)(C_6D_5)$ (**25**) is the subject of a kinetic study.

In chapter 5, the ROMP of a series of amino acid derived norbornene monomers is studied. The resultant polymers are fully characterised and a brief molecular modelling study is carried out on representative polymers chain lengths.

Chapter 6 contains experimental details to chapters 2–5.

Martyn Paul Coles (December 1995).

ABBREVIATIONS

NMR	Nuclear Magnetic Resonance	HETCOR	Heteronuclear Correlation
		COSY	Correlation Spectroscopy
δ	Chemical Shift	DEPT	Distortionless Enhancement by Polarisation Transfer
ppm	parts per million		
MAS	Magic Angle Spinning	NQS	Non-Quaternary Suppression
CP	Cross Polarisation	IR	Infra Red
DSC	Differential Scanning Calorimetry	GPC	Gel Permeation Chromatography
TGA	Thermal Gravometric Analysis	$[\alpha]$	Specific Optical Activity
		PDI	Polydispersity Index
T_g	Glass Transition Temperature	σ_c	cis vinylene content
		σ_t	trans vinylene content
M_n	Number average molecular weight	M_w	Weight average molecular weight
ROMP	Ring Opening Metathesis Polymerisation	k	Rate constant
		k_i	Rate constant of initiation
E_a	Activation Energy	k_p	Rate constant of propagation
$\Delta H^{\ddagger}$	Enthalpy of Activation	$\Delta S^{\ddagger}$	Entropy of Activation
X	Monoanionic ligand	L	Dianionic ligand
R	Alkyl Group	Cp	Cyclopentadienyl ligand
DEAC	Diethyl Aluminium Chloride	TMA	Trimethyl Aluminium
		MAO	Methyl Aluminoxane
TEA	Triethyl Aluminium	TMS	Trimethyl Silyl
THF	Tetrahydrofuran	*p*-tol	*para*-C_6H_4-CH_3
Ad	Adamantyl	Ar	2,6-diisopropyl phenyl
Ar'	2,4,6-tri^{t}butyl phenyl	DME	Dimethoxyethane
mes	mesityl	neophyl	2-methyl-2-phenyl propyl
LUMO	Lowest Unoccupied Molecular Orbital	HOMO	Highest Occupied Molecular Orbital

NOTE: For Cp containing complexes, a non IUPAC nomenclature has been adopted. Formulae are represented with the metal following the Cp ligand, i.e. $[Cp_xM(\text{other ligands})]$.

Contents **Page**

Chapter 1 :- Transition Metal Imido and Alkylidene Complexes. An Overview of Bonding and Applications to Polymerisation Catalysis.

Chapter 2 :- Imido Complexes of Group 5 and 6 Metals as α-Olefin Polymerisation Catalysts. Development of the Bis-Imido Chemistry of Chromium.

Chapter 3 :- Four and Five Coordinate Bis(Arylimido) Complexes of Chromium

Chapter 6 :- Experimental Details.

Appendices :- Crystal Data, Colloquia and Lectures.

Chapter One

Transition Metal Imido and Alkylidene Complexes. A Brief Overview of Bonding and Applications to Polymerisation Catalysis.

1.1 Introduction.

This thesis is concerned with the chemistry of mononuclear Group 5 and Group 6 complexes that contain one or more multiply bonded nitrogen atoms, present as imido ligands. This area of chemistry has generated many novel compounds with applications in homogeneous and heterogeneous catalysis, and such species have been recognised as crucial intermediates in enzymatic reactions (e.g. fixation of nitrogen by nitrogenase enzymes).

The aim of this thesis is therefore to explore the chemistry of early transition metal imido complexes, with particular attention being paid to the use of these compounds as catalytic species in polymerisation reactions. The major part of this study is concerned with exploiting the related symmetry properties of the frontier orbitals of the imido fragment (NR^{2-}) and the cyclopentadienyl anion ($C_5R_5^-$) in the synthesis of complexes related to the Group 4 'bent metallocene' family of compounds.

Chapter two details early results in the application of these compounds in α-olefin polymerisation catalysis, and proceeds to describe developments in the synthesis of a group of compounds that proved particularly promising in this field, the bis-imido complexes of chromium (VI). Chapters three and four continue to expand this area of chromium chemistry detailing the synthesis and reactivity of a range of novel compounds.

Chapter five approaches the catalysis study from a different angle, employing a transition metal imido complex that is already well established as a polymerisation catalyst to prepare novel polymeric materials. 'Schrock' type initiators for the Ring Opening Metathesis Polymerisation (ROMP) of cyclic olefins are used to generate a range of polymers from norbornene derived monomers.

The remainder of this chapter is devoted to a review of transition metal imido and alkylidene complexes, being divided into three sections. First, the synthesis and characterisation of these species are discussed, including a simplistic examination of the structure and bonding present, and the relationship with other transition metal species. The remaining two sections examine specific catalytic processes that these classes of

compounds are involved in, namely Ziegler-Natta type polymerisation of α-olefins and the ROMP of cyclic olefins.

1.2 Electronic Structure and Bonding.

This section gives a brief summary of the possible bonding modes of imido and alkylidene ligands, and investigates simple bonding descriptions of such species. Expansion of the bonding description allows a linear imido unit bonded to a transition metal to be related to a cyclopentadienyl ligand through the isolobal relationship. Finally a method of predicting the orientation of π-bonding ligands within a 'pseudo-tetrahedral' molecule is discussed.

1.2.1 Bonding Modes of Imido Ligands.

Although the first organoimido transition metal complex, $Os(N^tBu)O_3$ was reported less than 40 years ago,[1] numerous complexes are now known spanning Groups 4 - 9 of the transition series.[2] Five different bonding modes have been identified for the imido ligand, but this discussion is limited only to terminally bonded units (illustrated in figure 1.1)

(A) (B)

Figure 1.1 Bonding modes in terminal imido ligands.

In (A), the linear M-N-R arrangement arises through an sp hybridised N-atom that is donating its lone pair of electron to an empty metal d-orbital, giving a triple bonded species *via* one σ and two π interactions. Such ligands that possess two π-

symmetry orbitals, that can therefore form a triple bond to the metal have been referred to as Π_2 ligands.[3]

If the nitrogen atom is unable to donate its lone pair to the metal, for example if the d-orbitals are already filled or when competition exists for the available orbital with other π-bonding ligands, situation B may be expected to arise, where the lone pair resides on the nitrogen atom, which is sp^2 hybridised. This leads to a 'bent' imido unit, with the classic example being the complex $Mo(NPh)_2(S_2CNEt_2)_2$.[4] In this complex the linear imido ligand has an Mo-N-C_{ipso} angle of 169.4(4)° and a Mo=N distance of 1.754 Å, whilst in the remaining bent imido, the angle about the nitrogen atom is reduced to 139.9(4)° and the bond length has increased to 1.789 Å. Another example of bent imido ligands are found in the complex $Mn(N^tBu)_3Cl$[5] where the Mn–N–C bond angles fall in the range 138.5(3) - 141.8(3)°. This is consistent with a delocalisation of the two 4-electron and one 2-electron donation from the three imido ligands to give an eighteen electron Mn configuration.

Recently, the validity of the bent vs. linear argument has been questioned. Schrock and co-workers synthesised the tris-imido complex $Os(NAr)_3$[6] which possesses linear terminal imido groups (178 - 180°). If the previous arguments are adhered to and we designate these imido groups as four electron donors, the electron count of this compound is 20, exceeding the effective atomic number rule.[7] However due to severe competition for the available dπ-orbitals of the metal, not all of the ligand π electrons are donated. In three-fold symmetric complexes of this type, including other imido derivatives $[M(NR)_3X]$ (R = ^{t}Bu, M = Mn,[5] Re[8] ; R = Ar, M = Tc,[9] Re[10]) and $[M(NAr)_3L]$ (M = Mo,[11] W[12]) and the acetylene complexes $[Re(RC{\equiv}CR)_3X]$[13] and $[W(RC{\equiv}CR)_3L]$,[14] a ligand non-bonding orbital exists from a linear combination of the orbitals on the π-bonding ligands, occupied by two electrons thus effectively reducing the electron count to eighteen.

The 'twenty electron' complexes $Cp^*Ta(NPh)H$[15a] and $Cp_2Zr(N^tBu)(THF)$[16] have also been synthesised and crystallographically characterised, showing linear imido units of 177.8(9)° and 174.4(3)° respectively. Both complexes however have increased metal imido distances (1.831(10) Å and 1.826(4) Å respectively) suggesting that an

intermediate situation arises between bent and linear, illustrated below for the tantalum case. The imido nitrogen is sp hybridised, but the lone pair of electrons is principally found on the nitrogen atom, giving an intermediate bonding situation between (**II**) and (**III**) below (see also reference 15b for a detailed molecular orbital study on this complex)

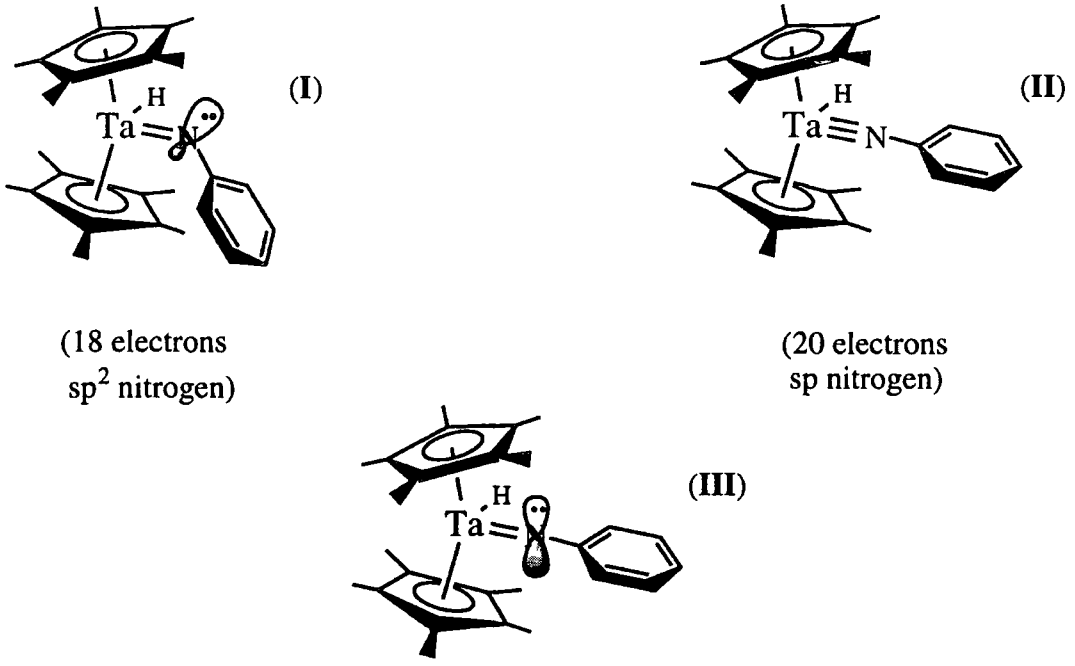

Figure 1.2 Bonding extremes in the complex Cp*Ta(NPh)H.[15]

1.2.2 Bonding Modes of Alkylidene Ligands.

The alkylidene ligand differs from the imido in that it has only one π symmetry orbital with which to interact with the metal centre and hence can from at most a double bond. In the past such ligands have been referred to as 'single faced' π ligands, and have more recently been termed Π_1 ligands.[3]

The bonding of an alkylidene ligand to a metal centre can be described in one of two ways illustrated in figure 1.3. Either the alkylidene fragment exists as a triplet that

combines with a triplet metal centre (**I**), or a singlet carbene fragment donates its electron pair to a metal centre, receiving back donation into the empty p-orbital on the carbon atom (**II**).

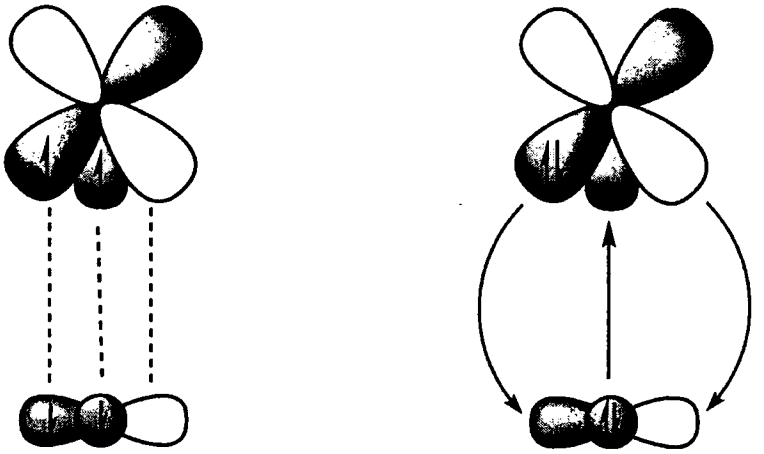

(I) **(II)**

Figure 1.3 Bonding in transition metal alkylidene complexes.

In case **I**, the covalent bond that forms resembles the carbon-carbon bond found in ethylene. This is the case where the carbon fragment possesses only hydrogen or alkyl substituents (i.e. CH_2 ; CHR ; CRR') and is known as an alkyl-carbene or more commonly an alkylidene. Complexes of this type were first established by Schrock in 1973[17] through the alkyl-alkylidene complex $Ta(=CH^tBu)(CH_2{}^tBu)_3$.

The carbene fragments of type **II** donate a lone pair of electrons to an empty d-orbital on the metal centre, and are stabilised by back-bonding. This type of bonding therefore resembles the Dewer-Chatt-Duncanson model for an olefin binding to a metal centre,[18] and such complexes are termed Fischer carbenes after their discoverer. These ligands typically have a heteroatom substituent with $p\pi$ lone pairs that can also contribute to stabilisation of the empty p-orbital on the carbene carbon atom.

The chemistry associated with each of the above ligand types differs considerably. The Fischer carbenes are electrophilic and tend to be found in low valent late transition metal complexes. The 'Schrock' type alkylidenes however possess a

nucleophilic carbon (as in ethylene) and are typically associate with early transition metals in high oxidation states that possess few d-electrons. Extensive *ab initio* calculations have been performed on both of these types of complex, enabling a further understanding of their bonding and reactivity.[19-23]

1.2.3 The Pseudo-Isolobal Relationship Between η^5-Cyclopentadienyl and Terminal Linear Imido Ligands.§

(§ - Assuming four electron donation from an sp hybridised nitrogen).

Examination of the frontier orbitals of the cyclopentadienyl (Cp) ring reveal an orbital of a_1 symmetry and a degenerate pair of e_1 symmetry orbitals (see figure 1.4). The a_1 orbital is σ with respect to the metal ligand axis, and the e_1 pair are π, denoting this ligand a Π_2 ligand.[3] The frontier orbitals of the terminal imido group have been shown to closely resemble those for the Cp ring,[24] also bonding to a metal *via* one σ and two π interactions.

The imido ligand can be regarded as a dianionic ligand NR^{2-} and the cyclopentadienyl group as monoanionic Cp^-. This is also illustrated in figure 1.4 with energy level diagrams showing that both ligands have six electrons in filled σ and π orbitals available for donation to a metal centre. Note that the Cp ligand also possesses an e_2 pair of δ-acceptor orbitals potentially available to form a δ bond. However, these interactions are expected to be weak and will have little effect on the metal ligand bond.

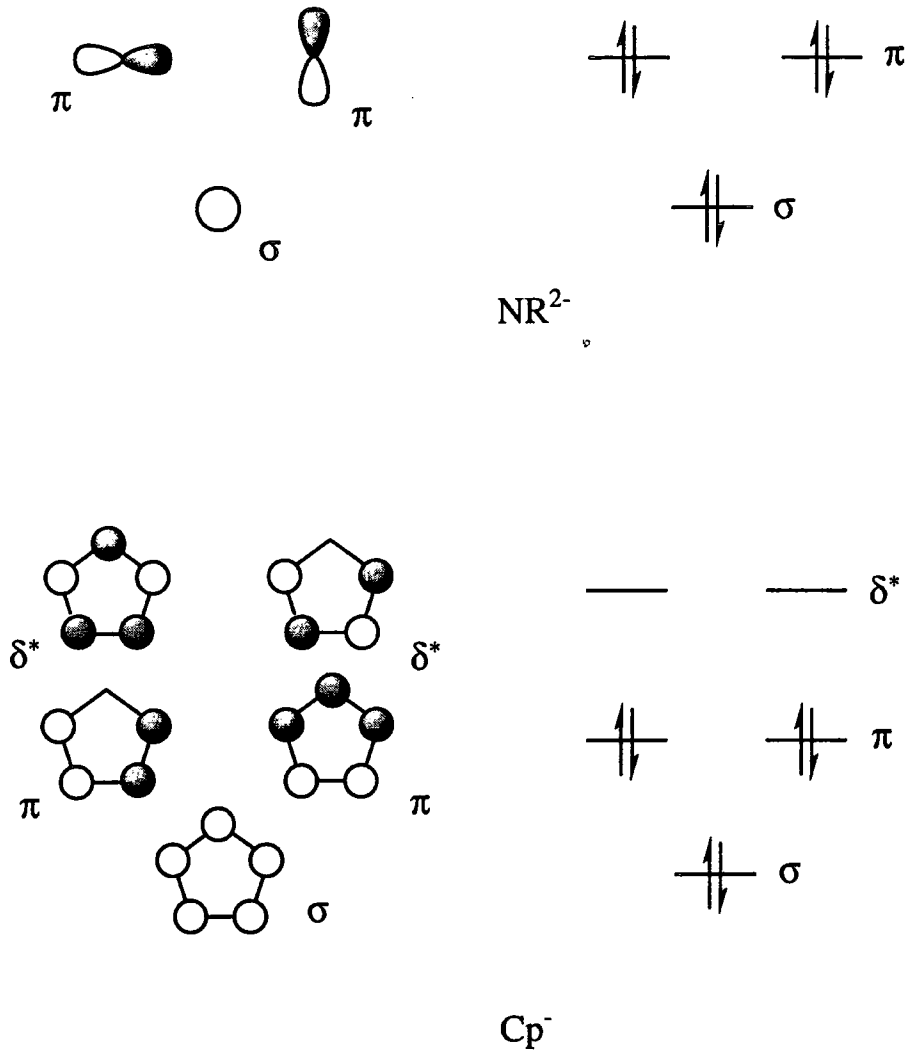

Figure 1.4 Simple molecular orbital and energy diagrams of the linear imido and cyclopentadienyl ligands.

1.2.4 The Isolobal Relationship between [Cp_2M], [CpM'(NR)] and [M''$(NR)_2$].

When considered as a neutral species, the cyclopentadienyl ligand contributes five electrons to the metal centre, being one more than the linear imido ligand. Hence it was postulated that replacement of a Cp ring by an imido ligand, accompanied by a shift of one group to the right in the periodic table, should result in a related series of compounds with an identical 'd' electron count. As both ligands bond through one σ and two π orbitals, the two resultant metal fragments were also predicted to possess similar frontier orbitals.

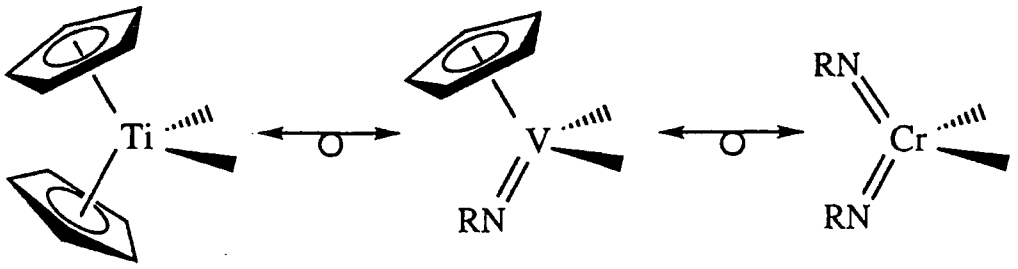

Figure 1.5 Isolobal series of [Cp_2M], [CpM'(NR)] and [M''$(NR)_2$] compounds.

The frontier orbital characteristics of the bis-cyclopentadienyl transition metals fragment have been calculated by Lauher and Hoffmann[25] using extended Hückel Molecular Orbitals (EHMO) and by Zhu and Kostic[26] using the Fenske-Hall method, providing good agreement between the two methods. Hoffmann demonstrated that, as the angle between the two imaginary ring centroid to metal bonds decrease from 180° (as in ferrocene) towards that of a bent metallocene, three new metal bonding orbitals are generated, illustrated below.

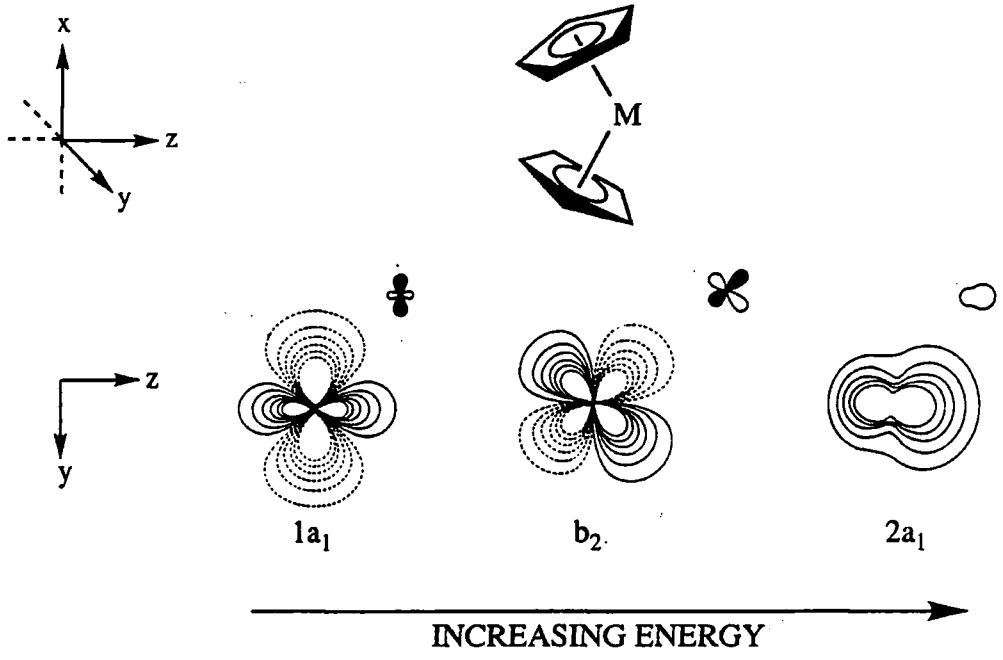

Figure 1.6 Bonding orbitals in a bent metallocene transition metal complex.

These orbitals project in the yz plane, which has been termed the equatorial binding plane in these complexes since this is where ligands bind to the metal. The b_2 orbital possesses mainly d_{yz} character, whilst the two a_1 orbitals are a combination of s, p_z, d_{z2} and d_{x2-y2}. The remaining higher energy b_1 and a_2 symmetry orbitals are generally too high in energy to contribute to the bonding,[25] and hence are not included in this discussion.

Gibson and co-workers[24] have carried out Fenske-Hall calculations on the isolobally related [CpNb(NR)] fragment, finding that the resultant frontier orbitals are similar in orientation and relative energies. A notable difference appears in the $2a_1$ orbital which receives a considerable contribution from the niobium d_{xz} orbital. This lies away from the 'equatorial binding plane' and may lead to differences in chemistry between the two classes of compound.

Continuing this analogy further, replacement of the remaining Cp group with another imido ligand, and moving to the Group 6 metals should give rise to isolobal bis(imido) metal species. Schrock[27] has recently performed SCF-X_α-SW calculations on the [$W(NAr)_2$] fragment and found that this too possesses two frontier orbitals of a_1 symmetry and one of b_2 symmetry in accordance with the above. Many comparative studies now exist between these three classes of compound,[24,27-30] and the main studies within this thesis are concerned with extending these to include the bis-imido complexes of chromium.

1.2.5 Triad Representations.[3]

This section summarises a recent method of examining the bonding patterns that exist in 'tetrahedral' transition metal complexes bearing π donor ligands. In order to facilitate visualisation of such compounds, the molecule is viewed along one of the metal ligand axes, the remaining three ligands defining a triangle (or triad) beneath (see figure 1.7a). The π symmetry orbitals available for bonding to a π donor ligand are illustrated in figure 1.7b. Although for simplicity these are shown as p-type orbitals,

they could also consist of the front pointing lobes of a metal dπ orbital, or more likely a hybrid of p and d metal orbitals.

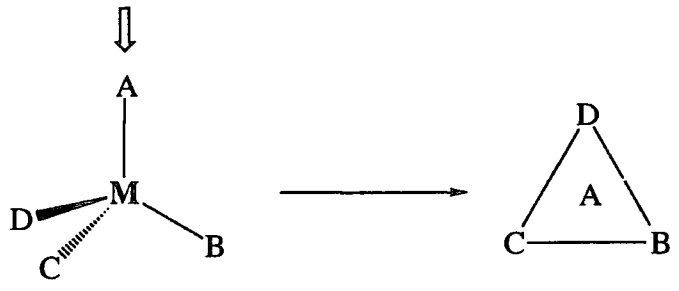

Figure 1.7a

Figure 1.7b

This theory adequately explains the orientation of a number of bonding situations. However, for the purposes of this brief review, the examples will be limited to those tetrahedral molecules possessing two dominant $\prod_2$ donor ligands. In such a situation, the orientation of a $\prod_1$ ligand can be predicted to occur in such a way as to limit the competition with the two other π donor ligands. For example, the complex $Cp_2Ta(=CHPh)(CH_2Ph)$[31] contains two strongly π donating Cp ligands ($\prod_2$ ligands), and a weaker $\prod_1$ alkylidene ligand. The orientation is therefore predicted to be such that the p-orbital of the alkylidene ligand bisects the two Cp ligands and points towards the purely σ bonding CH_2Ph group. In this situation, the substituents bound to the alkylidene α-carbon will appear perpendicular to the Ta–CH_2Ph bond as can be seen quite clearly from the original crystal structure[31] (see figure 1.8).

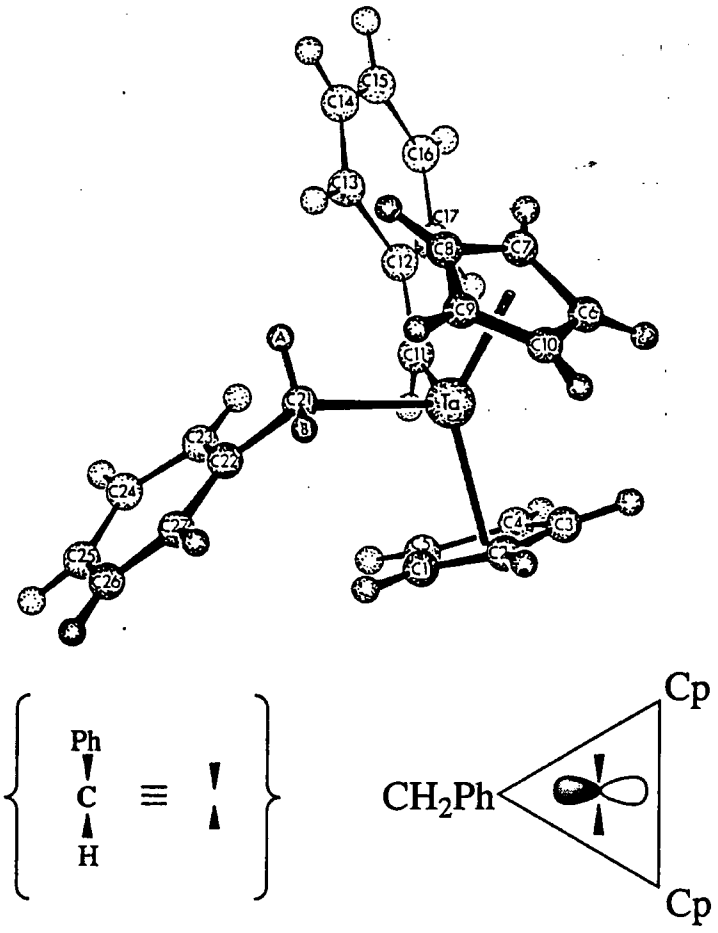

Figure 1.8 Crystal structure and triad representation of $Cp_2Ta(=CHPh)(CH_2Ph)$.

A similar situation can be predicted for amide complexes where two Π_2 ligands predominate the π bonding. The amide nitrogen can bond to the metal in two ways, illustrated below.

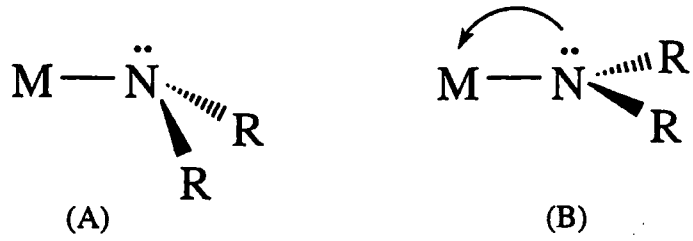

Figure 1.9 Possible bonding modes of a terminal amide ligand.

In the former case, the nitrogen retains its lone pair of electrons and is thus pyramidal sp^3 hybridised, interacting with the metal through σ bonds only. If the nitrogen donates its electrons to the metal, thus becoming a planar sp^2 hybridised atom, it becomes a single faced Π_1 (see section 1.2.2). This is likely to be the case for early transition metal complexes where low energy empty d-orbitals are available to accept π donation. We can therefore expect a similar orientation of the amide substituents in a complex dominated by two Π_2 interactions. This has previously be shown for the half-sandwich niobium complex CpNb(NAr)(NH^{t}Bu)Cl[32] and will later be shown for the case of bis-imido complexes of chromium.

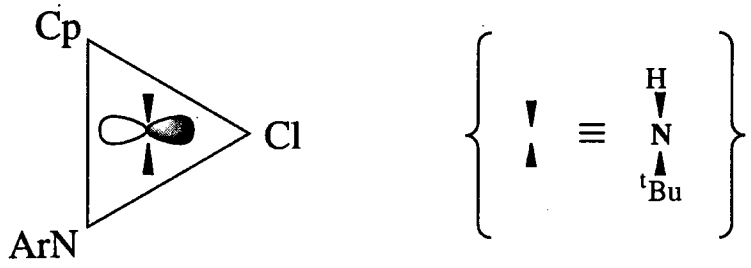

Figure 1.10 Triad representation of CpNb(NAr)(NH^{t}Bu)Cl.

1.3 Ziegler-Natta Type α-Olefin Polymerisation.

1.3.1 Introduction.

This section very briefly reviews the use of Group 4 bent metallocene complexes as precursors to the active catalytic species in the polymerisation of α-olefins, in particular ethylene. The development of the area is followed chronologically from early observations to recent developments in metal catalyst species and the co-catalyst employed to generate the active site. Finally complexes that are isolobal to Group 4 [Cp_2M] fragments are addressed and their potential use as polymerisation catalysts is investigated.

1.3.2 Metallocene Halide Complexes.

The original Ziegler-Natta polymerisation of α-olefins[33] is a heterogeneous process, thus proving relatively difficult to study using conventional techniques. This, along with the notorious non-uniformity of active sites in heterogeneous catalysis, caused a shift of attention to homogeneous systems where the active site is well defined and conventional techniques such as NMR can be used in their study.

An attractive model system fitting the above two criteria was that of the Group 4 bent metallocene complexes of the general formula Cp_2MX_2. In 1957 it was reported that homogeneous mixtures of Cp_2TiCl_2 and diethyl aluminium chloride (DEAC) catalysed the formation of polyethylene under conditions similar to those employed in heterogeneous Ziegler systems.[34] The simple coordination geometry consisting of only two cis ligand sites available for bonding (see section 1.2.4) was particularly favourable in this case, promising a relatively easy system to study.

Many reports followed this observation[35] and through spectroscopic, kinetic and isotope labelling studies of Breslow, Newburg and Long, and by Chien[36] the reaction mechanism was deduced to be :-

1. Formation of (alkyl)titanium complexes Cp_2TiRCl (R = Me / Et) by ligand exchange with the alkylaluminium co-catalyst.
2. Polarisation of the Cp_2Ti—Cl bond by the Lewis acidic aluminium centres in adducts of the form $Cp_2Ti(R)Cl.AlRCl_2$.
3. Insertion of the olefin into the Cp_2Ti–R bond of this (or a closely related) electron deficient species.

This was in good agreement with the original mechanism of heterogeneous polymerisation proposed by Cossee,[37] where cis-insertion of the olefin into a Ti–C bond at the surface of $TiCl_3$ was hypothesised. The reaction mechanism is schematically represented in figure 1.11 below, for the metallocene example.

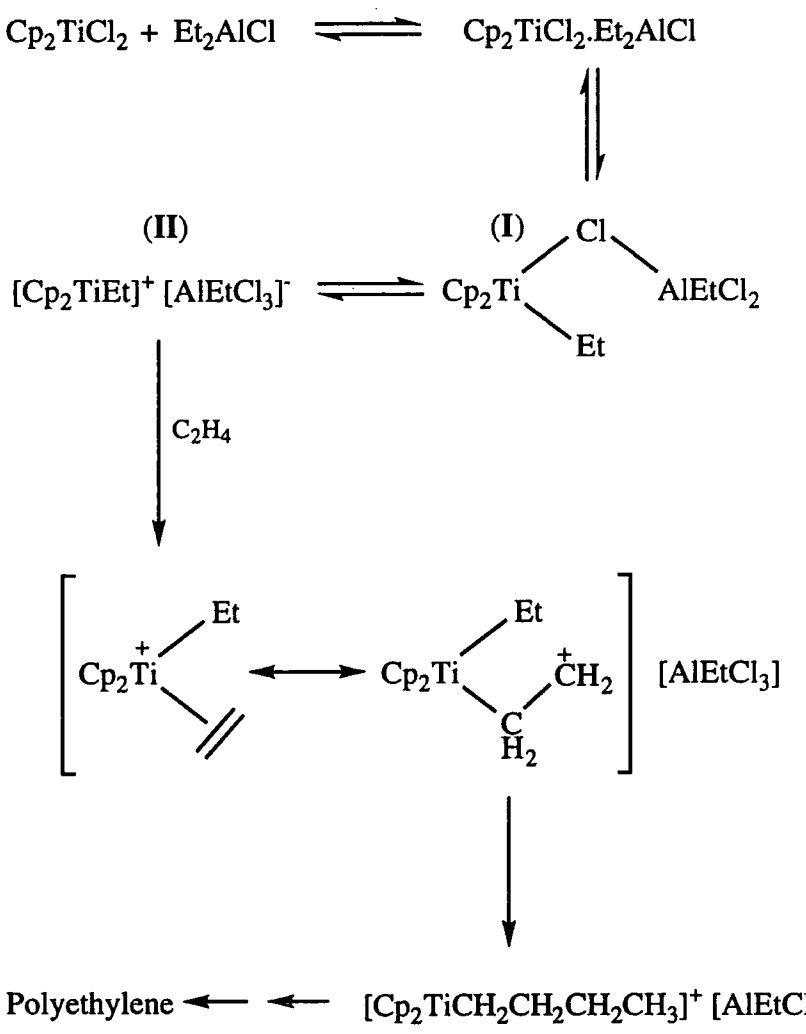

Figure 1.11 Proposed mechanism for Ziegler type polymerisation of ethylene.

1.3.3 Cationic Alkyl Species.

An important question that was not fully answered by this early work was whether the olefin inserts into the bimetallic species (**I** in figure 1.11) containing a bridged halogen (or alkyl group), or into the Ti–C bond of a discrete ion pair of the type $[Cp_2TiR]^+ [AlR_xCl_{4-x}]^-$. Work by Jordan and co-workers in 1986[38] showed that the tetraphenylborate salts of the cationic species $[Cp_2Zr(CH_3)(THF)]^+$ and $[Cp_2Zr(CH_2Ph)(THF)]^+$ will polymerise ethylene in the absence of any further activation, lending support to metallocene alkyl cations being the active components (see equation 1.1 below).

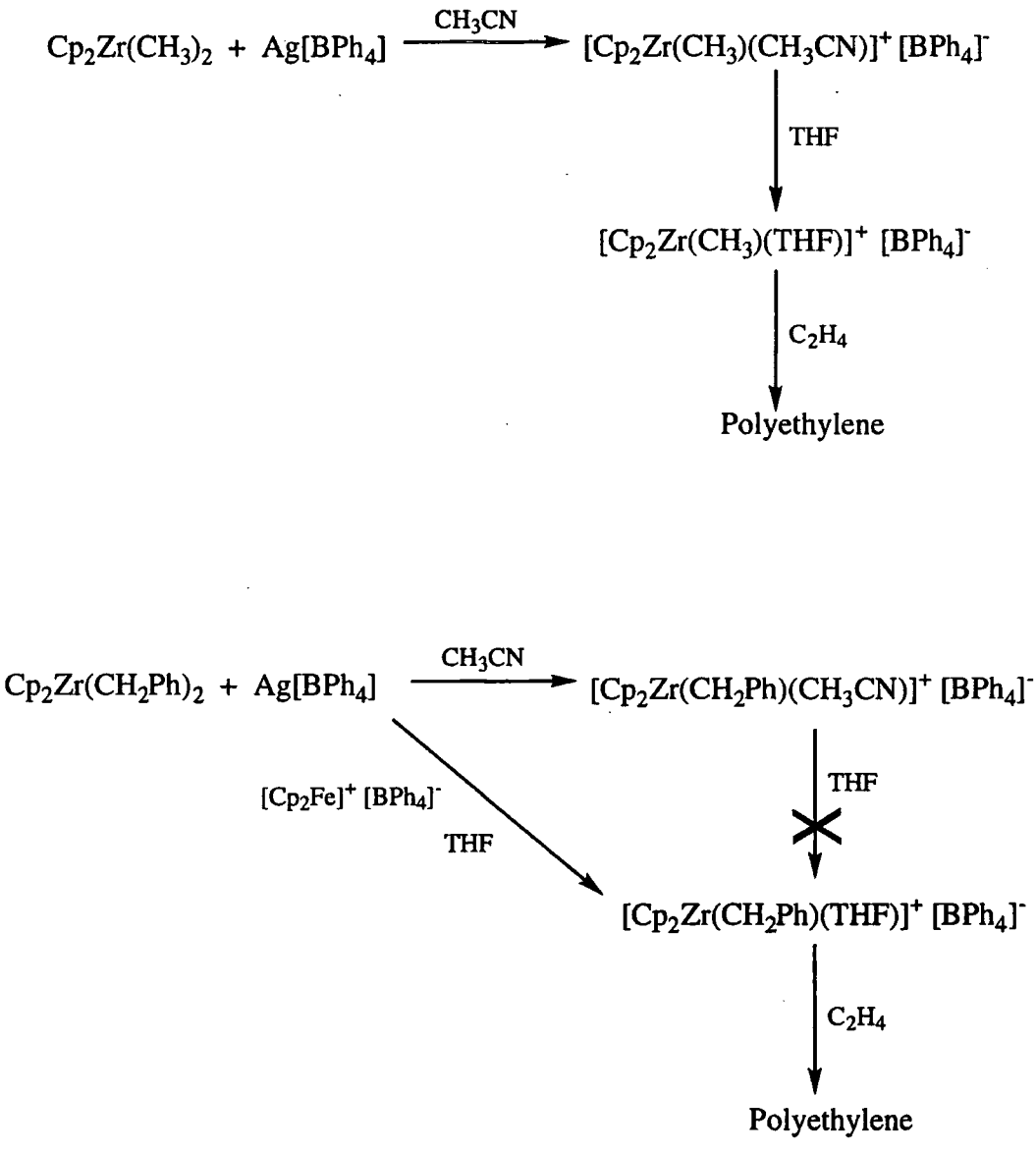

Equation 1.1 Generation of metallocene alkyl cations active for the polymerisation of ethylene.

Subsequent work has extended this area to include both titanium[39] and hafnium[40] complexes.

1.3.4 The Nature of the Anion.

Early kinetic work showed that the growth of a polymer chain alternates between a dormant state and one where the chain is actively growing, the so called 'intermittent growth' model. This was ascribed to the equilibrium between the Lewis

acid-base adducts (contact ions, dormant) and the dissociated species (separated ion pairs, active). This is illustrated below for the schematic ions A and B. Such systems are currently studied using modern techniques (e.g. multinuclear NMR).[41]

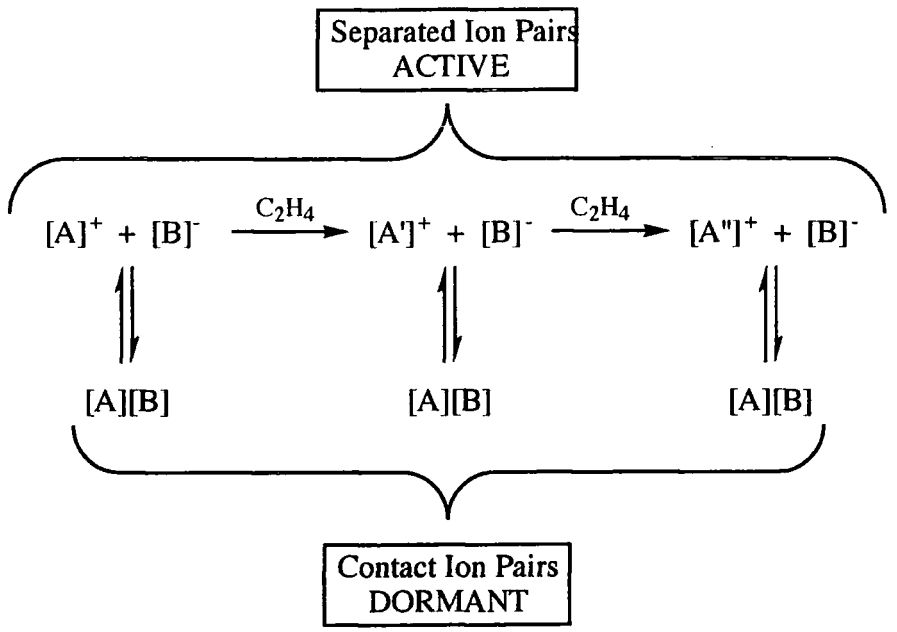

Figure 1.12 Intermittent growth model of polymerisation.

This has also been used to explain the inability of the metallocene alkylaluminium halide systems to polymerise propene and higher α-olefins, due to the insufficient capability of such monomers to displace the anion and generate the active separated pair.

A series of observations made in the mid-1970's led to the discovery that the addition of traces of water to Cp_2TiRCl and Cp_2TiCl_2-alkylaluminium systems, far from being a poison, increased the activity.[42] In the 1980's, Kaminsky and co-workers noted that water will also impart a surprisingly high activity to the otherwise inactive halogen-free system $Cp_2ZrMe_2 + AlMe_3$.[43] It was found that partial hydrolysis of the alkylaluminium co-catalyst was occurring, giving rise to the formation of aluminoxanes. Although the exact formulation of these species is not known, they are

generally thought of as linear and cyclic structures[44] as illustrated in figure 1.13 and are the subject of continued interest.[45]

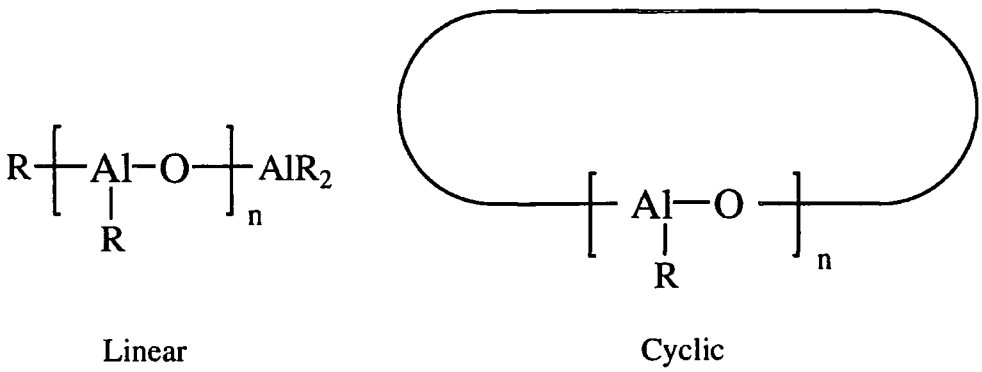

Figure 1.13 Proposed structures present in aluminoxanes.

The most widely used aluminoxane is derived from the partial hydrolysis of trimethyl aluminium (TMA), giving methyl aluminoxane (MAO), thought to contain residual TMA.[44] This effectively removes an alkyl group from the metallocene complex, forming a weakly interacting anion of the type [R—MAO]$^-$. In the presence of (even substituted) olefins, any contacts of the type $[Cp_2MR]^+$·····[R—MAO]$^-$ give way, allowing polymerisation to proceed through the 'naked' cation.

Another series of large, weakly interacting coordinating anions consist of the per-fluorinated tetraphenylborates, developed by Hlatky and Turner[46] and Marks.[47] In contrast to their protio-analogues where fairly strong interactions may still be present between the alkyl cation and the anion retarding or preventing polymerisation,[48] these anions are sufficiently weakly coordinated to be displaced by incoming olefin molecules.

The formation of the cationic metal species occurs in one of two main ways, illustrated in equation 1.2 for the case of dimethyl zirconocene.

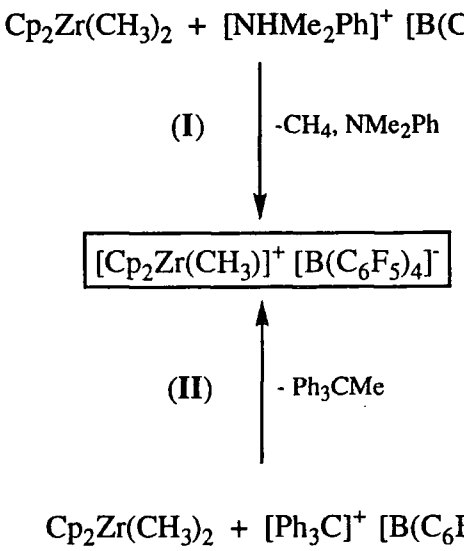

Equation 1.2 Formation of cationic alkyl species employing per-fluorinated tetraphenylborate.

In (**I**), the acidic proton of the anilinium complex protonates an alkyl group, eliminating the alkane and generating the alkyl cation. A possible drawback to this system is the coordination of the free aniline to the metal centre, competing with olefin complexation and polymerisation. In (**II**), the trityl group abstracts an alkyl ligand generating the cation directly.

The neutral species $B(C_6F_5)_3$ can also abstract a methyl group to form a complex of the type $[Cp'_2Zr(CH_3)^+\cdots\cdots H_3C—B(C_6F_5)_3^-]$. This has been crystallographically characterised for the above compound where Cp' = Me_2-C_5H_3,[48] and shows residual coordination contacts between the cationic zirconium and the counter ion, believed to resemble the contacts in the putative $[Cp_2MR]^+\cdots\cdots[R—MAO]^-$ complexes. Recently new fluorinated aryl(borates) have been developed which also promote polymerisation in metallocene systems.[49]

1.3.5 Isolobal and Isoelectronic Analogues to Bent-Metallocenes.

Exploiting the isolobal theory as outlined in section 1.2.4, many new complexes related to the Group 4 metallocenes have been shown to be active in the polymerisation

of ethylene. Complexes that retain the general bis-cyclopentadienyl framework include the neutral Group 3 complex $Cp^*_2Sc\text{-}R$[50] and neutral lanthanide complexes of the type $Cp^*_2Lu\text{-}CH_3$[51] and $Cp^*_2Sm(CH_3)(THF)$[52] whilst cationic actinide species are also known, for example $[Cp^*_2Th\text{-}CH_3]^+$.[53]

Jordan has replaced the uni-negative $C_5R_5^-$ ligand of $(C_5R_5)_2M(R)^+$ with the isolobal, di-negative dicarbollide ligand $(C_2B_9H_{11})^{2-}$ giving neutral complexes of the type $(Cp^*)(C_2B_9H_{11})M(R)$ where M = Zr, Hf,[54] which have proved moderately active in the polymerisation of ethylene (see figure 1.14). In several cases, a deactivation pathway exists where a hydridic B-H bond from the dicarbollide cluster coordinates to the metal centre, thus reducing activity.

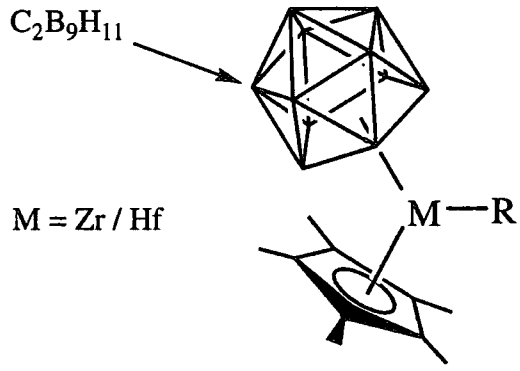

Figure 1.14 Jordan's dicarbollide 'metallocene' complex.

Recently, Bazan[55] has replaced a 'Cp' ligand of the metallocene framework with a dianionic ligand of the general formula $[C(CHR)_3]^{2-}$. When R = H, the complex isolated from the reaction of Cp^*ZrCl_3 and $TMM(Li.TMEDA)_2$ (where TMM = trimethylenemethane, $C(CH_2)_3$; TMEDA = tetramethylethylenediamine) is best considered as $(Cp^*)(TMM)ZrCl_2.Li(TMEDA)$ where bridging chlorine atoms exist between the zirconium and the lithium as observed by X-ray analysis. When R - Ph however, an analogous reaction gives what is best described as $[(Cp^*)(TBM)ZrCl_2]^-[Li(TMEDA)_2]^+$ (where TBM = tribenzylmethane) again observed crystallographically. The second complex is active for the polymerisation of ethylene upon treatment with

MAO, presumably by generating a neutral complex of the type $(Cp^*)(TBM)Zr(R)$ that initiates polymerisation.

Moving away from the Group 4 metals, half-sandwich imido complexes of the type $CpM(NR)Cl_2$ have been shown to be active catalysts in the presence of DEAC or MAO.[56] Kress has replaced the Cp ligand with the hydrotris(pyrazolyl)borato ligand of the general formula $[HB(C_3H_6N_2)_3]^-$ that is generally considered to be a Cp analogue.[57] A series of four vanadium imido derivatives have been synthesised and shown to polymerise ethylene in the presence of MAO.

Replacing the imido group instead of a Cp ligand in such complexes has also proved successful in the generation of active species. Nakamura et al[58] have synthesised complexes of the type $(\eta^5\text{-}C_5R_5)(\eta^4\text{-diene})MX_2$ (where M = Nb, Ta ; X = Cl, CH_3) which again show promising activity when activated by MAO.

Continuing the isolobal analogy, we have recently reported polymerisation activity from a Group 6 bis-imido complex.[59] This is detailed further in chapter 2 and forms the basis for much of the work in this thesis.

1.4 Living Ring Opening Metathesis Polymerisation.

1.4.1 Introduction.

In chemical terms, a metathesis reaction is one whereby two units, initially incorporated into a larger molecule are interchanged with one another. For the case of olefin metathesis, the exchanging units are alkylidene fragments, pairs of which compromise an olefin, as illustrated in equation 1.3.

$$2\ RHC{=}CHR' \rightleftharpoons RHC{=}CHR + 'RHC{=}CHR'$$

Equation 1.3 Generalised olefin metathesis reaction.

A particularly important application of this type of reaction is the Ring Opening Metathesis Polymerisation (or ROMP) of cyclic olefins. The first recorded example of this type of reaction was reported in a 1955 DuPont patent,[60] although it was only realised that this mechanism was occurring with hind-sight (see equation 1.4).

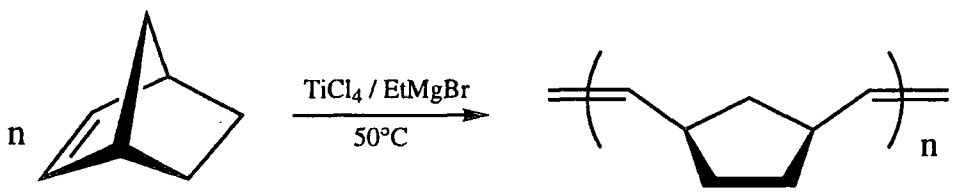

Equation 1.4

1.4.2 The Mechanism of Olefin Metathesis Reactions.

The original proposal for the mechanism of this reaction was based on pairwise processes involving metal bound cyclobutanes or related structures.[61] The currently accepted mechanism proposed by Chauvin and Herisson in 1970,[62] however, involves a [2 + 2] cycloaddition of the C=C bond of the olefin to a metal carbon double bond to yield a metallacyclobutane intermediate (see figure 1.15). This can then react to form either the original reactants (degenerate metathesis) or proceed to give the new olefin products, termed productive metathesis.

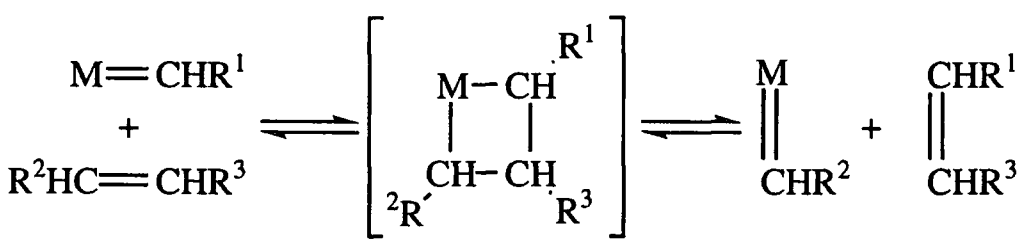

Figure 1.15 Proposed mechanism for olefin metathesis.

Support for this mechanism is forthcoming from labelling studies on cross metathesis reactions that show the products to be incompatible with a pairwise mechanism,[63] and the subsequent demonstration by Schrock, Osborn and Grubbs that

discrete metal alkylidene and metallacyclobutane complexes are active in this type of reaction.[64-66]

1.4.3 Classical Catalysts for ROMP.

These typically dual component systems were the first to be developed and can be either heterogeneous or homogeneous, although the distinction between the two is not always apparent. Such systems typically consist of a Lewis acidic metal species and a main group alkyl compound. An example of a heterogeneous system is WO_3 on SiO_2 support[67] with homogeneous systems including WCl_6 / EtOH / $EtAlCl_2$[68] and $MeReO_3$ / $AlCl_3$.[69] Many other examples are present in the literature and the reader is referred to Ivins' book for a full review of classical systems.[70]

Although such systems have gained commercial application, for example in the production of Norsorex (polynorbornene) and more recently in the Reaction Injection Moulding (RIM) of dicyclopentadiene,[71] the chemistry is not well defined. Variations exist depending on the rate of mixing of catalyst, co-catalyst and monomer, as well as the thermal and chemical history of the catalyst itself. Also the formation of the metal carbon bonds necessary for such a polymerisation to proceed only occur in low yield and tend to decompose over the time scale of a typical reaction. The high Lewis acidity of the metal species renders these systems sensitive to functional groups, limiting the number of monomers that can be successfully polymerised prompting the development of well-defined functional group tolerant catalysts.[72]

1.4.4 Well-Defined Catalysts for ROMP.

Two established well defined ROMP systems are Schrock's alkylidene complexes[73] and Grubbs' titanocene metallacyclobutane.[74] In the work presented in chapter five of this thesis, initiators of the type $M(NAr)(=CHR)(OR')_2$ (where M = Mo, W ; R = CMe_2Ph, CMe_3 ; R' = CMe_3, $CMe_2(CF_3)$, $CMe(CF_3)_2$) have been employed

(see figure 1.16), and hence the remainder of this section will concentrate in this area of ROMP.

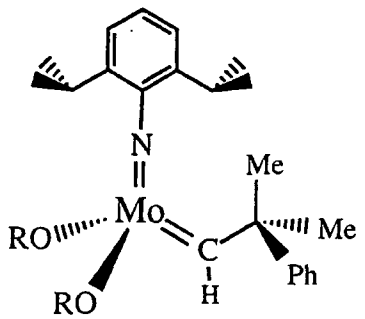

R = $OCMe_3$
$OCMe_2(CF_3)$
$OCMe(CF_3)_2$

Figure 1.16 Four coordinate 'Schrock' initiators.

In complexes of this type, the tetrahedral geometry about the metal allows relatively small substrates such as olefins to access the metal centre, permitting the formation of the intermediate metallacyclobutane (see section 1.4.2), which may be isolated and characterised in certain favourable cases.[75] The bulky alkoxide and 2,6-diisopropylphenylimido ligands help prevent ligand scrambling at this stage.

The X-ray structure of $W(NAr)(=CH^tBu)(O^tBu)_2$ is shown in figure 1.17, being typical of this range of catalysts. It is pseudo tetrahedral about the metal centre, with the alkylidene substituent pointing towards the imido ligand (the syn rotamer). The linear W=N triple bond forces the β-carbon of the alkylidene to lie in the same plane as the nitrogen, tungsten and α-carbon atoms.[76] The other possible isomer of this compound, where the alkylidene ligand is pointing away from the imido nitrogen (the anti rotamer) is present in solution forming an equilibrium mixture (see section 5.4.6).

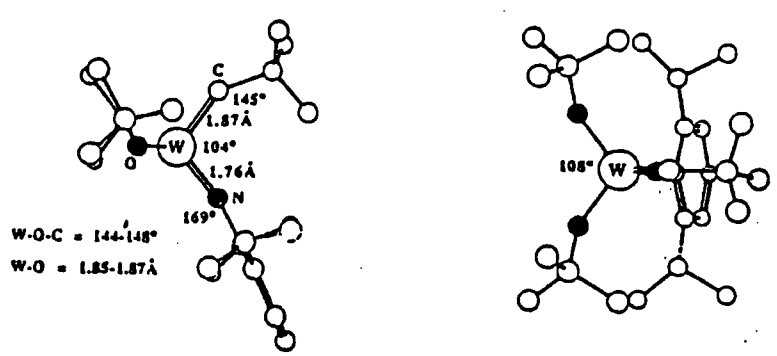

Figure 1.17 Crystal structure of $W(NAr)(=CH^tBu)(O^tBu)_2$.

Control over the activity of these compounds is accomplished by varying the alkoxide group. For example, W(NAr)(=CH^{t}Bu)(OCMe(CF$_3$)$_2$)$_2$ will metathesise cis-2-pentene at a rate of ~ 10^3 turnovers / minute in toluene at room temperature, whereas W(NAr)(=CH^{t}Bu)(O^{t}Bu)$_2$ the corresponding rate of metathesis is only 2 turnovers / hour.[73b] The reduced reactivity of ^{t}butoxide initiators is exploited in the polymerisation of cyclic olefins where both the molybdenum and tungsten analogues react with the strained double bond in norbornene to yield polymers, but will not metathesise the double bonds in the growing polymer chain, a phenomenon known as back-biting. This leads to production of polymers in a controlled 'living' manner.

1.4.5 The Mechanism of Living ROMP using Well-Defined Initiator Systems.

This is illustrated below for the relatively simple case of Mo(NAr)(=CH^{t}Bu)(O^{t}Bu)$_2$ and norbornene (figure 1.18).

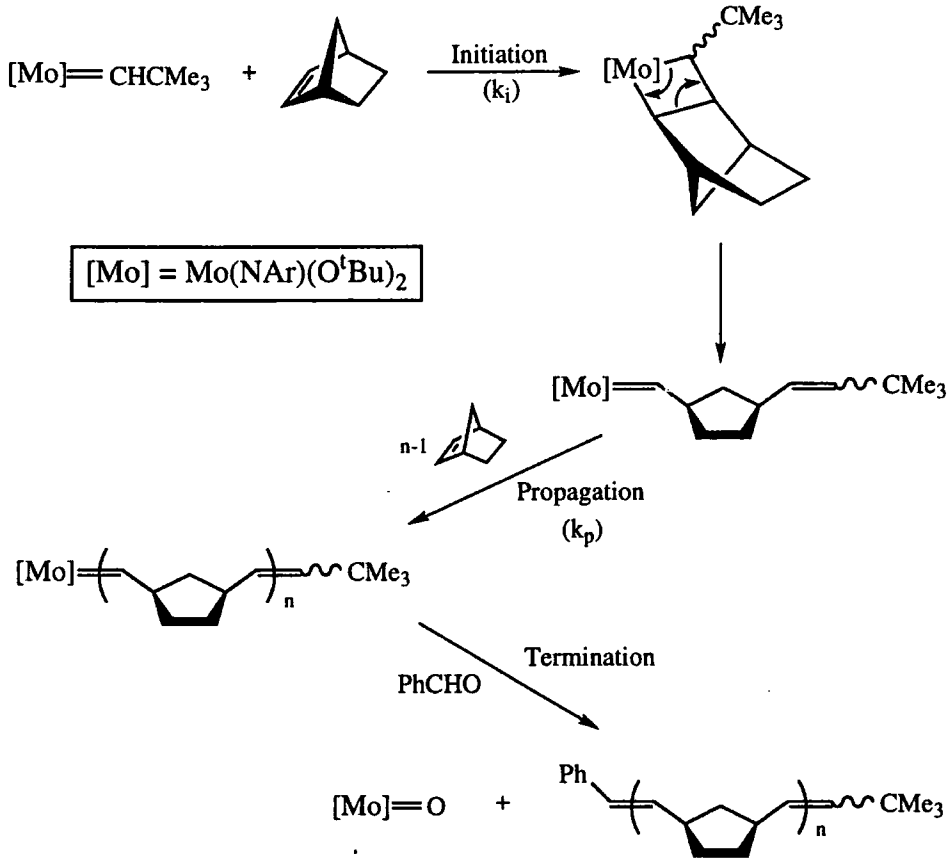

Figure 1.18 Mechanism of ROMP using well-defined initiators.

The initiator reacts with one equivalent of norbornene (rate = k_i) to form a metallacyclobutane which breaks productively to yield a new (propagating) alkylidene. This reacts with more monomer at the propagating rate k_p. The resulting polymer is termed living if the monomer adds irreversibly and chain transfer and chain termination are slow on the time scale of the reaction. Also, the rate of initiation must be favourable compared with the rate of propagation.[77,78]

The polymer is finally cleaved from the metal centre (termination of the polymerisation) in a 'Wittig like' capping process by reaction with an aldehyde (typically benzaldehyde or pivaldehyde) to give the mixed oxo-imido species $Mo(O)(NAr)(O^tBu)_2$.

1.4.6 Living ROMP of Functionalised Norbornene and Norbornadiene Derivatives.

Many simple alkyl substituted norbornenes have been polymerised using Schrock initiators[79] and recently there has been interest in the development of specific advanced materials employing this technique. In 1980, Feast and co-workers elegantly demonstrated a route into polyacetylene[80] *via* the preparation of a polymeric precursor. Stelzer[81] has employed a similar rationale behind the synthesis of poly(cyclopentadienylenevinylene), whereby the original polymeric precursor from the ROMP of a norbornene derivative is heated to eliminate the side groups and give the conjugated material (see figure 1.19).

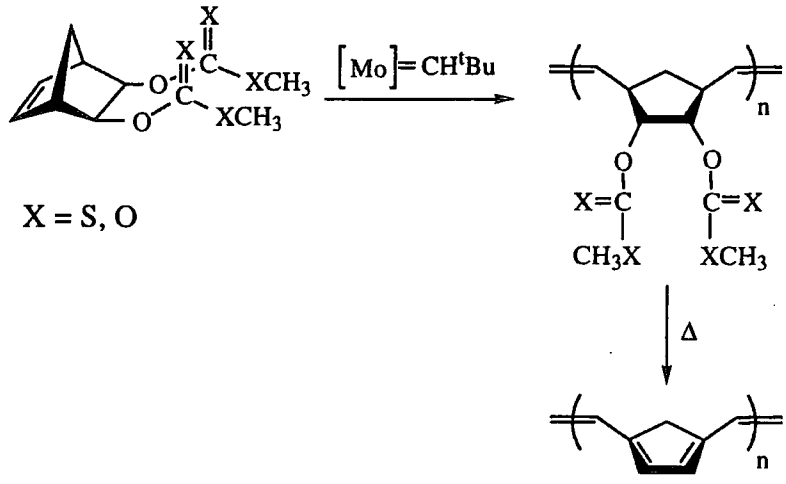

Figure 1.19 Synthesis of poly(cyclopentadienylenevinylene) *via* a polymeric precursor.

Producing polymers from norbornene molecules that already possess a polymeric substituent has led to new side chain liquid crystalline polymers (SCLCPs) being developed.[82] In many cases the mesogen is attached laterally to the polymer backbone, as illustrated in figure 1.20 from reference 82c.

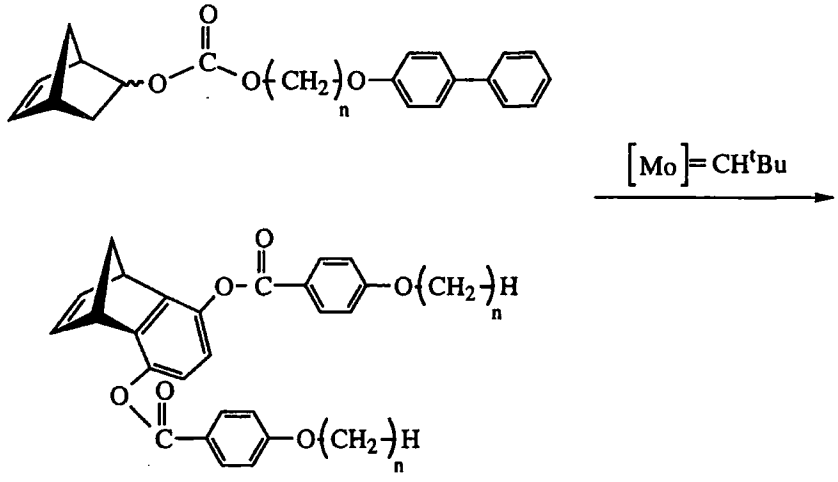

Figure 1.20 Synthesis of novel side chain liquid crystalline polymers (SCLCPs).

Feast *et al* have utilised a similar rationale to develop novel polymer topologies.[83] Combining anionic polymerisation of styrene and ROMP, so called

'polymer brushes' have been developed with a norbornene backbone and styrene side groups (see figure 1.21).

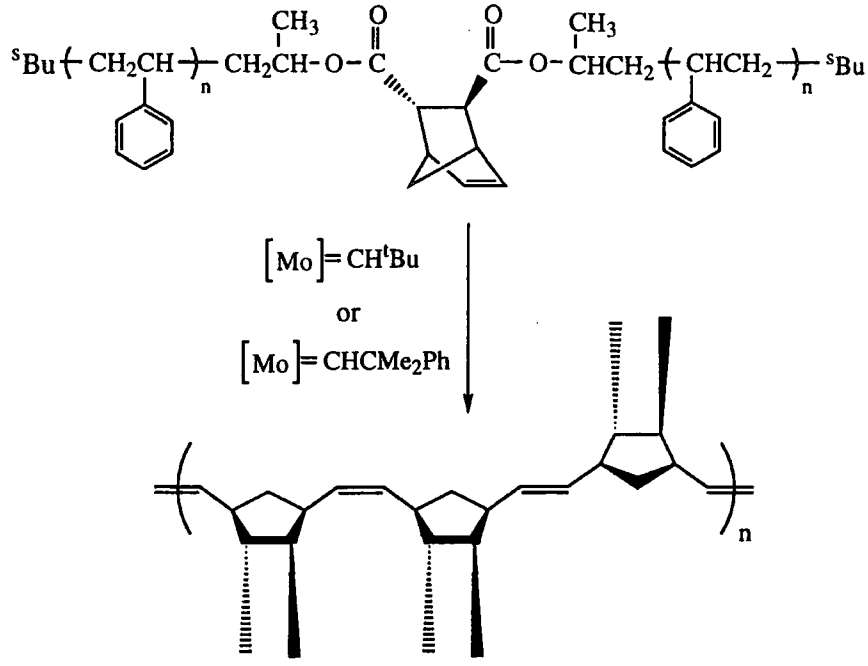

Figure 1.21 Synthesis of polymer brushes.

Schrock and co-workers have designed and synthesised a polymeric blue-light emitting electroluminescent material from the monomer illustrated below.[84] As a polymeric material, thin layers can be easily made, in this example either by static casting from THF or chloroform or by spin casting onto a glass substrate.

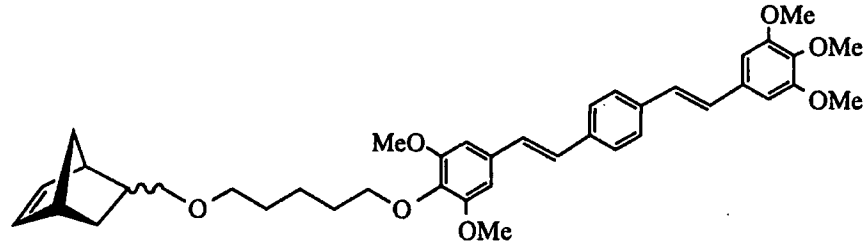

Figure 1.22 Monomer used in the preparation of an electroluminescent material.

By terminating a polymer chain with a lumophore, the dynamics of the polymer both in solution and in the solid state can be studied.[85] Such a system is also useful for studying electron transfer reaction within polymers. Schrock *et al* have achieved this for the polymers derived from the two monomers illustrated below by capping a living polymer with pyrenecaboxaldehyde.

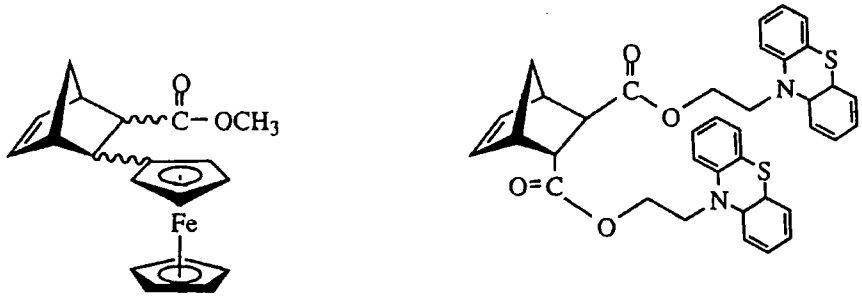

Figure 1.23

A recent review[86] has listed some of the expected properties of polymeric materials containing a C_{60} 'buckminsterfullerene' molecule, including electron, optical and catalytic properties. As well as combining features of C_{60} with the polymer, such systems should be much more processible than C_{60} itself, allowing spin coating or melt extrusion for example. In 1993 it was reported that addition of quadricyclone to C_{60} gave the stable 6,6 adduct illustrated below.[87] This has now been shown to undergo copolymerisation with norbornene employing the fluorinated initiator $Mo(NAr)(=CH^tBu)(OCMe(CF_3)_2)_2$.[88] The large excess of unsubstituted norbornene is present due to solubility problems associated with the C_{60} derived monomer.

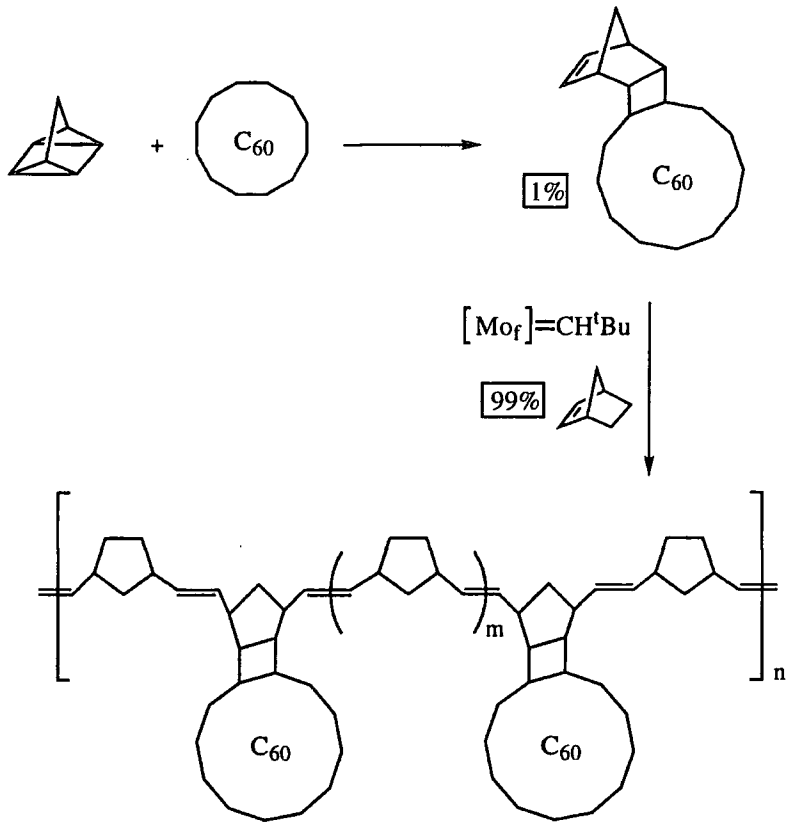

Figure 1.24

This section has briefly looked at some examples of ROMP used to prepare advanced materials. It is recognised that this is only a selection of the full range of such polymeric materials, but it is hoped that the versatility of the process has been demonstrated.

1.5 Summary

This chapter has attempted to highlight some of the vast range of chemistry associated with transition metal imido and alkylidene complexes. We have briefly discussed the bonding present in representative complexes and proceeded to examine two polymerisation processes with which these compounds are associated. The remaining chapters of this thesis further explore the chemistry and polymerisation activity of new species of this type.

1.6 References.

1. A.F. Clifford and C.S. Kobayshi, *Inorg. Synth.*, **1960**, *6*, 204.

2. For a recent comprehensive review, see D.E. Wigly, *Progress In Inorganic Chemistry*, **1995**, *42*, 239.

3. V.C. Gibson, *J. Chem. Soc. Dalton Trans.*, **1994**, 1607 ; V.C. Gibson, *Angew. Chem. Int. Ed. Engl.*, **1994**, *33*, 1565.

4. B.L. Haymore, E.A. Maatta and R.A.D. Wentworth, *J. Am. Chem. Soc.*, **1979**, *101*, 2063.

5. A.A Danopoulos, G. Wilkinson, T Sweet and M.B. Hursthouse, *J. Chem Soc., Chem. Commun.*, **1993**, 495.

6. J.T. Anhaus, T.P. Kee, M.H. Schofield and R.R. Schrock, *J. Am. Chem. Soc.*, **1990**, *112*, 1642 ; M.H. Schofield, T.P. Kee, J.T. Anhaus, R.R. Schrock, K.H. Johnson and W.M. Davis, *Inorg. Chem.*, **1991**, *30*, 3595.

7. W.A. Nugent and J.M. Mayer, *"Metal Ligand Multiple Bonds"*, Wiley, New York, 1988.

8. A.A Danopoulos, C.J. Longley, G. Wilkinson, B. Hussain and M.B. Hursthouse, *Polyhedron*, **1989**, *8*, 2657.

9. A.K. Burrell and J.C. Bryan, *Organometallics*, **1992**, *11*, 3501 ; A.K. Burrell and J.C. Bryan, *Angew. Chem. Int. Ed. Engl.*, **1993**, *32*, 94 ; A.K. Burrell, D.L. Clark, P.L. Gordon, A.P. Sattelberger and J.C. Bryan, *J. Am. Chem. Soc.*, **1994**, *116*, 3813 ; J.C. Bryan, A.K. Burrell, M.M. Miller, W.H. Smith, C.J. Burns and A.P. Sattelberger, *Polyhedron*, **1993**, *12*, 1769.

10. D.S. Williams, J.T. Anhaus, M.H. Schofield, R.R. Schrock and W.M. Davis, *J. Am. Chem. Soc.*, **1991**, *113*, 5480 ; D.S. Williams and R.R. Schrock, *Organometallics*, **1993**, *12*, 1148.

11. D.L. Morrison and D.E. Wigley, *J. Chem. Soc., Chem. Commun.*, **1995**, 79 ; D.L. Morrison and D.E. Wigley, *Inorg. Chem.*, **1995**, *34*, 2610.

12. Y. -W. Chao, P.M. Rodgers, D.E. Wigley, S.J. Alexander and A.L. Rheingold, *J. Am. Chem. Soc.*, **1991**, *113*, 6326 ; D.L. Morrison, P.M. Rodgers, Y.-W.

Chao, M.A. Bruck, C. Grittini, T.L. Tajima, S.J. Alexander, A.L. Rheingold and D.E. Wigley, *Organometallics*, **1995**, *14*, 2435.

13. A.B. Manion, T.K.G. Erikson, E. Spaltenstein and J.M. Mayer, *Organometallics*, **1989**, *8*, 1871 ; E. Spaltenstein, R.R. Conry, S.C. Critchlow and J.M. Mayer, *J. Am. Chem. Soc.*, **1989**, *111*, 8741.

14. D.P. Tate and J.M. Augl, *J. Am. Chem. Soc.*, **1963**, *85*, 2174 ; D.P. Tate, J.M. Augl, W.M.Ritchey, B.L. Ross and J.G. Grasselli, *J. Am. Chem. Soc.*, **1964**, *86*, 3261 ; R.M. Laine, R.E. Moriarty and R. Bau, *J. Am. Chem. Soc.*, **1972**, *94*, 1402 ; R.B. King, *Inorg Chem*, **1968**, *7*, 1044.

15. (a) G. Parkin, A. van Asselt, D.J. Leahy, L. Whinnery, N.G. Hua, R.W. Quan, L.M. Henling, W.P. Schaefer, B.D. Santarsiero and J.E. Bercaw, *Inorg. Chem.*, **1992**, *31*, 82. (b) K.A. Jørgensen, *Inorg. Chem.*, **1993**, *32*, 1521.

16. R.G. Bergman, F.J. Hollander and P.J. Walsh, *J. Am. Chem. Soc.*, **1988**, *110*, 8729.

17. R.R. Schrock, *J. Am. Chem. Soc.*, **1974**, *96*, 6796.

18. J.R. Collmann, L.S. Hegedus, J.R. Norton and R.G. Finke, *"Principles and Applications of Organometallic Chemistry"*, University Science Press, Mill Valley, CA, 1987.

19. A.K. Rappé and W.A. Goddard III, *J. Am. Chem. Soc.*, **1977**, *99*, 3966.

20. H. Nakatsuji, J. Ushio, S. Han and T. Yonezawa, *J. Am. Chem. Soc.*, **1983**, *105*, 426.

21. J. Ushio, H. Nakatsuji and T. Yonezawa, *J. Am. Chem. Soc.*, **1984**, *106*, 5892.

22. T.E. Taylor and M.B. Hall, *J. Am. Chem. Soc.*, **1984**, *106*, 1576.

23. E.A. Carter and W.A. Goddard III, *J. Am. Chem. Soc.*, **1986**, *108*, 2180.

24. D.N. Williams, J.P. Mitchell, A.D. Poole, U. Siemeling, W. Clegg, D.C.R. Hockless, P.A. O'Neil and V.C. Gibson, *J. Chem. Soc. Dalton Trans.*, **1992**, 739.

25. J.W. Lauher and R. Hoffmann, *J. Am. Chem. Soc.*, **1976**, *98*, 1729.

26. L. Zhu and N.M. Kostic, *J. Organomet. Chem.*, **1987**, *335*, 395.

27. D.S. Williams, M.H. Schofield and R.R. Schrock, *Organometallics*, **1993**, *12*, 4560.

28. For Half-Sandwich Group 5 examples :- A.D. Poole, V.C. Gibson and W. Clegg, *J. Chem. Soc., Chem. Commun.*, **1992**, 237 ; U. Siemeling and V.C. Gibson, *J. Organomet. Chem.*, **1992**, *426*, C25 ; J.K. Cockcroft, V.C. Gibson, J.A.K. Howard, A.D. Poole, U. Siemeling and C. Wilson, *J. Chem. Soc., Chem. Commun.*, **1992**, 1668 ; A.D. Poole, Ph.D. Thesis, University of Durham, 1992 ; V.C. Gibson, A.D. Poole, U. Siemeling and D.N. Williams, *J. Organomet. Chem.*, **1993**, *462*, C12.

29. For Bis-Imido Group 6 examples :- D.S. Williams, M.H. Schofield, J.T. Anhaus and R.R. Schrock, *J. Am. Chem. Soc.*, **1990**, *112*, 6728 ; I.A. Weinstock, R.R. Schrock, D.S. Williams and W.E. Crowe, *Organometallics*, **1991**, *10*, 1 ; P.W. Dyer, V.C. Gibson, J.A.K. Howard, B. Whittle and C. Wilson, *J. Chem. Soc., Chem. Commun.*, **1992**, 1666 ; P.W. Dyer, V.C. Gibson, J.A.K. Howard and C. Wilson, *J. Organomet. Chem.*, **1993**, *462*, C15 ; P.W. Dyer, V.C. Gibson, J.A.K. Howard, B. Whittle and C. Wilson, *Polyhedron*, **1995**, *1*, 103.

30. Other examples :- J. Sundermeyer and D. Runge, *Angew. Chem. Int. Ed. Engl.*,**1994**, *33*, 1255.

31. R.R. Schrock, L.W. Messerle, C.D. Wood and L.J. Guggenberger, *J. Am. Chem. Soc.* **1978**, *100*, 3793.

32. M. Jolly, Ph.D. Thesis, University of Durham, 1994.

33. J. Boor, *"Ziegler-Natta Catalysis and Polymerisations"*, Academic Press, New York, 1979.

34. G. Natta, P. Pino, G. Mazzanti and U. Giannini, *J. Am. Chem. Soc.*, **1957**, *79*, 2975 ; D.S. Breslow and N.R. Newburg, *J. Am. Chem. Soc.*, **1957**, *79*, 5072.

35. For reviews covering this period see :- H. Sinn and W. Kaminsky, *Adv. Organomet. Chem.*, **1980**, *18*, 99 ; P. Pino and R. Mülhaupt, *Angew. Chem. Int. Ed. Engl.*, **1980**, *19*, 857.

36. D.S. Breslow and N.R. Newburg, *J. Am. Chem. Soc.*, **1959**, *81*, 81 ; W.P. Long, *J. Am. Chem. Soc.*, **1959**, *81*, 5312 ; W.P. Long and D.S. Breslow, *J. Am. Chem. Soc.*, **1960**, *82*, 1953 ; J.C.W. Chien, *J. Am. Chem. Soc.*, **1959**, *81*, 86.

37. P. Cossee, *Tetrahedron Lett.*, **1960**, *17*, 12.

38. R.F. Jordan, W.E. Dasher and S.F. Echols, *J. Am. Chem. Soc.*, **1986**, *108*, 1718 ; R.F. Jordan, C.S. Bajgur, R. Willett and B. Scott, *J. Am. Chem. Soc.*, **1986**, *108*, 7410 ; R.F. Jordan, R.E. LaPointe, C.S. Bajgur, S.F. Echols and R. Willett, *J. Am. Chem. Soc.*, **1987**, *109*, 4111 ; R.F. Jordan, P.K. Bradley, N.C. Baenziger

and R.E. LaPointe, *J. Am. Chem. Soc.*, **1990**, *112*, 1289 ; R.F. Jordan, R.E. LaPointe, N. Baenziger and G.D. Hinch, *Organometallics*, **1990**, *9*, 1539 ; R.F. Jordan, *Adv. Organomet, Chem.*, **1991**, *32*, 325.

39. M. Bochmann and L.M. Wilson, *J. Chem. Soc., Chem. Commun.*, **1986**, 1610 ; M. Bochmann, L.M. Wilson, M.B. Hursthouse and R.L. Short, *Organometallics*, **1987**, *6*, 2556 ; M. Bochmann, L.M. Wilson, M.B. Hursthouse and M. Motevalli, *Organometallics*, **1988**, *7*, 1148 ; R. Taube and L. Krukowka, *J. Organomet. Chem.*, **1988**, *347*, C9 ; M. Bochmann, and A.J. Jaggar, *J. Organomet. Chem.*, **1992**, *424*, C5.

40. M. Bochmann and S.J. Lancaster, *J. Organomet. Chem.*, **1992**, *434*, C1 ; J.J.W. Eshuis, Y.Y. Tan, A. Meetsma, J.H. Teuben, J. Renkema and G.G. Evens, *Organometallics*, **1992**, *11*, 362.

41. J.J. Eisch, S.I. Pombrik and G-X. Zheng, *Makromol. Chem., Macromol. Symp.*, **1993**, *66*, 109 ; P.A. Deck and T.J. Marks, *J. Am. Chem. Soc.*, **1995**, *117*, 6128.

42. W.P. Long and D.S. Breslow, *Liebigs Ann. Chem.*, **1975**, 463.

43. A. Andresen, H.-G. Cordes, J. Herwig, W. Kaminsky, A. Merk, R. Mottweiler, J. Pein, H. Sinn and H.-J. Vollmer, *Angew. Chem. Int Ed. Engl.*, **1976**, *15*, 630 ; H. Sinn, W. Kaminsky, H.-J. Vollmer and R. Woldt, *Angew. Chem. Int. Ed. Engl.*, **1980**, *19*, 390.

44. L. Resconi, S. Bossi and L. Abis, *Macromolecules*, **1990**, *23*, 4489.

45. T. Sugano, K. Matsubara, T. Fujita and T. Takahashi, *J. Mol. Catal.*, **1993**, *82*, 93 ; C.J. Harlan, M.R. Mason and A.R. Barron, *Organometallics*, **1994**, *13*, 2957 and references therein ; I. Tritto, S.X. Li, M.C. Sacchi, P. Locatelli and G. Zannoni, *Macromolecules*, **1995**, *28*, 5358.

46. G.G. Hlatky, D.J. Upton and H.W. Turner, *US. Pat. Appl*, **1990**, 459921 - *Chem. Abstr.*, **1991**, *115*, 256897v.

47. X. Yang, C.L. Stern and T.J. Marks, *Organometallics*, **1991**, *10*, 840.

48. X. Yang, C.L. Stern and T.J. Marks, *J. Am. Chem. Soc.*, **1991**, *113*, 3623 ; X. Yang, C.L. Stern and T.J. Marks, *J. Am. Chem. Soc.*, **1994**, *116*, 10015.

49. L. Jia, X. Yang, A. Ishihara and T.J. Marks, *Organometallics*, **1995**, *14*, 3135 ; R. Quyoum, Q. Wang, M.-J. Tudoret, M.C. Baird and D.J. Gillis, *J. Am. Chem. Soc.*, **1994**, *116*, 6435.

50. B.J. Burger, M.E. Thompson, W.D. Cotter and J.E. Bercaw, *J. Am. Chem. Soc.*, **1990**, *112*, 1566.

51. P.L. Watson and G.W. Parshall, *Acc. Chem. Res.*,**1985**, *18*, 51.

52. W.J. Evans, L.R. Chamberlain, T.A. Ulibarri and J. Ziller, *J. Am. Chem. Soc.*, **1988**, *110*, 6423.

53. Z. Lin, J-F. LeMarechal, M. Sabat and T.J. Marks, *J. Am. Chem. Soc.*, **1987**, *109*, 4127.

54. D.J. Crowther, N.C. Baenziger and R.F. Jordan, *J. Am. Chem. Soc.*, **1991**, *113*, 1455 ; D.J. Crowther, R.F. Jordan, *Makromol. Chem., Macromol. Symp.*, **1993**, *66*, 121 ; R. Uhrhammer, D.J. Crowther, J.D. Olson, D.C. Swenson and R.F. Jordan, *Organometallics*, **1992**, *11*, 3098.

55. G.C. Bazan, G. Rodriguez and B.P. Cleary, *J. Am. Chem. Soc.*, **1994**, *116*, 2177.

56. (a) M.P. Coles and V.C. Gibson, *Polymer Bull.*, **1994**, *33*, 529. (b) M.C.W. Chan, Ph.D. Thesis, University of Durham, 1995. (c) See also this thesis, chapter 2.

57. S. Scheuer, J. Fischer and J. Kress, *Organometallics*, **1995**, *14*, 2627.

58. K. Mashima, S. Fujikawa and A. Nakamura, *J. Am. Chem. Soc.*, **1993**, *115*, 10990 ; K. Mashima, S. Fujikawa, Y. Tanaka, H. Urata, T. Oshiki, E. Tanaka and A. Nakamura, *Organometallics*, **1995**, *14*, 2633.

59. M.P. Coles, C.I. Dalby, V.C. Gibson, W. Clegg and M.R.J. Elsegood, *J. Chem. Soc., Chem. Commun.*, **1995**, 1709.

60 A.W. Anderson and N.G. Merckling, US. Pat. 2721189, *Chem. Abstr.*, **1955**, *50*, p3008i.

61. F.D. Mango and J. Schachtschneider, *J. Am. Chem. Soc.*, **1971**, *93*, 1123 ; G.S. Lewandos and R. Pettit, *J. Am. Chem. Soc.*, **1971**, *93*, 7087 ; R.H. Grubbs and T.K. Brunck, *J. Am. Chem. Soc.*, **1972**, 2538.

62. J.L. Herisson and Y. Chauvin, *Makromol. Chem.*, **1970**, *141*, 161.

63. T.J. Katz and R. Rothchild, *J. Am. Chem. Soc.*, **1976**, *98*, 2519 ; R.H. Grubbs, D.D. Carr, C. Hoppin and P.L. Burk, *J. Am. Chem. Soc.*, **1976**, *98*, 3478 ; T.J. Katz and J. McGinnis, *J. Am. Chem. Soc.*, **1977**, *99*, 1903.

64. R.R. Schrock, *Acc. Chem. Res.*, **1990**, *23*, 158.

65. J. Kress, J.A. Osborn, R.M.E. Green, K.J. Ivin and J.J. Rooney, *J. Am. Chem. Soc.*, **1987**, *109*, 899.

66. R.H. Grubbs and S. Swetnick, *J. Mol. Catal*, **1980**, *8*, 25.

67. F. Pennella, *J. Catal.*, **1981**, *69*, 206.

68. N. Calderon, E.A. Ofstead, J.P. Ward, W.A. Judy and K.W. Scott, *J. Am. Chem. Soc.*, **1968**, *90*, 4133.

69. W.A. Herrmann, J.G. Kuchler, J.K. Felixberger, E. Herdtweck and W. Wagner, *Angew. Chem., Int. Ed. Engl.*, **1988**, *27*, 394.

70. K.J. Ivin, *"Olefin Metathesis"*, Academic Press, London, 1983.

71. A. Bell, US Pat. 5319042, *Chem. Abstr.*, **1994**, *89*, p281440x.

72. R.R. Schrock, *J. Organomet. Chem.*, **1986**, *300*, 249.

73. (a) R.R. Schrock, J.S. Murdzek, G.C. Bazan, J. Robbins, M. DiMare and M. O'Regan, *J. Am. Chem. Soc.*, **1990**, *112*, 3875. (b) R.R. Schrock, R.T. DePue, J. Feldman, C.J. Schaverien, J.C. Dewan and A.H. Liu, *J. Am. Chem. Soc.*, **1988**, *110*, 1423. (c) R.R. Schrock, R.T. DePue, J. Feldman, K.B. Yap, D.C. Yang. W.M. Davis, L. Park, M. Dimare, M. Schofield, J.T. Anhaus, E. Walborsky, E. Evitt, C. Krüger and P. Betz, *Organometallics*, **1990**, *9*, 2262.

74. D.A. Straus and R.H. Grubbs, *Organometallics*, **1982**, *1*, 1658 ; L.R. Gilliom and R.H. Grubbs, *J. Am. Chem. Soc.*, **1986**, *108*, 733.

75. J. Feldman, W.M. Davis and R.R. Schrock, *Organometallics*, **1989**, *8*, 2266 ; J. Feldman, J.S. Murdzek, W.M. Davis and R.R. Schrock, *Organometallics*, **1989**, *8*, 2260 ; J. Robbins, G.C. Bazan, J.S. Murdzek, M.B. O'Regan and R.R. Schrock, *Organometallics*, **1991**, *10*, 2902.

76. R.R. Schrock, in *"Reactions of Coordinated Ligands"*, P.R. Braterman Ed., Plenum, New York, 1986.

77. L. Gold, *J. Chem. Phys.*, **1958**, *28*, 91.

78. A.H.E. Muller, *"Comprehensive Polymer Science"*, Pergamon, New York, Volume 3, Chapter 26, 1989.

79. G.C. Bazan, R.R. Schrock, H.N. Cho and V.C. Gibson, *Macromolecules*, **1991**, *24*, 4495 ; G.C. Bazan, R.R. Schrock, E. Khosravi, W.J. Feast and V.C. Gibson, *Polymer Comm.*, **1989**, *30*, 258 ; G.C. Bazan, R.R. Schrock, E. Khosravi, W.J.

Feast, V.C. Gibson, M.B. O'Regan, J.K. Thomas and W.M. Davis, *J. Am. Chem. Soc.*, **1990**, *112*, 8378.

80. J.H. Edwards and W.J. Feast, *Polymer*, **1980**, *21*, 595 ; J.H. Edwards, W.J. Feast and D.C. Bott, *Polymer*, **1984**, *25*, 395 ; W.J. Feast and J.N. Winter, *J. Chem. Soc., Chem. Commun.*, **1985**, 202.

81. M. Schimetta and F. Stelzer, *Macromolecules*, **1994**, *27*, 3769.

82. (a) Z. Komiya, C. Pugh and R.R. Schrock, *Macromolecules*, **1992**, *25*, 6586. (b) C. Pugh and R.R. Schrock, *Macromolecules*, **1992**, *25*, 6593. (c) C. Pugh, *Makromol. Chem., Macromol. Symp.*, **1994**, *77*, 325.

83. W.J. Feast, V.C. Gibson, A.F. Johnson, E. Khosravi and M.A. Mohsin, *Polymer*, **1994**, *35*, 3542.

84. J.-K. Lee, R.R. Schrock, D.R. Baigent and R.H. Friend, *Macromolecules*, **1995**, *28*, 1966.

85. D. Albagli, G.C. Bazan, R.R. Schrock and M.S. Wrighton, *J. Phys. Chem.*, **1993**, *97*, 10211.

86. A. Hirsch, *Adv. Mater.*, **1993**, *5*, 859.

87. M. Prato, M. Magginni, G. Scoranno and V. Lucchini, *J. Org. Chem.*, **1993**, *58*, 3613.

88. N.J. Zhang, S.R. Schricker, F. Wudl, M. Prato, M. Magginni and G. Scoranno, *Chemistry of Materials*, **1995**, *7*, 441.

Chapter Two

Imido Complexes of Group 5 and Group 6 Metals as α-Olefin Polymerisation Catalysts. Development of the Bis-Imido Chemistry of Chromium.

2.1 Introduction.

In view of the close isolobal relationship between Group 5 half-sandwich imido, Group 6 bis-imido compounds and Group 4 bent metallocenes (see section 1.2.4), we were interested in establishing any ethylene polymerisation activity of the imido complexes at an early stage. A series of simple dichloride compounds were targeted with a view to evaluating their capacity to polymerise ethylene upon activation by established co-catalysts such as DEAC and MAO. It was planned to follow up any positive results by synthesising well defined alkyl derivatives and evaluating their polymerisation capability as single component catalysts employing the $[B(C_6F_5)_4]^-$ counter-ion.

2.2 Half Sandwich Group 5 Imido and Group 6 Bis-Imido Compounds as Potential α-Olefin Polymerisation Catalysts.

2.2.1 Synthesis of $CpV(NR)Cl_2$ and $Cr(N^tBu)_2X_2$ [R = *p*-tol ; ^{t}Bu and X = OTMS ; Cl]

The synthetic route to $CpV(NR)Cl_2$ (where Cp = η^5-C_5H_5 and R = ^{t}Bu, *p*-CH_3-C_6H_4) was a modification of a method previously published by Maatta,[1] using ^{n}Bu$_3$Sn(Cp) rather than TMS(Cp) or Na(Cp) to introduce the cyclopentadienyl ring onto the vanadium centre (equations 2.1 and 2.2)

$$VOCl_3 + RN{=}C{=}O \longrightarrow V(NR)Cl_3 + CO_2$$

$$V(NR)Cl_3 + {}^nBu_3Sn(Cp) \longrightarrow CpV(NR)Cl_2 + {}^nBu_3Sn\text{-}Cl$$

Equations 2.1 and 2.2 Synthetic route to half-sandwich vanadium imido complexes.

The synthesis of the bis(^{t}butylimido) chromium precursors used in this study have also been previously described[2,3] and are summarised in equations 2.3 and 2.4. The initial reaction between CrO_2Cl_2 and the silylated amine was carried out in heptane and heated to 60°C overnight resulting in an improved yield to that reported by Nugent.[2]

$$CrO_2Cl_2 + 4\ ^tBuNH(TMS) \longrightarrow Cr(N^tBu)_2(OTMS)_2 + 2\ [^tBuNH_2(TMS)]Cl$$

$$Cr(N^tBu)_2(OTMS)_2 + 2\ BCl_3 \longrightarrow Cr(N^tBu)_2Cl_2 + 2\ BCl_2(OTMS)$$

Equations 2.3 and 2.4 Synthetic route to bis(^{t}butylimido) chromium complexes.

All compounds were isolated as pure crystalline materials whose NMR data corresponded with that previously published.

2.2.2 Testing for Catalytic Activity Employing Alkyl-Aluminium Reagents as Co-Catalysts.

Initial testing of these compounds as catalytic precursors for the polymerisation of ethylene was carried out at Durham using the experimental set-up illustrated in figure 2.1.

Full details of the polymerisation procedure appear in section 6.2.1 and are therefore only briefly discussed here. The ethylene was first passed through a drying column consisting of $CaCl_2$, molecular seives and P_2O_5 and then a silicone oil bubbler to which a few cm^3 of a DEAC solution had been added. The latter also served as a crude measure of the flow rate of the ethylene into the system.

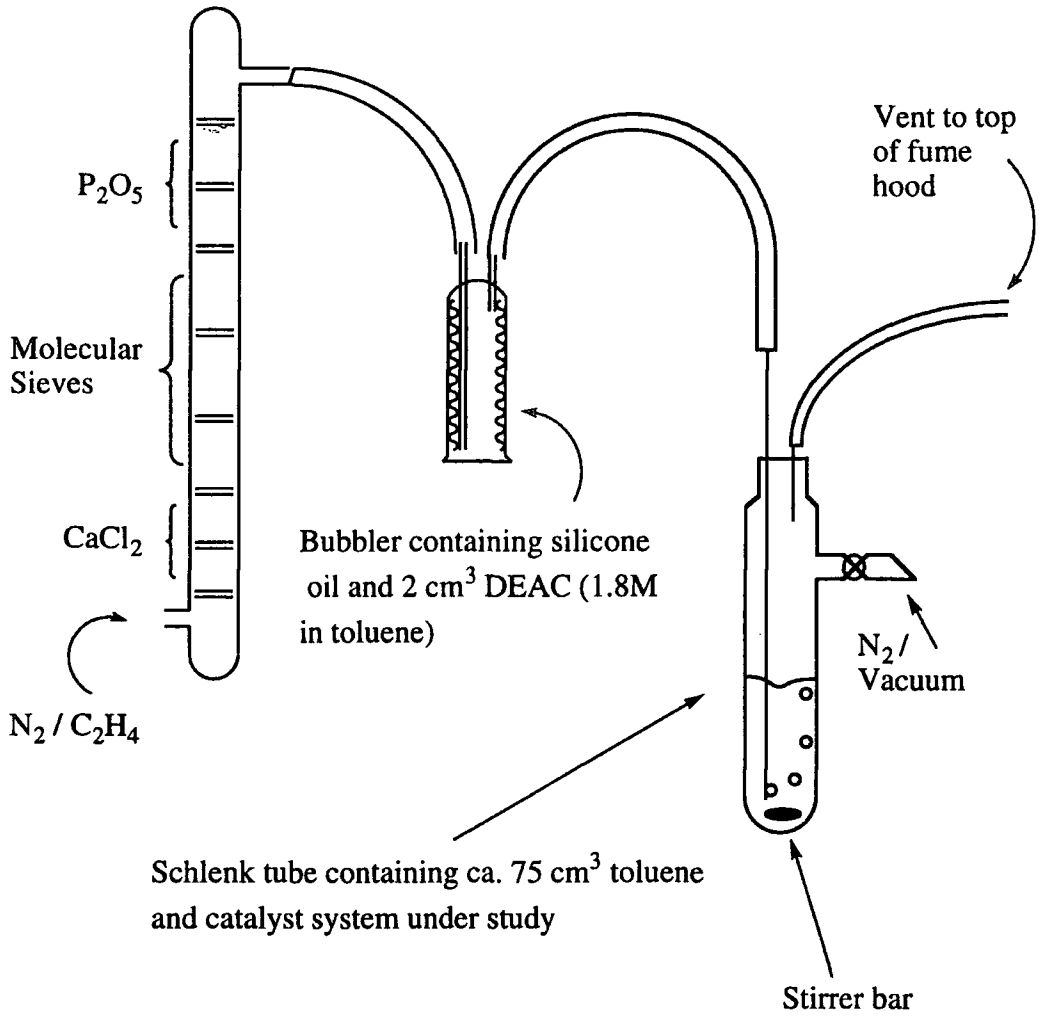

Figure 2.1 Experimental set-up for the screening of catalytic activity at Durham

The catalyst / co-catalyst solution was purged with ethylene for a predetermined length of time (typically one hour), before the polymerisation was terminated by flushing the system with N_2. Any polymer that formed was collected by filtration and washed free of metal residues by the action of acidified methanol followed by a methanol / toluene mixture, before drying under vacuum. The results are collected in table 2.1.

Run	Catalyst Precursor (mmol)	Co-Catalyst (equivalents)	Yield PE (g)	Activity (g $mmol^{-1}$ hr^{-1})
1	Cp_2TiCl_2 (0.078)	DEAC (3)	1.44	18.5
2	CpV(N*p*-tol)Cl_2 (0.081)	DEAC (3)	0.53	6.5
3	CpV(N*p*-tol)Cl_2 (0.161)	DEAC (3)	1.27	7.9
4	$Cr(N^tBu)_2(OTMS)_2$ (0.134)	DEAC (3)	0.09	0.7
5	$Cr(N^tBu)_2Cl_2$ (0.189)	DEAC (3)	0.39	2.1
6	$Cr(N^tBu)_2Cl_2$ (0.193)	DEAC (20)	1.73	9.0

Table 2.1 Results of ethylene polymerisation activity of vanadium and chromium species performed at Durham using alkyl aluminium co-catalysts.

The purpose of the first run was to ensure that the set-up was sufficiently free of poisons to allow polymerisation to occur and to establish an activity value with which new systems could be compared. All tests were performed at room temperature for a period of 1 hour unless stated otherwise.

Polymer was observed to form for each of the runs *2-6* indicating that active species were being generated upon treatment of the metal precursor complex with the alkyl-aluminium co-catalyst (testing of all precursors in the absence of co-catalyst gave no polymer). The macroscopic appearance of the polyethylene differed greatly between the vanadium and chromium systems (*vide infra*).

Doubling the concentration of the vanadium precursor in run *3* compared with run *2* resulted in only a slight increase in activity, suggesting that a similar number of active sites were being generated.

For the bis-imido chromium system, the dichloride (run *5*) was seen to be considerably more active than the bis-siloxide (run *4*) under otherwise identical

conditions. This is likely to be caused by the two sterically demanding siloxide groups around the metal centre hindering alkyl ligand exchange with the co-catalyst, necessary for polymerisation to proceed (see section 1.3.2). It may also reflect a stronger chromium oxygen bond (cf. chromium chlorine) through enhanced lone pair donation to the metal centre.

Increasing the ratio of $Cr(N^tBu)_2Cl_2$: DEAC from 1:3 to 1:20 (runs *5* and *6*) dramatically increases the activity. This may simply arise as more potential 'poisons' are being eliminated from the apparatus with an increased DEAC concentration. However, if inefficient activation of the precursor is occurring, the presence of a higher DEAC concentration may convert more of the dichloride to the active species giving a higher activity figure.

For the vanadium catalysts, a stringy polymer was seen to form rapidly around the ethylene injection point (typically 30 to 90 seconds). After an initial burst of activity however, the rate of polymer formation decreased considerably, consistent with a highly active but short lived catalytic species. Recent studies by Mr M.C.W. Chan in this group indicate that the rapid termination observed in this system is the result of bimolecular coupling of the active centres.[4] Generally the recovered samples of polyethylene were strongly coloured due to metal residues being trapped in the polymer. Removal of these impurities proved problematic in many cases, even after prolonged soaking in acidified methanol.

For the chromium complexes, the polymerisation was observed to proceed in a slower but more controlled manner. The polymer formed was a flocculent white precipitate dispersed throughout the toluene solution, resulting in a much cleaner polymer than that produced from the vanadium system.

The longer lived nature of the active species was confirmed by filtering the supernatant solution from the polymer and then treating with ethylene for a further hour. Polymer continued to form after four such repetitions of this process, although more DEAC was added to later runs, which may have been converting unreacted chromium precursor to the active species responsible for the production of polymer.

Characterising data on the polymers produced with both systems is presented later in this chapter (see section 2.2.4).

The next stage in the evaluation of these catalytic species was performed at BP Chemicals' Sunbury laboratory by Dr C.I. Dalby (Durham) and Mr B.J. Mills (BP Chemicals). Details of a typical polymerisation procedure appear in section 6.2.2. This system allowed testing to be performed under industrially relevant conditions, with elevated pressures of ethylene and on-line monitoring of both pressure and temperature.

Run	**Catalyst Precursor (mmol)**	**Co-Catalyst (Equivalents)**	**Temp. (°C)**	**Yield PE (g)**	**Activity (g mmol^{-1} hr^{-1} bar^{-1})**
1	$Cr(N^tBu)_2Cl_2$ (0.190)	DEAC (50)	28	5.64	2.97
2	$Cr(N^tBu)_2Cl_2$ (0.38)	DEAC (20)	50	1.30	0.33
3	$Cr(N^tBu)_2Cl_2$ (0.190)	DEAC (500)	50	0.90	0.47
4	$CpV(N$*p*-tol$)Cl_2$ (0.21)	DEAC (100)	30	0.21	0.10
5	$CpV(N$*p*-tol$)Cl_2$ (0.20)	DEAC (20)	50	0.45	0.23
6	$Cr(N^tBu)_2Cl_2$ (0.20)	TEA (50)	28	Negligible	-
7	$CpV(N$*p*-tol$)Cl_2$ (0.18)	TEA (50)	30	Negligible	-

(all performed at 10 bar pressure of ethylene).

Table 2.2 Results of polymerisation activity of vanadium and chromium species performed at Sunbury using alkyl aluminium co-catalysts.

A comparison of run *1* with the results of the one atmosphere tests carried out in Durham show that elevated pressure does not have a beneficial affect on the activity. Furthermore, increasing the temperature (runs *2* and *3*) also leads to decreased

activities, even when the co-catalyst ratio is increased to 500:1 (although at this ratio a slight increase in activity is observed over the experiment when 20 equivalents are employed). This suggests that a deactivation process may be occurring at elevated temperatures.

For the vanadium precursor, a 30-fold increase in co-catalyst ratio at 30°C (run *4*) reduces the activity of the system under 10 bar of ethylene compared with the one atmosphere tests. Increasing the temperature to 50°C (run *5*) results in slightly higher activities than at 30°C, but is still considerably less than found under one atmosphere of ethylene at Durham.

Therefore, at increased pressures of ethylene both systems show a reduction in activity when compared to values obtained at Durham. This may simply be due to the different experimental procedures at Sunbury as neither the chromium or vanadium compounds were tested under one atmosphere using this polymerisation rig. The presence of an increased number of poisons my also contribute to the lower activity figures, although at the very high ratios of co-catalyst used in runs *3* and *4* would be expected to compensate for this eventuality.

Surprisingly, when the co-catalyst was changed to a trialkyl aluminium reagent (triethyl aluminium, TEA) neither system proved to be active, implying that the presence of a halogen on the co-catalyst is crucial in the activation of these systems.

2.2.3 Testing for Catalytic Activity Employing Methylaluminoxane (MAO) as Co-Catalyst.

The Group 4 metallocene systems show a vast increase in activity and longevity of the polymerisation catalysts when MAO is employed as the co-catalyst.[5] The results of polymerisation experiments using both the vanadium and chromium imido precursors with MAO as the co-catalyst appear in table 2.3. The MAO was made from the reaction of aluminium sulphate hydrate and a solution of trimethyl aluminium in toluene and was kindly donated by Mr M.C.W. Chan.

Run	Catalyst Precursor (mmol)	Co-Catalyst (Equivalents)	Temp. (°C)	Yield PE (g)	Activity (g mmol^{-1} hr^{-1} bar^{-1})
1	Cp_2ZrCl_2 (0.008)	MAO (1500)	0	5.30	662.5
2	$Cr(N^tBu)_2Cl_2$ (0.04)	MAO (300)	25	0.19	4.4
3	$Cr(N^tBu)_2Cl_2$* (0.2)	MAO (500)	33	Negligible	-
4	$CpV(N$*p*$\text{-tol})Cl_2$ (0.007)	MAO (1715)	25	0.19	27.1
5	$CpV(N$*p*$\text{-tol})Cl_2$ (0.03)	MAO (400)	60	0.13	4.3

(* Performed at Sunbury under 10 atmospheres ethylene)

Table 2.3 Results of polymerisation activity of vanadium and chromium species performed at Sunbury and Durham using MAO as co-catalyst.

Run *1* demonstrated the integrity of the MAO and confirmed the very high activities found with the zirconocene dichloride precursor. Run *2* employing the bis-imido chromium dichloride shows that, although still active, there is no increase in the activity when compared to analogous experiments using DEAC as co-catalyst (see table 2.1). When performed at increased pressure (run *3*), only negligible amounts of polymer was recovered, as for the previous experiment with TEA as co-catalyst.

With the vanadium system however, there is a moderate increase in activity when employing a large excess of MAO (run *4*), although the activity is still markedly less than the zirconocene system. Increasing the temperature to 60°C (run *5*) again shows a decrease in the activity consistent with earlier observations that at higher temperatures, deactivation becomes more significant.

2.2.4 Analysis of Polyethylene Samples from Dichloride Precursors.

Although in principle PE is amongst the simplest of synthetic polymers, a vast array of products is possible, with for example, variations in the type and degree of branching and differences in the overall molecular weights of the polymer. This, coupled with co-monomer incorporation, has led to many different commercial applications for polyethylene. Illustrative examples of the three marketed grades of PE are shown in figure 2.2.

1. Low Density Polyethylene (LDPE) : From high pressure, radical initiated polymerisation processes giving a highly branched structure.

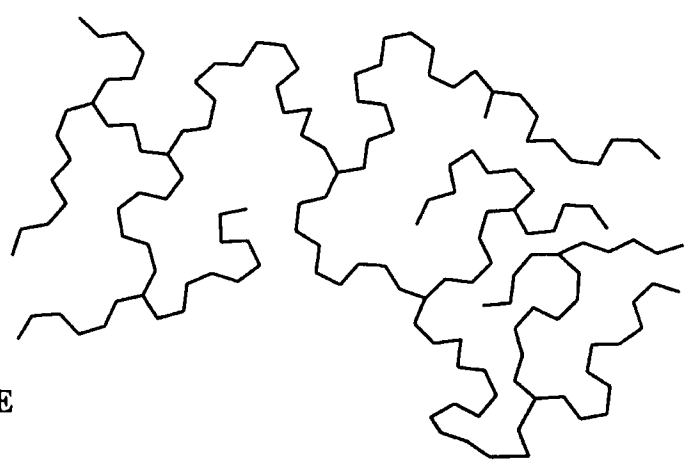

LDPE

2. High Density Polyethylene (HDPE) : Prepared using organometallic catalysts and consisting of structurally regular chains with few branching points.

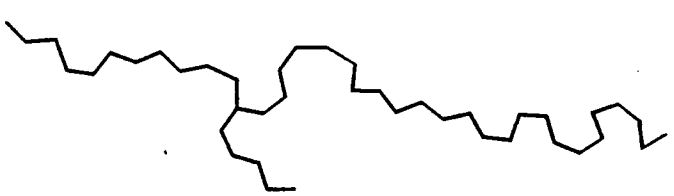

HDPE

3. Linear Low Density Polyethylene (LLDPE) : Bridges the gap between the 2 extremes and is actually a co-polymer of ethylene with 8-10% of another α-olefin such as hex-1-ene.

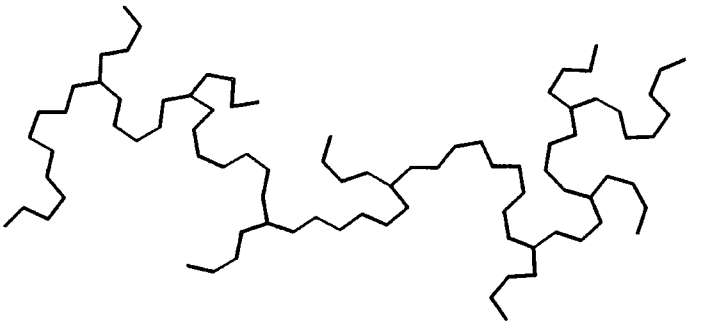

LLDPE

Figure 2.2 The three main forms of polyethylene

One of the most powerful tools in determining the microstructure of homopolymers and copolymers of polyethylene is ^{13}C NMR, where the extent and nature of any branching present has been studied and can now be routinely assigned. A comprehensive review of this procedure was recently published by Randall and covers a variety of ethylene copolymers.[6] Another valuable piece of information that can be gained from this technique is the molecular weight (M_n), calculated from the ratio between the integral of the chain end signals versus the main-chain methylene carbons. This figure varies with the amount of branching present but provides a rough indication of molecular weight. In principle, NMR data can also provide information on the termination mechanism occurring, for example ß-hydride elimination.

Representative samples of polyethylene generated by the vanadium and chromium catalyst systems have been analysed by ^{13}C NMR and high temperature gel permeation chromatography (GPC) at BP Chemicals analytical laboratory in Sunbury. The results are presented in table 2.4.

Sample	Catalyst Precursor	Co-Catalyst (Equivalents)	Branching (by ^{13}C NMR)	Molecular Weight (GPC)
1	$Cr(N^tBu)_2Cl_2$	DEAC (3)	None Detected	-
2	$Cr(N^tBu)_2Cl_2$	DEAC (20)	< 1 per 6000 C-atoms	-
3	$CpV(N^tBu)Cl_2$ (*)	DEAC (20)	< 1 per 5000 C-atoms	210000 (Main Peak)
4	$Cr(N^tBu)_2Cl_2$	DEAC (20)	None Detected	1200000 (Main Peak)

(* Chosen in preference over *p*-tol imido derivative since it produces a cleaner polymer)

Table 2.4 Molecular weights and degree of branching in PE samples

The ^{13}C NMR spectra show little or no evidence for branching in each of the polymers. In sample *2* the low level of branching is believed to be long chain ($\geq C_6$), but butyl branching is not excluded as signals are of such low intensity that the peaks unique to butyl branches may not be detected. For sample *3* however, the small peaks are most likely due to ethyl branches.

Both GPC traces show relatively broad molecular weight distributions (M_w/M_n = 26.1 and 30.1 for *3* and *4* respectively) when compared to polymers produced from zirconocene type catalysts, possibly indicating several differing active sites.

2.2.5 Summary

It has been demonstrated the both $CpV(N$*p*-tol$)Cl_2$ and $Cr(N^tBu)_2Cl_2$ are active ethylene polymerisation catalysts when activated with DEAC, producing high molecular weight polyethylene with little branching present. Increasing the pressure of ethylene does not have a beneficial effect on the activity figures. Increasing the temperature also leads to a reduction in activity, possibly due to bimolecular

termination processes. This suggests that performing the polymerisation run at reduced temperature will limit the amount of termination by this mechanism and should therefore result in higher activities, although this would then become of less industrial relevance.

Changing from DEAC to MAO showed no increase in activity for the chromium pro-catalyst. The vanadium system does show enhanced activity, although the increase is not as large as observed for zirconocene catalysts.

2.3 Synthesis, Structure and Polymerisation Activity of $Cr(N^tBu)_2(CH_2Ph)_2$.

2.3.1 Dialkyl Complexes of the $[Cr(N^tBu)_2]$ Moiety.

The next objective was the preparation of well-defined cationic alkyl catalysts based on the bis-imido chromium system. Such species derived from metallocene precursors have been shown to polymerise ethylene in the absence of a co-catalyst,[7] allowing a greater degree of control over the polymerisation process. It was also hoped that such species would provide insight into the factors influencing the activity of these imido systems. Therefore the synthesis of bis-imido dialkyl complexes of chromium was investigated.

In 1990 Schaverien published the synthesis of a range of dialkyl complexes for the ^{t}butylimido system of general formula $Cr(N^tBu)_2R_2$, where R = CH_2SiMe_3 ; CH_2CMe_3 ; CH_2CMe_2Ph.[8] He found that in all cases the product could only be isolated as an oil, which often leads to considerable difficulty in handling and purification, two factors of paramount importance in any catalytic study. Also reported in this paper were attempts to synthesise the dimethyl compound $Cr(N^tBu)_2Me_2$, which was never successfully purified even though a range of alkylating agents and conditions were tried. There is surprisingly no mention of attempts to prepare the bis-benzyl complex $Cr(N^tBu)_2(CH_2Ph)_2$ and hence this compound was targeted.

2.3.2 Reaction of $Cr(N^tBu)_2Cl_2$ with $PhCH_2MgCl$:

Preparation of $Cr(N^tBu)_2(CH_2Ph)_2$ (1)

Wilkinson and co-workers demonstrated that bis-aryl complexes of chromium can be synthesised from the reaction of the Grignard reagent and the bis-siloxide compound $Cr(N^tBu)_2(OTMS)_2$.[9] Attempts at synthesising the dialkyl complexes from this starting material however gave only intractable products[8] and the route employed by Schaverien utilised $Cr(N^tBu)_2Br_2$(pyridine) as the starting material. As improved synthetic routes have been developed that allow $Cr(N^tBu)_2Cl_2$ to be convienently prepared as a crystalline solid, this was chosen as the starting material for the preparation of the bis-benzyl complex. Reaction of $Cr(N^tBu)_2Cl_2$ with $PhCH_2MgCl$ in Et_2O proceeded smoothly affording $Cr(N^tBu)_2(CH_2Ph)_2$ in good yield.

$$Cr(N^tBu)_2Cl_2 + 2\ PhCH_2MgCl \longrightarrow Cr(N^tBu)_2(CH_2Ph)_2 + 2\ MgCl_2$$

(1)

Equation 2.5

Although initially isolated as a pure oil, the blood red compound can be induced to crystallise from a concentrated pentane solution at -30°C, or more easily from an acetonitrile solution at the same temperature.

The ^1H NMR spectrum (400MHz, C_6D_6) shows a singlet resonance at δ 2.49 corresponding to the methylene protons of the benzyl ligand, and a singlet at δ 1.20 due to the ^{t}butyl hydrogens of the imido ligands. The equivalence of the two imido ligands and the benzyl groups is consistent with a C_{2v} symmetric structure in solution. As this compound was to be the focus of a detailed study into the polymerisation of ethylene, the solid state structure was of considerable interest.

2.3.3 The Molecular Structure of $Cr(N^tBu)_2(CH_2Ph)_2$ (1).

Deep red crystals of **1** were grown from a saturated pentane solution at -30°C. A crystal of dimensions 0.52 x 0.44 x 0.34 mm was mounted under an inert oil and the structure was solved by Prof W. Clegg and Dr M.R.J. Elsegood of the University of Newcastle-Upon-Tyne. The molecular structure is illustrated in figure 2.3 and selected bond angles and distances are given in table 2.5.

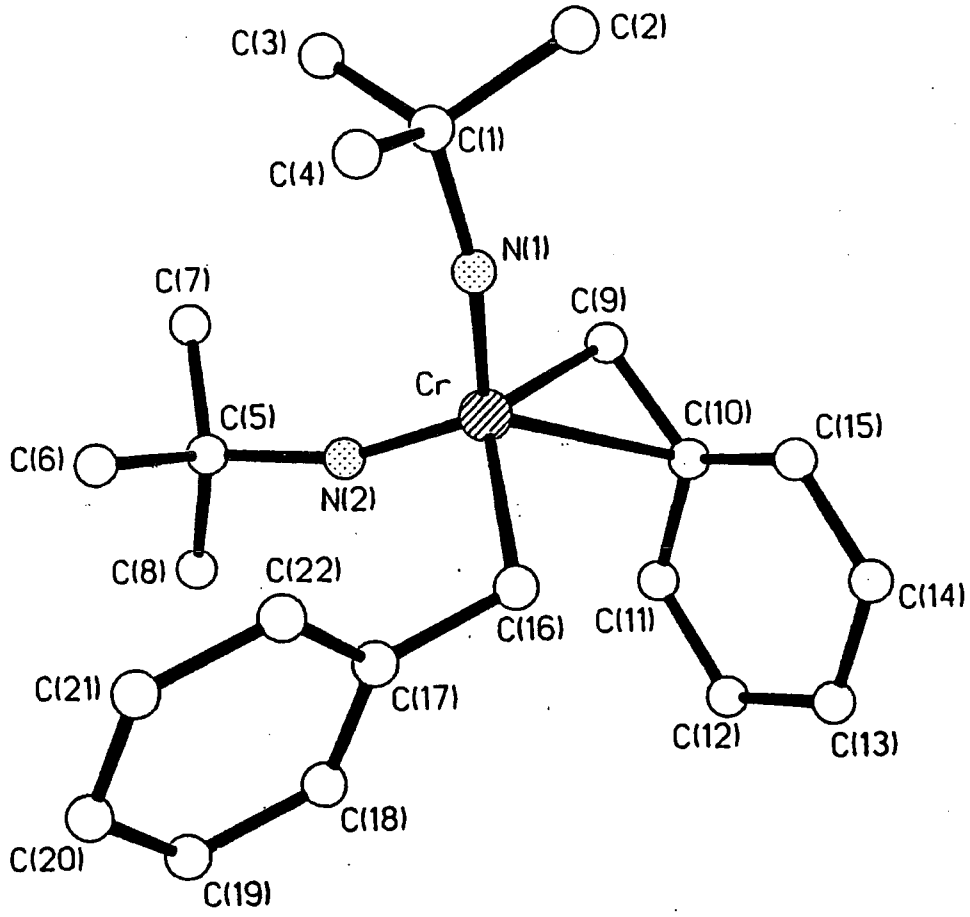

Figure 2.3 The molecular structure of $Cr(N^tBu)_2(CH_2Ph)_2$ (**1**)

Cr–N(1)	1.625(2)	Cr–N(2)	1.632(2)
Cr–C(9)	2.071(2)	Cr–C(16)	2.096(3)
Cr–C(10)	2.357(2)	N(1)–C(1)	1.447(2)
N(2)–C(5)	1.445(2)	C(9)–C(10)	1.443(3)
C(10)–C(11)	1.411(3)	C(10)–C(15)	1.406(3)
C(11)–C(12)	1.371(3)	C(12)–C(13)	1.384(3)
C(13)–C(14)	1.383(3)	C(14)–C(15)	1.375(3)
C(16)–C(17)	1.475(3)	C(17)–C(18)	1.402(3)
C(17)–C(22)	1.388(3)	C(18)–C(19)	1.375(3)
C(19)–C(20)	1.382(3)	C(20)–C(21)	1.383(3)
C(21)–C(22)	1.381(3)		

N(1)–Cr–N(2)	116.09(8)	N(1)–Cr–C(9)	100.66(8)
N(2)–Cr–C(9)	102.75(10)	N(1)–Cr–C(16)	102.86(8)
N(2)–Cr–C(16)	103.48(10)	C(9)–Cr–C(16)	131.93(8)
N(1)–Cr–C(10)	119.96(7)	N(2)–Cr–C(10)	114.38(7)
C(9)–Cr–C(10)	37.32(8)	C(16)–Cr–C(10)	94.86(7)
C(1)–N(1)–Cr	166.07(13)	C(5)–N(2)–Cr	160.60(13)
C(10)–C(9)–Cr	82.16(11)	C(15)–C(10)–C(11)	116.9(2)
C(15)–C(10)–C(9)	121.1(2)	C(11)–C(10)–C(9)	121.4(2)
C(15)–C(10)–Cr	99.13(11)	C(11)–C(10)–Cr	103.01(12)
C(9)–C(10)–Cr	60.52(9)	C(12)–C(11)–C(10)	121.3(2)
C(11)–C(12)–C(13)	120.5(2)	C(14)–C(13)–C(12)	119.5(2)
C(15)–C(14)–C(13)	120.4(2)	C(14)–C(15)–C(10)	121.4(2)
C(17)–C(16)–Cr	114.73(13)	C(22)–C(17)–C(18)	117.1(2)
C(22)–C(17)–C(16)	122.5(2)	C(18)–C(17)–C(16)	120.4(2)
C(19)–C(18)–C(17)	121.2(2)	C(18)–C(19)–C(20)	121.0(2)
C(19)–C(20)–C(21)	118.5(2)	C(22)–C(21)–C(20)	120.7(2)
C(21)–C(22)–C(17)	121.5(2)		

Table 2.5 Bond distances (Å) and angles (°) for $Cr(N^tBu)_2(CH_2Ph)_2$ (**1**).

It is immediately apparent that the solid state structure is different to that suggested by solution state NMR spectroscopy, the benzyl ligands being present in η^1 and η^2 coordination modes. This is in contrast to the metallocene complexes $Cp_2Ti(CH_2Ph)_2$[10] and $(Me_3SiC_5H_4)_2Zr(CH_2Ph)_2$[11] where each benzyl ligand is present in η^1 coordination and probably arises due to more space being present around the chromium centre in **1**.

The bond parameters for the η^2 ligand fall within the range found for other η^2-benzyl ligands,[12] with a reduced C(9)–C(10) bond length of 1.443(3) Å (cf. C(16)–C(17) bond length of 1.475(3) Å), a Cr–C(9)–C(10) angle of 82.16(11)° and elongated C_{ipso}–C_{ortho} distances (1.409(3) Å (av) cf. 1.395(3) Å for the η^1 CH_2Ph group). This is consistent with two electrons being removed from the π system of the phenyl ring and being provided to the metal centre *via* a carbon to chromium σ bond, illustrated as the two limiting forms of the resulting resonance hybrids in figure 2.4. This enables the η^2-benzyl ligand to function as a three electron donor and permits the complex to achieve a higher electron count.

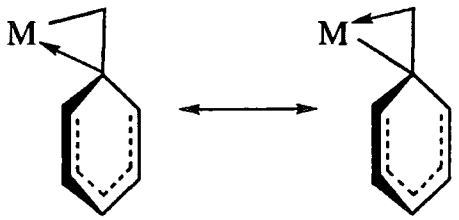

Figure 2.4 Resonance structures for η^2-benzyl ligand.

The *ipso*-carbon atom from the η^2-benzyl ligand is located between Cr–C(9) and Cr–C(16) and is approximately in the Cr–C(9)–C(16) plane (4.8° deviation) consistent with the metallocene-like frontier orbitals predicted for the [Cr(NR)$_2$] moiety. The N–Cr–N angle of 116.09(8)° and the Cr=N distances of 1.625(2) Å and 1.632(2) Å are comparable to those found in the related structures Cr(N^{t}Bu)$_2$(2,4,6-Me$_3$-C$_6$H$_2$)$_2$[10] and Cr(N^{t}Bu)$_2$Cl$_2$.[13]

2.3.4 Solid State ^{13}C NMR Study of 1.

η^1 and η^2 coordination of benzyl ligands have been observed in Group 6 cyclopentadienyl nitrosyl complexes.[14] For these compounds, low temperature solution state NMR studies (183K, CD_2Cl_2) can distinguish between the different benzyl ligands (see table 2.6). In the case of **1** however, the spectrum remains unchanged to -80°C.

Solid state CP / MAS NMR spectra were kindly recorded by Prof R.K. Harris and Mr T.V. Thompson. The spectra generally show an increase in complexity in accordance with a lowering of the symmetry due to the removal of molecular averaging present in solution. A non-quaternary suppression (NQS) experiment clearly distinguishes between the two C_{ipso} resonances, with the signal from the η^1-bound benzyl at 158 ppm and the *ipso* signal from the η^2-bound ligand resonating at 124 ppm (see figure 2.5).

Complex	δ C_{ipso} (η^1)	δ C_{ipso} (η^2)
$CpMo(NO)(\eta^1\text{-}CH_2Ph)(\eta^2\text{-}CH_2Ph)$ *	152.7	111.2
$CpW(NO)(\eta^1\text{-}CH_2Ph)(\eta^2\text{-}CH_2Ph)$ *	152.3	108.6
$Cp^*Mo(NO)(\eta^1\text{-}CH_2Ph)(\eta^2\text{-}CH_2Ph)$ *	152.8	115.0
$Mo(N^tBu)_2(\eta^1\text{-}CH_2Ph)(\eta^2\text{-}CH_2Ph)$[15] §	156	125
$Cr(N^tBu)_2(\eta^1\text{-}CH_2Ph)(\eta^2\text{-}CH_2Ph)$ §	158	124

(* 183K, CD_2Cl_2 : § CP / MAS Spectroscopy)

Table 2.6 Comparison of η^1-and η^2-bound C_{ipso} resonances.

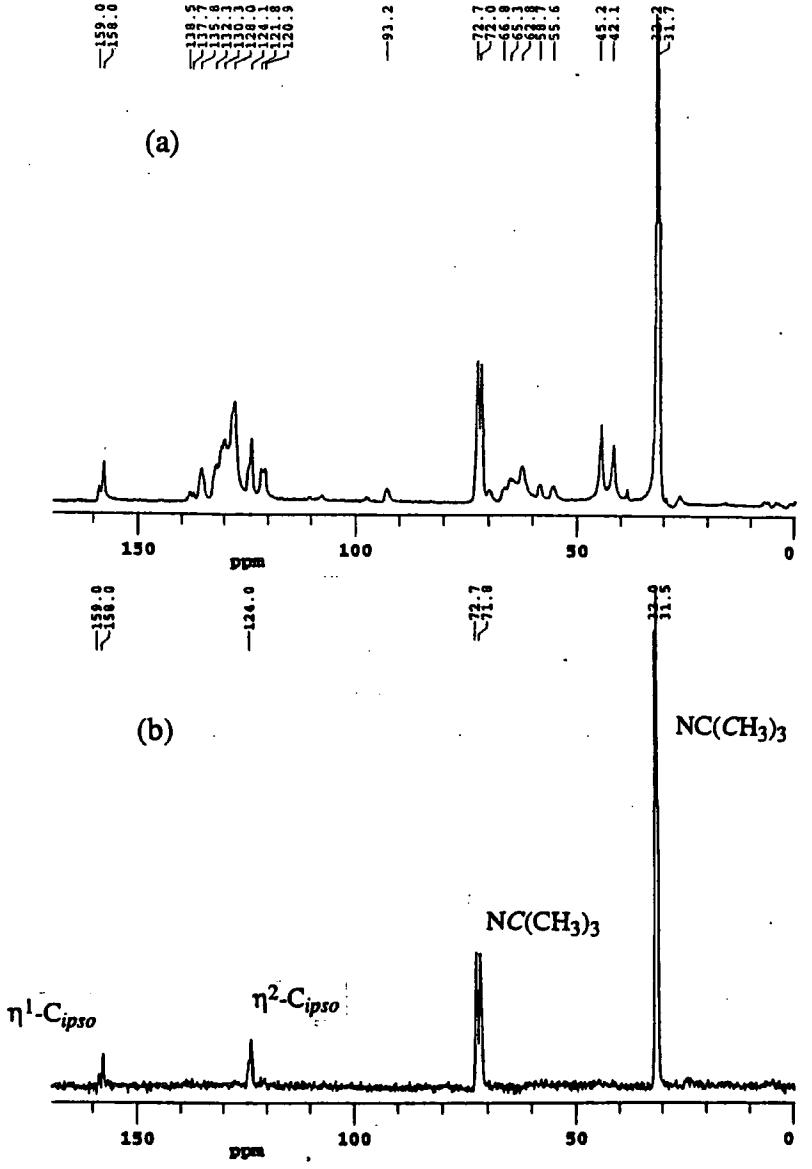

Figure 2.5 (a) Solid state CP / MAS ^{13}C NMR spectrum of (**1**) (b) With non-quaternary suppression.

2.3.5 Reaction of $Cr(N^tBu)_2(CH_2Ph)_2$ (1) with Alkyl Abstracting Reagents.

a) Reaction with $[Ph_3C][B(C_6F_5)_4]$:

Formation of $[Cr(N^tBu)_2(CH_2Ph)][B(C_6F_5)_4]$ (2).

Reaction of **1** with the trityl salt $[Ph_3C][B(C_6F_5)_4]$ gave the red cationic mono-benzyl complex $[Cr(N^tBu)_2(CH_2Ph)][B(C_6F_5)_4]$ (**2**) and Ph_3CCH_2Ph (100% conversion by NMR spectroscopy). **2** forms an immiscible oil in hydrocarbon solvents, but is soluble in CD_2Cl_2.

The ^1H NMR spectrum shows a downfield shift for both the benzyl methylene protons (δ 4.22 cf. δ 2.49 in **1**) and the ^{t}butyl hydrogen signal (δ 1.59 cf. δ 1.20 in **1**). ^{13}C NMR spectra show that the remaining benzyl ligand is bound in an η^2-fashion, the *ipso* C-atom resonating at 128.8 ppm with a small $^2J_{CH}$ coupling of 5.3 Hz to the methylene hydrogens. This was confirmed by heteronuclear decoupling experiments where the methylene protons were selectively irradiated causing the ^{13}C signal of the *ipso* carbon to collapse to a singlet. The oily nature of this product prevented the isolation of a pure solid material when the reaction was repeated on a preparative scale.

b) Reaction with $[PhNMe_2H][B(C_6F_5)_4]$:

Formation of $[Cr(N^tBu)_2(CH_2Ph)(NMe_2Ph)][B(C_6F_5)_4]$ (3).

An analogous experiment between **1** and $[PhNMe_2H][B(C_6F_5)_4]$ resulted in the formation of the mono-amine adduct $[Cr(N^tBu)_2(CH_2Ph)(NMe_2Ph)][B(C_6F_5)_4]$ (**3**). The ^1H NMR spectrum again reveals a shift to lower field for the CH_2Ph singlet of the remaining benzyl ligand (δ 3.84) and the $C(CH_3)_3$ peak of the imido ligands (δ 1.67). Also evident was the presence of bound amine (δ 1.67 for $PhNMe_2$), and the expected toluene by-product. The abundance of signals in the ^{13}C NMR spectrum prevented unambiguous assignments. Treatment of the base free cation **2** with one equivalent of $PhNMe_2$ gives the same equilibrium mixture containing **3**.

c) Reaction of (**2**) with PMe_3 :

*Formation of [Cr(N^{t}Bu)$_2$(CH$_2$Ph)(PMe$_3$)][B(C$_6$F$_5$)$_4$] (**4**).*

Treatment of **2** with 1 equivalent of PMe_3 in an NMR tube gave the mono-phosphine adduct $[Cr(N^tBu)_2(CH_2Ph)(PMe_3)][B(C_6F_5)_4]$ (**4**). Care was exercised in addition of the phosphine as an excess causes decomposition of the metal species, observable by the presence of additional signals, most noticeably in the ^{31}P NMR. The data are consistent with the formation of a 4-coordinate pseudo tetrahedral structure where the phosphine lies adjacent to the benzyl methylene group. NMR data supporting this shows the coupling of the methylene group to the phosphorus atom ($^3J_{PH}$ = 2 Hz in the ^{1}H NMR ; $^2J_{PC}$ = 4.5 Hz in the ^{13}C NMR), where no such coupling is evident for the C_{ipso} resonance, although this does show a small triplet of 5.3 Hz due to methylenic hydrogens in the proton coupled spectra. Similar observations have been made on complexes of the type $Mo(N^tBu)_2(L)(PMe_3)$, where L = an alkene or an alkyne.[15]

Reaction of the amine adduct **3** with 1 equivalent of PMe_3 causes displacement of the $PhNMe_2$ and formation of the mono-phosphine adduct **4**. A reaction scheme summarising this series of results is given in figure 2.6.

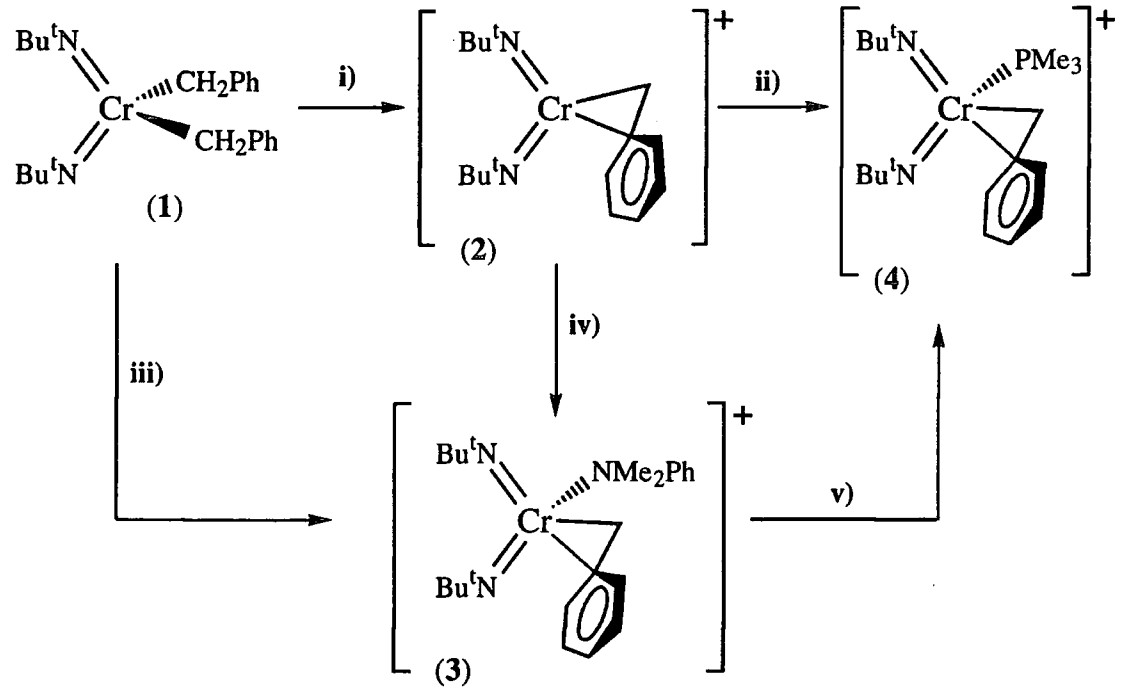

{ i) $[Ph_3C][B(C_6F_5)_4]$; ii) PMe_3 ; iii) $[PhNMe_2H][B(C_6F_5)_4]$; iv) $PhNMe_2$; v) PMe_3 }

Figure 2.6 Cationic benzyl species derived from $Cr(N^tBu)_2(CH_2Ph)_2$ (**1**).

2.3.6 Polymerisation Activity of $[Cr(N^tBu)_2(CH_2Ph)]^+$

Having established that **1** readily forms a cationic alkyl species upon reaction with alkyl abstraction reagents, the catalytic activity of this system was investigated at BP Chemicals, Sunbury. A summary of the results appear in table 2.7.

The initial run was performed at 30°C under 10 atmospheres of ethylene and gave an activity figure 50.2 g $mmol^{-1}$ hr^{-1} bar^{-1}. This is an order of magnitude higher than observed for the dual component $Cr(N^tBu)_2Cl_2$ / co-catalyst system, showing that the well-defined cationic alkyl catalysts are considerably more active and readily polymerise ethylene at elevated pressure. Increasing the temperature to 50°C gave a slight increase in activity (run *2*), although at 75°C (run *3*) the activity falls, possibly due to slight decomposition of the active species at this temperature.

Run	Catalyst Precursor (mmol)	Co-Catalyst (Equivalents)	Pressure (bar)	Temperature (°C)	Time (mins)	Yield (g)	Activity (g $mmol^{-1}$ hr^{-1} bar^{-1})
1	$Cr(N^tBu)_2(CH_2Ph)_2$ (0.13)	$[PhNMe_2H][B(C_6F_5)_4]$ (1)	10	30	60	65.4	50.2
2	$Cr(N^tBu)_2(CH_2Ph)_2$ (0.13)	$[PhNMe_2H][B(C_6F_5)_4]$ (1)	10	50	60	75.5	57.8
3	$Cr(N^tBu)_2(CH_2Ph)_2$ (0.13)	$[PhNMe_2H][B(C_6F_5)_4]$ (1)	10	75	60	42.0	31.6
4	$Cr(N^tBu)_2(CH_2Ph)_2$ (0.13)	$[PhNMe_2H][B(C_6F_5)_4]$ (1)	5 / 10 / 15 / 19	50	130	198.5	-
5	$Cr(N^tBu)_2(CH_2Ph)_2$ (0.13)	$[PhNMe_2H][B(C_6F_5)_4]$ (5)	10	50	60	87.0	65.4
*6**	$Cr(N^tBu)_2(CH_2Ph)_2$ (0.13)	$[Ph_3C][B(C_6F_5)_4]$ (1)	10	50	60	33.4	25.7
*7**	$Cr(N^tBu)_2(CH_2Ph)_2$ (0.13)	$B(C_6F_5)_3$ (1)	10	50	60	-	-

(Catalyst / co-catalyst dissolved in 50 cm^3 toluene except * where dissolved in CH_2Cl_2)

Table 2.7 Results of polymerisations using $[Cr(N^tBu)_2(CH_2Ph)][B(C_6F_5)_4]$.

The computer trace generated from run 2 is displayed in figure 2.7, showing the rate of ethylene flow into the autoclave, the pressure in the reactor, the temperature of the autoclave and the temperature of the water being supplied to the water jacket around the autoclave. This is representative of a typical trace produced from this catalyst system.

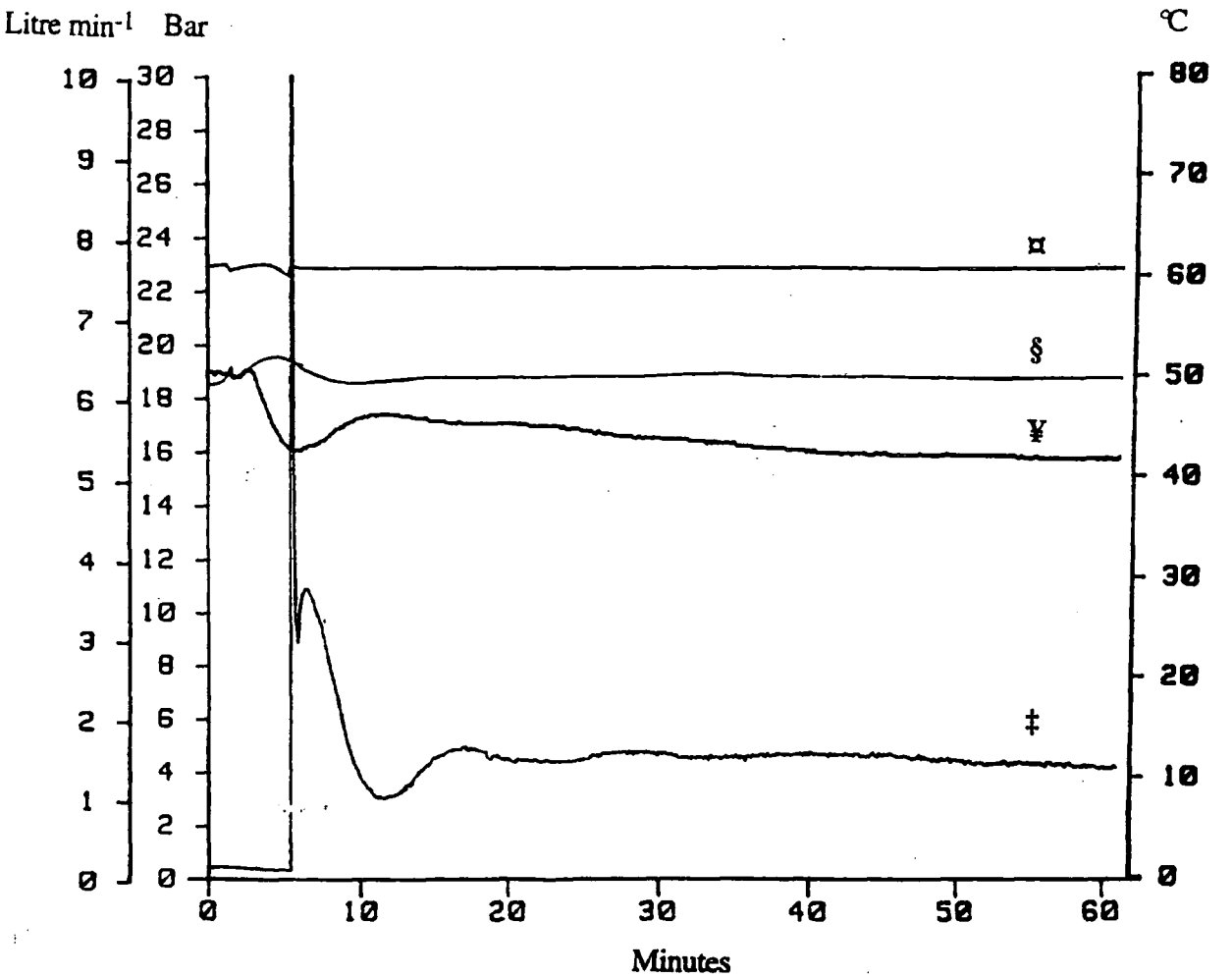

Pressure	¤	Water in temperature	¥
Reactor Temperature	§	Ethylene flow	‡

Figure 2.7 Computer generated trace from polymerisation run 2.

The catalyst is injected at time = 0, causing an immediate increase in reactor temperature, indicating that an exothermic reaction is occurring. The temperature of the water being supplied to the autoclave automatically lowers to compensate for this temperature rise, which has the effect of reducing the pressure in the autoclave, negating the need for more ethylene to be admitted.

After approximately five minutes however, sufficient ethylene has been consumed to register as a drop of pressure in the autoclave and hence ethylene flows into the reactor in order to maintain a constant pressure. Over the next ten minute period the system reaches equilibrium, with the resultant flow of ethylene into the reactor levelling out at approximately 1.5 litre min^{-1}. This flow rate is maintained until the polymerisation is terminated 60 minutes after the initial injection of the catalyst. Thus the well-defined cationic alkyl chromium catalyst is remarkably long-lived in comparison with its well-defined cationic zirconocene counterparts.

Run *4* revealed a near linear activity pressure relationship, with ethylene pressures of 5, 10 15 and 19 bar affording ethylene consumption rates of 0.5, 1.0, 1.5 and 2 litre min^{-1}. This run also serves to emphasise the long-lived nature of the catalyst system as polymer was still being produced after over two hours.

A five-fold increase in the amount of $[PhNMe_2H][B(C_6F_5)_4]$ (run *5*) gave only a modest increase in the activity of the system. This suggests that the reaction between the dialkyl complex and the co-catalyst proceeds to high yield even in a 1 : 1 ratio, supported by the NMR experiments where 100% conversion is observed.

Run *6* shows that, although a cationic alkyl species is still generated through the reaction of the dialkyl with the trityl salt $[Ph_3C][B(C_6F_5)_4]$, the activity is less then for the corresponding experiment using the anilinium salt (run *2*). Reaction of **1** with the neutral boron complex $B(C_6F_5)_3$, which is known to generate active species for zirconocene dimethyl complexes,[16] does not promote any activity for the bis-benzyl complex, probably as a consequence of the small size of the Lewis acid centre and the relative bulk of the benzyl ligand. In general, the use of the neutral boron reagent appears to be largely restricted to methyl derivatives.

2.3.7 Analysis of Polyethylene Samples Employing 1 as Precursor.

High temperature GPC traces were recorded at Sunbury on the PE samples generated using the trityl and anilinium borate salts and the results appear in table 2.8.

Run	Co-Catalyst (Equivalents)	M_n	M_w	M_w / M_n	M_p*
2	$[PhNMe_2H][B(C_6F_5)_4]$ (1)	5800	505500	87	500000 550000
6	$[Ph_3C][B(C_6F_5)_4]$ (1)	4000	539500	135	357000

(* Main Peaks in the GPC Trace)

Table 2.8 GPC data on selected samples of polyethylene using $Cr(N^tBu)_2(CH_2Ph)_2$ as catalyst precursor.

Both polymers are of relatively high molecular weight with main peak (M_p) molecular weights of the order of half a million. The molecular weight distributions, however, are quite large as a result of a multi-modal distribution (see figure 2.8). This may suggest that more than one active site is generated, each capable of producing polymer at a different rate, although the NMR study showed that initially only one cationic species is produced.

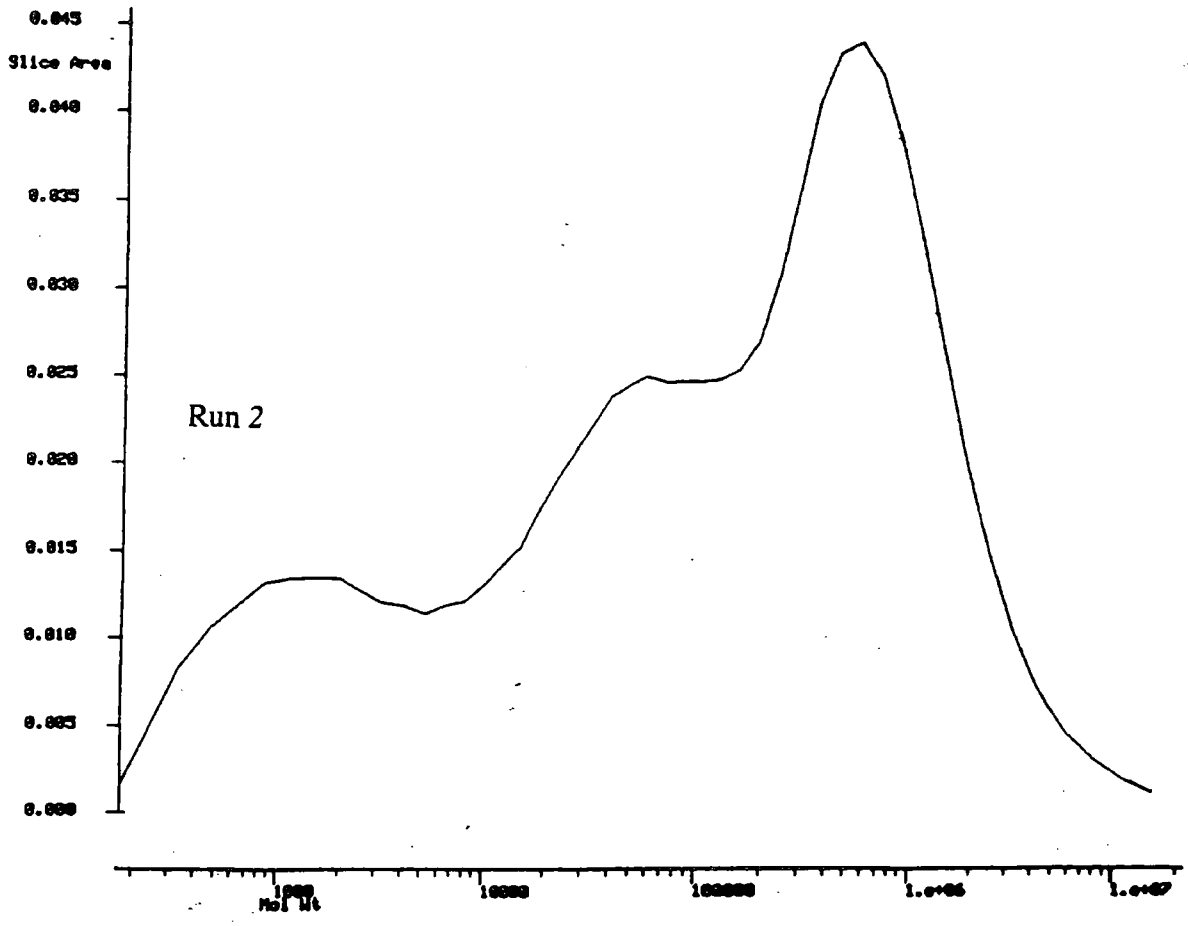

Figure 2.8 GPC trace of the polymer produced from $[Cr(N^tBu)_2(CH_2Ph)][B(C_6F_5)_4)]$ (Run *2*).

2.3.8 Summary

A well defined, single component cationic alkyl polymerisation catalyst based on bis-imido chromium complexes has been established, demonstrating high activity for the polymerisation of ethylene. NMR studies have allowed the nature of the species generated upon treatment with anilinium and trityl borate salts to be studied.

These promising results prompted an interest in developing routes into related but hitherto unknown chromium imido species. Despite the synthetic entry into the bis(^{t}butylimido) chromium system, there had been no reports of the analogous adamantylimido compounds and therefore these became the next focus of our attention.

2.4 Synthesis of Bis(Adamantylimido) Chromium Compounds.

2.4.1 Introduction.

Due to similar electronic properties of the ^{t}butyl and adamantyl substituents, a route to bis(adamantylimido) chromium complexes analogous to that developed by Nugent and Harlow for the synthesis of ^{t}butylimido complexes was investigated.[2,17] It was envisaged that the adamantyl substituent might lend favourable crystallinity characteristics to dialkyl derivatives. Figure 2.9 shows the labelling scheme adopted for the adamantylimido group with respect to NMR assignments.

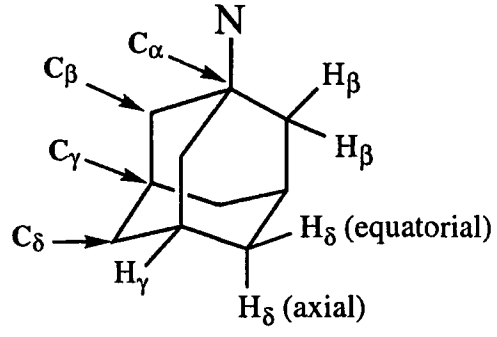

Figure 2.9 Labelling scheme for the adamantylimido ligand.

2.4.2 Reaction of CrO_2Cl_2 with AdNH(TMS) :

Preparation of $Cr(NAd)_2(OTMS)_2$ (5)

The silylated adamantylamine was prepared according to equation 2.6, a method that has proved successful for the production of the ^{t}butyl analogue.

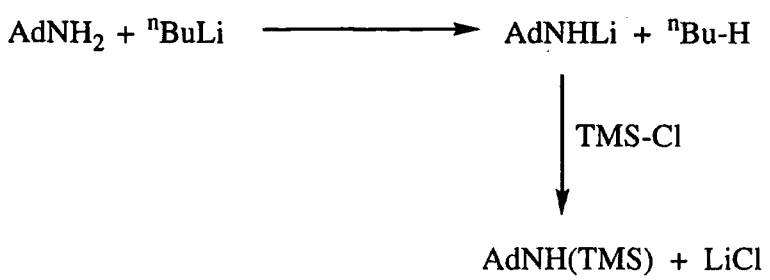

Equation 2.6

Chromyl chloride was added to a heptane solution of the silylated amine and the mixture was heated to 60°C overnight resulting in a red solution and a precipitate, presumed to be $[AdNH_2(TMS)]^+Cl^-$. This reaction was worked-up in a manner analogous to that employed for the preparation of $Cr(N^tBu)_2(OTMS)_2$. However, this gave a mixture of products by proton NMR spectroscopy, indicated by the presence of overlapping adamantyl proton signals in the 1.30–2.15 ppm region of the spectrum.

A further recrystallisation from a concentrated toluene solution at -30°C was required to afford pure $Cr(NAd)_2(OTMS)_2$ (**5**) as a brown amorphous solid in 26% overall yield. The ^1H NMR spectrum (see figure 2.10) shows that the β-protons exhibit a slight coupling to the γ-protons of 2.8Hz. The γ-protons resonate as a singlet centred at δ 1.91, which is broad in appearance due to long range coupling to other protons on the adamantyl cage. The δ–hydrogens are present in both axial and equatorial positions and hence give rise to an AB quartet splitting pattern. This is again broadened due to long range coupling to other protons present on the adamantyl cage.

Attempts at isolating further crops of **5** by concentration of the mother liquor were unsuccessful, an unidentified orange powder being recovered. Although the presence of an amide group attached to the chromium centre was suggested from the ^1H NMR (broad singlet at 11.53 ppm) and the I.R. (strong absorption at 3275 cm^{-1}) in this complex, unambiguous assignment of a structure was not achieved due to complicated overlap of signals in the adamantyl region in the ^1H NMR spectrum and elemental analyses that were not consistent with any reasonable formulation.

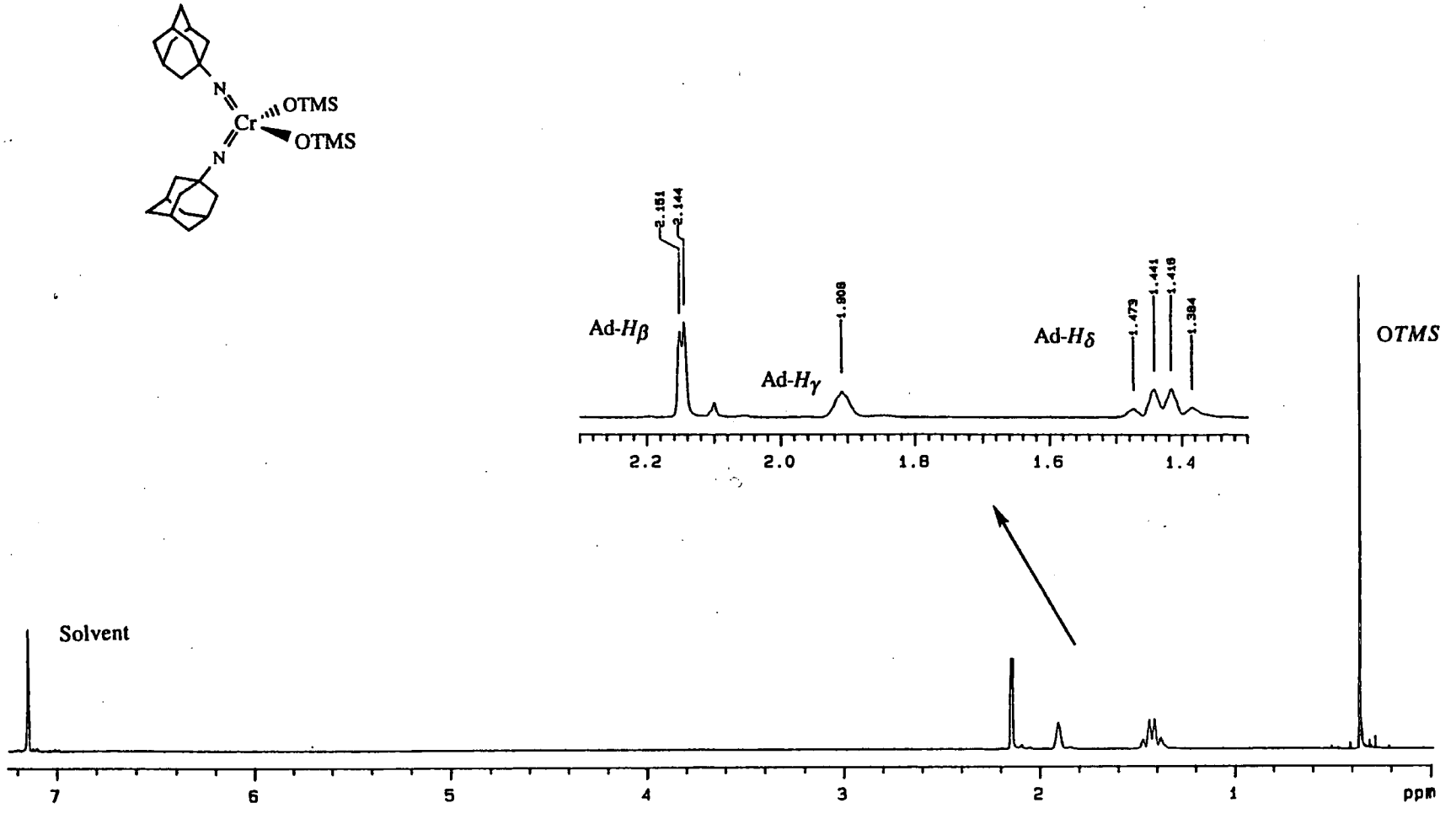

Figure 2.10 ^{1}H NMR spectrum (400MHz, C_6D_6) of $Cr(NAd)_2(OTMS)_2$ (**5**).

2.4.3 Reaction of $Cr(NAd)_2(OTMS)_2$ (5) with BCl_3 :

Preparation of $Cr(NAd)_2Cl_2$ (6).

In an analogous reaction to that reported for the ^{t}butylimido system,[3] the bis-siloxide compound **5** was smoothly converted to the dichloride $Cr(NAd)_2Cl_2$ (**6**) through treatment with BCl_3 (see equation 2.7).

$$\underset{(5)}{Cr(NAd)_2(OTMS)_2} + 2\,BCl_3 \longrightarrow \underset{(6)}{Cr(NAd)_2Cl_2} + 2\,BCl_2(OTMS)$$

Equation 2.7 Synthesis of $Cr(NAd)_2Cl_2$ (**6**).

As for **5** the product was insoluble in pentane and even hot (60°C) heptane, but could be readily extracted from the boron residues by employing toluene as the solvent at room temperature. Recrystallisation at -30°C gave analytically pure $Cr(NAd)_2Cl_2$ in 82% yield, although the crude solid obtained upon removal of the volatile component was also found to be sufficiently pure for subsequent reactions.

2.4.4 Reaction of $Cr(NAd)_2Cl_2$ (6) with 2 Electron Donor Ligands (L):

Preparation of $Cr(NAd)_2Cl_2(L)$ [L = PMe_3 (7) ; Pyridine (8)].

As expected, the Lewis acidic dichloride **6** reacts readily with both PMe_3 and pyridine to form the stable adducts $Cr(NAd)_2Cl_2(PMe_3)$ (**7**) and $Cr(NAd)_2Cl_2$(pyridine) (**8**) respectively. Both complexes are sparingly soluble in toluene but can be recrystallised from THF (for **7**) and CH_2Cl_2 (for **8**) as yellow–orange amorphous powders.

For 5 coordinate complexes of this type, the most likely geometries are trigonal bipyramidal and square pyramidal. Examples of the former case include the closely related complex $Cr(N^tBu)_2Cl_2(PMe_2Ph)$,[3] where the two imido ligands adopt equatorial

positions that minimise the competition for available d-orbitals. The distribution of ligands about chromium in the bimetallic species $[CrO(NSiMe_3)(pyridine)]_2(\mu\text{-}OSiMe_3)_2$ is, however, midway between the two extremes.[18] In the absence of a solid state structure, no conclusions can be drawn as to the preferred orientation of ligands about the metal, although the analogous complex $Cr(NAr)_2Cl_2(pyridine)$ has been shown to adopt a square pyramidal geometry (see section 3.3.3).

2.4.5 Reaction of $Cr(NAd)_2Cl_2$ (6) with Grignard Reagents :

Preparation of $Cr(NAd)_2R_2$ [R = CH_2Ph (9) ; CH_2CMe_2Ph (10) ; CH_2CMe_3 (11)].

The dichloride **6** was reacted with a range of Grignard reagents in diethyl ether to afford the dialkyl complexes $Cr(NAd)_2R_2$ (equation 2.8).

$$Cr(NAd)_2Cl_2 \text{ (6)} + 2\,RMgCl \longrightarrow Cr(NAd)_2R_2 + 2\,MgCl_2$$

R =			
CH_2Ph	(**9**)	64%
CH_2CMe_2Ph	(**10**)	76%
CH_2CMe_3	(**11**)	55%

Equation 2.8 Formation of chromium bis(adamantylimido) dialkyl species.

Each compound was isolated as a red crystalline material from a concentrated pentane solution at -30°C, whereas $Cr(N^tBu)_2(CH_2CMe_2Ph)_2$ and $Cr(N^tBu)_2(CH_2CMe_3)_2$ have only been prepared as oils.[8] The analytical data are consistent with the formation of the monomeric dialkyl complexes (**9–11**). Some of the structural features of this group of compounds are discussed in the following sections.

2.4.6 Solid State Structure of $Cr(NAd)_2(CH_2Ph)_2$ (9).

In the absence of crystals suitable for X-ray analysis, a solid state ^{13}C NMR study was performed by Prof. R.K. Harris and Mr T.V. Thompson to determine the bonding modes of the benzyl ligands in **9**. The non-quaternary suppression experiment shows the η^1 bound *ipso*-carbon signal at 156.6 ppm and the η^2 *ipso*-carbon at 122.8 ppm, correlating well with shifts found for $Cr(N^tBu)_2(CH_2Ph)_2$ using this technique (section 2.3.4). This leads us to conclude that in the solid state, the benzyl ligands adopt an η^1 and η^2 bonding arrangement about the chromium centre. At room temperature in solution, rapid interchange of these two bonding modes results in a time averaged ^1H and ^{13}C NMR spectrum where the two ligands are equivalenced.

A recent crystallographic study has been performed at Newcastle showing that this is indeed the case for **10**, with one benzyl ligand η^1 and the other showing an η^2 bonding mode. Unfortunately, the crystals were of very poor quality precluding any bond length and angle refinement, but the connectivity of the atoms was observable and is in agreement with the solid state ^{13}C NMR data.

2.4.7 The Molecular Structure of $Cr(NAd)_2(CH_2CMe_2Ph)_2$ (10).

Red, prismatic crystals of **10** were grown from a concentrated pentane solution at -30°C, and an X-ray study was performed on a crystal of dimensions 0.74 x 0.40 x 0.24 mm. The molecular structure is shown in figure 2.11 and selected bond angles and distances appear in table 2.9.

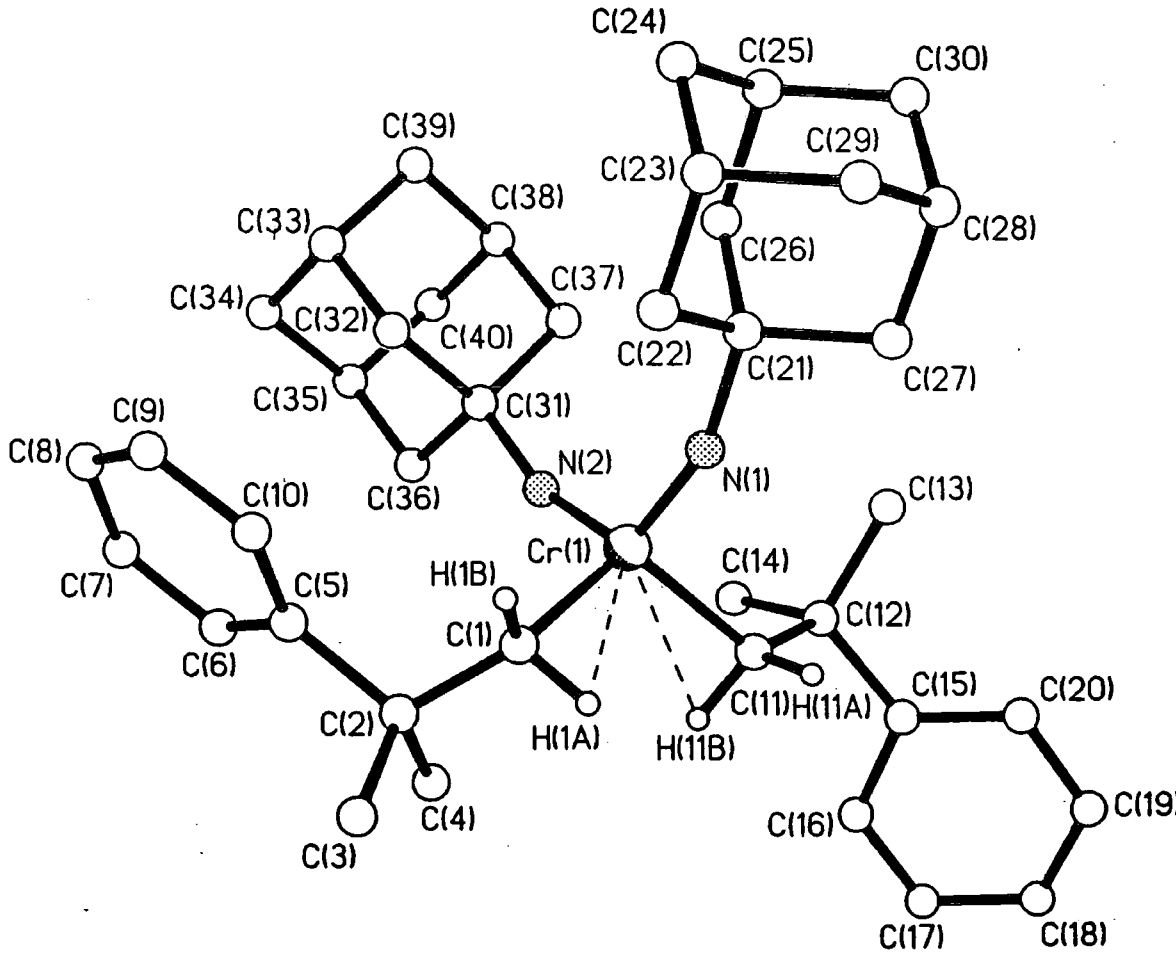

Figure 2.11 Molecular structure of **10** showing the presence of α-agostic interactions.

Cr–N(1)	1.635(2)	Cr–N(2)	1.636(2)
Cr–C(1)	2.027(3)	Cr–C(11)	2.029(2)
C(1)–C(2)	1.536(3)	C(2)–C(4)	1.534(4)
C(2)–C(5)	1.538(3)	C(2)–C(3)	1.539(4)
C(5)–C(6)	1.394(4)	C(5)–C(10)	1.395(4)
C(6)–C(7)	1.394(4)	C(7)–C(8)	1.378(4)
C(8)–C(9)	1.377(4)	C(9)–C(10)	1.388(4)
C(11)–C(12)	1.530(4)	C(12)–C(13)	1.527(4)
C(12)–C(14)	1.535(4)	C(12)–C(15)	1.540(3)
C(15)–C(20)	1.387(4)	C(15)–C(16)	1.394(4)
C(16)–C(17)	1.378(4)	C(17)–C(18)	1.369(4)
C(18)–C(19)	1.365(5)	C(19)–C(20)	1.407(5)
N(1)–C(21)	1.444(3)	C(21)–C(26)	1.529(4)
C(21)–C(22)	1.540(4)	C(21)–C(27)	1.540(3)
N(2)–C(31)	1.453(3)	C(31)–C(37)	1.538(3)
C(31)–C(36)	1.540(3)	C(31)–C(32)	1.542(3)

N(1)–Cr–N(2)	115.90(10)	N(1)–Cr–C(1)	101.89(11)
N(2)–Cr–C(1)	109.56(10)	N(1)–Cr–C(11)	107.83(11)
N(2)–Cr–C(11)	108.83(10)	C(1)–Cr–C(11)	112.81(11)
C(2)–C(1)–Cr	122.6(2)	C(4)–C(2)–C(1)	109.7(2)
C(4)–C(2)–C(5)	112.0(2)	C(1)–C(2)–C(5)	111.4(2)
C(4)–C(2)–C(3)	107.7(2)	C(1)–C(2)–C(3)	108.0(2)
C(5)–C(2)–C(3)	107.9(2)	C(6)–C(5)–C(10)	117.3(2)
C(6)–C(5)–C(2)	122.1(2)	C(10)–C(5)–C(2)	120.5(2)
C(5)–C(6)–C(7)	121.2(2)	C(8)–C(7)–C(6)	120.3(3)
C(9)–C(8)–C(7)	119.3(3)	C(8)–C(9)–C(10)	120.6(3)
C(9)–C(10)–C(5)	121.3(3)	C(12)–C(11)–Cr	126.6(2)
C(13)–C(12)–C(11)	108.7(2)	C(13)–C(12)–C(14)	108.6(2)
C(11)–C(12)–C(14)	110.0(2)	C(13)–C(12)–C(15)	111.7(2)
C(11)–C(12)–C(15)	108.4(2)	C(14)–C(12)–C(15)	109.4(2)
C(20)–C(15)–C(16)	116.7(2)	C(20)–C(15)–C(12)	123.4(2)
C(16)–C(15)–C(12)	119.9(2)	C(17)–C(16)–C(15)	122.2(3)
C(18)–C(17)–C(16)	120.4(3)	C(19)–C(18)–C(17)	119.3(3)
C(18)–C(19)–C(20)	120.7(3)	C(15)–C(20)–C(19)	120.7(3)
C(21)–N(1)–Cr	161.4(2)	N(1)–C(21)–C(26)	111.6(2)
N(1)–C(21)–C(22)	108.7(2)	N(1)–C(26)–C(27)	108.6(2)
C(31)–N(2)–Cr	159.8(2)	N(2)–C(31)–C(37)	111.3(2)
N(2)–C(31)–C(36)	108.7(2)	N(2)–C(31)–C(32)	109.8(2)

Table 2.9 Bond distances (Å) and angles (°) for $Cr(NAd)_2(CH_2CMe_2Ph)_2$ (**10**).

The structure reveals a distorted tetrahedral geometry about the chromium atom with inter-ligand angles in the range 101.89(11)–115.90(10)°. The largest angle is located between the two imido ligands as expected, where repulsion of the π-electron density forces the ligands apart and increases the angle from idealised values. The bulk of the adamantyl groups may also influence this angle as in the analogous structure $Cr(NAr)_2(CH_2CMe_2Ph)_2$ (see section 4.2.7), the N=Cr=N angle is 113.3(2)°.

The coordinates of the methylene hydrogen atoms H(1A), H(1B), H(11A) and H(11B) were refined, with isotropic displacement parameters tied to those of the carrier carbon atoms. These show relatively close chromium–hydrogen contacts for Cr···H(1A) and Cr···H(11B) with distances of 2.28 Å and 2.35 Å respectively, indicating the possible presence of weak α-agostic type interactions.[19] The Cr–C–H_α angles of 92.3° and 95.9° for Cr–C(1)–H(1A) and Cr–C(11)–H(11B) respectively are also consistent with such an interaction being present and are comparable to those found in the isolobal structures $[CpNb(NAr)(CH_2CMe_3)_2]$[21] and $[Mo(NAr)(N^tBu)(CH_2CMe_3)_2]$.[22] The shorter distance and smaller angle indicate that the former interaction is the stronger of the two. The Cr–H bonds lie close to the plane containing the metal and the two

methylene carbon atoms as predicted from the metallocene like frontier orbitals of the $[Cr(NR)_2]$ moiety.

The infra-red stretching frequencies of agostic C–H systems have been shown to occur in the region ν(C–H) ca. 2700-2350 cm^{-1}, lower than that of normal C–H stretches. This is attributed to a lengthening of the C–H bond through interaction with the metal centre. The infra-red spectrum of **10** recorded as a nujol mull shows the presence of weak absorptions in the range 2608–2750 cm^{-1} which may arise from such an agostic C–H stretch, though isotopic labelling studies have not been performed to confirm these assignments.

The $^1J_{CH}$ coupling constant of the methylene carbon atoms in **10** is 123.41Hz, which is higher than predicted if static agostic interactions were present (75–100Hz), but falls in the range expected for non-agostic CH_2 groups (120–130Hz). In a fluxional system however, the reduction in coupling constant for the agostic C–H bond is compensated for by a rise in $^1J_{CH}$ of the remaining C–H bond, caused by an increase in the *s*-character of the bond. The average value may then occur in the range found for non-agostic C–H bonds even though agostic interactions are present.

2.4.8 ^{13}C NMR of $Cr(NAd)_2X_2$ Compounds ; Investigation of Chemical Shifts.

Studies have been performed on a diverse range of d^0 ^{t}butylimido complexes which show a good correlation between the difference in chemical shift of the α and β carbon resonances ($\Delta\delta$) and the electron density at the imido N-atom.[9,22,23] A decrease in the electron density at the imido nitrogen atom causes a downfield shift of the α carbon signal, whilst the β carbon atom resonates at higher field, resulting in a greater value of $\Delta\delta$. Thus determining $\Delta\delta$ values allows a qualitative estimation of the amount of electron donation from the ^{t}butylimido ligand to the metal centre.

The structural and electronic similarities between the ^{t}butyl and adamantyl groups prompted a comparative study into the $\Delta\delta$ values for the adamantylimido ligand, where $\Delta\delta$ is also derived from the difference in chemical shift between the C_α and C_β

signals. The results appear below in table 2.10 for the $Cr(NAd)_2X_2$ complexes (the values for the analogous $Cr(N^tBu)_2X_2$ compounds are also displayed for comparison).

Compound	C_α (ppm)	C_β (ppm)	$\Delta\delta$	Reference
$Cr(NAd)_2(OTMS)_2$	80.1	44.9	35.2	Compound **5**
$Cr(NAd)_2Cl_2$	85.4	43.5	41.9	Compound **6**
$Cr(NAd)_2(CH_2Ph)_2$	72.8	44.5	28.3	Compound **9**
$Cr(NAd)_2(CH_2CMe_2Ph)_2$	73.3	45.2	28.1	Compound **10**
$Cr(NAd)_2(CH_2CMe_3)_2$	73.1	45.7	27.4	Compound **11**
$Cr(N^tBu)_2(OTMS)_2$	77.8	31.3	46.5	22
$Cr(N^tBu)_2Cl_2$	82.7	30.0	52.7	8
$Cr(N^tBu)_2(CH_2Ph)_2$	72.0	31.6	40.4	Compound **1**
$Cr(N^tBu)_2(CH_2CMe_2Ph)_2$	71.7	31.8	39.9	8
$Cr(N^tBu)_2(CH_2CMe_3)_2$	71.4	33.5	37.9	8

Table 2.10 Values of $\Delta\delta$ for $Cr(NAd)_2X_2$ and $Cr(^tBu)_2X_2$.

The value for compound **1** of 40.4 is in the range found by Schaverien for other ^{t}butylimido dialkyl derivatives. For the series of bis(adamantylimido) chromium compounds, a parallel trend is observed but a comparison of the absolute values between the two systems is meaningless owing to the difference in β-carbon environments, where these atoms experience a much more strained geometry in the adamantyl complexes giving rise to lower field resonances.

Both the bis-siloxide **5** and the dichloride **6** have a much larger $\Delta\delta$ value than the dialkyl species. This is indicative of the greater electron withdrawing capacity of the oxygen and chlorine atoms resulting in reduced electron density at the imido N-atom through greater donation to the electron deficient metal.

2.4.9 Summary.

A modification of the existing route into bis(^{t}butylimido) chromium chemistry has allowed a range of adamantylimido complexes to be synthesised. These electron deficient compounds form adducts upon treatment with the two electron donors PMe_3 and pyridine. A series of dialkyl compounds were also synthesised and as envisaged, the exchange of a ^{t}butyl group for an adamantyl cage allowed the isolation of these entities as crystalline materials. This permitted a solid state ^{13}C NMR study to be performed on the bis-benzyl complex $Cr(NAd)_2(CH_2Ph)_2$ (**9**) allowing a deduction to be made concerning the bonding modes of the two alkyl ligands. An X-ray study of the complex $Cr(NAd)_2(CH_2CMe_2Ph)_2$ (**10**) revealed a pseudo tetrahedral geometry around the chromium and also the presence of two weak α-agostic interactions. Studies are currently being undertaken to probe the activity of the bis-benzyl complex towards α-olefin polymerisation.

2.5 References.

1. D.D. Devore, J.D. Lichtenhan, F. Takusagawa and E.A. Maatta, *J. Am. Chem. Soc.*, **1987**, *109*, 7408.

2. W.A. Nugent and R.L. Harlow, *Inorg. Chem.*, **1980**, *19*, 777.

3. A.A. Danopoulos, W.-H. Leung, G. Wilkinson, B. Hussain-Bates and M.B. Hursthouse, *Polyhedron*, **1990**, *9*, 2625.

4. M.C.W. Chan, Ph.D. Thesis, University of Durham, 1995.

5. H. Sinn, W. Kaminsky, H.-J. Vollmer and R. Woldt, *Angew. Chem. Int. Ed. Engl.*, **1980**, *19*, 390. ; A. Andresen, H.-G. Cordes, J. Herwig, W. Kaminsky, A. Merck, R. Mottweiler, J. Pein, H. Sinn and H.-J. Vollmer, *Angew. Chem. Int. Ed. Engl.*, **1976**, *15*, 630.

6. J.C. Randall, *Rev. Macromol. Chem. Phys.*, **1989**, *C29 (2 & 3)*, 201.

7. R.F. Jordan, W.E. Dasher and S.F. Echols, *J. Am. Chem. Soc.*, **1986**, *108*, 1718 ; R.F. Jordan, C.S. Bajgur, R. Willett and B. Scott, *J. Am. Chem. Soc.*, **1986**, *108*, 7410 ; R.F. Jordan, R.E. LaPointe, C.S. Bajgur, S.F. Echols and R. Willett, *J. Am. Chem. Soc.*, **1987**, *109*, 4111 ; R.F. Jordan, P.K. Bradley, N.C. Baenziger and R.E. LaPointe, *J. Am. Chem. Soc.*, **1990**, *112*, 1289 ; R.F. Jordan, *Adv. Organomet, Chem.*, **1991**, *32*, 325.

8. N. Meijboom, C.J. Schaverien and A.G. Orpen, *Organometallics*, **1990**, *9*, 774.

9. (a) M.B. Hursthouse, M. Motevalli, A.C. Sullivan and G. Wilkinson, *J. Chem. Soc., Chem. Commun.*, **1986**, 1398. (b) A.C. Sullivan, G. Wilkinson, M. Motevalli and M.B. Hursthouse, *J. Chem. Soc. Dalton Trans.*, **1988**, 53.

10. J. Scholz, F. Rehbaum, K.-H. Thiele, R. Goddard, P. Betz and C. Krüger, *J. Organomet. Chem.*, **1993**, *443*, 93.

11. K.-H. Thiele, U. Böhme and J. Sieler, *Z. Anorg. Allg. Chem.*, **1993**, *619*, 1951.

12. R.F. Jordan, R.E. LaPointe, N. Baenziger and G.D. Hinch, *Organometallics*, **1990**, *9*, 1539, and references therein.

13. A.A. Danopoulos, G. Wilkinson, T.K.N. Sweet and M.B. Hursthouse, *J. Chem. Soc. Dalton Trans.*, **1995**, 2111.

14. P. Legzdins, R.H. Jones, E.C. Phillips, V.C. Yee, J. Trotter and F.W.B. Einstein, *Organometallics*, **1991**, *10*, 986.

15. P.W. Dyer, V.C. Gibson, J.A.K. Howard, B. Whittle and C. Wilson, *Polyhedron*, **1995**, *14*, 103.

16. X. Yang, C.L. Stern and T.J. Marks, *J. Am. Chem. Soc.*, **1991**, *113*, 3623. ; X. Yang, C.L. Stern and T.J. Marks, *J. Am. Chem. Soc.*, **1994**, *116*, 10015.

17. W.A. Nugent and R.L. Harlow, *J. Chem. Soc., Chem. Commun.*, **1979**, 342.

18. Hon-wah Lam, G. Wilkinson, B. Hussain-Bates and M.B. Hursthouse, *J. Chem. Soc. Dalton Trans.*, **1993**, 1477.

19. M. Brookhart and M.L.H. Green, *J. Organomet. Chem.*, **1983**, *250*, 395 ; M. Brookhart, M.L.H. Green and L.L. Wong, *Progress In Inorganic Chemistry*, **1988**, *36*, 1.

20. A.D. Poole, D.N. Williams, A.M. Kenwright, V.C. Gibson, W. Clegg, D.C.R. Hockless and P.A. O'Neil, *Organometallics*, **1993**, *12*, 2549.

21. A. Bell, W. Clegg, P.W. Dyer, M.R.J. Elsegood, V.C. Gibson and E.L. Marshall, *J. Chem. Soc., Chem. Commun.*, **1994**, 2547.

22. W.A. Nugent, R.J. McKinney, R.V. Kasowski and F.A. Van-Catledge, *Inorganica Chimica Acta*, **1982**, *65*, L91.

23. M. Jolly, Ph.D. Thesis, University of Durham, 1994.

Chapter Three

Four and Five Coordinate Bis(Arylimido) Complexes of Chromium.

3.1 Introduction.

In general, arylimido ligands often bestow favourable solubility and crystallinity characteristics to imido complexes and may even confer enhanced stability to their derivatives. Consequently, bis(arylimido) complexes of chromium were targeted. Once a synthetic route had been developed, it was postulated that changing the substituents on the aryl ring would allow 'fine-tuning' of the steric and electronic environment at the metal centre.

Previous attempts at the synthesis of arylimido complexes of chromium using established methodologies had proved unsuccessful.[1] Exchange of an existing imido ligand with a free aniline molecule has proved to be a powerful method of synthesising arylimido complexes of molybdenum.[2]

3.2 Preparative Routes into Arylimido Chromium Chemistry.

3.2.1 Reaction of $Cr(N^tBu)_2Cl_2$ with $ArNH_2$ (Ar = 2,6-^{i}Pr$_2$C$_6$H$_3$) :

Formation of $Cr(NAr)_2(NH^tBu)Cl$ (12).

Initial NMR studies between $Cr(N^tBu)_2Cl_2$ and $ArNH_2$ conducted at room temperature in C_6D_6 showed a rapid colour change from red-black to purple on mixing. The ^1H NMR spectrum revealed that both starting materials had been consumed giving clean signals corresponding to a single new product.

Upon performing the reaction on a preparative scale, the new product was isolated and found to be $Cr(NAr)_2(NH^tBu)Cl$ (**12**).[3] Both ^{t}butylimido groups had thus successfully been replaced by arylimido ligands, a residue of the ^{t}butylimido group remaining bound to the metal as an amide ligand. **12** arises as the product rather than the dichloride $Cr(NAr)_2Cl_2$ due to the preferential loss of a molecule of HCl and not a second molecule of $^tBuNH_2$ in the last stage of the reaction sequence (see equation 3.1). Although illustrated as involving initial coordination of the amine to the metal

centre (i.e. an intramolecular proton transfer), such species were not directly observed and hence intermolecular transfer of the proton to the imido ligand can not be ruled out.

Reaction with one molar equivalent of $ArNH_2$ did not allow the mixed imido complex $Cr(N^tBu)(NAr)Cl_2$ to be isolated as for molybdenum,[2] but gave a mixture of starting dichloride and **12** in reduced yield. This suggests the mixed imido complex is more reactive towards exchange with another molecule of aniline than the initial starting material.

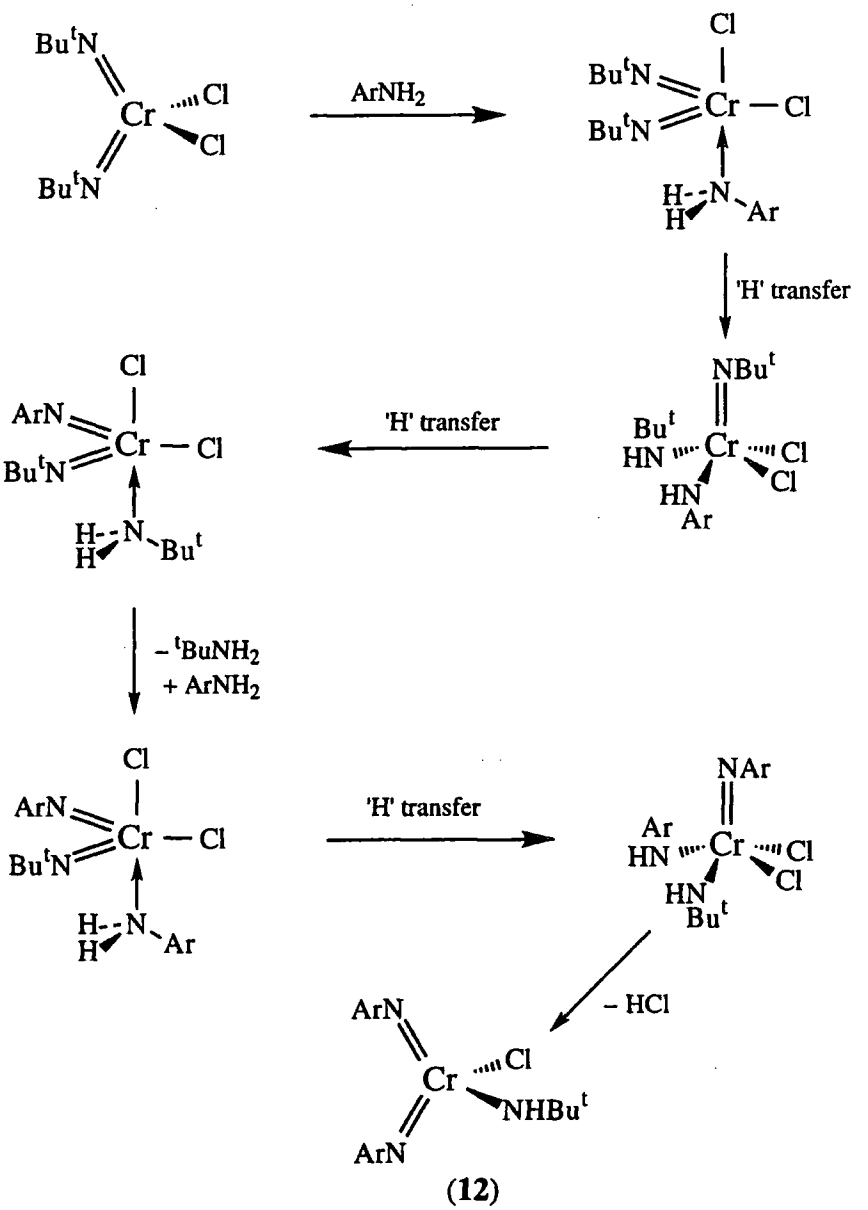

Equation 3.1 Proposed mechanism for the formation of $Cr(NAr)_2(NH^tBu)Cl$ (**12**).

The ^{1}H NMR spectrum (400 MHz, C_6D_6) shows a characteristically high frequency signal for the nitrogen bound proton of the ^{t}butylamido ligand at 11.84 ppm. The two imido ligands are inequivalent at room temperature as a consequence of the amido group aligning with its substituents orientated towards the imido ligands (see sections 1.2.5 and 3.2.2). This is most clearly evident in the ^{1}H NMR spectrum by the presence of two septets at δ 3.89 and δ 3.76 for the *iso*-propyl methine protons. The IR spectrum shows a band of medium intensity at 3225 cm^{-1} assigned to the N-H stretch of the amide ligand.

3.2.2 Molecular Structure of Cr(NAr)$_2$(NH^{t}Bu)Cl (12).

Crystals of **12** were grown from a concentrated pentane solution at -30°C resulting in the formation of dark red prisms. The molecular structure is shown in figure 3.1 and selected bond lengths and angles are collected in table 3.1.

The molecule is pseudo-tetrahedral with angles about the chromium centre falling in the range 106.18(13)–111.96(13)°. The N=Cr=N angle of 109.3(2)° is smaller than has been observed for ^{t}butylimido and adamantylimido analogues[4] but is comparable to those found in other tetrahedral arylimido chromium compounds.[5] This reflects the planarity of the aryl ring and its ability to rotate about the N–C$_{ipso}$ bond to reduce steric interactions.

The Cr=N–Ar angles deviate from 180° to a greater extent than typically observed for bis(imido) complexes of this type, with values of 157.0(3)° and 159.4(3)° The Cr=NAr bond lengths of 1.643(3) Å and 1.654(4) Å are longer than observed for ^{t}butylimido derivatives (1.58 - 1.63 Å),[4] a consequence of π-bonding between the imido nitrogen and the aryl C$_{ipso}$ bond giving rise to a reduction of Cr-N π-bond order. The Cr-N$_{amide}$ bond length of 1.813(3) Å compares to values found for molybdenum and tungsten ^{t}butylamides, which fall in the range 1.93 - 2.05 Å.[6] The shorter distance in **12** is not fully compensated by the smaller ionic radius of chromium (0.52 Å) compared to molybdenum and tungsten (0.62 Å) and may therefore reflect stronger π-bonding between the amido nitrogen and the chromium.

The amido hydrogen position, H(1) was freely refined with the isotropic temperature factor set to be 120% of that of N(1). The N(1)–H(1) distance is found to be 0.849 Å, with the Cr–N(1)–H(1) angle equal to 113.6° and the C(1)–N(1)–H(1) angle equal to 108.2°

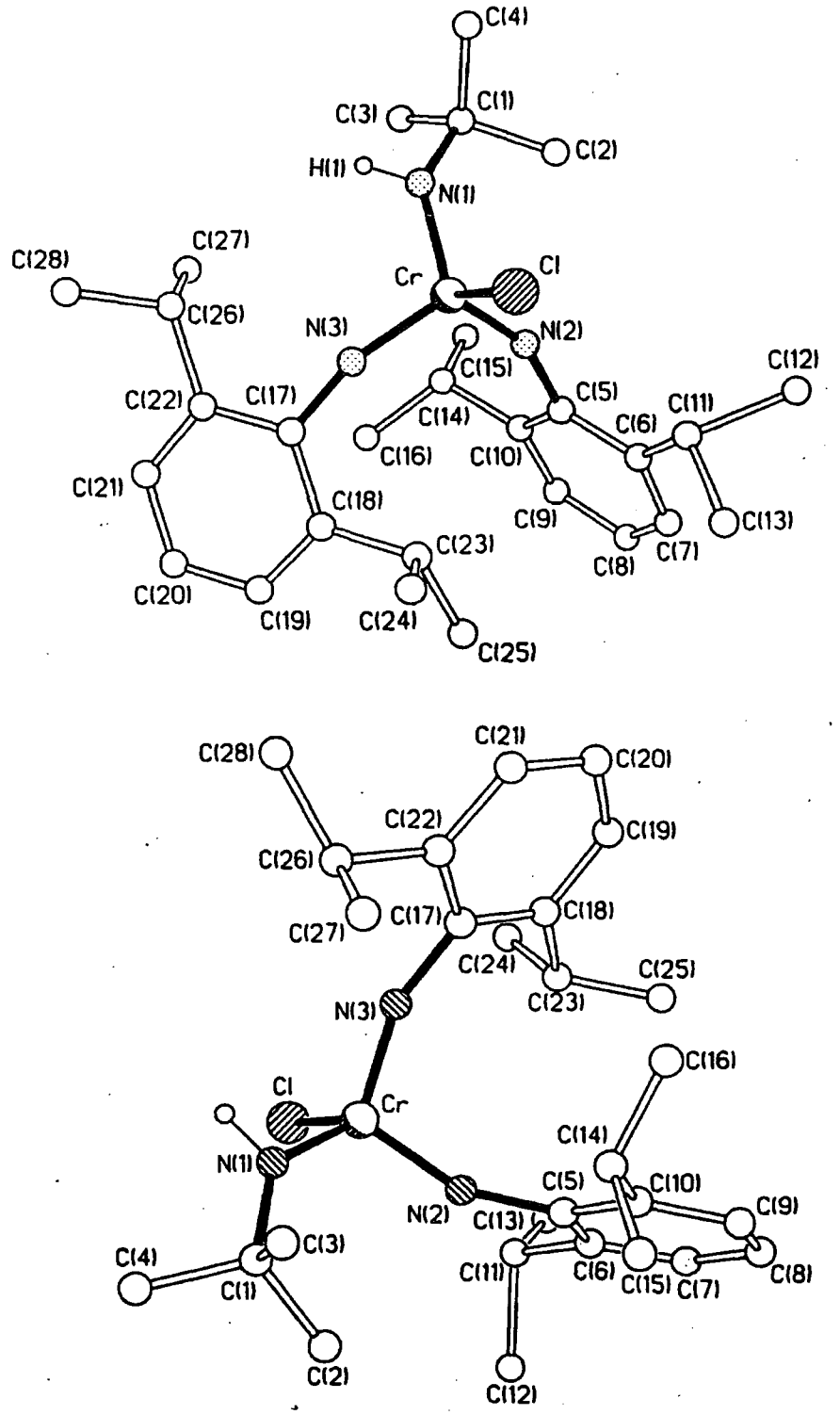

Figure 3.1 Two views of the molecular structure of $Cr(NAr)_2(NH^tBu)Cl$ (**12**).

Cr–N(2)	1.643(3)	Cr–N(3)	1.654(4)
Cr–N(1)	1.813(3)	Cr–Cl	2.247(2)
N(1)–C(1)	1.479(6)	C(1)–C(3)	1.517(7)
C(1)–C(2)	1.524(7)	C(1)–C(4)	1.536(6)
N(2)–C(5)	1.392(5)	C(5)–C(10)	1.405(6)
C(5)–C(6)	1.413(6)	C(6)–C(7)	1.378(6)
C(6)–C(11A)	1.513(6)	C(6)–C(11)	1.513(6)
C(7)–C(8)	1.368(6)	C(8)–C(9)	1.378(6)
C(9)–C(10)	1.389(6)	C(10)–C(14)	1.517(6)
C(11)–C(13)	1.494(7)	C(11)–C(12)	1.74(2)
C(11A)–C(12A)	1.395(12)	C(11A)–C(13A)	1.494(7)
C(14)–C(16)	1.524(7)	C(14)–C(15)	1.529(7)
N(3)–C(17)	1.380(5)	C(17)–C(22)	1.402(6)
C(17)–C(18)	1.429(6)	C(18)–C(19)	1.380(6)
C(18)–C(23)	1.501(6)	C(19)–C(20)	1.383(6)
C(20)–C(21)	1.378(6)	C(21)–C(22)	1.394(6)
C(22)–C(26)	1.522(6)	C(23)–C(24)	1.517(6)
C(23)–C(25)	1.529(6)	C(26)–C(28)	1.516(7)
C(26)–C(27)	1.526(7)		

N(2)–Cr–N(3)	109.3(2)	N(2)–Cr–N(1)	110.1(2)
N(3)–Cr–N(1)	110.6(2)	N(2)–Cr–Cl	108.63(13)
N(3)–Cr–Cl	106.18(13)	N(1)–Cr–Cl	111.96(13)
C(1)–N(1)–Cr	136.7(3)	N(1)–C(1)–C(3)	109.4(4)
N(1)–C(1)–C(2)	110.1(4)	C(3)–C(1)–C(2)	111.2(4)
N(1)–C(1)–C(4)	106.1(4)	C(3)–C(1)–C(4)	110.4(4)
C(2)–C(1)–C(4)	109.4(4)	C(5)–N(2)–Cr	157.0(3)
N(2)–C(5)–C(10)	120.9(4)	N(2)–C(5)–C(6)	117.0(4)
C(10)–C(5)–C(6)	122.0(4)	C(7)–C(6)–C(5)	117.3(4)
C(7)–C(6)–C(11A)	122.5(4)	C(5)–C(6)–C(11A)	120.2(4)
C(7)–C(6)–C(11)	122.5(4)	C(5)–C(6)–C(11)	120.2(4)
C(8)–C(7)–C(6)	121.8(4)	C(7)–C(8)–C(9)	120.3(4)
C(8)–C(9)–C(10)	121.4(4)	C(9)–C(10)–C(5)	117.2(4)
C(9)–C(10)–C(14)	119.8(4)	C(5)–C(10)–C(14)	123.0(4)
C(13)–C(11)–C(6)	113.7(4)	C(13)–C(11)–C(12)	97.7(7)
C(6)–C(11)–C(12)	106.7(5)	C(12A)–C(11A)–C(13A)	120.5(8)
C(12A)–C(11A)–C(6)	113.8(6)	C(13A)–C(11A)–C(6)	113.7(4)
C(10)–C(14)–C(16)	112.0(4)	C(10)–C(14)–C(15)	111.3(4)
C(16)–C(14)–C(15)	110.7(4)	C(17)–N(3)–Cr	159.4(3)
N(3)–C(17)–C(22)	118.1(4)	N(3)–C(17)–C(18)	120.0(4)
C(22)–C(17)–C(18)	122.0(4)	C(19)–C(18)–C(17)	116.3(4)
C(19)–C(18)–C(23)	121.8(4)	C(17)–C(18)–C(23)	121.7(4)
C(18)–C(19)–C(20)	122.5(4)	C(21)–C(20)–C(19)	120.3(4)
C(20)–C(21)–C(22)	120.6(4)	C(21)–C(22)–C(17)	118.2(4)
C(21)–C(22)–C(26)	120.7(4)	C(17)–C(22)–C(26)	121.0(4)
C(18)–C(23)–C(24)	110.4(4)	C(18)–C(23)-C(25)	113.6(4)
C(24)–C(23)–C(25)	110.3(4)	C(28)–C(26)–C(22)	113.2(4)
C(28)–C(26)–C(27)	110.9(4)	C(22)–C(26)–C(27)	110.0(4)

Table 3.1 Bond distances (Å) and angles (°) for $Cr(NAr)_2(NH^tBu)Cl$ (**12**).

The 'triad representation' of **12** is illustrated in figure 3.2,[7] the molecule being displayed with the amide–metal bond projecting towards the viewer (see section 1.2.5). This clearly shows the amido ligand orientated so the donor p-orbital lies in the Cr–N(1)–Cl plane, thus avoiding direct competition for π bonding with the strong π donor imido groups. Such an orientation is consistent with those seen in bent metallocene and half-sandwich imido metal complexes.[7,8]

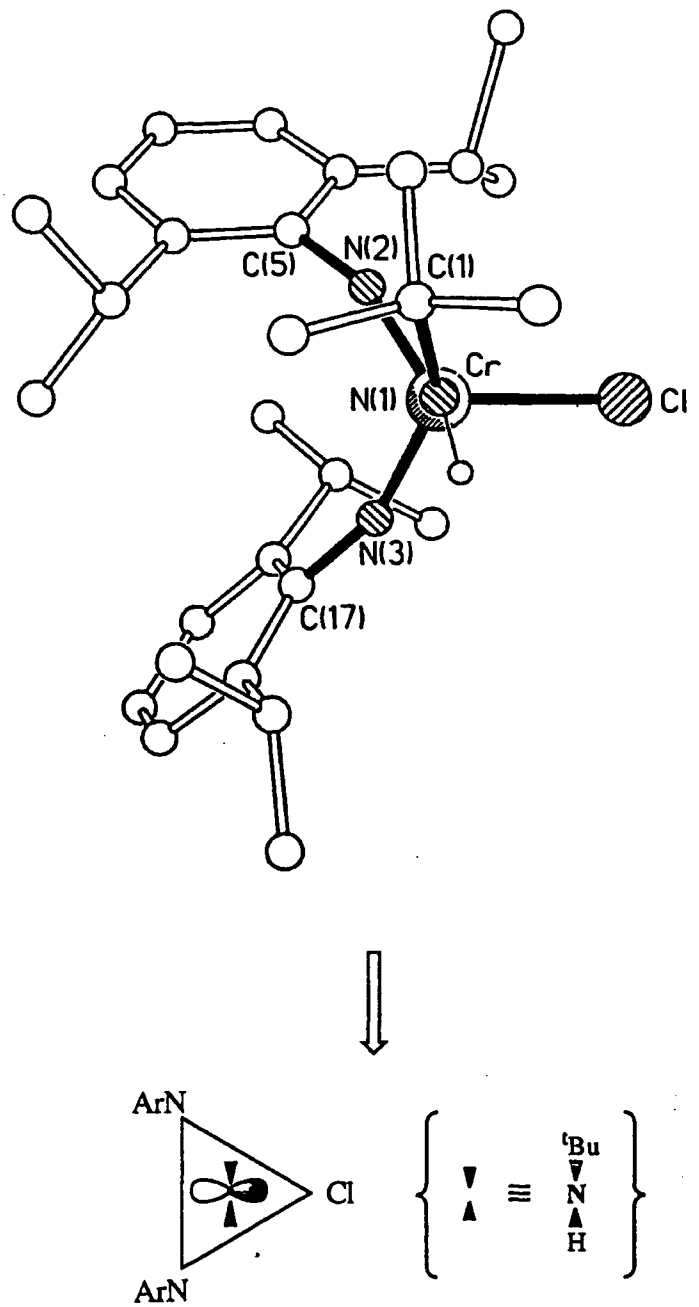

Figure 3.2 View of **12** along N(1) - Cr vector.

3.2.3 Reaction of $Cr(N^tBu)_2Cl_2$ with LiNHAr (Ar = 2,6-^{i}Pr$_2$C$_6$H$_3$).

Another potential route into arylimido chemistry of chromium is *via* reaction of the halide species $Cr(N^tBu)_2Cl_2$ with LiNHAr. It was envisaged that the arylamido species would form initially, proceeding to react by intramolecular 'H-atom' transfer to give the arylimido, ^{t}butylamido compound as illustrated in equation 3.2.

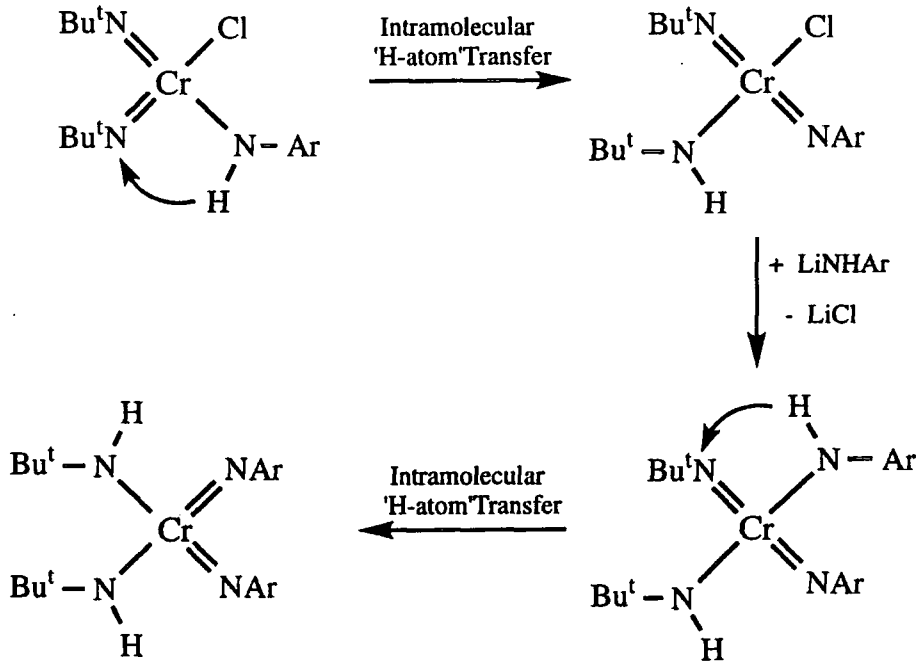

Equation 3.2 Formation of arylimido ligand by reaction with LiNHAr.

Reaction of $Cr(N^tBu)_2Cl_2$ with two equivalents of LiNHAr in Et_2O resulted only in isolation of **12** in reduced yield (26% cf. > 60% yield for $Cr(N^tBu)_2Cl_2$ + 2 $ArNH_2$). The proposed mechanistic pathway involves the reaction of the first ^{t}butylamido ligand generated with LiNHAr, in preference to replacement of the second chloride ligand, giving the arylamido ligand and liberating $LiNH^tBu$. This can then undergo the intramolecular proton transfer leading directly to the formation of $Cr(NAr)_2(NH^tBu)Cl$. Attempted reaction with one equivalent of LiNHAr to isolate either $Cr(N^tBu)_2(NHAr)Cl$ or the rearranged product $Cr(NAr)(N^tBu)(NH^tBu)Cl$ gave rise to a mixture of starting dichloride and **12**, again suggesting that the initial product from this reaction is more reactive than the starting dichloride (see section 3.2.1).

3.2.4 Reaction of $Cr(N^tBu)_2Cl_2$ with $Ar'NH_2$ (where Ar' = 2,4,6-$^tBu_3C_6H_2$) :

Preparation of $Cr(NAr')(N^tBu)Cl_2$ (13).

There is no reaction between $Cr(N^tBu)_2Cl_2$ and the bulky aniline 2,4,6-$^tBu_3$-C_6H_2 ($Ar'NH_2$) at room temperature most likely due to increased steric congestion around the aniline nitrogen atom hindering its initial coordination to the chromium centre, or possibly impairing proton transfer to the imido N-atom. Heating the mixture to 60°C in heptane for 1 week, however, results in the formation of the mixed imido compound $Cr(NAr')(N^tBu)Cl_2$ (**13**), with liberation of one equivalent of $^tBuNH_2$. Repeated recrystallisation from heptane or pentane is necessary to completely remove traces of unreacted amine from the complex. The reaction does not proceed further, even when heated at 100°C in toluene for 2 weeks.

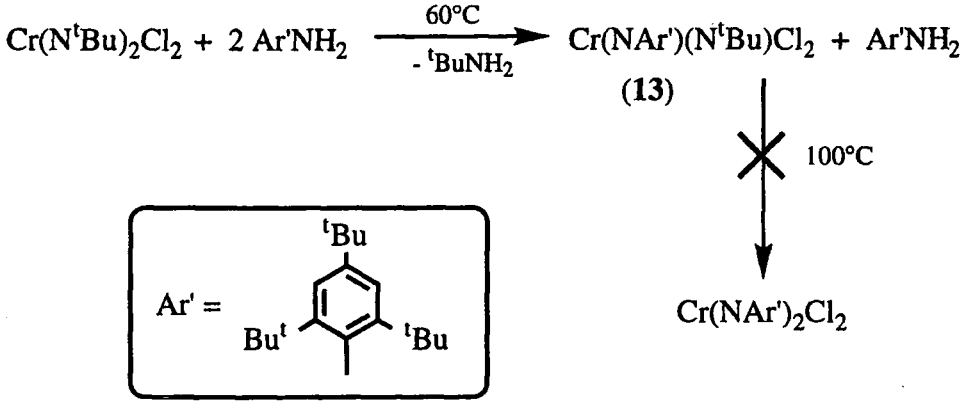

Equation 3.3 Reaction of $Cr(N^tBu)_2Cl_2$ with $Ar'NH_2$.

The ^1H NMR spectrum shows three ^{t}butyl signals in the ratio 2:1:1 at 1.52, 1.16 and 1.03 ppm, corresponding to *ortho*-^{t}butyl, imido-^{t}butyl and *para*-^{t}butyl groups respectively. The equivalent aryl protons resonate to slightly lower field than the protio impurity in C_6D_6, being located at 7.35 ppm.

3.2.5 Other Attempted Amine Exchange Reactions.

The reaction between $Cr(N^tBu)_2Cl_2$ and the parent aniline $PhNH_2$ resulted in isolation of a small amount of green paramagnetic material, implying that reduction of the metal centre had occurred. The successful reaction between 2,6- (and 2,4,6-) substituted anilines suggested that the presence of *ortho* substituents on the aryl ring may be important in this reaction pathway, either by stabilising intermediates or the final product.

For $2,6\text{-}Me_2C_6H_3NH_2$ and $2\text{-}^tBuC_6H_4NH_2$ a colour change from red-black to purple was observed at low temperature on mixing, suggesting that a similar reaction was occurring to that observed for exchange with $2,6\text{-}^iPr_2C_6H_3NH_2$. On work-up however, the isolated solid consisted of a mixture of products for both cases that proved impossible to separate by conventional methods. With $2,6\text{-}Cl_2C_6H_3NH_2$ the solution adopted a green colour, indicating that reduction had occurred, as seen for the reaction with $PhNH_2$. No tractable product was isolated from this reaction.

The 'H-atom' transfer route to arylimido chromium complexes is therefore sensitive to both the steric and electronic properties of the aniline. Facile reduction of the metal centre also needs to be considered when selecting anilines as potential sources of imido ligands.

3.3 Preparation of the Dichloride $Cr(NAr)_2Cl_2$ (14) and the Formation of Adducts.

3.3.1 Reaction of $Cr(NAr)_2(NH^tBu)Cl$ (12) with BCl_3 :

*Preparation of $Cr(NAr)_2Cl_2$ (**14**).*

BCl_3 was again employed as the chlorinating reagent for this reaction due to success with both the ^{t}butylimido and adamantylimido systems and facile separation of the product from the boron residues (equation 3.4).

$$\underset{\textbf{(12)}}{Cr(NAr)_2(NH^tBu)Cl} + BCl_3 \xrightarrow[2\text{ hours}]{CH_2Cl_2} \underset{\textbf{(14)}}{Cr(NAr)_2Cl_2} + BCl_2(NH^tBu)$$

Equation 3.4 Formation of $Cr(NAr)_2Cl_2$ (**14**).

Although originally reported as being purified by sublimation,[3] a concentrated pentane or heptane solution maintained at -30°C will yield pure **14** as red crystalline plates. **14** can be made without isolation of the intermediate complex **12**, but care must be taken since unreacted $ArNH_2$ from the imido ligand exchange results in the dichloride being isolated as an oil that cannot be induced to crystallise.

3.3.2 Reaction of $Cr(NAr)_2Cl_2$ (14) with Pyridine :

Preparation of $Cr(NAr)_2Cl_2$(pyridine) (15).

Reaction between the dichloride and pyridine in toluene failed to induce precipitation of the adduct (cf. $Cr(N^tBu)_2Cl_2$[1] and $Cr(NAd)_2Cl_2$[9]), but removal of the solvent followed by recrystallisation from pentane, CH_2Cl_2 or diethyl ether resulted in isolation of $Cr(NAr)_2Cl_2$(pyridine) (**15**) as a pure crystalline material.

The ^1H NMR spectrum and elemental analysis are consistent with the mono-adduct, with the proton spectrum showing typical low field signals at δ 8.97 (H_{ortho}), δ 7.89 (H_{para}) and δ 7.50 (H_{meta}) for the bound pyridine ligand (see figure 3.3). Wilkinson has found that the related compound $Cr(N\text{-}C_6H_2Me_3\text{-}2,4,6)_2Cl_2$ will form the bis-pyridine adduct,[5] most likely due to the reduced size of the *ortho*-aryl substituents.

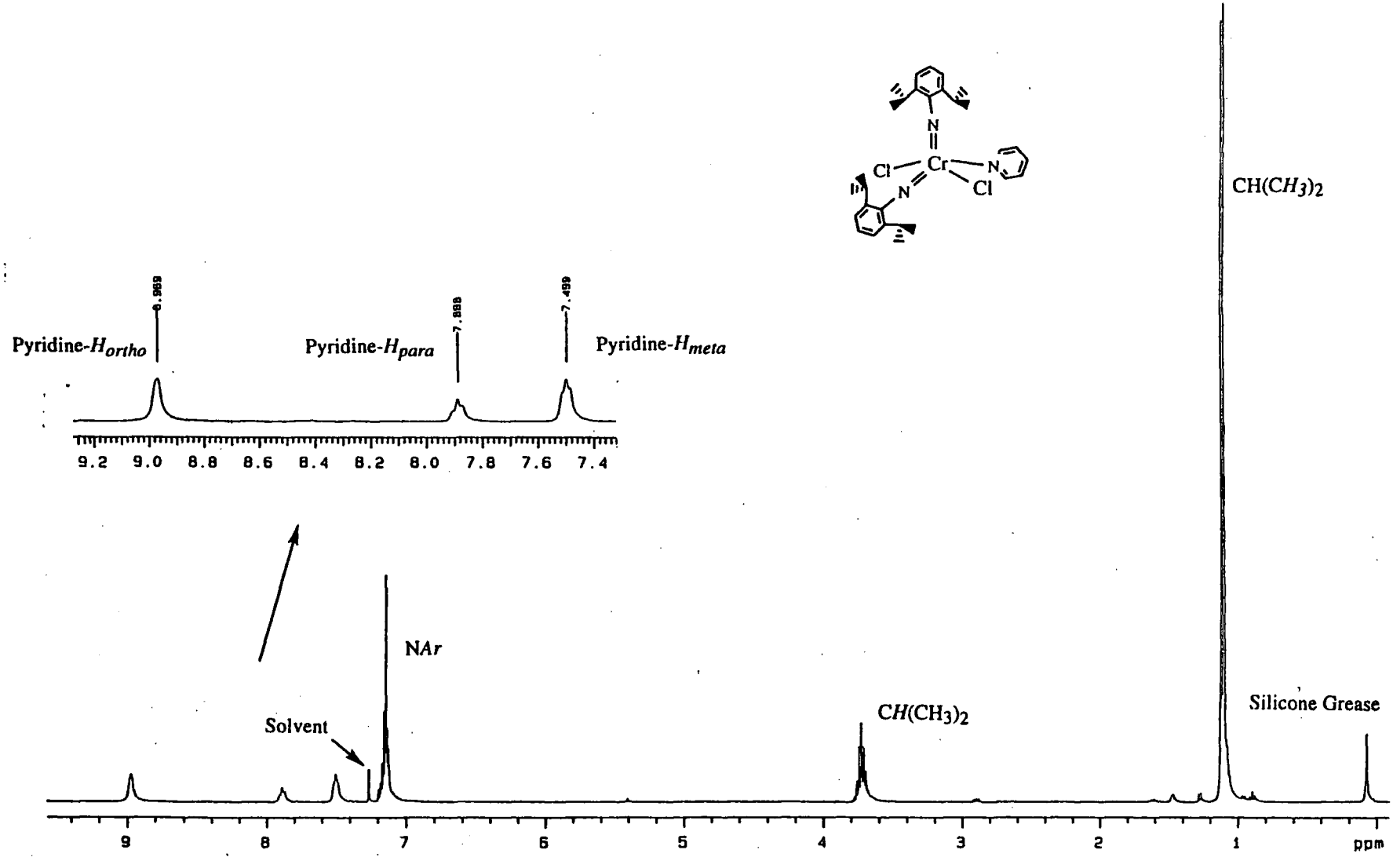

Figure 3.3 ^{1}H NMR spectrum (400MHz, $CDCl_3$) of $Cr(NAr)_2Cl_2$(pyridine) (**15**).

3.3.3 Molecular Structure of $Cr(NAr)_2Cl_2$(pyridine) (15).

Dark red cubic crystals of **15** were grown on cooling of a warm (30°C) concentrated pentane solution to room temperature. A crystal of dimensions 0.52 x 0.24 x 0.14 mm was mounted under an inert oil and X-ray data was collected and solved at Newcastle. The molecular structure is illustrated in figure 3.4 and selected bond distances and angles are given in table 3.2.

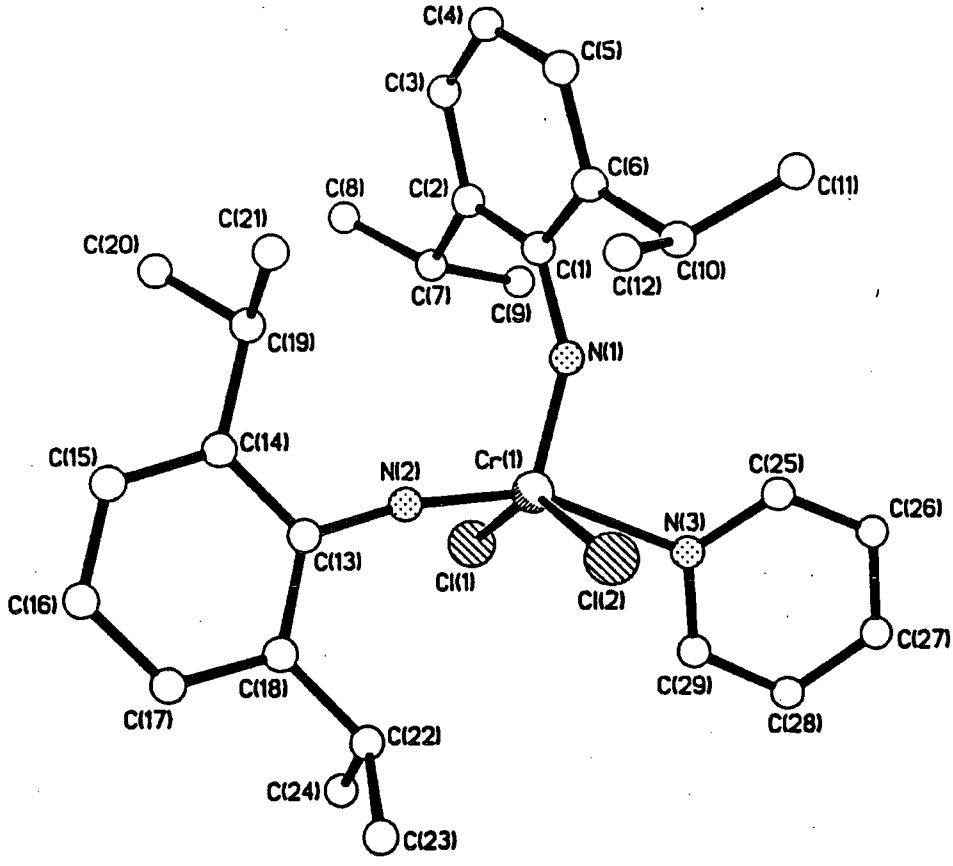

Figure 3.4 Molecular structure of $Cr(NAr)_2Cl_2$(pyridine) (**15**).

Cr–N(2)	1.671(3)	Cr–N(1)	1.673(2)
Cr–N(3)	2.135(2)	Cr–Cl(1)	2.2994(10)
Cr–Cl(2)	2.3042(10)	N(1)–C(1)	1.391(4)
C(1)–C(2)	1.414(4)	C(1)–C(6)	1.418(4)
C(2)–C(3)	1.390(4)	C(3)–C(4)	1.380(5)
C(4)–C(5)	1.378(5)	C(5)–C(6)	1.391(4)
N(2)–C(13)	1.354(4)	C(13)–C(18)	1.424(4)
C(13)–C(14)	1.428(4)	C(14)–C(15)	1.385(4)
C(15)–C(16)	1.386(5)	C(16)–C(17)	1.385(5)
C(17)–C(18)	1.391(5)	N(3)–C(29)	1.322(4)
N(3)–C(25)	1.399(4)	C(25)–C(26)	1.382(5)
C(26)–C(27)	1.362(6)	C(27)–C(28)	1.370(6)
C(28)–C(29)	1.389(5)		

(C-C Distances of *iso*-propyl groups in the range 1.512(4)–1.535(5) Å)

N(2)–Cr–N(1)	110.99(12)	N(2)–Cr–N(3)	150.03(11)
N(1)–Cr–N(3)	98.86(11)	N(2)–Cr–Cl(1)	88.89(9)
N(1)–Cr–Cl(1)	103.13(9)	N(3)–Cr–Cl(1)	81.50(7)
N(2)–Cr–Cl(2)	92.42(9)	N(1)–Cr–Cl(2)	106.04(9)
N(3)–Cr–Cl(2)	81.64(7)	Cl(1)–Cr–Cl(2)	148.15(4)
C(1)–N(1)–Cr	148.9(2)	N(1)–C(1)–C(2)	120.2(3)
N(1)–C(1)–C(6)	117.8(3)	C(2)–C(1)–C(6)	122.0(3)
C(3)–C(2)–C(1)	117.6(3)	C(3)–C(2)–C(7)	122.4(3)
C(1)–C(2)–C(7)	119.9(3)	C(4)–C(3)–C(2)	121.1(3)
C(5)–C(4)–C(3)	120.6(3)	C(4)–C(5)–C(6)	121.6(3)
C(5)–C(6)–C(1)	117.0(3)	C(5)–C(6)–C(10)	121.2(3)
C(1)–C(6)–C(10)	121.7(3)	C(13)–N(2)–Cr	172.6(2)
N(2)–C(13)–C(18)	119.6(3)	N(2)–C(13)–C(14)	119.2(3)
C(18)–C(13)–C(14)	121.2(3)	C(15)–C(14)–C(13)	117.9(3)
C(15)–C(14)–C(19)	123.1(3)	C(13)–C(14)–C(19)	119.0(3)
C(14)–C(15)–C(16)	121.1(3)	C(17)–C(16)–C(15)	120.9(3)
C(16)–C(17)–C(18)	121.1(3)	C(17)–C(18)–C(13)	117.7(3)
C(17)–C(18)–C(22)	120.9(3)	C(13)–C(18)–C(22)	121.3(3)
C(29)–N(3)–C(25)	117.6(3)	C(29)–N(3)–Cr	123.0(2)
C(25)–N(3)–Cr	119.4(2)	N(3)–C(25)–C(26)	123.1(3)
C(27)–C(26)–C(25)	118.9(4)	C(26)–C(27)–C(28)	118.6(3)
C(27)–C(28)–C(29)	119.5(4)	N(3)–C(29)–C(28)	122.4(4)

(Angles within *iso*-propyl groups in the range 109.0(3)–114.6(3)°)

Table 3.2 Bond distances (Å) and angles (°) for $Cr(NAr)_2Cl_2$(pyridine) (**15**).

This molecule is best described as a distorted square pyramid, with two trans chlorine atoms, the pyridine and one imido group forming the base of the pyramid (angles range from 81.50(7) - 92.42(9)°) and the remaining imido ligand located at the apex. Both the pyridine and the aryl ring of the basal imido ligand are rotated so that they are approximately perpendicular to the plane defined by the base of the structure, presumably to minimise steric interactions with the two chlorine atoms.

The chromium imido distances of 1.673(2) and 1.671(3) Å for Cr–N(1) and Cr–N(2) respectively are relatively long compared to those found in four coordinate chromium imido complexes[4,5] a possible consequence of the increased electron count at the metal centre leading to a reduction in metal-ligand bond orders. The two angles about the imido nitrogen atoms differ greatly however, with Cr–N(2)–C(13) within the expected range for linear imido ligands at 172.6(2)°, but the Cr–N(1)–C(1) angle of 148.9(2)° is closer to the theoretical value of 120° for a two electron 'bent' imido ligand.[13] It is unlikely that the apical imido ligand is donating only two electrons to the

metal centre, with the reduced Cr–N–C_{ipso} angle more likely a consequence of steric factors around the chromium.

3.3.4 Reaction of $Cr(NAr)_2Cl_2$ (14) with PMe_3 :

Formation of $Cr(NAr)_2Cl_2(PMe_3)$ (16).

An NMR scale reaction between the dichloride **14** and exactly one equivalent of PMe_3 in C_6D_6 results in the formation of the monophosphine adduct $Cr(NAr)_2Cl_2(PMe_3)$ (**16**). A sharp doublet centred at 1.53 ppm ($^2J_{PH}$ = 10.8Hz) is present in the ^1H NMR spectrum corresponding to PMe_3 that is bound to the chromium centre. The ^{31}P NMR spectrum indicates that all of the free phosphine has been consumed since no peak is evident at -62 ppm, the expected chemical shift for the phosphorus nucleus in uncoordinated PMe_3. A large peak at 5.16 ppm in the ^{31}P NMR spectrum is assigned to the bound PMe_3 ligand in **16**, and a smaller peak at 28.14 ppm is caused by an unidentified side product.

Removal of the solvent from the NMR tube and subjecting the residue to vacuum for one hour demonstrated the stability of complex **16** to vacuum. Reintroduction of C_6D_6 to the NMR tube and subsequent recording of the ^1H and ^{31}P NMR spectra revealed that the PMe_3 was still bound to the chromium centre.

Introduction of a further molar equivalent of PMe_3 to the sample *via* gas bulb resulted in rapid decomposition of the adduct. The proton NMR spectrum showed a broadening of all peaks consistent with paramagnetic side products, and a precipitate was also formed. ^{31}P NMR spectra indicated the presence of a small amount of **16** and a major new species with a phosphorus resonance at 30.88 ppm. This resonance is located within the range normally associated with phosphazene species of the type $Y_3P{=}NZ$, where the chemical shifts for the majority of such compounds are found in the range +50 to -50 ppm (e.g. $Me_3P{=}NH$ δ 13 ppm).[11]

It is therefore postulated that, due to steric crowding about the chromium in complex **16**, there is insufficient space to allow another molecule of PMe_3 to bind, rather it attacks the imido ligand to form the complex $Me_3P{=}NAr$ and paramagnetic

decomposition products. In an analogous reaction, Wilkinson reports the formation of the bis-phosphine complex $Cr(N\text{-}C_6H_2Me_3\text{-}2,4,6)_2Cl_2(PMe_3)_2$,[5] where the initial five coordinate monophosphine species is postulated to have sufficient space about the metal to allow the second molecule of PMe_3 to bind. The resulting six coordinate species is then stable to attack by the phosphine at the imido ligands.

Repeated attempts to scale up the reaction to allow isolation of either **16** or the postulated phosphazene were unsuccessful. No precipitate was observed when one equivalent of the phosphine was admitted to a toluene solution of **14**, and subsequent removal of the volatile component resulted only in an oily residue that could not be purified, though the presence of the product was identified by NMR. Reaction of **14** with excess PMe_3 to try and encourage decomposition and allow isolation of the putative phosphazene $Me_3P{=}NAr$ were also unsuccessful. Although a pale precipitate was observed to form, insufficient quantities were isolated to allow full characterisation.

3.3.5 Attempted Reaction of $Cr(NAr)_2Cl_2$ (14) with PPh_3.

Dr P.W. Dyer of this group has previously shown that PPh_3 will react with $Cr(N^tBu)_2Cl_2$ to form the monoadduct $Cr(N^tBu)_2Cl_2(PPh_3)$.[12] It was hoped that the use of a bulkier phosphine would allow isolation of either the adduct, or allow characterisation of the decomposition products.

Excess PPh_3 was added as a toluene solution to the dichloride and the mixture allowed to stir at ambient temperature for 4.5 hours. NMR spectroscopy (^1H and ^{31}P) showed that no reaction had occurred after this time, so the reaction was heated to 60°C and stirred for a further three days. Removal of the toluene and recrystallisation from pentane resulted in isolation of only starting materials, as identified by ^1H and ^{31}P NMR spectroscopy. The expected adduct formation, or decomposition did therefore not occur, most likely as a consequence of unfavourable steric interactions between the imido and phosphine phenyl substituents.

3.4 Attempted Synthesis of the [Cr(NR)$_3$] Functionality.

3.4.1 Introduction.

Initial publications by Wilkinson's group on the ^{t}butylimido chromium system report failure to access the tris-imido complex Cr(N^{t}Bu)$_3$ from the precursor Cr(N^{t}Bu)$_2$(NH^{t}Bu)Cl.[4a] It was hoped that changing the imido substituent to 2,6-^{i}Pr$_2$C$_6$H$_3$ may have a beneficial effect on the stability of such tris-imido complexes.

3.4.2 Using Cr(NAr)$_2$(NH^{t}Bu)Cl (12) as a Potential Precursor.

In order to synthesise the non-symmetrical tris imido complex Cr(NAr)$_2$(N^{t}Bu) from **12**, it is necessary to remove one molecule of HCl. NMR experiments have shown that this does not occur spontaneously on warming the sample to 60°. Reaction of **12** with the strong neutral base NEt$_3$ resulted only in the recovery of starting materials, as did reaction with the anionic base ^{t}BuLi. Attempts at generating Cr(NR)$_3$ during the initial formation of **12** by performing the amine exchange reaction in the presence of excess NEt$_3$ gave only Cr(NAr)$_2$(NH^{t}Bu)Cl on work-up.

There was no reaction between **12** and one equivalent of LiNHAr in Et$_2$O. It was hoped that formation of either Cr(NAr)$_2$(NH^{t}Bu)(NHAr) or Cr(NAr)$_2$(NHAr)Cl would result, providing another potential route into the desired complexes. Repeating the reaction in THF at 60°C gave a colour change from red-purple to green, indicative of reduction occurring. No tractable product was isolated from this reaction.

3.4.3 Using $Cr(NAr)_2Cl_2$ (14) as a Potential Precursor.

a) Reaction with LiNHAr :

Preparation of $Cr(NAr)_2(NHAr)Cl$ (17).

Although reaction of $Cr(N^tBu)_2Cl_2$ with LiNHAr gave only $Cr(NAr)_2(NH^tBu)Cl$ (**12**) on work up (see section 3.2.3), which itself does not react further with LiNHAr (see section 3.4.2), the reaction between $Cr(NAr)_2Cl_2$ and LiNHAr in THF proceeds smoothly to afford $Cr(NAr)_2(NHAr)Cl$ (**17**) in moderate yield. **17** can be extracted from LiCl using pentane as the solvent and, on cooling of this solution to ca. -30°C, small purple crystals of $Cr(NAr)_2(NHAr)Cl$ form (see equation 3.5)

$$\underset{\textbf{(14)}}{Cr(NAr)_2Cl_2} + LiNHAr \xrightarrow{THF} \underset{\textbf{(17)}}{Cr(NAr)_2(NHAr)Cl} + LiCl$$

Equation 3.5

The ^1H NMR spectrum again shows a low field shift for the amide proton at 12.22 ppm with the corresponding N-H stretch in the IR spectrum at 3345 cm^{-1}. The highly fluxional nature of this molecule is evident from the observation of only one well defined septet at room temperature due to the *iso*-propyl methine proton, the remaining signals having broadened into the baseline. A similar broadening is also evident for the *iso*-propyl doublets, although two set of aryl peaks are distinguishable in a 2:1 ratio, presumably corresponding to the imido and amido ligands respectively.

The proton decoupled ^{13}C NMR spectrum reflects the fluxionality of the molecule at room temperature, with many aromatic signals evident as broad singlets. Recording the spectrum at -80°C in D_8-toluene resolves these signals into two separate peaks, by slowing the molecular motions present within the molecule. The high field aliphatic ^{13}C NMR signals are not sufficiently resolved to allow unambiguous assignment.

A variable temperature ^1H NMR study of **17** in D_8-toluene from room temperature to -80°C causes the *iso*-propyl septet previously broadened into the baseline to sharpen, whilst the signal present at room temperature resolves itself into two separate septets. At -20°C there are three distinct signals at 4.06, 3.95 and 3.33 ppm each of equal intensity corresponding to two inequivalent imido ligands and the amide ligand. It can be assumed that the molecular motion has been slowed to such an extent at this temperature that the amide is 'frozen' on the NMR time scale in the position where its substituents are aligned towards the imido groups, thus rendering them inequivalent.

b) Molecular structure of $Cr(NAr)_2(NHAr)Cl$ (**17**).

Crystals of **17** suitable for an X-ray study were isolated from a concentrated pentane solution maintained at -30°C overnight and the structure of a crystal of dimensions 0.44 x 0.40 x 0.17 mm was solved at Newcastle by Prof W. Clegg and Dr M.R.J Elsegood. The molecular structure is illustrated in figure 3.5 and selected bond distances and angles appear in table 3.3.

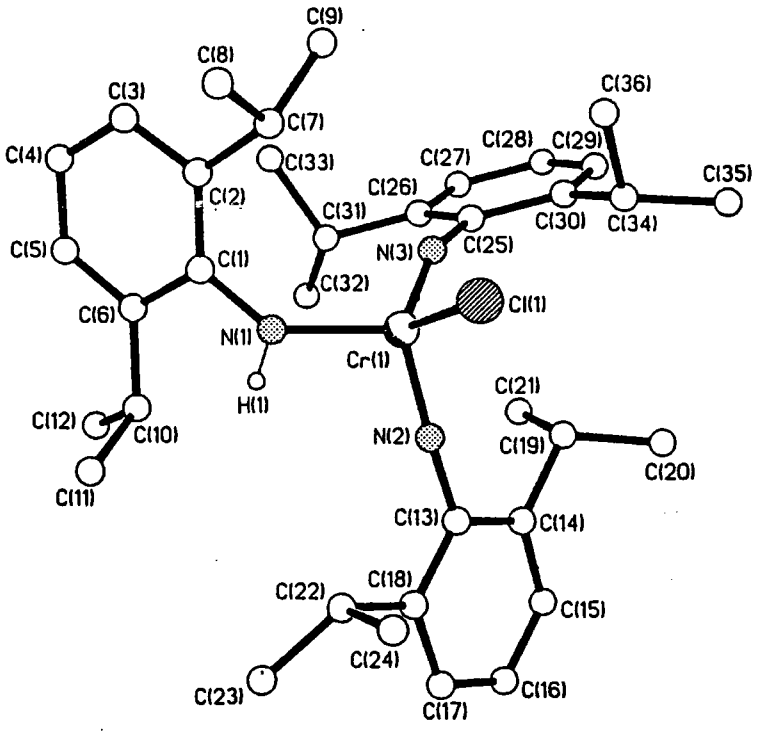

Figure 3.5 (a) Molecular structure of $Cr(NAr)_2(NHAr)Cl$ (**17**).

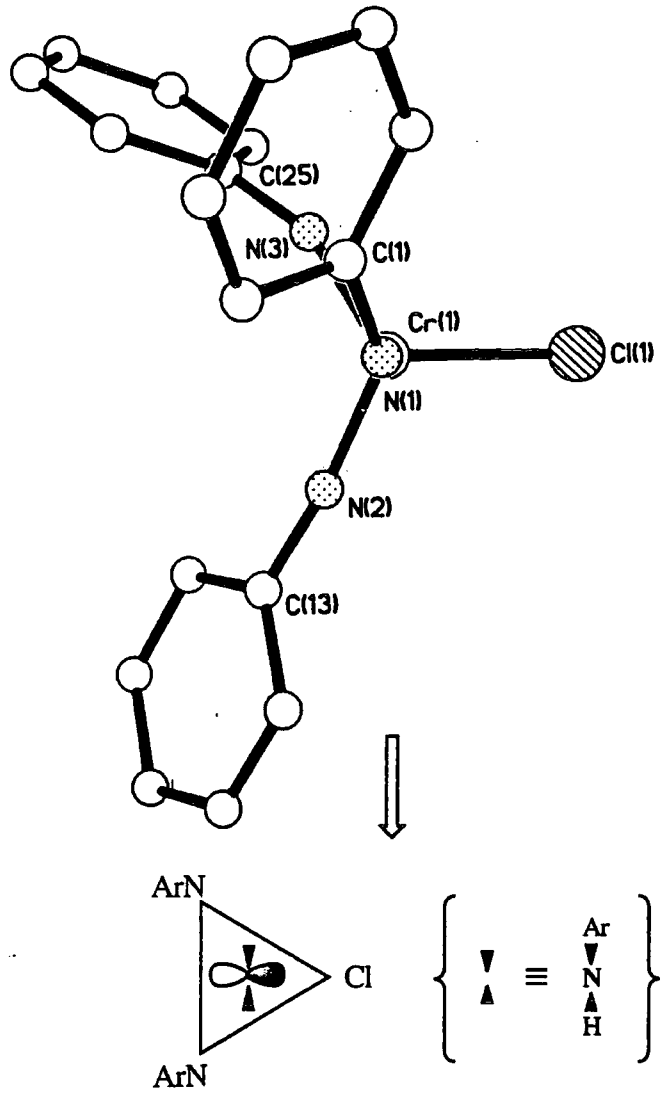

Figure 3.5 (b) View along the N(1)–Cr vector showing the arrangement of the amide substituents (*iso*-propyl groups omitted for clarity).

Cr–N(2)	1.651(3)	Cr–N(3)	1.657(3)
Cr–N(1)	1.843(3)	Cr–Cl	2.2297(10)
N(1)–C(1)	1.418(4)	C(1)–C(2)	1.404(5)
C(1)–C(6)	1.414(5)	C(2)–C(3)	1.399(5)
C(3)–C(4)	1.385(5)	C(4)–C(5)	1.374(5)
C(5)–C(6)	1.393(5)	N(2)–C(13)	1.386(4)
C(13)–C(14)	1.410(5)	C(13)–C(18)	1.415(5)
C(14)–C(15)	1.395(5)	C(15)–C(16)	1.375(5)
C(16)–C(17)	1.371(5)	C(17)–C(18)	1.394(5)
N(3)–C(25)	1.388(4)	C(25)–C(26)	1.408(4)
C(25)–C(30)	1.422(4)	C(26)–C(27)	1.393(5)
C(27)–C(28)	1.382(5)	C(28)–C(29)	1.396(5)
C(29)–C(30)	1.382(5)		

(C-C Distances of *iso*-propyl groups in the Range 1.495(5)–1.542(5) Å)

N(2)–Cr–N(3)	114.69(13)	N(2)–Cr–N(1)	105.34(13)
N(3)–Cr–N(1)	108.73(12)	N(2)–Cr–Cl	105.80(10)
N(3)–Cr–Cl	109.37(9)	N(1)–Cr–Cl	112.94(10)
C(1)–N(1)–Cr	135.6(2)	C(2)–C(1)–C(6)	121.9(3)
C(2)–C(1)–N(1)	119.9(3)	C(6)–C(1)–N(1)	118.1(3)
C(3)–C(2)–C(1)	117.8(3)	C(3)–C(2)–C(7)	118.7(3)
C(1)–C(2)–C(7)	123.4(3)	C(4)–C(3)–C(2)	121.0(4)
C(5)–C(4)–C(3)	120.3(3)	C(4)–C(5)–C(6)	121.7(3)
C(5)–C(6)–C(1)	117.4(3)	C(5)–C(6)–C(10)	121.6(3)
C(1)–C(6)–C(10)	121.1(3)	C(13)–N(2)–Cr	172.7(2)
N(2)–C(13)–C(14)	120.9(3)	N(2)–C(13)–C(18)	117.7(3)
C(14)–C(13)–C(18)	121.3(3)	C(15)–C(14)–C(13)	117.8(3)
C(15)–C(14)–C(19)	121.0(3)	C(13)–C(14)–C(19)	121.2(3)
C(16)–C(15)–C(14)	121.1(4)	C(17)–C(16)–C(15)	120.8(3)
C(16)–C(17)–C(18)	121.1(4)	C(17)–C(13)–C(18)	117.8(3)
C(17)–C(18)–C(22)	121.4(3)	C(13)–C(18)–C(22)	120.7(3)
C(25)–N(3)–Cr	157.3(2)	N(3)–C(25)–C(26)	119.4(3)
N(3)–C(25)–C(30)	118.6(3)	C(26)–C(25)–C(30)	122.0(3)
C(27)–C(26)–C(25)	117.7(3)	C(27)–C(26)–C(31)	121.2(3)
C(25)–C(26)–C(31)	121.2(3)	C(28)–C(27)–C(26)	121.8(3)
C(27)–C(28)–C(29)	119.1(3)	C(30)–C(29)–C(28)	122.3(3)
C(29)–C(30)–C(25)	117.1(3)	C(29)–C(30)–C(34)	122.8(3)
C(25)–C(30)–C(34)	120.2(3)		

(Angles within *iso*-propyl groups in the range 109.2(3)–115.0(3)°)

Table 3.2 Bond distances (Å) and angles (°) for $Cr(NAr)_2(NHAr)Cl$ (**17**).

The molecule is pseudo-tetrahedral about the chromium atom with angles in the range 105.34(13) – 114.69(13)°, the largest of which is located between the multiply bonded imido ligands as expected. The $Cr{=}N_{imido}$ bond lengths of 1.651(3) Å for Cr-N(2) and 1.657(3) Å for Cr-N(3) are comparable to those observed in the structures **12** and **15**, with the $Cr–N_{amide}$ bond of 1.843(3) Å slightly longer than that found in $Cr(NAr)_2(NH^tBu)Cl$ (1.813(3) Å). This is due to π-bonding between the amide nitrogen and the C_{ipso} atom of the aryl ring (1.418(4) Å cf. 1.479(6) Å for N(1)–C(1) in the amide ligand of **12**) causing a reduction in the $Cr–N_{amide}$ bond order. The angles at the imido nitrogen atoms consist of a near linear arrangement for Cr–N(2)–C(13) of 172.7(2)°, while the angle at N(3) is reduced to 157.3(2)°, a likely consequence of the presence of three large aryl groups about the chromium atom.

As for **13**, when viewed along the N(1)–Cr vector, the arrangement of the substituents on the amide ligand is such that they are aligned towards the imido groups

perpendicular to the Cr–Cl bond thus minimising competition for available π-bonds (see figure 3.5b).

3.5 Preparation and Reactivity of d^2 Chromium bis-Phosphine Complexes.

3.5.1 Introduction

Bis-phosphine complexes of Group 4 bent metallocenes[13] and Group 5 half sandwich imido species[14] have been previously reported in the literature, and have been shown to react with a variety of unsaturated substrates.

Dr. P.W. Dyer and Miss B. Whittle of this group extended this area of chemistry to include the bis-imido complexes of molybdenum,[15] where the nature of the imido ligand was found to have an important influence on the product. This is illustrated in equations 3.6 and 3.7, where the ^{t}butylimido ligand results in a binuclear imido-bridged species whereas the arylimido product is mononuclear.

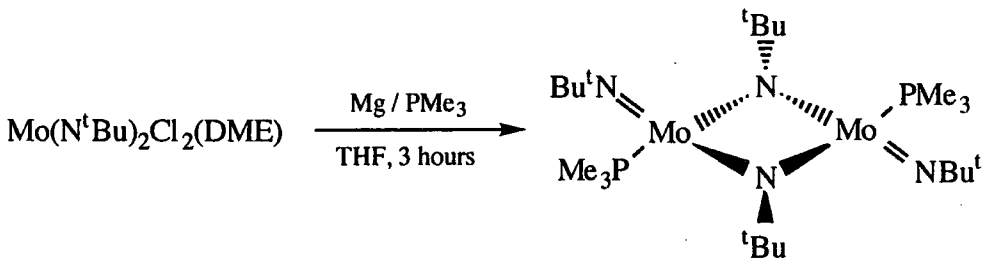

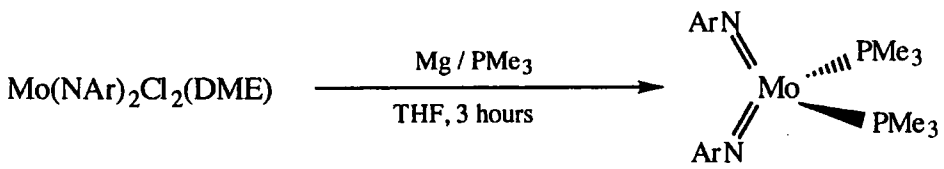

Equations 3.6 and 3.7 Reduction of bis-imido molybdenum complexes in the presence of PMe_3.

Attempts at reducing $Cr(N^tBu)_2Cl_2$ with magnesium, in the presence of PMe_3, resulted in isolation of a small amount of paramagnetic material, which could not be identified.[12]

3.5.2 Reduction of $Cr(NAr)_2Cl_2$ (14) with Mg in the Presence of PMe_3 :

Preparation of $Cr(NAr)_2(PMe_3)_2$ (18).

The reaction between $Cr(NAr)_2Cl_2$ (**14**) and magnesium was carried out in the presence of only a small excess of PMe_3 (2.1 equivalents compared to 4 equivalents for the above molybdenum examples) due to the suspected susceptibility of the imido ligand to attack by the phosphine (see section 3.3.4). The THF solution changes from red to green on warming to room temperature suggesting that a reductive process is occurring. Pure $Cr(NAr)_2(PMe_3)_2$ (**18**) is isolated as extremely air and moisture sensitive green crystals from a concentrated pentane solution at -30°C.

$$\underset{\textbf{(14)}}{Cr(NAr)_2Cl_2} + Mg \xrightarrow[THF]{PMe_3} \underset{\textbf{(18)}}{Cr(NAr)_2(PMe_3)_2} + MgCl_2$$

Equation 3.8.

Elemental analysis is in agreement with the mononuclear bisphosphine complex **18** as shown in equation 3.8. The ^1H NMR spectrum (figure 3.6) is consistent with a C_{2v} symmetry product in which the imido and phosphine ligands are equivalent. The doublet from the phosphine methyl groups remains sharp at room temperature in contrast to the equivalent signal in $Mo(NAr)_2(PMe_3)_2$ where $\upsilon_{1/2}$ = 36Hz, a possible indication of a more tightly bound PMe_3 ligand in the chromium case.

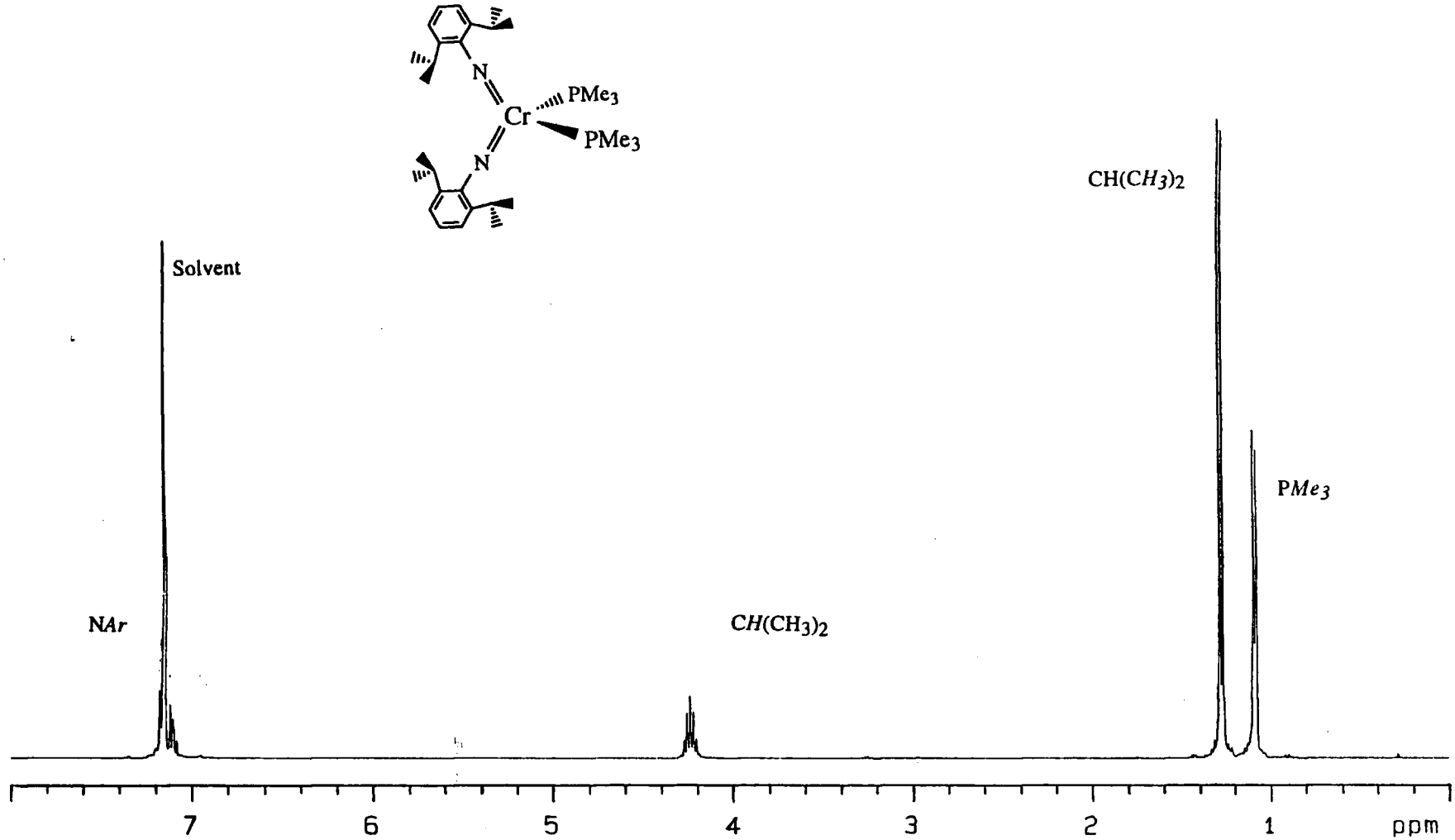

Figure 3.6 ^{1}H NMR spectrum (400MHz, C_6D_6) of $Cr(NAr)_2(PMe_3)_2$ (**18**)

3.5.3 Reduction of $Cr(NAr)_2Cl_2$ (14) with Mg in the Presence of PMe_2Ph :

Preparation of $Cr(NAr)_2(PMe_2Ph)_2$ (19).

In an analogous reaction between **14** and magnesium in the presence of PMe_2Ph, the bis-phosphine complex $Cr(NAr)_2(PMe_2Ph)_2$ (**19**) was isolated as a highly moisture and oxygen sensitive green crystalline compound. The ^1H NMR spectrum shows equivalent imido groups and the chemical shift of the bound phosphorus nuclei in the ^{31}P NMR spectrum is 68.09 ppm

Neither complex gave crystals of sufficient quality to allow a structural determination. Schrock *et al* however have predicted that d^2 bis-imido complexes will preferentially adopt a tetrahedral arrangement around the metal centre,[16] as observed in the complex $W(NAr)_2(PMePh_2)_2$.[17]

3.5.4 Reactions of $Cr(NAr)_2(PMe_3)_2$ (18) with Unsaturated Hydrocarbons (a Preliminary Investigation by NMR Spectroscopy).

Group 4 bent metallocene bis-phosphine complexes[13a] and the isolobal Group 5 half-sandwich imido analogues[14] have been shown to readily undergo reactions with a variety of unsaturated hydrocarbons. This has been extended to include bis-imido, bis-phosphine complexes of tungsten and molybdenum.[12,18] This section probed the reaction of $Cr(NAr)_2(PMe_3)_2$ (**18**) with ethylene, propylene and diphenylacetylene in attempts to observe the formation of adducts.

The reaction between $Cr(NAr)_2(PMe_3)_2$ (**18**) and ten equivalents of ethylene shows a rapid reaction (by NMR). There is a shift of all the imido signals in the ^1H NMR spectrum to higher field, and the collapse of the P*Me*$_3$ doublet into a broad signal, possibly indicating a rapid exchange process with free phosphine. There are also two new broad signals at 2.91 and 2.13 ppm, possibly from the interaction of ethylene with the chromium centre. The ^{31}P NMR spectrum shows that ca. 95% of the starting material has been converted to a new species which gives a broad resonance at 40.21

ppm. The resonances at 2.91 and 2.13 ppm do not sharpen on cooling to -80°C in CD_2Cl_2 and prolonged standing in this solvent led to decomposition after 12 hours.

By contrast, the attempted reaction with excess propylene failed to form a new complex, even after prolonged heating to 60°C (several weeks). Both the ^1H and ^{31}P NMR spectra were consistent with the presence of unreacted starting materials. This is presumably due to the methyl substituent on the olefin causing more steric crowding at the metal centre.

A reaction between **18** and one equivalent of C_2Ph_2 was carried out in a sealed NMR tube. No reaction occurred at room temperature, but heating the mixture to 60°C resulted in the formation of a new complex tentatively assigned as $Cr(NAr)_2(PhC{\equiv}CPh)(PMe_3)$. The ^1H NMR spectrum showed new aromatic signals for the acetylene phenyl groups and a upfield shift of the *iso*-propyl methine septet of the imido ligands. The presence of free PMe_3 was indicated by a broad signal to high field.

The ^{31}P NMR spectrum also indicated that PMe_3 had been liberated in the reaction (broad peak at -62 ppm), and that the starting material had been converted to a new species with a phosphorus chemical shift of 30.89 ppm. It did not prove possible to drive the reaction to completion implying an equilibrium between **18** and the acetylene adduct. Further studies will be required on reactions of $Cr(NAr)_2(PMe_3)_2$ with unsaturated hydrocarbons in order to isolate and fully characterise the products.

3.6 Summary.

A route into bis(arylimido) chromium chemistry has been successfully developed for Ar = 2,6-$^{i}Pr_2C_6H_3$. The dichloride (**14**) can be easily accessed *via* treatment of $Cr(NAr)_2(NH^tBu)Cl$ (**12**) with BCl_3 providing a convenient entry point into a range of novel complexes (see figure 3.7).

The arylimido ligand allows the chromium (IV) bis-phosphine complexes $Cr(NAr)_2(PMe_3)_2$ (**18**) and $Cr(NAr)_2(PMe_2Ph)_2$ (**19**) to be isolated as crystalline solid materials. Complex **18** has been shown to react with both ethylene and diphenylacetylene on an NMR scale.

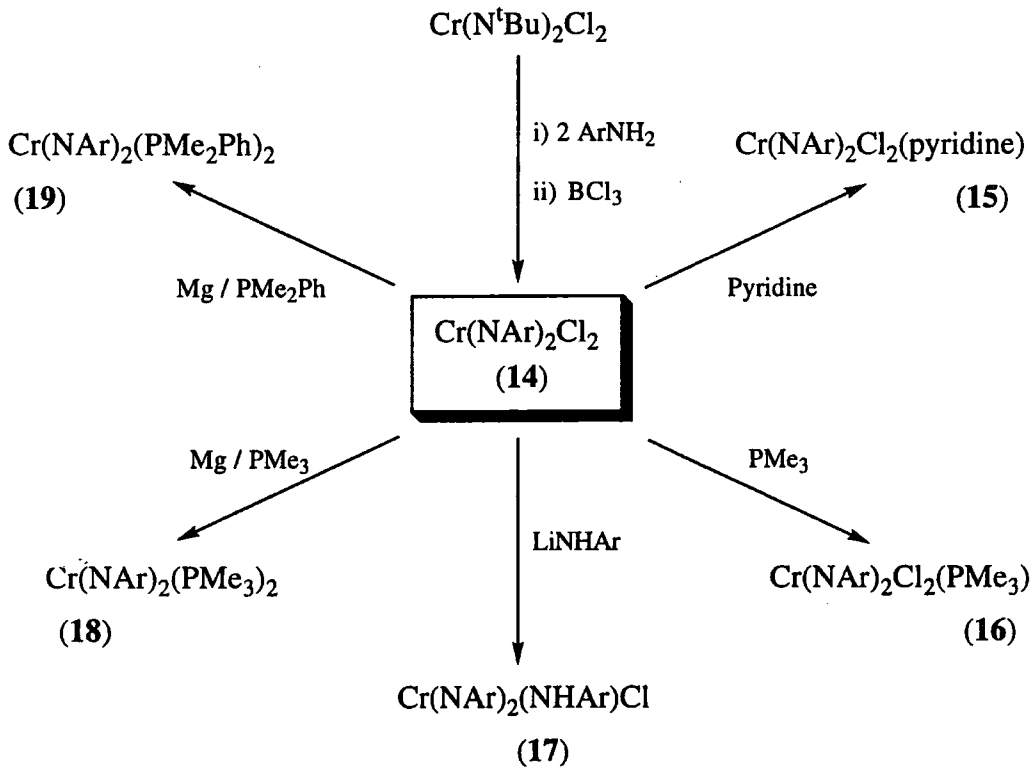

Figure 3.7 Summary of reactions of $Cr(NAr)_2Cl_2$ (**14**).

3.7 References.

1. N. Meijboom, C.J. Schaverien and A.G. Orpen, *Organometallics*, **1990**, *9*, 774.

2. (a) A. Bell, W. Clegg, P.W. Dyer, M.R.J. Elsegood, V.C. Gibson and E.L. Marshall, *J. Chem. Soc., Chem. Commun.*, **1994**, 2247. (b) A. Bell, W. Clegg, P.W. Dyer, M.R.J. Elsegood, V.C. Gibson and E.L. Marshall, *J. Chem. Soc., Chem. Commun.*, **1994**, 2547. (c) A. Barker, A. Bell, C. Beresford, M.C.W. Chan, W. Clegg, M.P. Coles, P.W. Dyer, M.R.J. Elsegood, V.C. Gibson, E.L. Marshall, *manuscript in preparation.*

3. M.P. Coles, C.I. Dalby, V.C. Gibson, W. Clegg and M.R.J. Elsegood, *Polyhedron*, **1995**, *14*, 2455.

4. (a) A.A. Danopoulos, Wa-Hung Leung, G. Wilkinson, B. Hussain-Bates and M.B. Hursthouse, *Polyhedron*, **1990**, *21*, 2625. (b) M.B. Hursthouse, M. Motevalli, A.C. Sullivan and G. Wilkinson, *J. Chem. Soc., Chem. Commun.*, **1986**, 1398. (c) M.B. Hursthouse, M. Motevalli, A.C. Sullivan and G. Wilkinson, *J. Chem. Soc. Dalton Trans.*, **1988**, 53. (d) W.-H. Leung, A.A. Danopoulos, G. Wilkinson, B. Hussain-Bates and M.B. Hursthouse, *J. Chem. Soc. Dalton Trans.*, **1991**, 2051. (e) Hon-Wah Lam, G. Wilkinson, B. Hussain-Bates and M.B. Hursthouse, *J. Chem. Soc. Dalton Trans.*, **1993**, 1477.

5. A.A. Danopoulos, G. Wilkinson, T.K.N. Sweet and M.B. Hursthouse, *J. Chem. Soc. Dalton Trans.*, **1995**, 2111.

6. W.A. Nugent and R.L. Harlow, *Inorg. Chem.*, **1980**, *19*, 777 ; D. M.-T. Chan, W.C. Fultz, W.A. Nugent, D.C. Roe and T.H. Tulip, *J. Am. Chem. Soc.*, **1985**, *107*, 251 ; P. Legzdins, S.J. Rettig and K.J. Ross, *Organometallics*, **1993**, *12*, 2103 ; N. Bryson, M.-T. Youinou and J.A. Osborn, *Organometallics*, **1991**, *10*, 3389.

7. V.C. Gibson, *J. Chem. Soc. Dalton Trans.*, **1994**, 1607 ; V.C. Gibson, *Angew. Chem. Int. Ed. Engl.*, **1994**, *33*, 1565.

8. M. Jolly, Ph.D. Thesis, University of Durham, 1994.

9. See this thesis, section 2.4.4.

10. W.A. Nugent and J.M. Mayer, *"Metal Ligand Multiple Bonds"*, Wiley and Sons, New York, 1988.

11. J.C. Tebby and S.S. Krishnamurthy, *"CRC Handbook of Phosphorus-31 Nuclear Magnetic Resonance Data"*, Chapter 14, p409.

12. P.W. Dyer, Ph.D. Thesis, University of Durham, 1994.

13. (a) L.B. Kool, M.D. Rausch, H.G. Alt, M. Heberhold, U. Thewalt and B. Wolf, *Angew. Chem. Int. Ed. Engl.*, **1985**, *24*, 394. (b) L.B. Kool, M.D. Rausch, H.G. Alt, M. Heberhold, B. Honold and U. Thewalt, *J. Organomet. Chem.*, **1987**, *320*, 37. (c) T. Takahashi, D.R. Swanson and E. Negishi, *Chem. Letters*, **1987**, 623.

14. A.D. Poole, Ph.D. Thesis, University of Durham, 1992 ; U. Siemeling and V.C. Gibson, *J. Organomet. Chem.*, **1992**, *426*, C25 ; A.D. Poole, V.C. Gibson and W. Clegg, *J. Chem. Soc., Chem. Commun.*, **1992**, 237 ; A.D. Poole and V.C. Gibson, *J. Chem. Soc., Chem. Commun.*, **1995**, 2261.

15. (a) P.W. Dyer, V.C. Gibson, J.A.K. Howard, B. Whittle and C. Wilson, *J. Chem. Soc., Chem. Commun.*, **1992**, 1666. (b) P.W. Dyer, V.C. Gibson, J.A.K. Howard and C. Wilson, *J. Organomet. Chem.*, **1993**, *462*, C15. (c) P.W. Dyer, V.C. Gibson, J.A.K. Howard, B. Whittle and C. Wilson, *Polyhedron*, **1995**, *14*, 103. (d) B. Whittle, M.Sc. Thesis, University of Durham, 1993.

16. D.S. Williams, M.H. Schofield, J.T. Anhaus and R.R. Schrock, *J. Am. Chem. Soc.*, **1990**, *112*, 6728 ; M.H. Schofield, T.P. Kee, J.T. Anhaus, R.R. Schrock, K.H. Johnson and W.M. Davis, *Inorg. Chem.*, **1991**, *30*, 3595.

17. J.T. Anhaus, T.P. Kee, M.H. Schofield and R.R. Schrock, *J. Am. Chem. Soc.*, **1990**, *112*, 1642.

18. D.S. Williams, M.H. Schofield and R.R. Schrock, *Organometallics*, **1993**, *12*, 4560.

Chapter Four

Alkyl and Alkylidene Complexes of Bis(Arylimido) Chromium.

4.1 Introduction

Chromium alkyl derivatives are of considerable interest as precursors to well-defined α-olefin polymerisation catalysts. In this chapter, syntheses of bis(arylimido) chromium alkyl derivatives are addressed where it was envisaged that the arylimido group might lend stability and crystallinity to such species.

4.2 Synthesis of $Cr(NAr)_2R_2$ (R = 2,4,6-$Me_3C_6H_2$; CH_2Ph ; CH_3 ; CH_2CMe_2Ph ; CH_2CMe_3).

4.2.1 Reaction of $Cr(NAr)_2Cl_2$ (14) with 2,4,6-$Me_3C_6H_2MgBr$:

Preparation of $Cr(NAr)_2(C_6H_2Me_3$-2,4,6$)_2$ (20).

Previous work by Wilkinson *et al*[1] has shown that aryl complexes of the Group 6 triad (where aryl = 2,4,6-$Me_3C_6H_2$; 2,6-$Me_2C_6H_3$; *o*-MeC_6H_4) can be accessed *via* the reaction of the bis-siloxide species with the aryl Grignard reagent. This allowed isolation of the first σ-organochromium (VI) compound $Cr(N^tBu)_2(C_6H_2Me_3$-2,4,6$)_2$ (equation 4.1).

$$M(N^tBu)_2(OSiR_3)_2 + R'MgBr \longrightarrow M(N^tBu)_2R'_2 + 'MgBr(OSiR_3)'$$

M = Cr, Mo : R = Me
W : R = Ph

M = Cr : R' = mesityl ; 2,6 xylyl
Mo : R' = mesityl ; 2,6 xylyl ; *o*-tolyl
W : R' = mesityl ; 2,6 xylyl

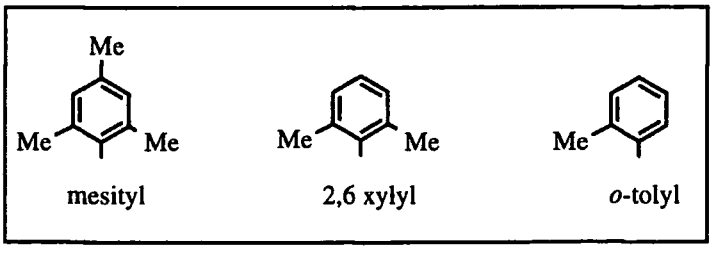

Equation 4.1

However the bis-siloxide species have not proved to be good precursors to dialkyl derivatives.[2] We were prompted therefore to explore the use of the dichloride **14** as an entry point into both the aryl and alkyl chemistry of the bis(arylimido) chromium fragment.

The reaction between **14** and the mesityl Grignard reagent 2,4,6-$Me_3C_6H_2MgBr$ proceeds smoothly according to equation 4.2 to afford **20** as a yellow-green crystalline complex in good yield. The ^1H NMR spectrum (400MHz, C_6D_6) shows typical shifts for the methyl groups of the mesityl ligands, with the *ortho*-substituents resonating at 2.97 ppm and the *para*-methyl group being found at 2.08 ppm. The mesityl group exhibits a low-field ^{13}C NMR shift of 202.91 ppm for the *ipso*-carbon atom bonded directly to the chromium atom.

$$Cr(NAr)_2Cl_2 + 2,4,6\text{-}Me_3C_6H_2MgBr \xrightarrow{Et_2O} Cr(NAr)_2(C_6H_2Me_3\text{-}2,4,6)_2 + \text{'MgBrCl'}$$

(14) **(20)**

Equation 4.2

There is no evidence either for coupling of the mesityl groups, or migration of this group to the imido nitrogen atom as Nugent observed in the similar reaction between $Cr(N^tBu)_2(OTMS)_2$ and diphenylzinc.[3] This is a likely consequence of the steric protection afforded by the *ortho*-methyl substituents.

4.2.2 Reaction of $Cr(NAr)_2Cl_2$ (14) with $PhCH_2MgCl$:

Preparation of $Cr(NAr)_2(CH_2Ph)_2$ (21).

Having previously demonstrated that $Cr(N^tBu)_2(CH_2Ph)_2$ (**1**) is a precursor to cationic alkyl species that are active for the polymerisation of ethylene,[4] an important

goal was to synthesise analogous compounds bearing new imido ligands in order to allow stereo-electronic effects to be probed. The reaction between $Cr(NAr)_2Cl_2$ (**14**) and $PhCH_2MgCl$ in Et_2O readily forms the arylimido complex $Cr(NAr)_2(CH_2Ph)_2$ (**21**) in good yield as dark green crystals.

The room temperature ^1H NMR spectrum (400MHz, C_6D_6) is consistent with a C_{2v} symmetric species in solution as shown by equivalent imido and benzyl ligands. There is a marked low field shift of the benzyl methylene proton signal to δ 3.41 compared with values of δ 2.49 and δ 2.57 for the ^{t}butylimido and adamantylimido analogues respectively. It is possible that changing the nature of the imido group maybe having a large effect on the bonding of the benzyl ligands, or alternatively the downfield shift may arise as a consequence of a ring-current effect associated with the aryl substituents of the imido ligands.

To further understand these changes in the bonding of the alkyl groups to the metal centre and to determine whether an η^1 / η^2 bonding pattern is retained for the benzyl ligands in **21**, a single crystal X-ray study was performed at the University of Newcastle upon Tyne.

4.2.3 Molecular Structure of $Cr(NAr)_2(CH_2Ph)_2$ (21).

Single crystals of **21** were isolated from a concentrated pentane solution at -30°C, and a crystal of dimensions 0.37 x 0.16 x 0.16 mm was mounted under an inert oil. The molecular structure was solved and is illustrated in figure 4.1 below, with selected bond lengths and angles presented in table 4.1

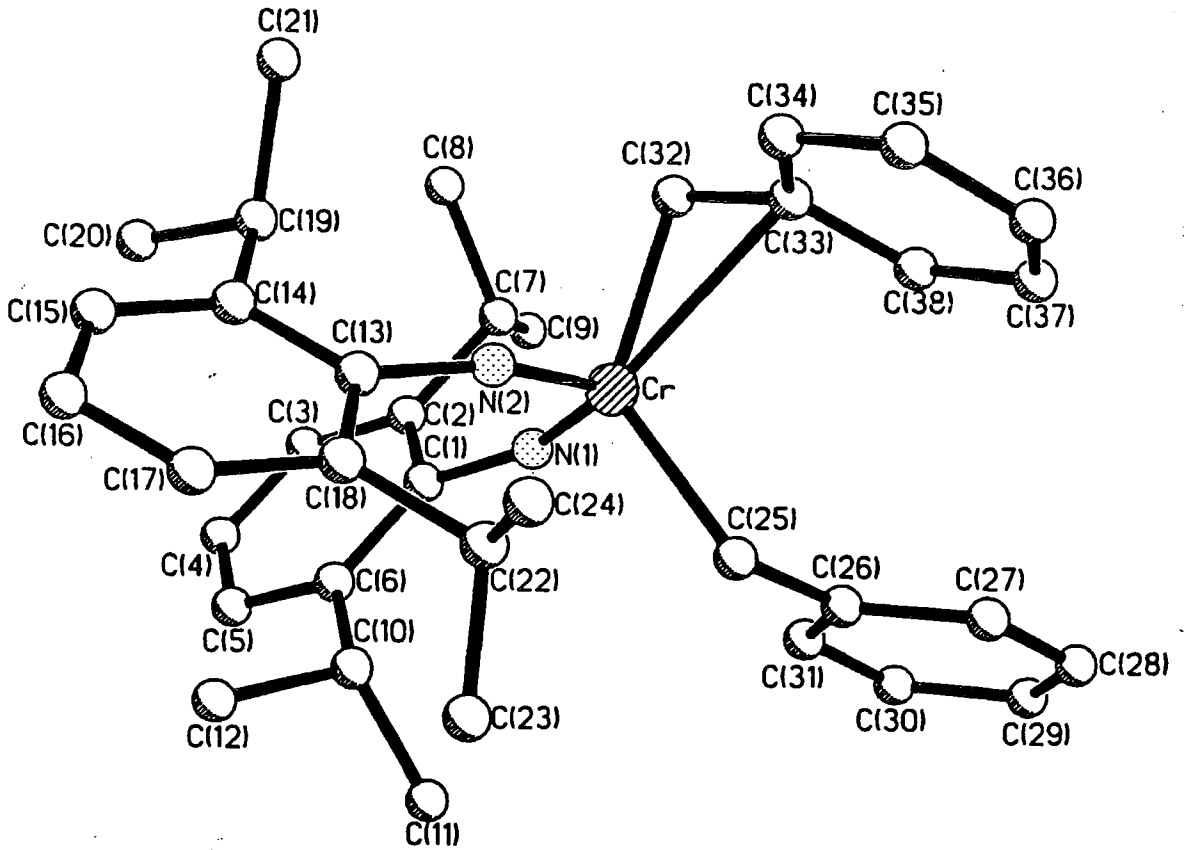

Figure 4.1 Molecular structure of $Cr(NAr)_2(CH_2Ph)_2$ (**21**).

Cr–N(1)	1.650(4)	Cr–N(2)	1.660(4)
Cr–C(32)	2.040(5)	Cr–C(25)	2.077(4)
Cr–C(33)	2.498(5)	N(1)–C(1)	1.396(6)
C(1)–C(6)	1.416(7)	C(1)–C(2)	1.428(6)
C(2)–C(3)	1.395(7)	C(3)–C(4)	1.377(8)
C(4)–C(5)	1.384(7)	C(5)–C(6)	1.398(6)
N(2)–C(13)	1.377(6)	C(13)–C(18)	1.411(7)
C(13)–C(14)	1.422(6)	C(14)–C(15)	1.376(7)
C(15)–C(16)	1.402(8)	C(16)–C(17)	1.374(7)
C(17)–C(18)	1.378(8)	C(25)–C(26)	1.505(7)
C(26)–C(31)	1.377(7)	C(26)–C(27)	1.416(7)
C(27)–C(28)	1.378(7)	C(28)–C(29)	1.366(7)
C(29)–C(30)	1.378(8)	C(30)–C(31)	1.387(7)
C(32)–C(33)	1.463(7)	C(33)–C(34)	1.399(7)
C(33)–C(38)	1.406(8)	C(34)–C(35)	1.387(8)
C(35)–C(36)	1.368(9)	C(36)–C(37)	1.371(9)
C(37)–C(38)	1.384(8)		

(C-C Distances of *iso*-propyl groups in the range 1.449(9)–1.540(7) Å)

N(1)–Cr–N(2)	109.7(2)	N(1)–Cr–C(32)	105.9(2)
N(2)–Cr–C(32)	104.4(2)	N(1)–Cr–C(25)	103.6(2)
N(2)–Cr–C(25)	103.3(2)	C(32)–Cr–C(25)	129.1(2)
N(1)–Cr–C(33)	137.3(2)	N(2)–Cr–C(33)	100.7(2)
C(32)–Cr–C(33)	35.8(2)	C(25)–Cr–C(33)	97.4(2)
C(1)–N(1)–Cr	154.2(3)	N(1)–C(1)–C(6)	121.0(4)
N(1)–C(1)–C(2)	117.9(4)	C(6)–C(1)–C(2)	121.1(4)
C(3)–C(2)–C(1)	117.1(5)	C(3)–C(2)–C(7)	121.5(4)
C(1)–C(2)–C(7)	121.4(4)	C(4)–C(3)–C(2)	122.1(5)
C(3)–C(4)–C(5)	120.7(5)	C(4)–C(5)–C(6)	120.4(5)
C(5)–C(6)–C(1)	118.7(5)	C(5)–C(6)–C(10)	120.5(5)
C(1)–C(6)–C(10)	120.8(4)	C(13)–N(2)–Cr	157.8(3)
N(2)–C(13)–C(18)	118.7(4)	N(2)–C(13)–C(14)	120.3(4)
C(18)–C(13)–C(14)	121.0(5)	C(15)–C(14)–C(13)	116.9(4)
C(15)–C(14)–C(19)	122.4(4)	C(13)–C(14)–C(19)	120.6(4)
C(14)–C(15)–C(16)	122.8(5)	C(17)–C(16)–C(15)	118.4(5)
C(16)–C(17)–C(18)	122.5(5)	C(17)–C(18)–C(13)	118.3(4)
C(17)–C(18)–C(22)	121.6(5)	C(13)–C(18)–C(22)	120.1(5)
C(26)–C(25)–Cr	117.0(3)	C(31)–C(26)–C(27)	116.9(5)
C(31)–C(26)–C(25)	122.7(5)	C(27)–C(26)–C(25)	120.3(4)
C(28)–C(27)–C(26)	120.9(5)	C(29)–C(28)–C(27)	120.9(5)
C(28)–C(29)–C(30)	119.2(5)	C(29)–C(30)–C(31)	120.4(5)
C(26)–C(31)–C(30)	121.6(5)	C(33)–C(32)–Cr	89.4(3)
C(34)–C(33)–C(38)	117.1(5)	C(34)–C(33)–C(32)	123.0(5)
C(38)–C(33)–C(32)	119.8(5)	C(34)–C(33)–Cr	111.1(4)
C(38)–C(33)–Cr	101.2(3)	C(32)–C(33)–Cr	54.7(2)
C(35)–C(34)–C(33)	121.5(5)	C(36)–C(35)–C(34)	119.1(6)
C(35)–C(36)–C(37)	121.8(6)	C(36)–C(37)–C(38)	119.1(6)
C(37)–C(38)–C(33)	121.3(6)		

(Angles within *iso*-propyl groups in the range 109.2(5)–113.5(4)°)

Table 4.1 Bond distances (Å) and angles (°) for $Cr(NAr)_2(CH_2Ph)_2$ (**21**).

The benzyl ligands are present in an η^1 / η^2 bonding pattern as observed for $Cr(N^tBu)_2(CH_2Ph)_2$ (**1**) and deduced for $Cr(NAd)_2(CH_2Ph)_2$ (**9**). The main bond parameters for both benzyl ligands are collected in table 4.2 with the corresponding values for **1**, enabling comparisons to be made between the two molecules.

Bond Length or Bond Angle	**$Cr(N^tBu)_2(CH_2Ph)_2$ (1)**	**$Cr(NAr)_2(CH_2Ph)_2$ (21)**
η^1-benzyl		
$Cr–CH_2$	2.096(3) Å	2.077(4) Å
$Cr–CH_2–C_{ipso}$	114.73(13)°	117.0(3)°
η^2-benzyl		
$Cr–CH_2$	2.071(2) Å	2.040(5) Å
$Cr–C_{ipso}$	2.357(2) Å	2.498(5) Å
$Cr–CH_2–C_{ipso}$	82.16(11)°	89.4(3)°

Table 4.2 Bond lengths and angles for the η^1 and η^2 benzyl ligands in **1** and **21**.

The bond distances and angles for the η^2-benzyl ligand again fall into the expected range for such a bonding mode. Both the η^1 and η^2 $Cr–CH_2$ bond lengths are shorter for **21** compared with **1** most likely as a consequence of the greater electrophilicity of the chromium centre in **21**. This is caused by a reduction in bond order between the imido groups and the chromium centre for **21**, arising from π-bonding between the imido nitrogen and the *ipso*-carbon of the aryl group (evident from the reduction in $N_{imido}–C$ bond length from 1.446(av) Å in **1** to 1.387(av) Å in **21**).

The η^2-interaction in **21**, however, seems to be weaker than that observed in **1**, with an increase in the $Cr–C_{ipso}$ distance from 2.357(2) Å to 2.498(5) Å and a corresponding increase in the $Cr–CH_2–C_{ipso}$ angle of 7.24°. This maybe a consequence of more effective σ-bonding between chromium and the two methylene carbon atoms of the benzyl ligands or due to increased steric repulsion between the arylimido substituents and the η^2-benzyl ligand.

4.2.4 Preliminary Testing of $Cr(NAr)_2(CH_2Ph)_2$ (21) as a Catalyst Precursor for the Polymerisation of Ethylene.

A polymerisation experiment was performed using the ethylene screening rig at Sunbury by Mr B.J. Mills and Dr. C.I. Dalby to evaluate the effect that changing the imido group would have on the polymerisation activity. The anilinium salt $[PhNMe_2H][B(C_6F_5)_4]$ was employed to generate the alkyl cation and the procedure was identical to that described in section 6.2.2. The experiment was performed at 50°C under 10 atmospheres of ethylene for 60 minutes, resulting in isolation of 14.5g of polyethylene. This corresponds to an activity of 18.9 g $mmol^{-1}$ hr^{-1} bar^{-1}.

This is some what lower than the ^{t}butylimido analogue (57.8 g $mmol^{-1}$ hr^{-1} bar^{-1}) and may be a result of stronger binding of the aniline by-product to the more electrophilic chromium centre. A way of overcoming this potential problem is to use the trityl salt $[Ph_3C][B(C_6F_5)_4]$ to generate the cation, where the 1,1,1,2-tetraphenylethane side product is unlikely to coordinate to the metal centre.

4.2.5 Reaction of $Cr(NAr)_2Cl_2$ (14) with MeMgBr :

Preparation of $Cr(NAr)_2(CH_3)_2$ (22).

Amongst the bent metallocene dialkyl complexes active for the polymerisation of α-olefins, the bis-benzyl and dimethyl compounds have proved to be the most readily converted to the cationic alkyl complex necessary for polymerisation to proceed.[5] The dimethyl complexes also allow neutral boron species (e.g. $B(C_6F_5)_3$) to be employed in the generation of the alkyl cation.

Although the bis-benzyl complexes $Cr(NR)_2(CH_2Ph)_2$ (where R = ^{t}Bu ; Ad ; Ar) have been successfully synthesised, the corresponding dimethyl complexes have thus far remained elusive. Schaverien reports the synthesis of $Cr(N^tBu)_2(CH_3)_2$,[2] but he was only able to isolate it as an impure oil. Our attempts to prepare the analogous adamantylimido complex resulted only in isolation of a paramagnetic species that we were unable to characterise.

The reaction between **14** and methylmagnesium bromide however proceeds smoothly to afford the very air and moisture sensitive dimethyl complex $Cr(NAr)_2(CH_3)_2$ (**22**), according to equation 4.3. Although too soluble in hydrocarbon solvents to allow ready recrystallisation, the complex can be recovered as a deep green microcrystalline solid from a concentrated acetonitrile solution at -30°C.

$$Cr(NAr)_2Cl_2 + 2\,MeMgBr \xrightarrow{Et_2O} Cr(NAr)_2(CH_3)_2 + \text{'MgBrCl'}$$

(14) **(22)**

Equation 4.3

The ^1H NMR spectrum shows a singlet resonance at 1.83 ppm with a corresponding ^{13}C NMR signal at 49.73 ppm ($^1J_{CH}$=130.45Hz) for the metal-bound methyl carbons. These data are closely comparable to the analogous molybdenum complex $Mo(NAr)_2(CH_3)_2$[6] whose crystal structure has been determined to reveal a monomeric structure.

4.2.6 Reaction of $Cr(NAr)_2Cl_2$ (14) with $PhMe_2CCH_2MgCl$:

Preparation of $Cr(NAr)_2(CH_2CMe_2Ph)_2$ (23).

The bis-neophyl complex $Cr(NAr)_2(CH_2CMe_2Ph)_2$ (**23**) can be isolated as a dark green crystalline compound from the reaction between the dichloride **14** and 2-methyl-2-phenylpropyl magnesium chloride.

The ^1H NMR spectrum (400MHz, C_6D_6) reveals equivalent imido and alkyl ligands about the metal centre with the neophyl methylene groups resonating at δ 2.15, a shift value comparable to other bis-neophyl complexes. The corresponding ^{13}C NMR signal at 96.23 ppm differs by ca. 7 ppm from those observed in both the ^{t}butyl and adamantylimido cases (86.1 and 85.5 ppm respectively), but is similar to the shift for an arylimido complex recently reported by Wilkinson and co-workers (92.8 ppm).[8]

4.2.7 Molecular Structure of $Cr(NAr)_2(CH_2CMe_2Ph)_2$ (23).

Dark green crystals of **23** were grown from a concentrated pentane solution maintained at -30°C, and a crystal of dimensions 0.56 x 0.36 x 0.26 mm was isolated and its structure solved at Newcastle. The asymmetric unit contains two crystallographically independent molecules, one of which is shown in figure 4.2; bond lengths and angles for both molecules are given in table 4.3.

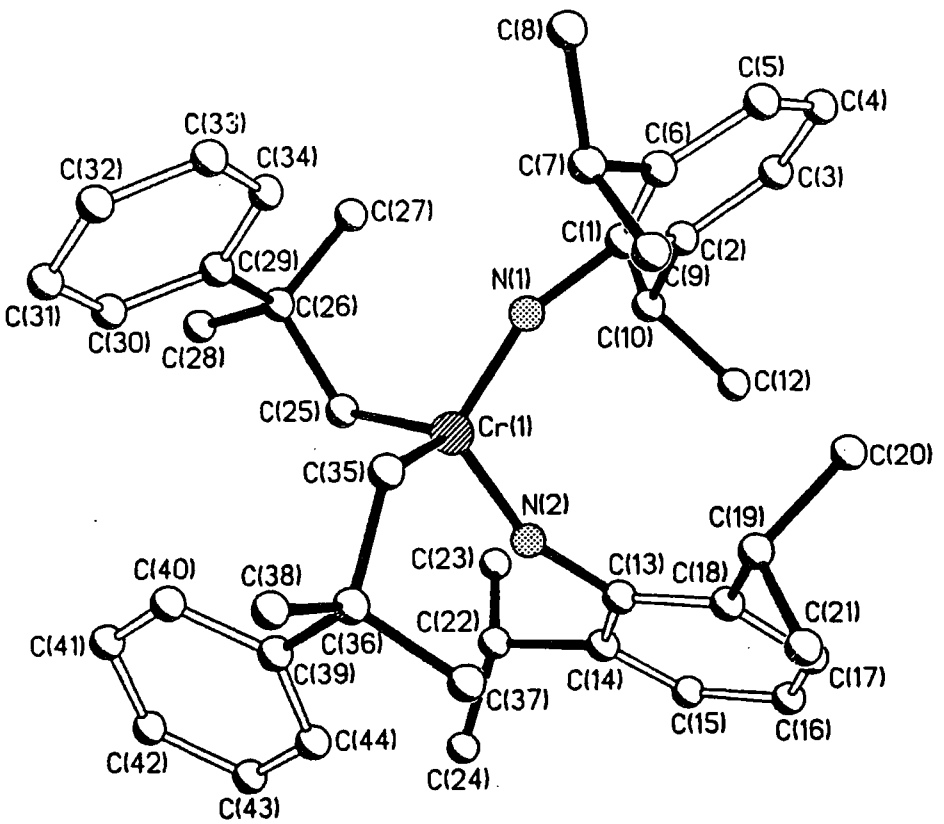

Figure 4.2 Molecular structure of $Cr(NAr)_2(CH_2CMe_2Ph)_2$ (**23**).

Molecule (i).

Cr(i)–N(2i)	1.640(4)	Cr(i)–N(1i)	1.649(4)
Cr(i)–C(25i)	2.021(5)	Cr(i)–C(35i)	2.021(5)
N(1i)–C(1i)	1.390(6)	C(1i)–C(6i)	1.407(7)
C(1i)–C(2i)	1.418(7)	C(2i)–C(5i)	1.387(7)
C(3i)–C(4i)	1.372(7)	C(3i)–C(6i)	1.394(7)
C(4i)–C(5i)	1.381(7)	N(2i)–C(13i)	1.386(6)
C(13i)–C(14i)	1.419(7)	C(13i)–C(18i)	1.423(7)
C(14i)–C(15i)	1.388(7)	C(15i)–C(16i)	1.371(8)
C(16i)–C(17i)	1.383(8)	C(17i)–C(18i)	1.390(7)
C(25i)–C(26i)	1.540(7)	C(26i)–C(27i)	1.531(7)
C(26i)–C(29i)	1.542(7)	C(26i)–C(28i)	1.547(7)
C(35i)–C(36i)	1.549(7)	C(36i)–C(37i)	1.523(7)
C(36i)–C(39i)	1.537(8)	C(36i)–C(38i)	1.556(7)

N(2i)–Cr(i)–N(1i)	113.3(2)	N(2i)–Cr(i)–C(25i)	105.2(2)
N(1i)–Cr(i)–C(25i)	106.5(2)	N(2i)–Cr(i)–C(35i)	107.4(2)
N(1i)–Cr(i)–C(35i)	107.6(2)	C(25i)–Cr(i)–C(35i)	117.2(2)
C(1i)–N(1i)–Cr(i)	158.2(4)	N(1i)–C(1i)–C(2i)	117.5(4)
N(1i)–C(1i)–C(6i)	121.7(4)	C(2i)–C(1i)–C(6i)	120.8(5)
C(5i)–C(2i)–C(1i)	118.1(5)	C(5i)–C(2i)–C(7i)	120.9(5)
C(1i)–C(2i)–C(7i)	121.0(5)	C(4i)–C(3i)–C(6i)	121.5(5)
C(3i)–C(4i)–C(5i)	119.8(5)	C(4i)–C(5i)–C(2i)	121.7(5)
C(3i)–C(6i)–C(1i)	118.0(5)	C(3i)–C(6i)–C(10i)	118.9(5)
C(1i)–C(6i)–C(10i)	123.0(5)	C(13i)–N(2i)–Cr(i)	158.9(4)
N(2i)–C(13i)–C(14i)	118.0(5)	N(2i)–C(13i)–C(18i)	121.3(5)
C(14i)–C(13i)–C(18i)	120.7(5)	C(15i)–C(14i)–C(13i)	118.3(5)
C(15i)–C(14i)–C(22i)	121.0(5)	C(13i)–C(14i)–C(22i)	120.6(5)
C(16i)–C(15i)–C(14i)	121.4(5)	C(15i)–C(16i)–C(17i)	120.2(6)
C(16i)–C(17i)–C(18i)	121.9(5)	C(17i)–C(18i)–C(13i)	117.4(5)
C(17i)–C(18i)–C(19i)	119.6(5)	C(13i)–C(18i)–C(19i)	122.9(5)
C(26i)–C(25i)–Cr(i)	121.3(4)	C(27i)–C(26i)–C(25i)	110.8(4)
C(27i)–C(26i)–C(29i)	111.3(5)	C(25i)–C(26i)–C(29i)	110.3(4)
C(27i)–C(26i)–C(28i)	106.4(5)	C(25i)–C(26i)–C(28i)	107.3(4)
C(29i)–C(26i)–C(28i)	110.6(4)	C(36i)–C(35i)–Cr(i)	120.0(4)
C(37i)–C(36i)–C(39i)	112.4(5)	C(37i)–C(36i)–C(35i)	112.4(5)
C(39i)–C(36i)–C(35i)	110.4(4)	C(37i)–C(36i)–C(38i)	107.6(5)
C(39i)–C(36i)–C(38i)	108.5(5)	C(35i)–C(36i)–C(38i)	107.5(4)

Molecule (ii).

Cr(ii)–N(2ii)	1.643(4)	Cr(ii)–N(1ii)	1.643(4)
Cr(ii)–C(25ii)	2.023(5)	Cr(ii)–C(35ii)	2.027(5)
N(1ii)–C(1ii)	1.390(6)	C(1ii)–C(6ii)	1.415(7)
C(1ii)–C(2ii)	1.418(7)	C(2ii)–C(5ii)	1.385(7)
C(3ii)–C(4ii)	1.383(8)	C(3ii)–C(6ii)	1.373(8)
C(4ii)–C(5ii)	1.391(7)	N(2ii)–C(13ii)	1.386(6)
C(13ii)–C(14ii)	1.415(7)	C(13ii)–C(18ii)	1.422(7)
C(14ii)–C(15ii)	1.381(7)	C(15ii)–C(16ii)	1.378(8)
C(16ii)–C(17ii)	1.388(8)	C(17ii)–C(18ii)	1.386(7)
C(25ii)–C(26ii)	1.539(7)	C(26ii)–C(27ii)	1.523(8)
C(26ii)–C(29ii)	1.533(7)	C(26ii)–C(28ii)	1.552(7)
C(35ii)–C(36ii)	1.547(7)	C(36ii)–C(37ii)	1.535(7)
C(36ii)–C(39ii)	1.535(7)	C(36ii)–C(38ii)	1.538(7)

N(2ii)–Cr(ii)–N(1ii)	112.1(2)	N(2ii)–Cr(ii)–C(25ii)	106.3(2)
N(1ii)–Cr(ii)–C(25ii)	105.6(2)	N(2ii)–Cr(ii)–C(35ii)	107.1(2)
N(1ii)–Cr(ii)–C(35ii)	106.5(2)	C(25ii)–Cr(ii)–C(35ii)	119.4(2)
C(1ii)–N(1ii)–Cr(ii)	155.6(4)	N(1ii)–C(1ii)–C(2ii)	121.6(5)
N(1ii)–C(1ii)–C(6ii)	117.7(5)	C(2ii)–C(1ii)–C(6ii)	120.8(5)
C(5ii)–C(2ii)–C(1ii)	118.3(5)	C(5ii)–C(2ii)–C(7ii)	121.4(5)
C(1ii)–C(2ii)–C(7ii)	120.4(5)	C(4ii)–C(3ii)–C(6ii)	121.1(5)
C(3ii)–C(4ii)–C(5ii)	120.3(5)	C(4ii)–C(5ii)–C(2ii)	121.6(5)
C(3ii)–C(6ii)–C(1ii)	117.9(5)	C(3ii)–C(6ii)–C(10ii)	118.4(5)
C(1ii)–C(6ii)–C(10ii)	123.7(5)	C(13ii)–N(2ii)–Cr(ii)	161.8(4)
N(2ii)–C(13ii)–C(14ii)	117.4(4)	N(2ii)–C(13ii)–C(18ii)	121.6(5)
C(14ii)–C(13ii)–C(18ii)	121.0(5)	C(15ii)–C(14ii)–C(13ii)	117.6(5)
C(15ii)–C(14ii)–C(22ii)	119.9(5)	C(13ii)–C(14ii)–C(22ii)	122.5(5)
C(16ii)–C(15ii)–C(14ii)	122.2(5)	C(15ii)–C(16ii)–C(17ii)	119.7(5)
C(16ii)–C(17ii)–C(18ii)	121.3(5)	C(17ii)–C(18ii)–C(13ii)	118.2(5)
C(17ii)–C(18ii)–C(19ii)	121.0(5)	C(13ii)–C(18ii)–C(19ii)	120.7(5)

C(26ii)–C(25ii)–Cr(ii)	118.6(4)	C(27ii)–C(26ii)–C(25ii)	112.3(5)
C(27ii)–C(26ii)–C(29ii)	110.4(4)	C(25ii)–C(26ii)–C(29ii)	109.6(4)
C(27ii)–C(26ii)–C(28ii)	107.0(5)	C(25ii)–C(26ii)–C(28ii)	108.7(4)
C(29ii)–C(26ii)–C(28ii)	108.7(4)	C(36ii)–C(35ii)–Cr(ii)	122.7(3)
C(37ii)–C(36ii)–C(39ii)	110.6(4)	C(37ii)–C(36ii)–C(35ii)	106.9(4)
C(39ii)–C(36ii)–C(38ii)	110.9(4)	C(37ii)–C(36ii)–C(38ii)	111.3(4)
C(39ii)–C(36ii)–C(38ii)	110.2(4)	C(35ii)–C(36ii)–C(38ii)	106.8(4)

Table 4.3 Bond distances (Å) and angles (°) for $Cr(NAr)_2(CH_2CMe_2Ph)_2$ (**23**).

The arrangement of ligands about the chromium is pseudo tetrahedral, with angles in the range 105.2(2)–117.2(2)° for molecule (i) and 105.6(2)–119.4(2)° for molecule (ii). The Cr=N distances of 1.644 Å (av) molecule (i) and 1.643 Å (av) molecule (ii) are comparable to those observed in other structures presented in this work, as are the Cr=N–Ar angles of 158.6° (av) molecule (i) and 158.7° (av) molecule (ii). Unexpectedly, the Cr-C_α distances in **23** do not show a significant shortening when compared to the adamantylimido analogue, in contrast to the comparison between the ^{t}butylimido and arylimido bis-benzyl structures, indicating that a steric influence may be more important in determining the M–C distances rather than electrophilicity.

Surprisingly, the largest angle about the chromium atom is located between the two alkyl ligands and not the two imido groups, where repulsion of the π-electron density in the two multiple bonds may be expected to force the ligands apart. Calculations performed on the compound $Cr(N^tBu)_2(C_6H_2Me_3\text{-}2,4,6)_2$,[1] where the largest angle in the CrN_2C_2 tetrahedron is located between the ancillary aryl ligands, show that there is no significant steric interaction between the ^{t}butyl groups of the imido ligands. The most likely explanation for the distribution of angles in this case is the interaction of a C–H bond of one of the *ortho*-methyl groups with the metal centre, prompting investigation into the interaction of the alkyl ligands with the chromium in complex **23.**

Unfortunately, the crystals of **23** were of insufficient quality to allow detection of the hydrogen atoms to any degree of accuracy. The coupling constant of 125.88Hz for the methylene carbon atom is in the range found for hydrogens attached to a 'normal' sp^3 hybridised carbon. This $^1J_{CH}$ value, however, may arise as a result of

averaging of 'normal' and agostic C–H bonds as detailed in section 2.4.7. No evidence of α-agostic interactions were observable in the Nujol mull IR spectrum of **23**.

4.2.8 Reaction of $Cr(NAr)_2Cl_2$ (14) with Me_3CCH_2MgCl :

Preparation of $Cr(NAr)_2(CH_2CMe_3)_2$ (24).

The bis-neopentyl complex $Cr(NAr)_2(CH_2CMe_3)_2$ (**24**) was synthesised in an analogous manner to the bis-neophyl complex **23** (see equation 4.4).

$$Cr(NAr)_2Cl_2 + 2\,Me_3CCH_2MgCl \xrightarrow{Et_2O} Cr(NAr)_2(CH_2CMe_3)_2 + MgCl_2$$

(14) **(24)**

Equation 4.4

The elemental analysis is consistent with displacement of both chlorides to give the dialkyl complex **24**. ^1H NMR spectrum again shows equivalent imido and alkyl ligands consistent with C_{2v} symmetry about the metal centre.

4.2.9 Molecular Structure of $Cr(NAr)_2(CH_2CMe_3)_2$ (24).

Maintaining a concentrated pentane solution of **24** at -30°C for 48 hours afforded crystals of suitable quality for an X-ray study at Newcastle. A crystal of dimensions 0.57 x 0.55 x 0.48 mm was selected and mounted under an inert oil. The molecular structure is shown in figure 4.3 with selected bond lengths and angles collected in table 4.4.

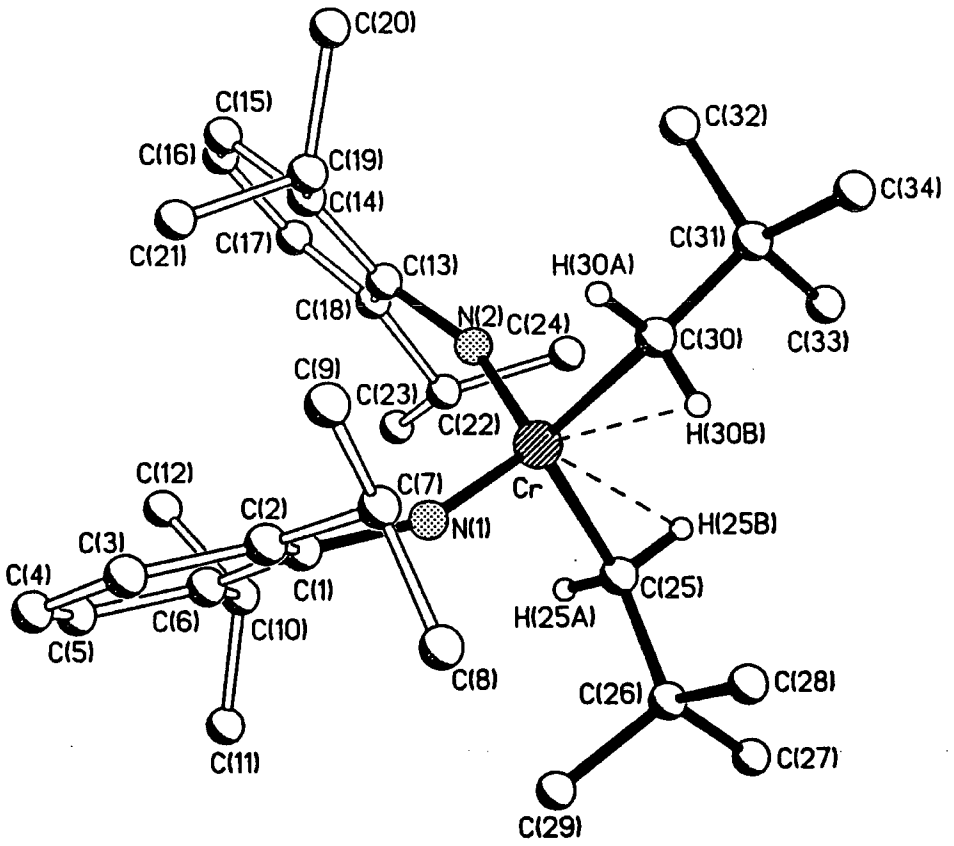

Figure 4.3 Molecular structure of $Cr(NAr)_2(CH_2CMe_3)_2$ (**24**).

Cr–N(2)	1.642(2)	Cr–N(1)	1.646(2)
Cr–C(25)	2.030(2)	Cr–C(30)	2.042(2)
N(1)–C(1)	1.392(3)	C(1)–C(6)	1.414(3)
C(1)–C(2)	1.418(3)	C(2)–C(3)	1.383(3)
C(3)–C(4)	1.387(3)	C(4)-C(5)	1.373(3)
C(5)–C(6)	1.393(3)	N(2)–C(13)	1.394(3)
C(13)–C(14)	1.411(3)	C(13)–C(18)	1.419(3)
C(14)–C(15)	1.395(3)	C(15)–C(16)	1.376(3)
C(16)–C(17)	1.384(3)	C(17)–C(18)	1.385(3)
C(25)–C(26)	1.534(3)	C(26)–C(29)	1.529(3)
C(26)–C(28)	1.530(3)	C(26)–C(27)	1.535(3)
C(30)–C(31)	1.540(3)	C(31)–C(32)	1.526(3)
C(31)–C(33)	1.528(3)	C(31)–C(34)	1.536(3)

(C-C Distances of *iso*-propyl groups in the range 1.512(4)–1.534(3) Å)

N(2)–Cr–N(1)	111.71(8)	N(2)–Cr–C(25)	107.18(9)
N(1)–Cr–C(25)	105.84(9)	N(2)–Cr–C(30)	106.15(9)
N(1)–Cr–C(30)	106.97(9)	C(25)–Cr–C(30)	119.07(9)
C(1)–N(1)–Cr	156.2(2)	N(1)–C(1)–C(6)	121.5(2)
N(1)–C(1)–C(2)	117.4(2)	C(6)–C(1)–C(2)	121.1(2)
C(3)–C(2)–C(1)	118.1(2)	C(3)–C(2)–C(7)	121.7(2)
C(1)–C(2)–C(7)	120.1(2)	C(2)–C(3)–C(4)	121.3(2)
C(5)–C(4)–C(3)	120.0(2)	C(4)–C(5)–C(6)	121.8(2)
C(5)–C(6)–C(1)	117.7(2)	C(5)–C(6)–C(10)	119.3(2)
C(1)–C(6)–C(10)	123.1(2)	C(13)–N(2)–Cr	158.3(2)
N(2)–C(13)–C(14)	120.9(2)	N(2)–C(13)–C(18)	117.7(2)
C(14)–C(13)–C(18)	121.4(2)	C(15)–C(14)–C(13)	117.6(2)
C(15)–C(14)–C(19)	119.5(2)	C(13)–C(14)–C(19)	123.2(2)
C(16)–C(15)–C(14)	121.6(2)	C(15)–C(16)–C(17)	120.2(2)
C(16)–C(17)–C(18)	121.3(2)	C(17)–C(18)–C(13)	117.9(2)
C(17)–C(18)–C(22)	122.5(2)	C(13)–C(18)–C(22)	119.6(2)
C(26)–C(25)–Cr	119.9(2)	C(29)–C(26)–C(28)	109.4(2)
C(29)–C(26)–C(25)	110.6(2)	C(28)–C(26)–C(25)	111.2(2)
C(29)–C(26)–C(27)	108.6(2)	C(28)–C(26)–C(27)	108.8(2)
C(25)–C(26)–C(27)	108.2(2)	C(31)–C(30)–Cr	120.3(2)
C(32)–C(31)–C(33)	109.5(2)	C(32)–C(31)–C(34)	108.4(2)
C(33)–C(31)–C(34)	108.4(2)	C(32)–C(31)–C(30)	110.9(2)
C(33)–C(31)–C(30)	111.4(2)	C(34)–C(31)–C(30)	108.2(2)

(Angles within *iso*-propyl groups in the range 108.7(2)–113.9(2)°)

Table 4.4 Bond distances (Å) and angles (°) for $Cr(NAr)_2(CH_2CMe_3)_2$ (**24**).

Compound **24** crystallises as a single molecule per unit cell allowing an accurate determination of atomic positions. In particular, the hydrogens on the metal attached methylenes were located. The Cr=N distances of 1.642(2) and 1.646(2) Å are comparable to those found in the bis-neophyl complex, and the Cr=N-Ar angles of 156.2(2) and 158.3(2)° are also very similar.

There are two α-agostic interactions present (as for $Cr(NAd)_2(CH_2CMe_2Ph)_2$ (**10**)), one from each alkyl ligand of the complex, giving chromium hydrogen distances of 2.33 Å for each interaction. The reduction in Cr–C–H_α angles from predicted tetrahedral values to 97.2° for both Cr–C(25)–H(25B) and Cr–C(30)–H(30B) lend further support for the presence of such interactions.

Spectroscopically, the $^1J_{CH}$ value of 123.2Hz cannot be used to infer the presence of an agostic interaction, due to rapid averaging which weights the coupling constant towards a 'normal' sp^3-hybridised value. The IR spectrum (Nujol mull) also does not provide any conclusive evidence since no absorption is observed in the

appropriate region of the spectrum. It should be noted, however, that infra-red spectroscopy is not a reliable technique for detecting agostic interactions.

4.3 Reactions of the Dialkyl Complex $Cr(NAr)_2(CH_2CMe_3)_2$ (24).

4.3.1 Reaction of $Cr(NAr)_2(CH_2CMe_3)_2$ (24) with C_6D_6 :

Formation of $Cr(NAr)_2(CHDCMe_3)(C_6D_5)$ (25).

It was noted that on standing, a C_6D_6 solution of **24** in a sealed NMR tube slowly converted to a new species with 100% conversion over ca. 7 days at room temperature. The ^1H NMR spectrum of this new complex no longer exhibits a signal at δ 2.52 previously assigned to the protons of the neopentyl methylene group, but has been replaced by a broader signal of much lower intensity at δ 2.85. There also appears to be a reduction in the symmetry about the chromium centre, reflected in the *iso*-propyl methyl resonance which now appears as two doublets centred at 1.12 and 1.09 ppm. Also present in the spectrum is an intense singlet at 0.90 ppm assigned to free neopentane. The spectrum is shown in figure 4.4 along with that of the dialkyl precursor complex for comparison.

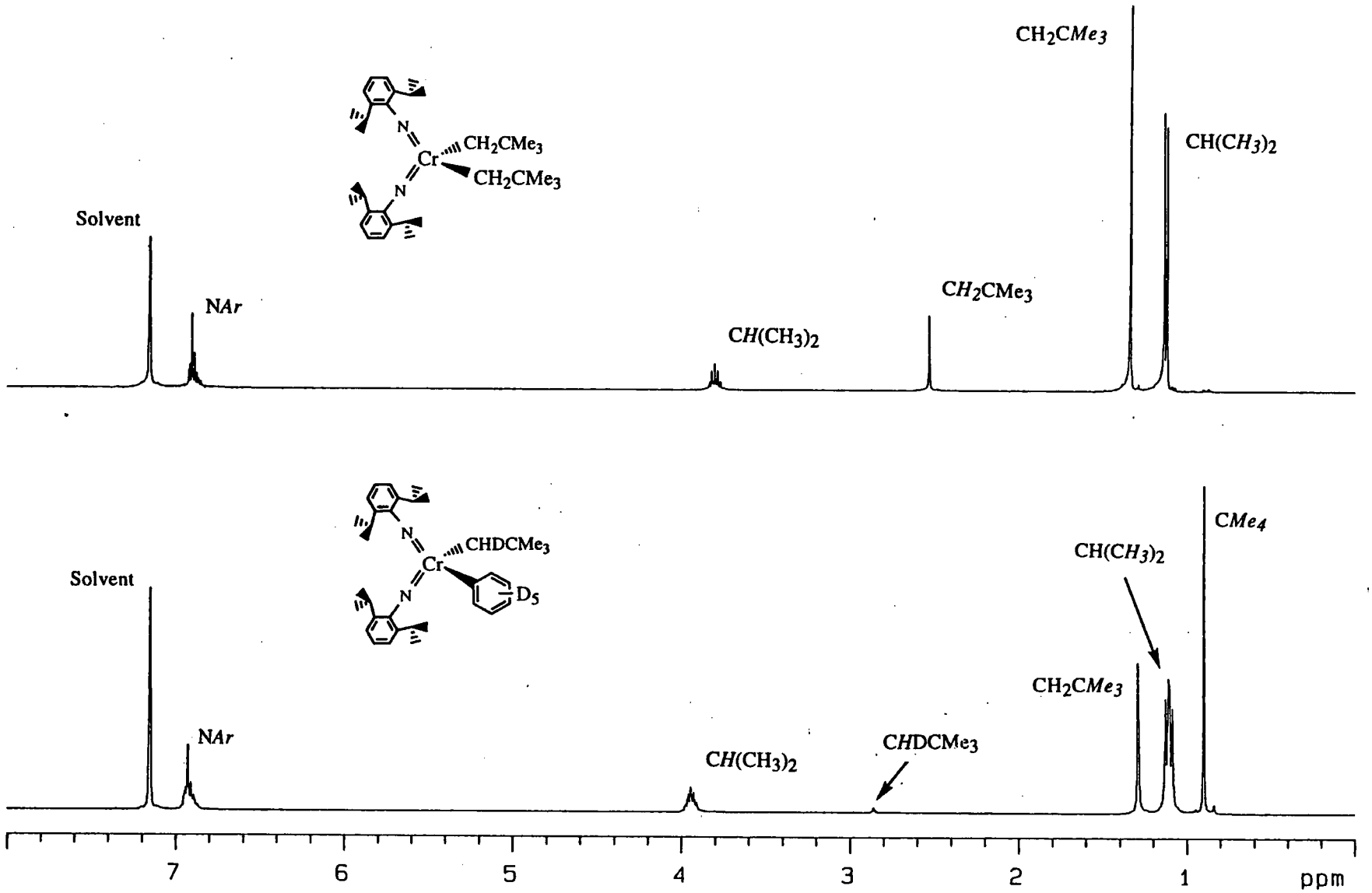

Figure 4.4 ^{1}H NMR spectra of (a) $Cr(NAr)_2(CH_2CMe_3)_2$ (**24**) and (b) $Cr(NAr)_2(CHDCMe_3)(C_6D_5)$ (**25**).

The generation of one equivalent of neopentane suggests that an α-H abstraction process is occurring to generate a bis-imido alkylidene species of the type $[Cr(NAr)_2(CHCMe_3)]$. Such a mechanism is well precedented in poly-alkyl complexes, and was first exploited by Schrock to synthesise the first tantalum alkylidene complex[9] (equation 4.5).

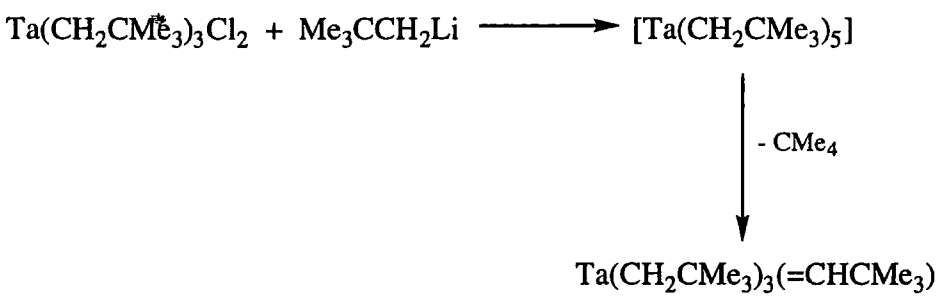

Equation 4.5

These species are typically characterised by a low field shift for both the α-proton and α-carbon atoms of the alkylidene ligand. A detailed examination of the NMR data revealed no such signals for **25** indicating the absence of an alkylidene ligand in the new complex. The ^{13}C NMR spectra, however, reveal 1:1:1 triplets at 192.17 ppm and 135.74 ppm suggesting that the deuterio solvent has become incorporated in the final product. The former resonance is assigned to the *ipso*-carbon of a deuterio phenyl ligand, experiencing a similar low field shift to that observed for C_{ipso} of the aryl ligands in $Cr(NAr)_2(C_6H_2Me_3\text{-}2,4,6)_2$ (**20**). The second signal can not be unambiguously assigned to a particular carbon of the phenyl ligand, and the other carbon resonances are coincident with the solvent peak. A 1:1:1 triplet at 97.98 ppm ($^1J_{CD}$=19.56Hz) is also present in the ^{13}C NMR spectrum and is assigned to the metal bound carbon of a mono-deuterated neopentyl ligand.

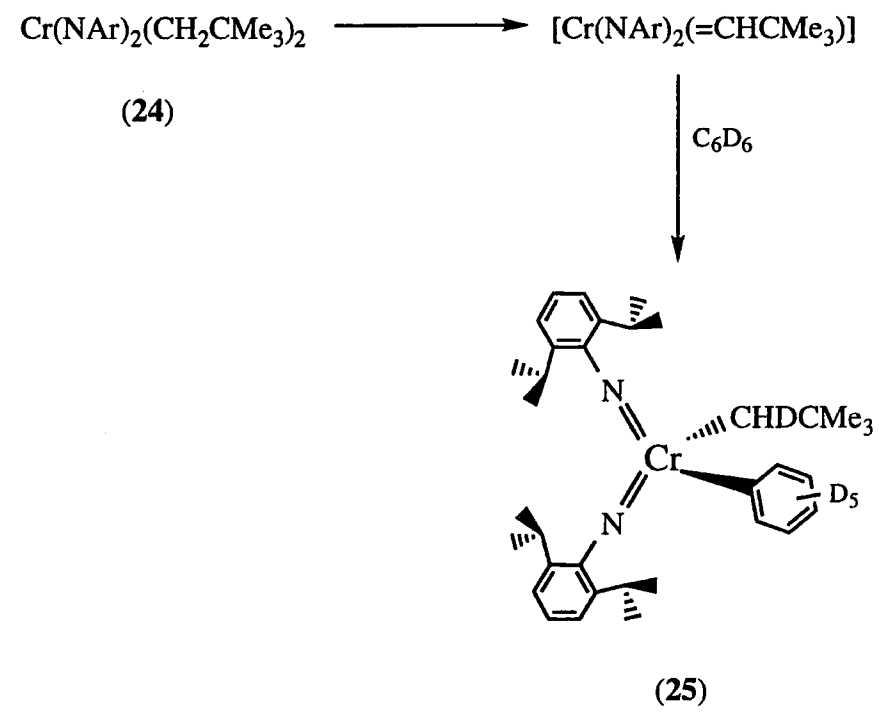

(24)

(25)

Equation 4.6

The broad peak at δ 2.85 in the ^{1}H NMR spectrum is therefore assigned to the methylene proton of the mono-deuterated neopentyl ligand C*H*DCMe$_3$, with the broadness attributed to its proximity to the deuterium atom with nuclear spin I=1. The overall reaction is summarised in equation 4.6.

In a recent publication by Hessen[10] the bent metallocene complex Cp$_2$Ti(CH$_2$CMe$_3$)$_2$ is also observed to undergo thermal α-H abstraction on attaining room temperature, eliminating neopentane and producing the nascent species [Cp$_2$Ti(=CHCMe$_3$)], which is isolobal to the putative [Cr(NAr)$_2$(=CHCMe$_3$)] complex. Hessen also found that in the absence of a base (e.g. PMe$_3$) to trap such a species, activation of C-H bonds (or C-D bonds) of the hydrocarbon solvent occurred across the metal-carbon double bond.

4.3.2 A Kinetic Study of the Conversion of $Cr(NAr)_2(CH_2CMe_3)_2$ (24) to $Cr(NAr)_2(CHDCMe_3)(C_6D_5)$ (25).

The conversion of **24** to **25** was followed by ^1H NMR spectroscopy (see figure 4.5), with experimental details presented in section 6.4.7.

For a first order process, A converting to B, the rate law is expressed as :

$$\frac{-d[A]}{dt} = k[A] \qquad \textbf{Equation 4.7}$$

A typical plot of concentration versus time is shown in figure 4.6.

If $[A]_t$ corresponds to the concentration of species A at time t, defining the boundary condition that the initial concentration of A at the commencement of the experiment (i.e. t = 0) is $[A]_0$, integration of equation 4.7 gives :

$$[A]_t = [A]_0 \exp(-kt) \qquad \textbf{Equation 4.8}$$

A log plot of the concentration of **24** versus time thus shows that the reaction is first order with respect to loss of **24** (see figure 4.7). Determination of the rate constant k can be achieved from a computer program to fit the best curve f(t) = a exp (-kt) + c for a first order exponential decay (figure 4.6), or by measuring the gradient of the line (equal to -k) in figure 4.7.

Figure 4.5 Conversion of $Cr(NAr)_2(CH_2CMe_3)_2$ (**26**) to $Cr(NAr)_2(CHDCMe_3)(C_6D_5)$ (**27**) with time.

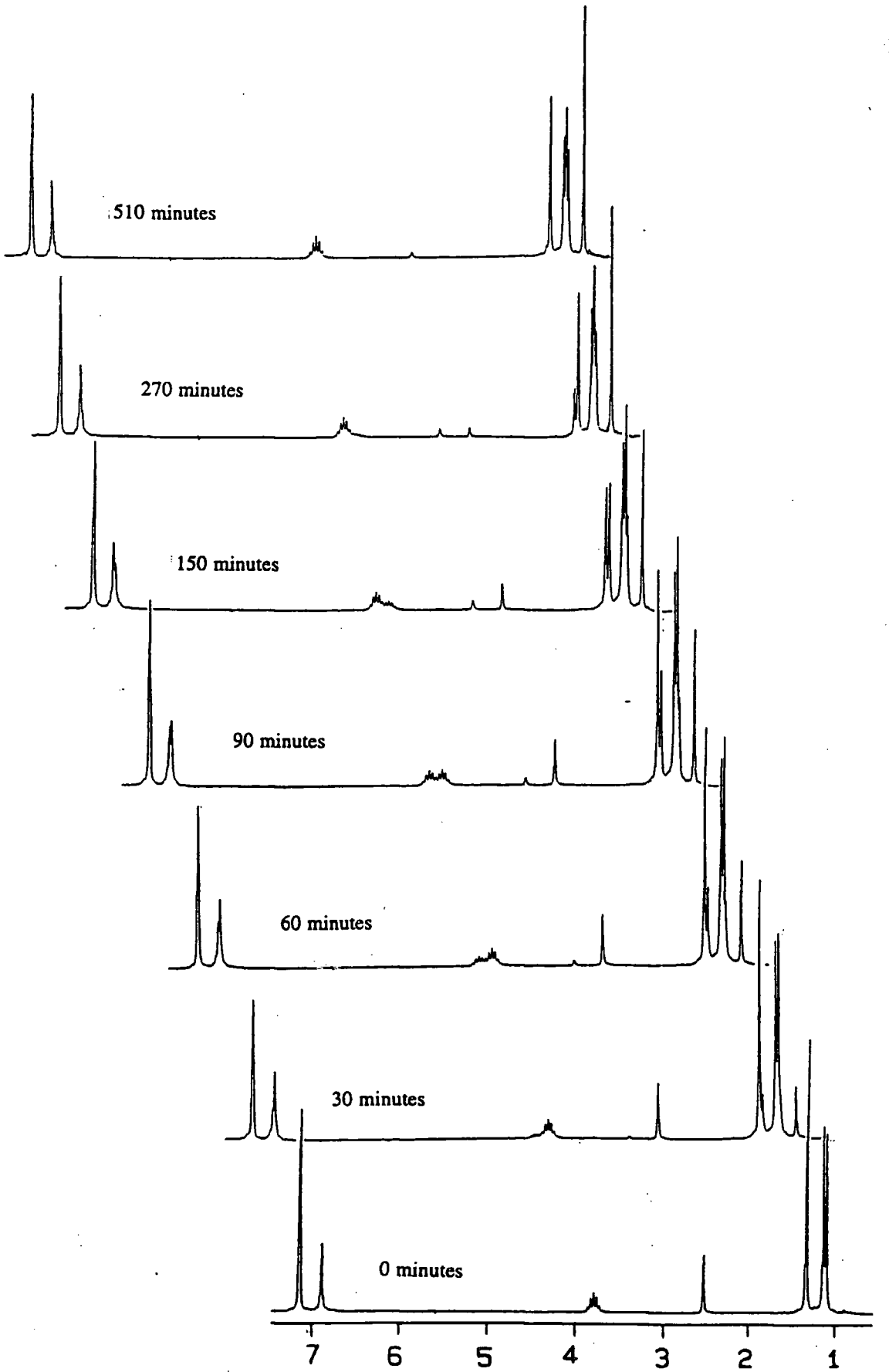

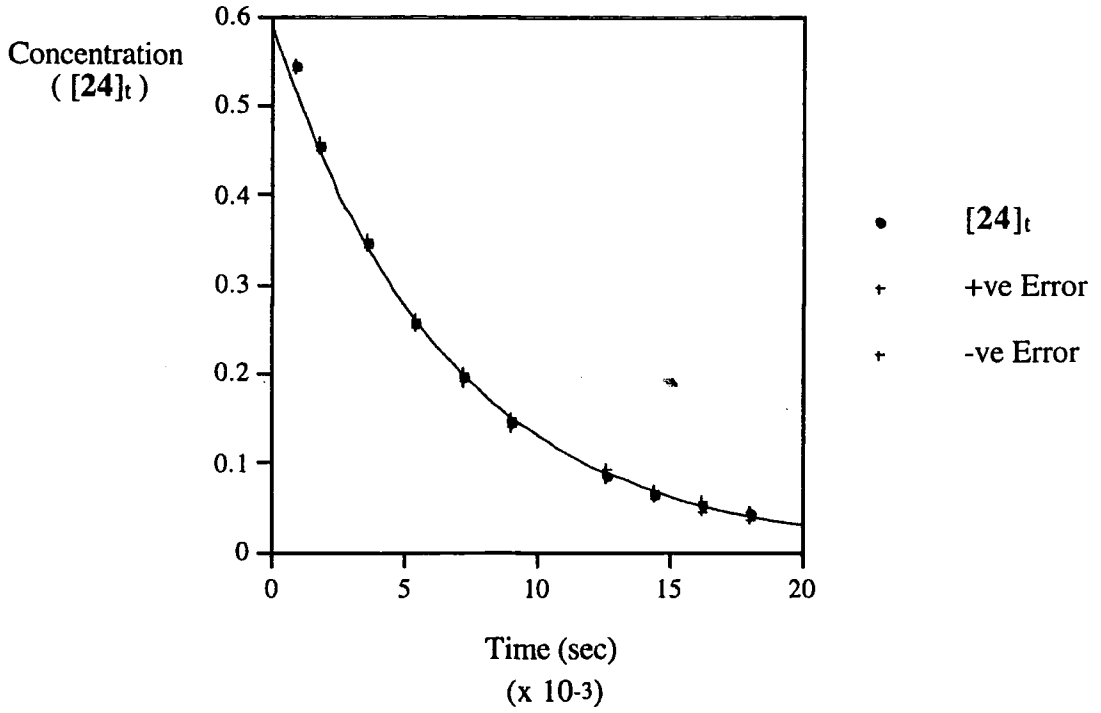

Figure 4.6 Graph of the exponential decay of complex **24** with time in C_6D_6 at 315K.

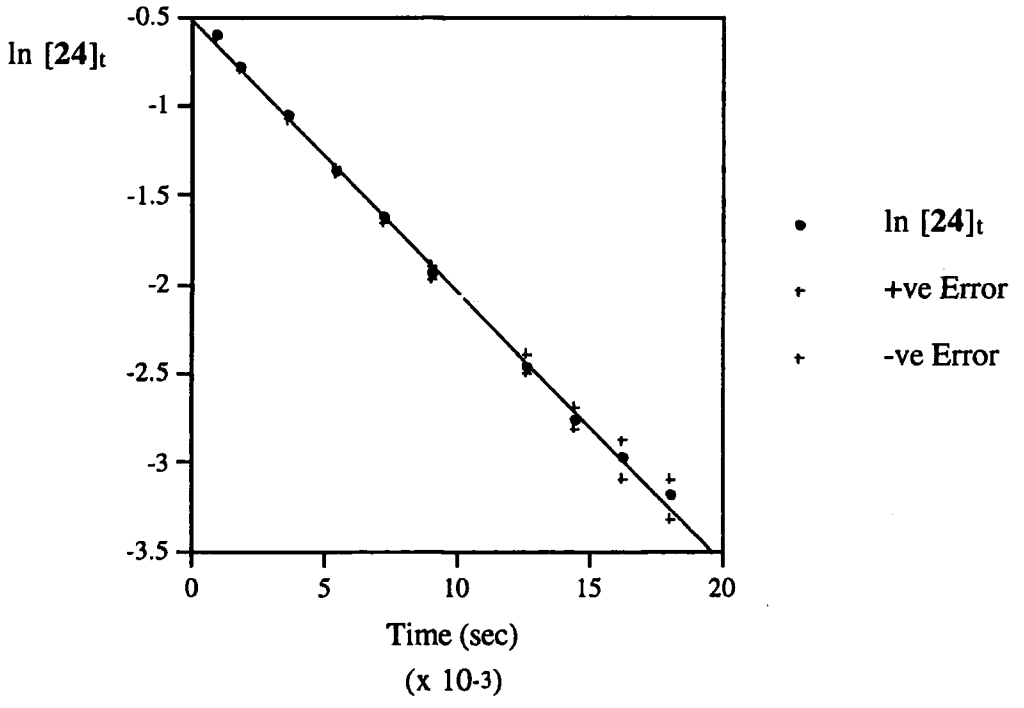

Figure 4.7 Graph of ln (concentration of **24**) versus time in C_6D_6 at 315K.

Values for the rate constants determined at different temperatures using both methods are displayed in table 4.5 for comparison.

Temp. (K)	*k* from Concentration vs. Time Plots (x 10^5 s^{-1})	*k* from ln (Concentration) vs. Time Plots (x 10^5 s^{-1})
303	3.68 (± 0.23)	3.67 (± 0.21)
307	6.68 (± 0.43)	6.76 (± 0.32)
309.5	9.90 (± 0.46)	9.87 (± 0.44)
313	11.97 (± 1.15)	11.88 (±1.06)
315	15.20 (±0.69)	15.23 (± 0.62)
318	28.55 (± 3.46)	28.59 (± 3.45)

Table 4.5 Comparison of first order rate constants obtained employing two different graphical methods.

There is a good correlation between the two calculated values at each temperature. The errors were calculated by taking the maximum deviation from the average ^{1}H NMR integral value (taken as ± 0.2), and either solving the equation for the exponential decay employing these new values (in figure 4.6), or measuring the deviation of the gradient of the new line from that calculated with the original values (in figure 4.7). Of the two methods, the plot of concentration versus time (figure 4.6) introduces less errors into the calculation by excluding the arithmetic problem associated with taking logarithms of small numbers. The errors are noted to generally increase as the temperature is raised which is attributed partly to the acquisition time of the spectra gaining in significance as the experiments proceed more rapidly.

To confirm first order behaviour under the experimental conditions used in these experiments, two kinetic runs were carried out at the same temperature using different concentrations of **24**. If first order kinetics is observed, the rate constant will be independent of the concentration of initial substrates. Although no quantitative values for the concentration were considered, doubling the quantity of **24** from 10 mg

to 20 mg in approximately the same amount of C_6D_6 had no significant effect on the rate constant, confirming first order behaviour.

4.3.3 Activation Parameters for the Conversion of 24 to 25.

The rate constant increases as the temperature is raised (see figure 4.8), and from this temperature dependence, activation parameters can be calculated.

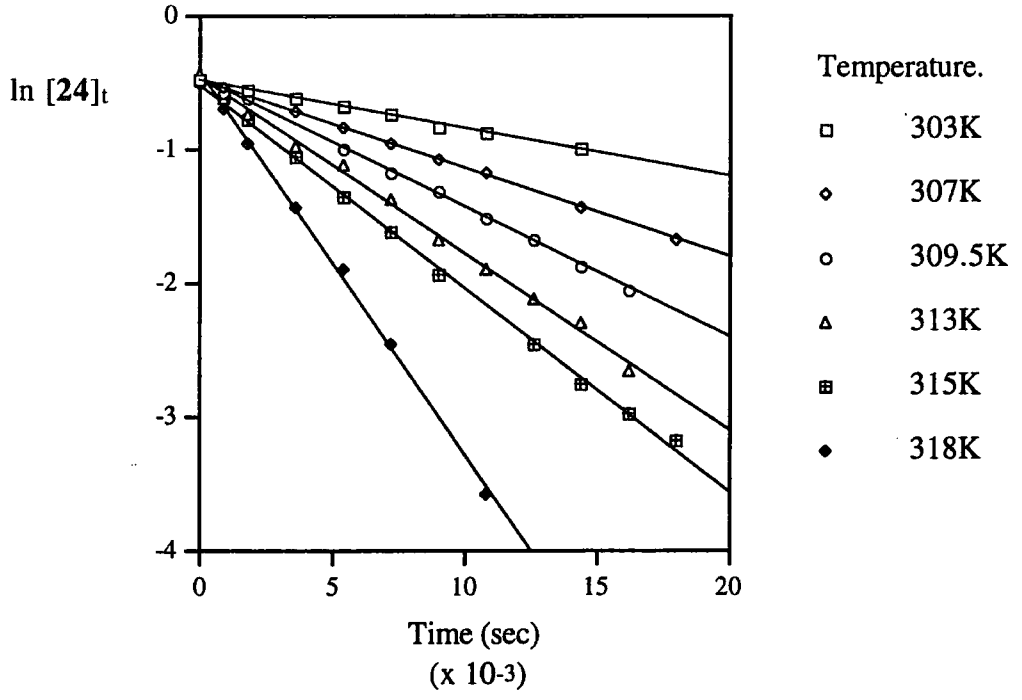

Figure 4.8 Graph displaying variation of rate constant (gradient of the line) with temperature.

The activation energy (E_a), being defined as the difference in energy between the reactants and the transition state, is related to the rate constant *via* the Arrhenius equation given below.

$$k = A \exp\left(\frac{-E_a}{RT}\right)$$ **Equation 4.9**

(Where A = the pre-exponential factor).

A plot of ln *k* versus 1/T therefore gives a straight line of gradient ($-E_a/R$), with an intercept being equal to ln A. The observed rate constants for the conversion of **24** to **25** over the temperature range 30°C to 45°C (303K - 318K) have been displayed in table 4.5 and are presented as an Arrhenius plot in figure 4.9.

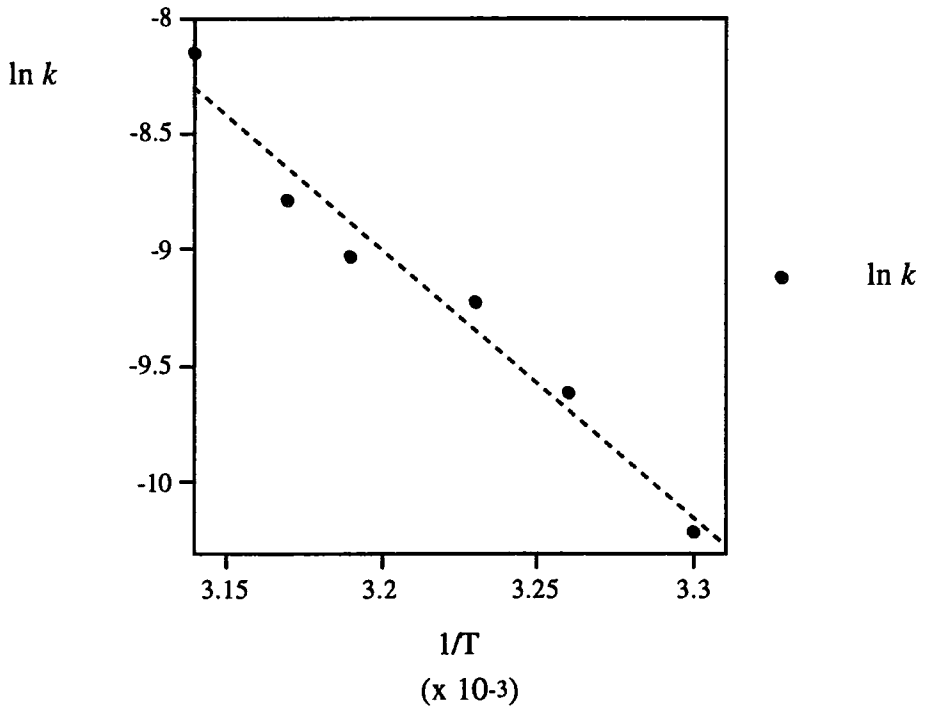

Figure 4.9 Arrhenius plot of the conversion of **24** to **25**.

Thus, for the conversion of **24** to **25**, the activation energy (E_a) and pre-exponential factors are calculated to be :

$$E_a = 96.2\ (\pm\ 3)\ \text{kJ mol}^{-1}$$

$$A = 1.47 \times 10^{12}\ \text{s}^{-1}$$

The enthalpy of activation ($\Delta H^{\ddagger}$) and entropy of activation ($\Delta S^{\ddagger}$) are found from the Eyring equation (equation 4.10), where k_B is the Boltzmann constant and h is Planck's constant :

$$k = \frac{k_B T}{h} \exp\left(\frac{-\Delta H^{\ddagger}}{RT}\right) \exp\left(\frac{-\Delta S^{\ddagger}}{R}\right)$$

Equation 4.10.

This can again be displayed graphically as a plot of ln (k/T) versus 1/T, allowing $\Delta H^{\ddagger}$ to be determined from the gradient, and $\Delta S^{\ddagger}$ from the intercept (see figure 4.10).

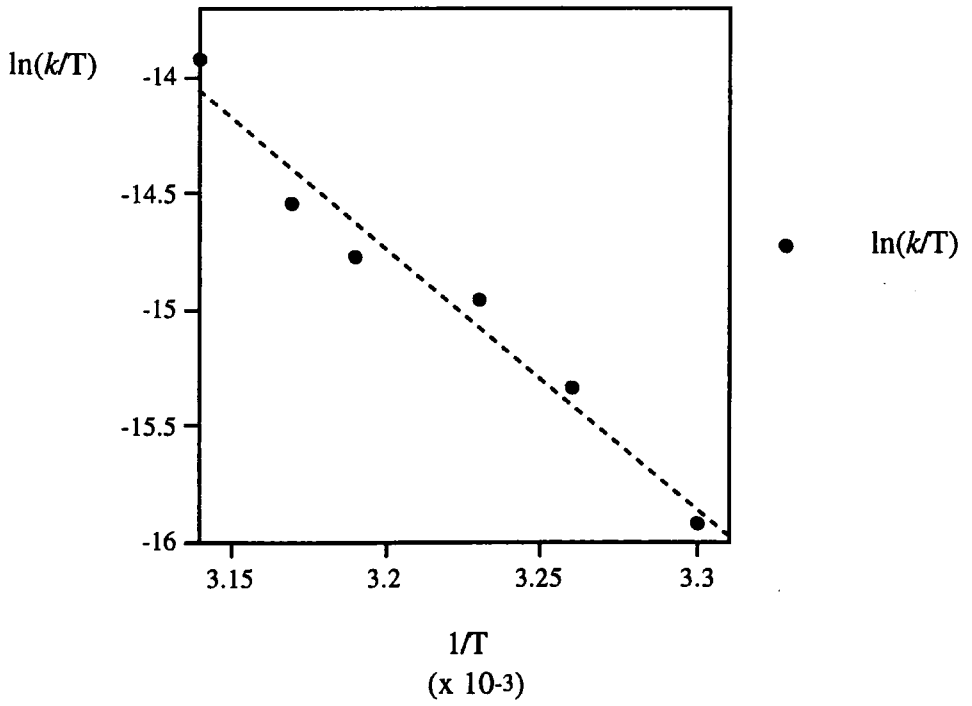

Figure 4.10 Eyring plot of the conversion of **24** to **25**.

Figure 4.10 gives values for the enthalpy and entropy of activation of :

$\Delta H^{\ddagger} = 93.7 (\pm 2.6)$ kJ mol^{-1}

$\Delta S^{\ddagger} = -20 (\pm 6)$ JK^{-1} mol^{-1}

These compare favourably with Hessen's calculations for the conversion of $Cp_2Ti(CH_2CMe_3)_2$ to $Cp_2Ti(CHDCMe_3)(C_6D_5)$ where the values of $\Delta H^{\ddagger}$ = 76.1 kJ mol^{-1} and $\Delta S^{\ddagger}$ = -49.8 JK^{-1} mol^{-1} are reported.[14] The lower value of the enthalpy of activation is reflected in the reduced stability of the bis-neopentyl titanium complexes $(C_5H_4R)_2Ti(CH_2CMe_3)_2$ where if R = H, the complex can be stored as a solid at -40°C, but if R = Me, the complex is unstable even at this temperature. The corresponding chromium dialkyl complex **24** is stable indefinitely in the solid state at room temperature.

The rate determining step for this reaction is believed to be the loss of neopentane to give the intermediate bis-imido alkylidene species. This would be expected to be unstable, reacting with a molecule of C_6D_6 immediately upon formation. The negative value for the entropy of activation $\Delta S^{\ddagger}$ reveals that the system is more ordered in the transition state than in the ground state. This may be a result of a four-membered transition state of the type illustrated in figure 4.11, where the freedom of the neopentyl ligands is reduced.

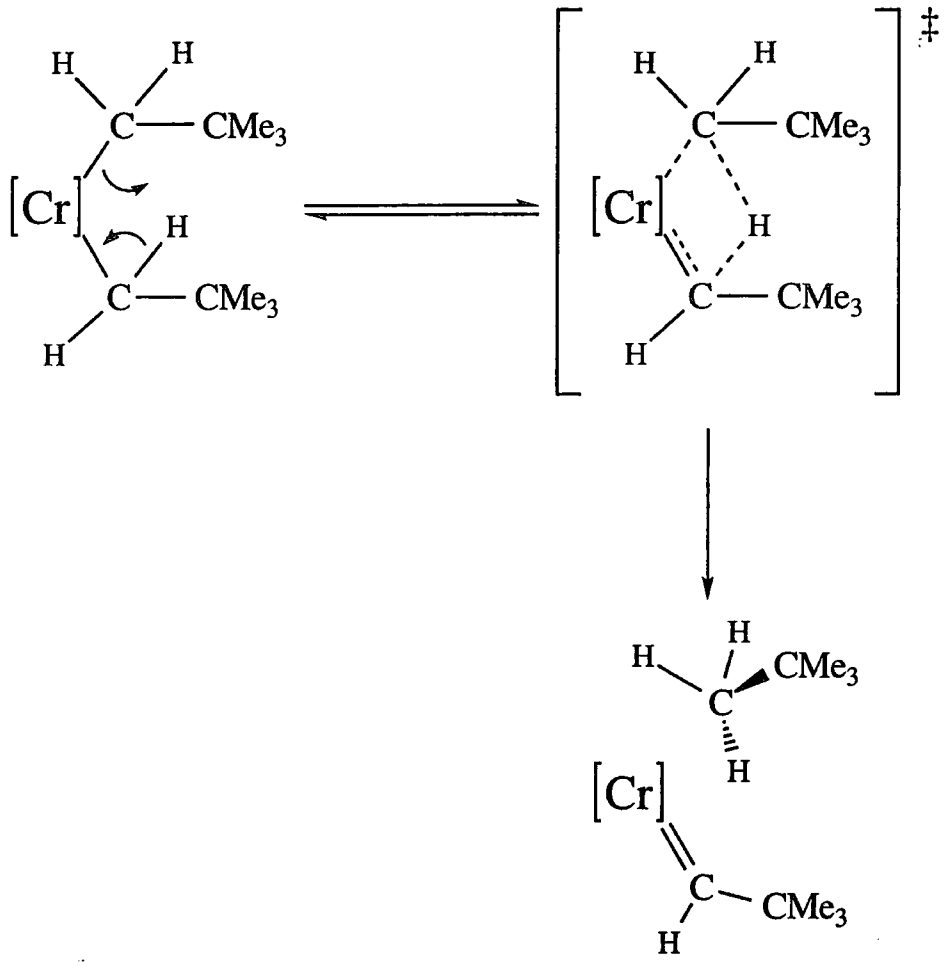

Figure 4.11 Proposed transition state in the conversion of **24** to **25**.

4.3.4 Effect of Solvent on the Conversion of 24 to 25.

To aid our understanding of the mechanistic processes occurring during the conversion of **24** to **25**, similar ^{1}H NMR experiments were performed in D_{10}-*p*-xylene (CD_3–C_6D_4–CD_3) and D_8–THF. Although these reactions obviously give rise to different products, by comparing the rate constant associated with the first order decay of **24** in these solvents, certain conclusions can be made. The graph of ln $[\mathbf{24}]_t$ versus time for these reactions is displayed in figure 4.12, along with that of the reaction in D_6–benzene at the same temperature. As the rate constant is independent of concentration, for the purpose of comparison the vertical scale has been altered to allow the separate experiments to be viewed on the same axes.

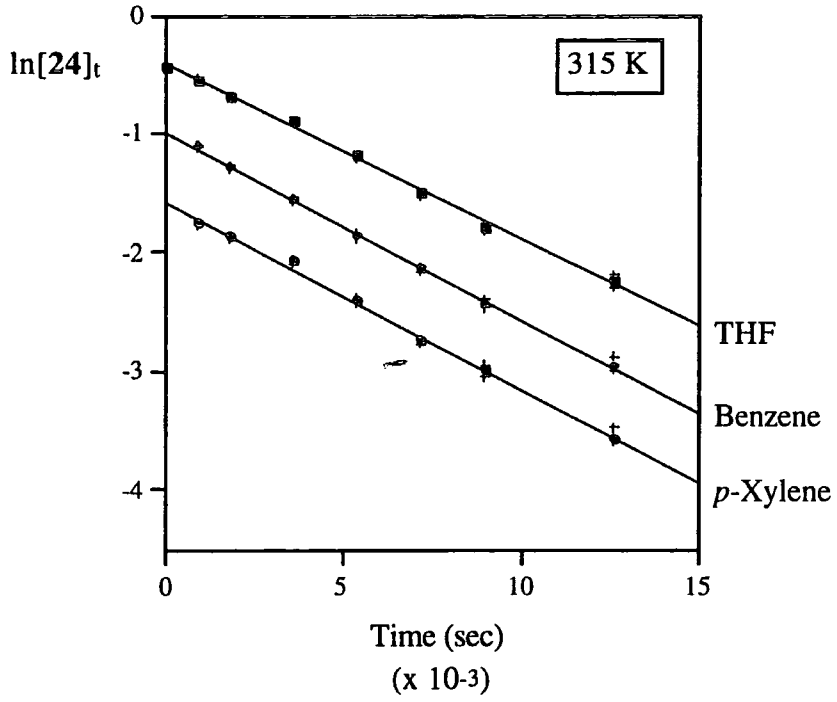

Figure 4.12 Effect of solvent on the decomposition of **24**.

The rate constant calculated from the gradients of the above graph are displayed in table 4.6.

Solvent	***k*** **(x 10^5 s^{-1})**
C_6D_6	15.2 (± 0.62)
D_8–THF	14.7 (± 0.35)
D_{10}–*p*-xylene	15.8 (± 0.67)

Table 4.6 Comparison of rate constant of the decay of **24** in different solvents.

The calculated rate constants are comparable in each of the experiments leading us to conclude that the solvent is not playing a role in the rate determining step of the reaction mechanism. If for example the solvent was responsible for promoting the loss of CMe_4 by forcing the two alkyl ligands together, we might have expected a coordinating solvent (e.g. THF) would cause an increase in the observed rate constant.

This is clearly not the case. It is reasonable to conclude that loss of CMe_4 is the rate determining step, the intermediate alkylidene then being trapped in a fast reaction with the solvent.

4.3.5 Reaction of $Cr(NAr)_2(CH_2CMe_3)_2$ (24) with D_{12}-Cyclohexane.

To investigate the activation of sp^3 C–D bonds, the reaction of $Cr(NAr)_2(CH_2CMe_3)_2$ (**24**) with cyclohexane was probed. The reaction however resulted only in decomposition of the starting dialkyl to paramagnetic species that could not be characterised, although evolution of neopentane was observed. A possible explanation is that the intermediate $[Cr(NAr)_2(=CHCMe_3)]$ complex is forming, as seen by the generation of neopentane, but that this is unable to react with the solvent, possibly for steric reasons. Consequently, it may be reacting with itself (inter or intramolecularly) or simply decomposing to generate a paramagnetic species. It will be of interest to establish whether or not smaller hydrocarbons such as methane or ethane can be activated.

4.3.6 Reaction of $Cr(NAr)_2(CH_2CMe_3)_2$ (24) with D_8-THF

Formation of $Cr(NAr)_2(=CHCMe_3)(THF)$ (26)

By employing the coordinating NMR solvent D_8-THF, it is possible to trap out and observe the intermediate alkylidene complex formed by the α-H abstraction of neopentane as the base adduct $Cr(NAr)_2(=CHCMe_3)(THF)$ (**26**), according to equation 4.11.

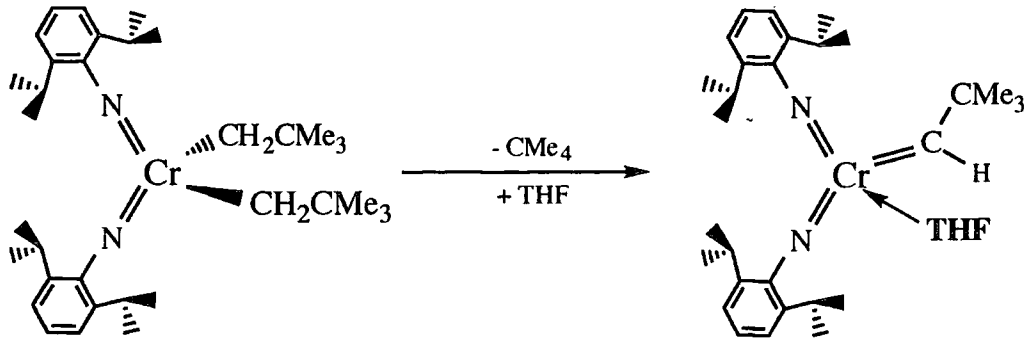

(24) (26)

Equation 4.11

This reaction again proceeds cleanly on an NMR scale with 100% conversion to the alkylidene complex as seen in the ^{1}H and ^{13}C NMR spectra illustrated in figures 4.13 and 4.14. **26** shows typical spectroscopic features associated with metal alkylidene complexes, including a low field shift of 14.62 ppm in the ^{1}H NMR spectrum for the alkylidene α-proton. The predicted orientation of the alkylidene[11] is with the substituents pointing towards the imido groups, analogous to the bis-imido amide complexes **12** and **17**, as illustrated in figure 4.15 (see section 1.2.5 for full discussion).

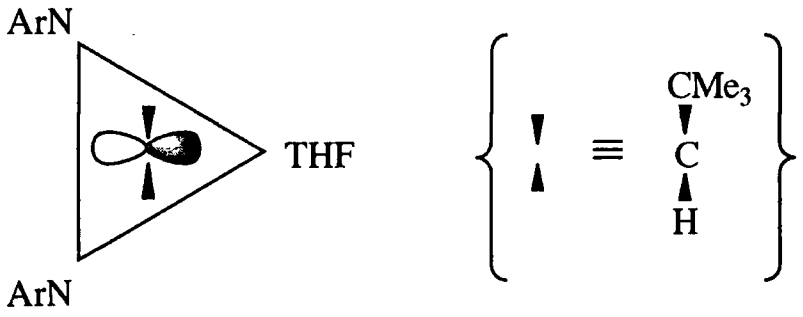

Figure 4.15 Predicted bonding arrangement of the alkylidene ligand in the complex $Cr(NAr)_2(=CHCMe_3)(THF)$ (**26**).

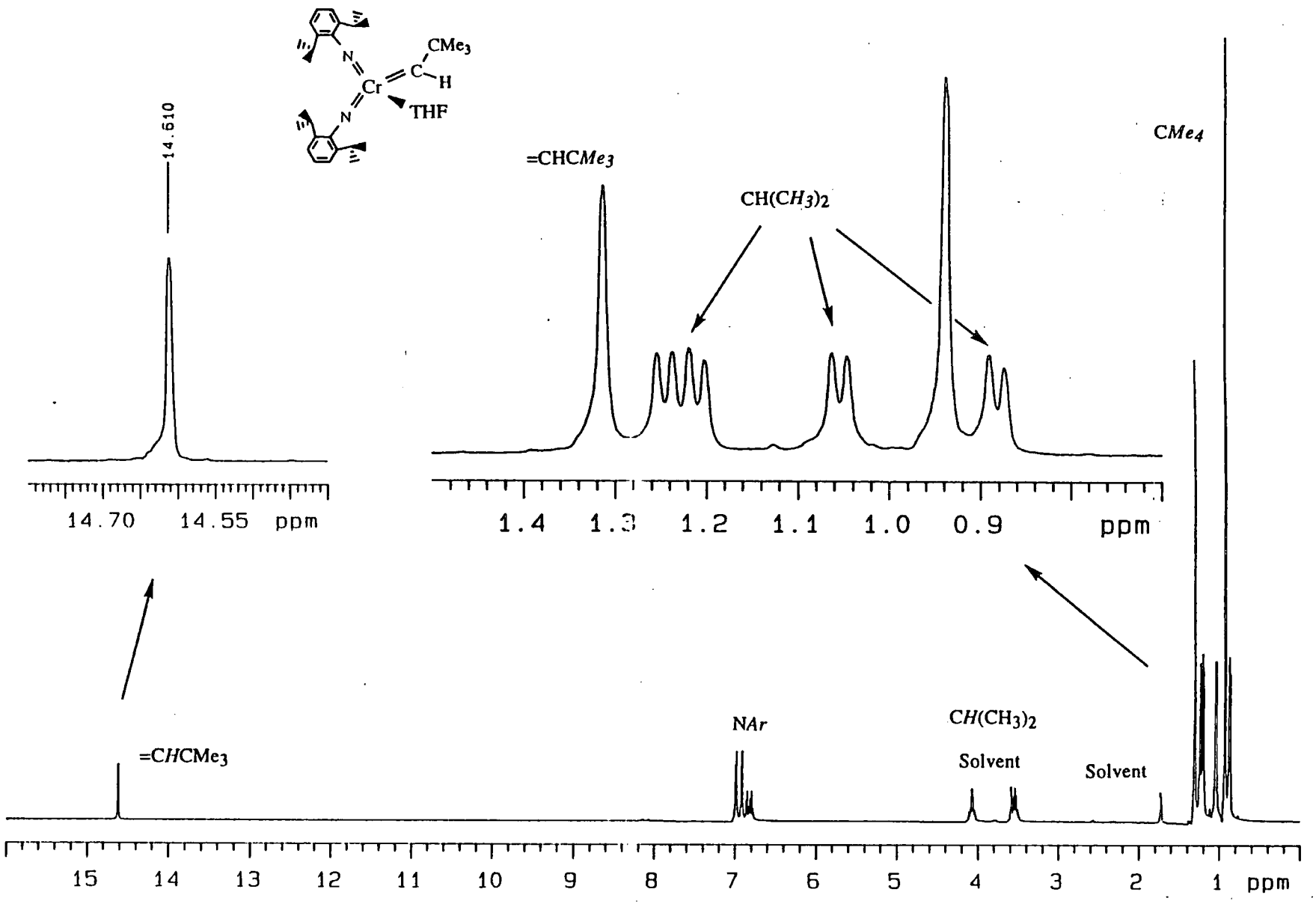

Figure 4.13 ^{1}H NMR spectrum (400MHz, D_8-THF) of $Cr(NAr)_2(=CHCMe_3)(THF)$ (**26**).

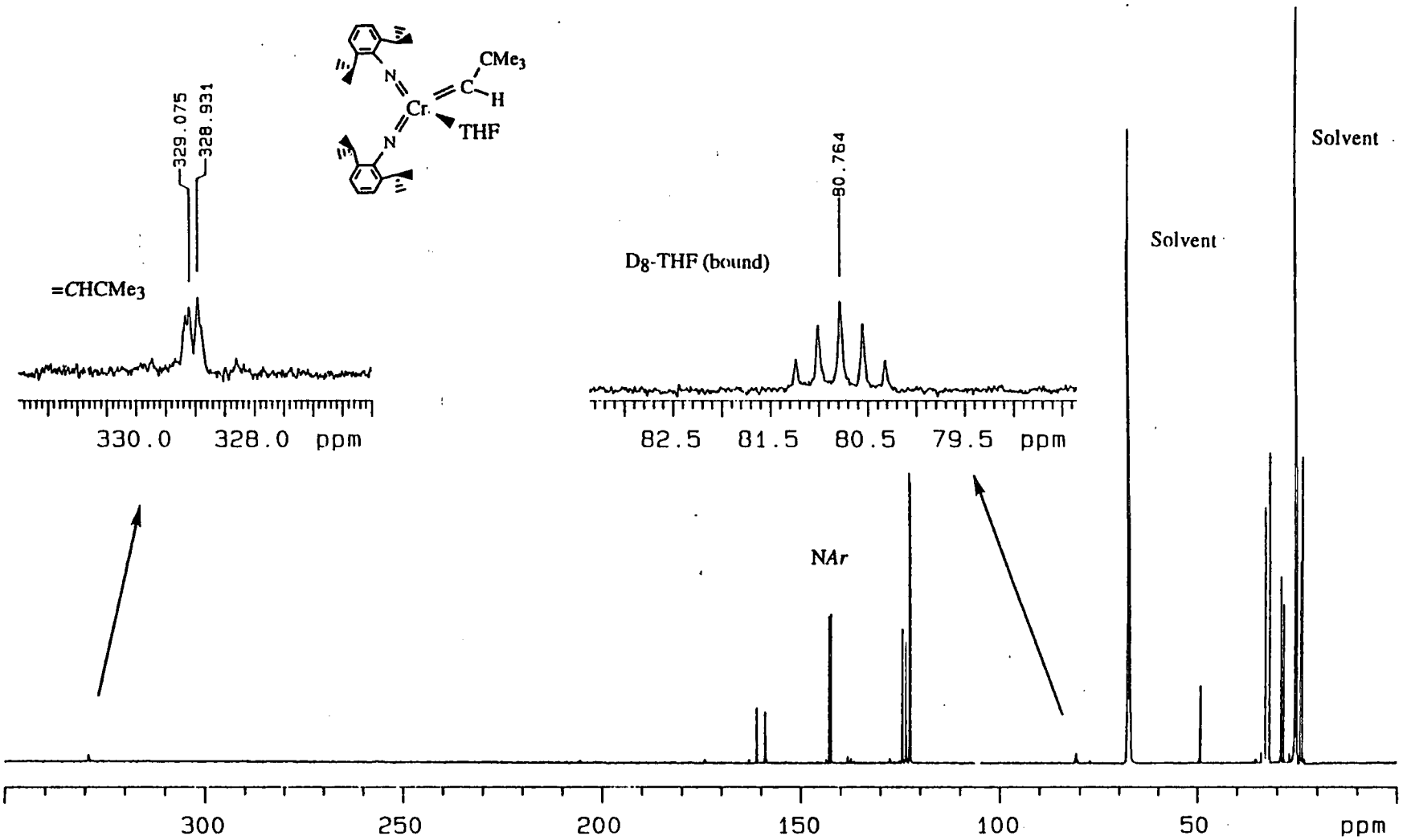

Figure 4.14 ^{13}C NMR spectrum (100MHz, D_8-THF) of $Cr(NAr)_2(=CHCMe_3)(THF)$ (**26**).

(Note : Alkylidene carbon experiences splitting from the α-proton even in the decoupled experiment due to the extreme low field shift of the resonance).

Consistently, the NMR (^1H and ^{13}C) data show inequivalence of the imido groups giving rise to two distinct septets at δ 4.07 and δ 3.54, and four doublets centred at 1.24, 1.21, 1.05 and 0.88 ppm for the *iso*-propyl methine and methyl groups respectively.

The ^{13}C NMR (figure 4.14) also shows a low field shift for the α-carbon of the alkylidene ligand at δ 328.00, with a C-H coupling constant of 14.48Hz. Careful examination of the spectra shows the presence of a signal due to the α-carbons of the coordinated D_8-THF at 80.77 ppm, with a quintet splitting caused by the two attached deuterium atoms. The other signal was not located, most likely due to overlap with other signals.

Although attempted on a preparative scale, a clean product was not isolated due to the oily nature of the species.

4.3.7 Reaction of $Cr(NAr)_2(=CHCMe_3)(THF)$ (26) with PMe_3 :

Preparation of $Cr(NAr)_2(=CHCMe_3)(PMe_3)$ (27).

26 was reacted with PMe_3 in an attempt to generate a crystalline product, as observed for the isolobal half-sandwich niobium analogue $CpNb(NAr)(=CHPh)(PMe_3)$.[12] Initial attempts at generation of the alkylidene directly from the dialkyl species employing the phosphine as base were unsuccessful, due to the sensitivity of the imido ligands to this reagent (see section 3.3.2). The indirect method of preparation by generating the THF adduct $Cr(NAr)_2(=CHCMe_3)(THF)$ (**26**) and then displacement of the base with PMe_3 however proved successful.

Treatment of **26** with one equivalent of PMe_3 in D_8-THF results in the rapid formation of $Cr(NAr)_2(=CHCMe_3)(PMe_3)$ (**27**) with 100% conversion (equation 4.12).

$$Cr(NAr)_2(=CHCMe_3)(THF) + PMe_3 \xrightarrow[30\ mins]{THF} Cr(NAr)_2(=CHCMe_3)(PMe_3) + THF$$

(26) (27)

Equation 4.12

The ^1H NMR spectrum reveals coupling between the alkylidene α-proton and the phosphorus atom resulting in a doublet with $^3J_{PH}$=6.40Hz. The imido ligands retain their non-equivalence suggesting a structure analogous to that illustrated in figure 4.15 with the alkylidene ligand orientated with the substituents pointed towards the imido ligands. The ^{13}C NMR spectrum again shows a high field shift for the α-carbon of the alkylidene ligand, with a doublet at 339.93 ppm ($^2J_{CP}$=26.25Hz) caused by coupling to phosphorus atom of the phosphine ligand.

This experiment was performed on a preparative scale by addition of one equivalent of PMe_3 to $Cr(NAr)_2(CH_2CMe_3)_2$ (**24**) that had been stirring in THF for 5 days, without isolation of the intermediate THF adduct (**26**). The resulting bright red solid proved extremely soluble in THF but could be induced to crystallise from a concentrated heptane solution at -30°C, affording pure $Cr(NAr)_2(=CHCMe_3)(PMe_3)$ in excellent yield (88%). Unfortunately, crystals suitable for an X-ray study were not forthcoming from this solvent, and work is continuing towards this goal.

4.4 Further Studies into Reactions of the Chromium Alkylidene Moiety [$Cr(NAr)_2(=CHCMe_3)$].

4.4.1 Introduction.

The ability of the transient species [$Cr(NAr)_2(=CHCMe_3)$] to activate sp^2 and sp^3 C-H bonds has been briefly investigated in the preceding section. Amongst other

well documented reactions of transition metal alkylidene complexes are reactions with olefins, either to form stable metallacyclobutane species through addition across the metal carbon double bond,[13] or if the correct conditions are met, to allow metathesis to occur,[14] whereby the different end groups of olefin molecules are exchanged *via* a metallacyclobutane intermediate. An important variation of this process is the Ring Opening Metathesis Polymerisation process (ROMP),[15] whereby the olefin is incorporated into a strained cyclic conformation prior to reaction and metathesis leads to the formation of a polymeric material (see section 1.4 for an introduction to ROMP and chapter five for a study into this process). It was therefore of interest to investigate the reactions of the chromium alkylidene species discussed previously with unsaturated substrates.

4.4.2 Reaction of $Cr(NAr)_2(=CHCMe_3)(THF)$ (26) with Norbornene.

A standard method employed to test the ROMP capability of a potential catalyst is to mix the compound with a solution of bicyclo[2.2.1]hept-2-ene (norbornene). This is a highly strained cyclic olefin that readily undergoes ROMP to form polymers that have been extensively studied.[16,17]

To investigate whether the chromium alkylidene $Cr(NAr)_2(=CHCMe_3)(THF)$ was able to promote the polymerisation of norbornene, a simple NMR experiment was performed whereby a mixture of **26** and 10 equivalents of norbornene was monitored in C_6D_6 over a three day period. If polymerisation was occurring, the ^1H and ^{13}C NMR signals corresponding to norbornene are expected to shift to known values for the resulting polymer.[17] The ^1H NMR spectrum of **26** and norbornene, however, showed no change upon mixing, with the signals of both species remaining unchanged even after heating to 50°C. Prolonged exposure to this temperature caused a decomposition of the chromium species to paramagnetic side products observed by a gradual loss of all signals corresponding to complex **26**. This reflects an instability of the chromium alkylidene compounds to heat.

It was initially postulated that the lack of polymerisation activity was due to the THF molecule being too strongly bound to the chromium centre. Dissociation or displacement of the THF by the incoming norbornene may be required to enable the reaction to proceed, although for the well-defined initiators of molybdenum and tungsten adduct formation with PMe_3 and quinuclidene as models for olefin binding show that five coordinate species are readily formed.[18] This may not be the case for the smaller chromium metal however.

4.4.3 Reaction of $Cr(NAr)_2(CH_2CMe_3)_2$ (24) with Norbornene in C_6D_6.

As the THF adducts of the bis-imido alkylidene complex appear too stable to allow the ROMP of norbornene, it was hypothesised that reaction of the initial dialkyl complex with C_6D_6 in the presence of norbornene to generate the alkylidene *in situ* may result in polymerisation. To investigate this, a mixture of $Cr(NAr)_2(CH_2CMe_3)_2$ (**24**) and norbornene in C_6D_6 was monitored by proton NMR. Unexpectedly, compound **24** was found to retain the C-D activation activity detailed in section 4.3, forming almost exclusively $Cr(NAr)_2(CHDCMe_3)(C_6D_5)$ (**25**), even in the presence of norbornene where it was envisaged that reaction with the olefin would occur preferentially. A very small amount of polynorbornene was evident in the NMR, although this was most likely a result of side reactions occurring.

4.4.4 Reaction of $Cr(NAr)_2(CH_2CMe_3)_2$ (24) with Norbornene in D_{12}-Cyclohexane.

The reaction of **24** in D_{12}-cyclohexane (section 4.3.5) showed that neopentane was generated during the course of this reaction, suggesting the transient formation of $[Cr(NAr)_2(=CHCMe_3)]$. In the absence of an available substrate this was seen to decompose without any apparent C-D activation of the solvent, prompting us to employ cyclohexane as a potential solvent for the ROMP of norbornene. It was reasoned that if the alkylidene is being generated and there is no facile C-D activation pathway to

follow, the complex may be forced to react with the olefin, as expected for such transition metal alkylidene complexes.

Unfortunately no polymerisation activity was evident, with the reaction following a similar pathway to that observed between **24** and D_{12}-cyclohexane in the absence of an olefin. The complex **24** therefore seems extremely unreactive towards olefins.

4.4.5 Reaction of $Cr(NAr)_2(CH_2CMe_3)_2$ (24) with Ethylene in C_6D_6.

It was postulated that the lack of reactivity of the chromium alkylidene species with norbornene may be due to a steric restraint on the approach of the olefin bond to the metal carbon multiple bond. It was therefore decided that a less sterically demanding olefin molecule should be investigated, ethylene being the obvious choice. It was hypothesised that the following reaction pathway would be favourable, resulting in a metallacyclobutane complex analogous to Grubbs' titanocene initiators.[19]

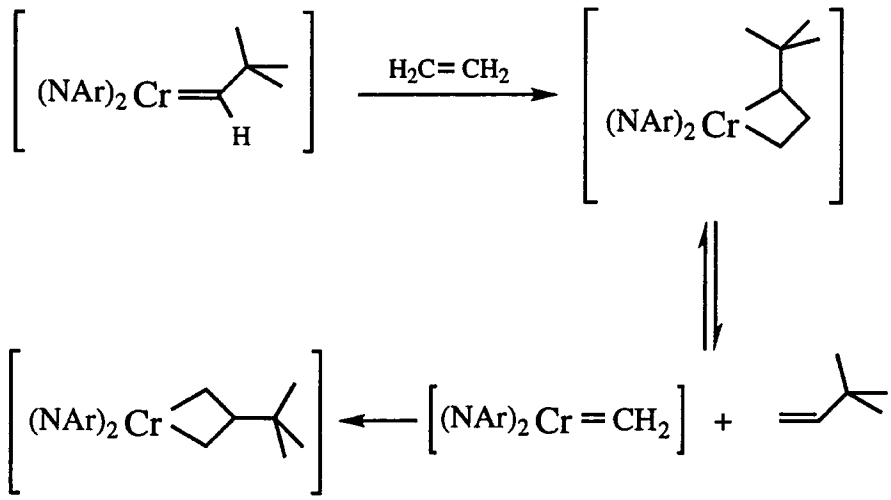

Equation 4.13 Proposed mechanism of the reaction between $[Cr(NAr)_2(=CHCMe_3)]$ and ethylene leading to the formation of metallacyclobutane intermediates.

Unexpectedly, there was still no observable reaction between the chromium complex and the olefin, with the only reaction pathway evident being the C-D activation of the deuterio-benzene. It was concluded that the putative chromium

alkylidene species [$Cr(NAr)_2(=CHCMe_3)$] is therefore unreactive towards olefins, with the preferred reaction being the activation of C-D bonds. The possible reason for this is discussed in the following section.

4.4.6 Rationalisation of the Observed Reactivity of the Chromium Alkylidene Species [$Cr(NAr)_2(=CHCMe_3)$].

The frontier orbitals of the bis-imido Group 6 complexes are analogous to those possessed by the Group 4 bent metallocene complexes[20] (see section 1.2.4). The bonding between the alkylidene fragment and [$Cr(NAr)_2$] is therefore such that the substituents on the α-carbon of the alkylidene are aligned in the N-Cr-N plane. Such an orientation of the alkylidene in this system is likely to cause unfavourable steric interactions between the bulky ^{t}butyl group of the alkylidene and the aryl groups of the imido ligands. This will lead to a destabilisation of the complex if this arrangement is adopted.

Rotation of the alkylidene ligand about the metal-carbon double bond is well documented for the Schrock type alkylidene complexes,[21] leading to different isomeric forms of the complex known as rotamers[22] (see section 5.4.6). In order to rotate about the metal carbon double bond, the π-interaction has to be broken, resulting in the localisation of an electron on both the metal and carbon, effectively a diradical species. In a rotation of this fashion, the substituents of the alkylidene ligand are orientated away from the imido groups, thus reducing the unfavourable steric interactions and hence causing a reduction in the energy of the complex (figure 4.16). If this proposed diradical form has a sufficiently long lifetime, it is possible that it may dominate the subsequent reactivity of the alkylidene complex.

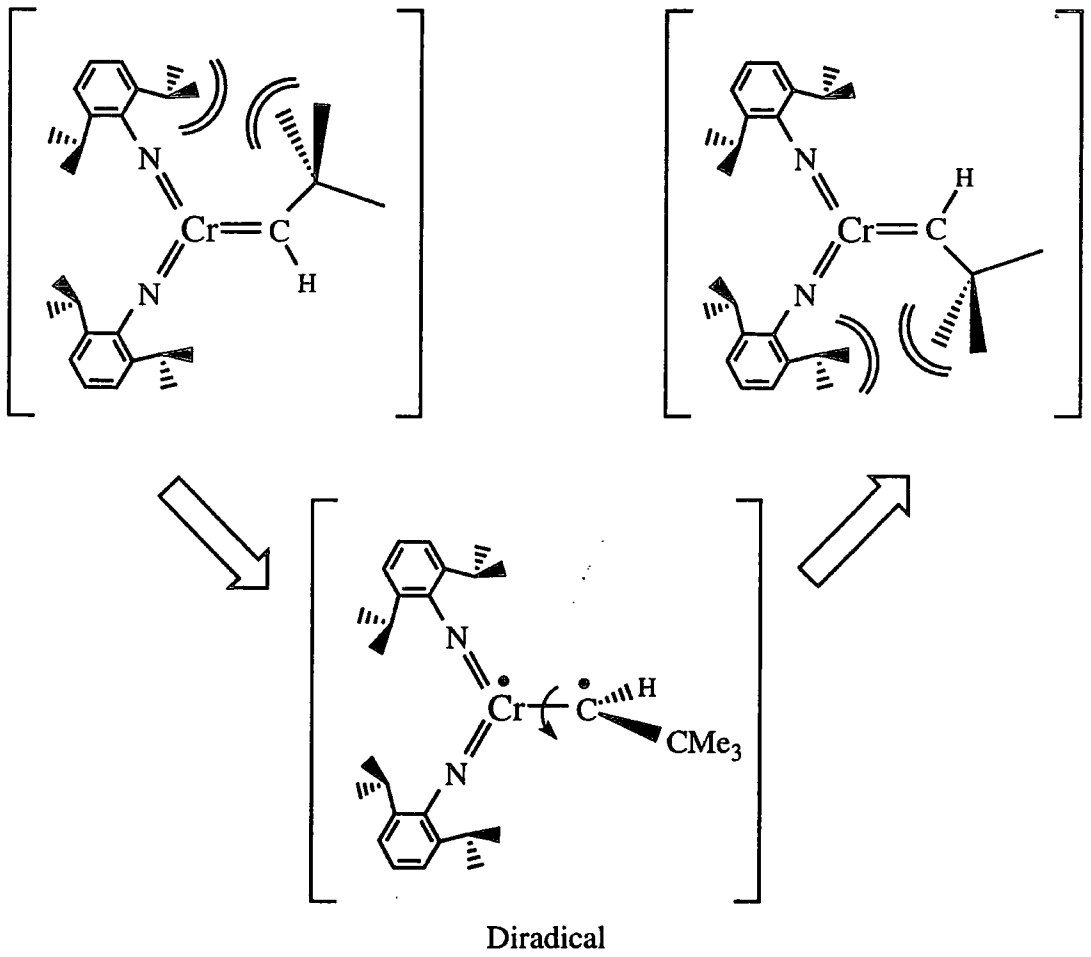

Diradical

Figure 4.16 Proposed diradical intermediate generated on rotation of the chromium alkylidene double bond.

It is suggested, therefore, that in view of the lack of reactivity of the bis-imido chromium alkylidene species [$Cr(NAr)_2(=CHCMe_3)$] towards olefins, the diradical species is dominating the solution reactivity. Such a diradical species may be the origin of the C–D activation reactivity since radical species are well known to be able to cleave C–H bonds (see figure 4.17).

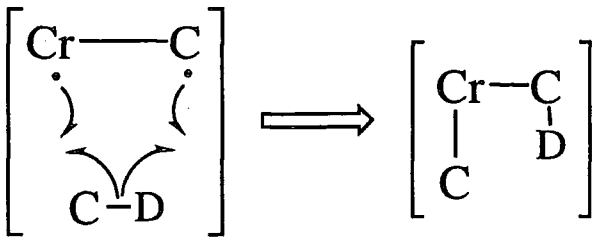

Figure 4.17 Proposed mechanism for the activation of C-D bonds *via* a diradical intermediate.

Further studies will be required to probe the nature of the metal-carbon bond in these interesting chromium compounds.

4.5 References.

1. M.B. Hursthouse, M. Motevalli, A.C. Sullivan and G. Wilkinson, *J. Chem. Soc., Chem. Commun.*, **1986**, 1398 ; A.C. Sullivan, G. Wilkinson, M. Motevalli and M.B. Hursthouse, *J. Chem. Soc. Dalton Trans.*, **1988**, 53.

2. N. Meijboom, C.J. Schaverien and A.G. Orpen, *Organometallics*, **1990**, *9*, 774.

3. W.A. Nugent and R.L. Harlow, *J. Am. Chem. Soc.*, **1980**, *102*, 1759.

4. M.P. Coles, C.I. Dalby, V.C. Gibson, W. Clegg and M.R.J. Elsegood, *J. Chem. Soc., Chem. Commun.*, **1995**, 1709 ; See also this thesis, section 2.3.

5. R.F. Jordan, W.E. Dasher and S.F. Echolls, *J. Am. Chem. Soc.*, **1986**, *108*, 1718 ; R.F. Jordan, C.S. Bajgur, R. Willett and B. Scott, *J. Am. Chem. Soc.*, **1986**, *108*, 7410 ; R.F. Jordan, R.E. LaPointe, C.S. Bajgur, S.F. Echols and R. Willett, *J. Am. Chem. Soc.*, **1987**, *109*, 4111 ; M. Bochmann, A.J. Jaggar and J.C. Nicholls, *Angew. Chem. Int. Ed. Engl.*, **1990**, *29*, 780.

6. V.C. Gibson and G.L.P. Walker, unpublished results.

7. W.A. Nugent and R.L. Harlow, *J. Am. Chem. Soc.*, **1980**, *102*, 1759.

8. A.A. Danopoulos, G. Wilkinson, T.K.N. Sweet and M.B. Hursthouse, *J. Chem. Soc. Dalton Trans.*, **1995**, 2111.

9. R.R. Schrock, *J. Am. Chem. Soc.*, **1974**, *96*, 6796.

10. H. van der Hiejden and B. Hessen, *J. Chem. Soc., Chem. Commun.*, **1995**, 145.

11. V.C. Gibson, *J. Chem. Soc. Dalton Trans.*, **1994**, 1607 ; V.C. Gibson, *Angew. Chem. Int. Ed. Engl.*, **1994**, *33*, 1565.

12. J.K. Cockcroft, V.C. Gibson, J.A.K. Howard, A.D. Poole, U. Siemeling and C. Wilson, *J. Chem. Soc., Chem. Commun.*, **1992**, 1668.

13. J. Feldman, J.S. Murdzek, W.M. Davis and R.R. Schrock, *Organometallics*, **1989**, *8*, 2260 ; J. Feldman, W.M. Davis and R.R. Schrock, *Organometallics*, **1989**, *8*, 2266 ; R.R. Schrock, J.S. Murdzek, G.C. Bazan, J. Robbins, M. DiMare and M.B. O'Regan, *J. Am. Chem. Soc.*, **1990**, *112*, 3875 ; J. Robbins, G.C. Bazan, J.S. Murdzek, M.B. O'Regan and R.R. Schrock, *Organometallics*, **1991**, *10*, 2902.

14. R.R. Schrock, R. DePue, J. Feldman, C.J. Schaverien, J.C. Dewan and A.H. Lui, *J. Am. Chem. Soc.*, **1990**, *110*, 1423 ; H.H. Fox, R.R. Schrock and R. O'Dell, *Organometallics*, **1994**, *13*, 635.

15. R.R. Schrock, *Acc. Chem. Res.*, **1990**, *23*, 158 ; R.R. Schrock, R.T. DePue, J. Feldman, K.B. Yap, D.C. Yang, W.M. Davis, L. Park, M. DiMare, M. Schofield, J. Anhaus, E. Walborsky, E. Evitt, C. Krüger and P. Betz, *Organometallics*, **1990**, *9*, 2262.

16. R.R. Schrock, J. Feldman, R.H. Grubbs and L. Cannizzo, *Macromolecules*, **1987**, *20*, 1169.

17. K.J. Ivin, *"Olefin Metathesis"*, Academic Press, London, 1983.

18. R.R. Schrock, W.E. Crowe, G.C. Bazan, M. DiMare, M.B. O'Regan and M.H. Schofield, *Organometallics*, **1991**, *10*, 1832.

19. T.R. Howard, J.B. Lee and R.H. Grubbs, *J. Am. Chem. Soc.*, **1980**, *102*, 6876 ; J.B. Lee, G.J. Gajola, W.P. Schaefer, T.R. Howard, T. Ikariya, D.A. Straus and R.H. Grubbs, *J. Am. Chem. Soc.*, **1981**, *103*, 7358 ; J.B. Lee, K.C. Ott and R.H. Grubbs, *J. Am. Chem. Soc.*, **1982**, *104*, 7491 ; R.H. Grubbs and L.R. Gilliom, *J. Am. Chem. Soc.*, **1986**, *108*, 733.

20. D.N. Williams, J.P. Mitchell, A.D. Poole, U. Siemeling, W. Clegg, D.C.R. Hockless, P.A. O'Neil and V.C. Gibson, *J. Chem. Soc. Dalton Trans.*, **1992**, 739.

21. R.R. Schrock, W.E. Crowe, G.C. Bazan, M. DiMare, B. O'Regan and M.H. Schofield, *Organometallics*, **1991**, *10*, 1832.

22. J.H. Oskam and R.R. Schrock, *J. Am. Chem. Soc.*, **1992**, *114*, 7588 ; W.J. Feast, V.C. Gibson, K.J. Ivin, A.M. Kenwright and E. Khosravi, *J. Chem. Soc., Chem. Commun.*, **1994**, 1399.

Chapter Five

Ring Opening Metathesis Polymerisation of Amino Acid Derived Norbornene Monomers.

5.1 Introduction.

This chapter details a study undertaken into the ring-opening metathesis polymerisation (ROMP) of a series of *N*-norbornenyl-amino acid ester monomers by well defined molybdenum initiators of the general formula $Mo(NAr)(=CHR)(OR')_2$[1] ($Ar = 2,6\text{-}^{i}Pr_2C_6H_3$, $R = CMe_2Ph$, $R' = {}^{t}Bu$ **[I]**, $CMe_2(CF_3)$ **[II]** and $CMe(CF_3)_2$ **[III]**). It has long been established that transition metal alkylidene complexes of this type promote the living polymerisation of substituted norbornene monomers,[2] displaying tolerance to a range of functional groups.[3]

The polymerisation of this class of monomer was explored since the presence of an amino acid side group gives rise effectively to a synthetic biopolymer. This is of great interest as many naturally occurring polymers such as proteins and nucleic acids spontaneously arrange themselves into well defined secondary and tertiary structures, with precise chemical and biological functions that are totally dependent upon their overall conformation. Control over the many aspects of the polymer assembly is therefore a pre-requisite if the overall properties of the resultant materials are to be influenced.

The inclusion of optically active amino acid residues in the side chain also allows access to a chiral polymer. By comparing the specific optical rotation of different polymers, the origin of the chirality can be addressed and related to the structure of the polymer. This study was further complemented by a brief molecular modelling study, whereby sample molecules were generated and the conformation at the lowest energy was investigated.

5.2 *N*-Norbornenyl Alanine Methyl Ester Monomers.

5.2.1 Monomer Synthesis.

All of the monomers examined in this chapter were kindly provided by Dr M. North and his research group from the University of Wales in Bangor as part of a larger

collaborative programme concerned with the synthesis of bioactive macromolecules. The synthesis has been recently published[4] and is summarised in equations 5.1 and 5.2.

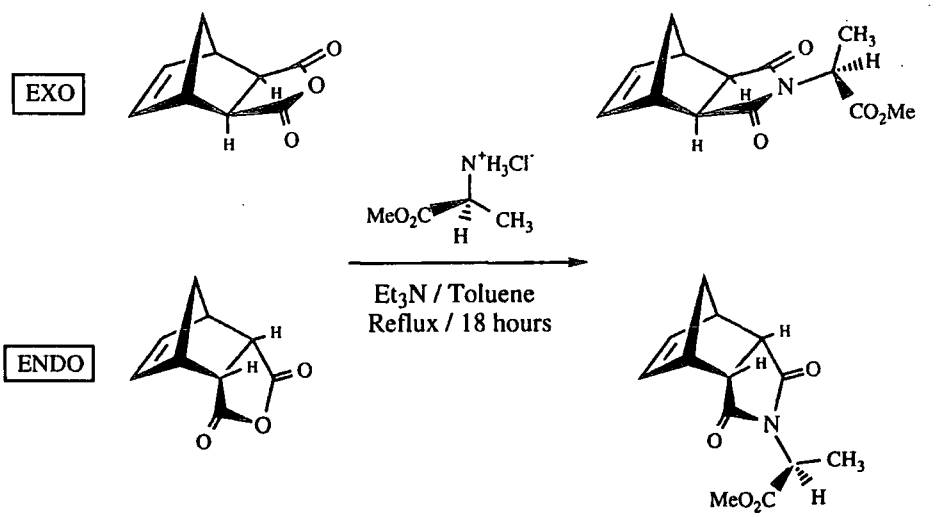

Equation 5.1 High temperature route for the synthesis of *exo-* and *endo- N*-norbornenyl-alanine methyl ester monomers.

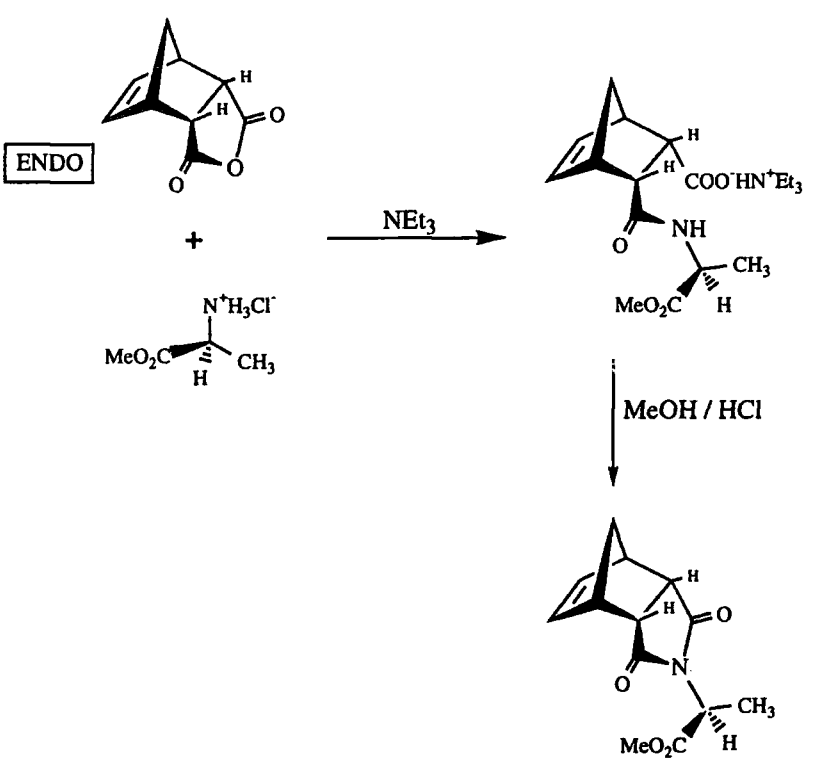

Equation 5.2 Low temperature route for the synthesis of *endo- N*-norbornenyl-alanine methyl ester monomers.

This study involved the R (dextrorotatory, D), S (lavorotatory, L) and the racemic mixture (DL) derived monomers of both the *exo* and *endo* forms of norbornene. Each monomer was provided as a white crystalline solid that was dried *in vacuo* prior to use. Occasionally the sample was of insufficient purity to allow polymerisation studies to proceed, the most likely contaminant being $[NEt_3H]^+Cl^-$.[5] In these cases recrystallisation from a saturated Et_2O solution at -30°C circumvented the problem.

It has been noted previously that *exo*-norbornene derivatives undergo ROMP more readily than their *endo* counterparts, which in some cases may be completely resistant to polymerisation.[6] Preliminary molecular modelling experiments were carried out on representative *exo* and *endo* monomers to examine their relative energies and different conformations.

5.2.2 Introduction to Molecular Modelling Programs.

A molecular mechanics model describes a molecule as an assembly of point charges (atoms), linked by springs (bonds). A mathematical function, the force field, defines the freedom of bond lengths and angles, along with Van der Waals and electrostatic interactions between non-bonded atoms. These force fields fit data from *ab-initio* quantum mechanical calculations to obtain parameters, which are checked against available experimental data (e.g. X-Ray diffraction data) to ensure a reliable model.

An important function these programs perform is to minimise any structures whose coordinates are entered into the computer, that is to investigate different conformations of the molecule until the lowest energy structure is found. The force field function is iteratively minimised to find probable, low energy conformations for a molecule. The mathematical algorithm employed for this study was that of *Steepest Descent* which, although a robust algorithm, slowly converges as it only considers the first derivative of the energy change (the gradient) and uses an inefficient linear search routine.

A limitation of such a process is that the minimisation will take the given conformation of a molecule and move it to the *nearest* minimum energy. This may not be the lowest energy conformation of that molecule (the 'global' minimum) as the algorithms used in this program are specifically designed to ignore any solutions that result in an increased energy. Thus, in figure 5.1, the global minimum is never reached as the program will not allow the conformation to change towards **X** as the energy is increasing.

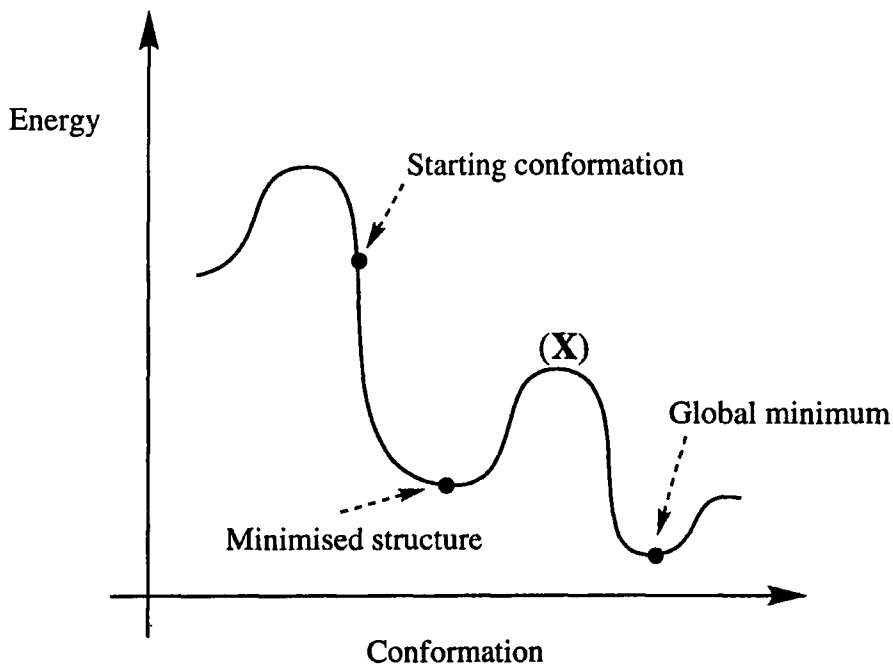

Figure 5.1 Graph of conformation vs. energy for a minimisation procedure.

A molecular dynamics experiment allows high energy barriers to be traversed in the search for the global minimum (see section 5.5), but for the relatively simple case of the monomers, the minimisation process is sufficient to show any important differences in conformation and energy between the *exo* and *endo* isomers.

5.2.3 Molecular Modelling of (D-*Endo*) and (D-*Exo*)*N*-Norbornenyl Alanine Methyl Esters.

As an illustrative example, both of the above monomers were constructed using the molecular simulation program *Discover* running within Biosym's graphical molecular modelling interface, Insight II (the C_4N ring was considered as a planar entity based on reported crystal structures of related compounds[7]). A minimisation program was subsequently carried out over 2000 iterations, and then an additional 10 to see whether convergence had been reached. The results are displayed in table 5.1.

Monomer	Energy after 2000 Iterations (kJ).	Energy after 2010 Iterations (kJ).	Energy Difference (kJ).
exo-D	43.87	43.83	0.03
endo-D	47.50	47.46	0.04

Table 5.1 The comparative energies of *exo*-D and *endo*-D monomers after minimisation.

The difference in energy between 2000 and 2010 iterations is such a small fraction of the overall energy of the molecules (0.07% and 0.08% for *exo* and *endo* respectively) that convergence has effectively been achieved. The two examples are illustrated in figure 5.2.

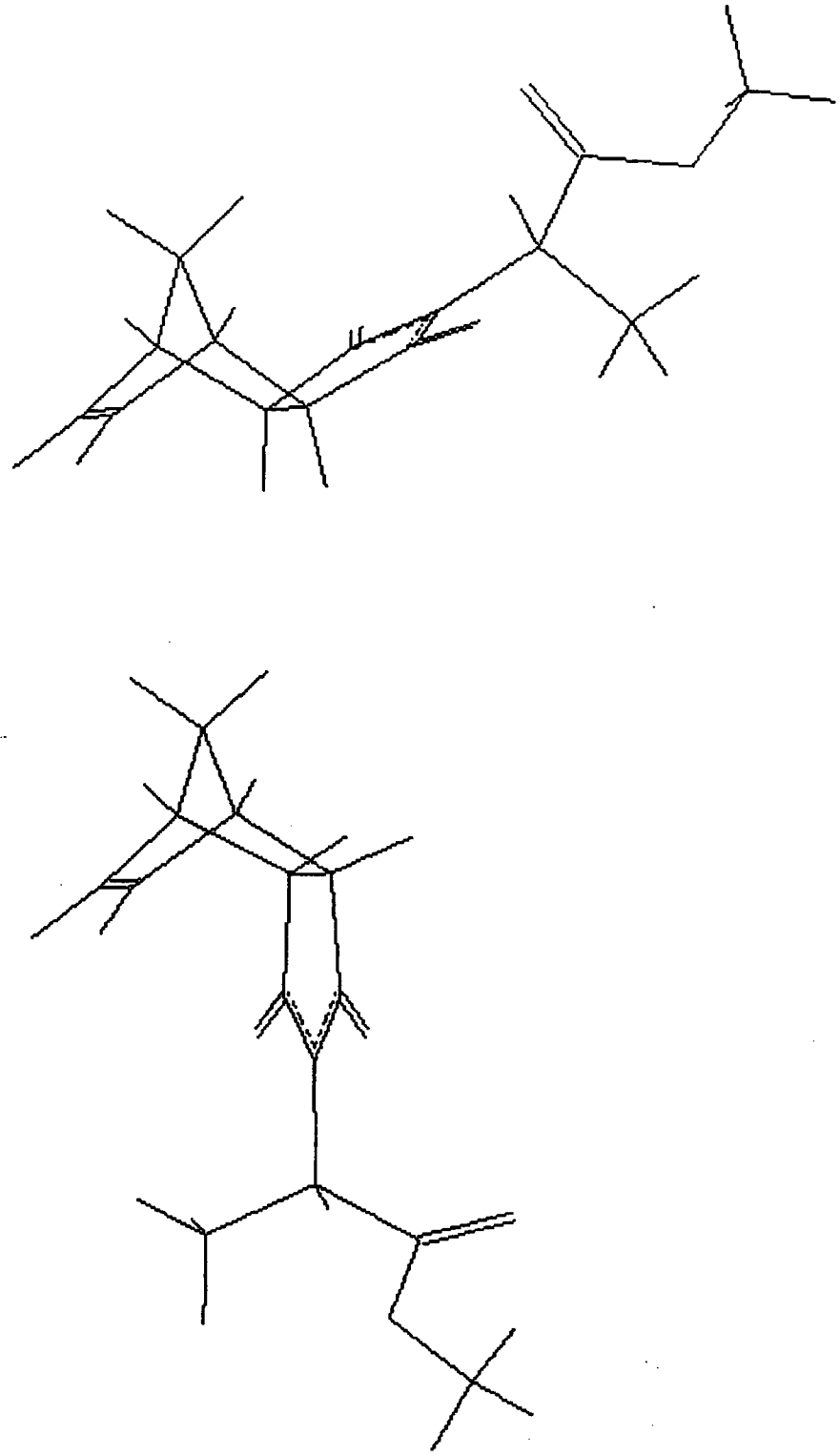

Figure 5.2 Minimised *exo*-D and *endo*- D monomers.

5.2.4 Discussion of Results from Molecular Modelling.

The two final energies of the minimised structures show the *exo* monomer having 3.63 kJ less energy than the *endo*. This difference in energy can not be the cause of the resistance to polymerisation that has been reported for other norbornene *endo* isomers, as the higher energy gives a less stable structure that may be more likely to undergo ROMP. The relative orientations of the *N*-functionalised maleimide moieties are of significance however. Assuming that the attack of the metal-alkylidene occurs only at the *exo*-face of the norbornene ring,[8] the lower reactivity of the *endo* isomer arises as a result, not of initial interactions, but steric interference once ring-opening of the bicyclic structure has occurred. This causes the substituents to be cis to one another both in the metallacyclobutane intermediate, and in the 5-membered ring formed upon ring opening. A much preferred orientation is when the substituents on the resultant ring and intermediate metallacycle are positioned further away, as in the case for the *exo* derived monomers. This is illustrated in figure 5.3 and 5.4, and has been studied for the case of fluoro-alkyl substituted norbornenes by Risse,[6] where the activity towards polymerisation has been correlated with the size of the *endo* substituent.

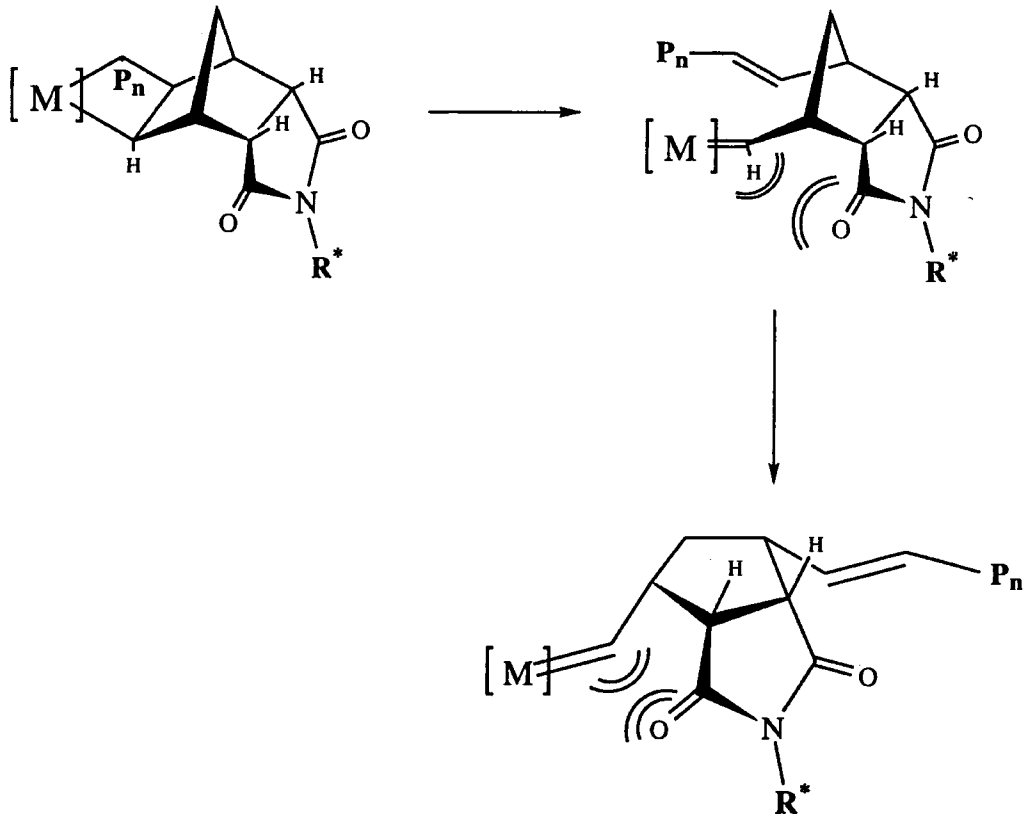

Figure 5.3 Ring-opening of *endo*-substiuted norbornene showing steric crowding of the cis arrangement.

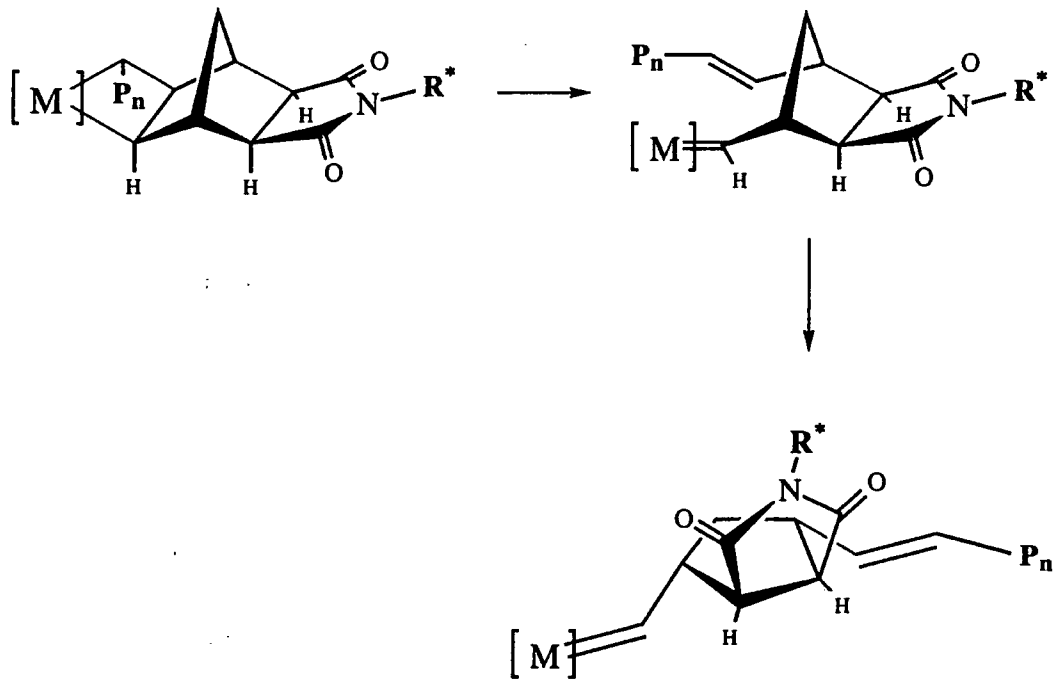

Figure 5.4 Ring-opening of *exo*-substituted norbornene showing reduced steric crowding of the trans arrangement.

In this study, the interactions illustrated above for the *endo*-monomers were insufficient to prevent polymerisation from occurring, but influenced the microstructure of the resultant polymers (see section 5.4.6).

5.3 Determination of the 'Living' Nature of the Polymerisation Process.

5.3.1 Living Polymerisation Processes.

Many of the desirable physical and chemical properties of a polymer are dependent upon the microstructure and molecular weight distribution of that sample. It is therefore one of the major objectives within polymer synthesis to gain the maximum control over these criteria. So called 'living' polymerisation mechanisms have thus far provided the greatest degree of control over the synthesis of polymers, and there currently exist examples of such processes within anionic,[9] cationic,[10] radical,[11] ROMP[12] and Ziegler-Natta[13] polymerisations. The experimental criteria defining living polymerisations have been investigated by Quirk and Lee[14] and are summarised below.

1. Polymerisation proceeds until all the monomer has been consumed. Introduction of additional monomer causes polymerisation to continue.
2. The number average molecular weight (M_n) is a linear function of conversion.
3. The number of polymer molecules (and active sites) remains constant.
4. Narrow molecular weight polymers are produced.
5. Molecular weight can be controlled by stoichiometry.
6. Block copolymers can be formed by sequential monomer addition.
7. Chain-end functionalised polymers can be prepared in quantitative yields.

5.3.2 Living Ring Opening Metathesis Polymerisations.

The alkylidene protons of Schrock-type initiators resonate at low field (**I** = δ 11.30, **II** = δ 11.67, **III** = δ 12.12) in ^{1}H NMR spectra (400 MHz in C_6D_6 at 298K) which provides an excellent handle for the study of these polymerisation processes, being clear of most other proton signals. If ring opening has occurred, the signal of the new alkylidene proton should correspond to a doublet for ring-opened norbornene monomers, usually appearing slightly down-field from the unreacted alkylidene resonance. This splitting occurs as a result of coupling between the α and β protons of the new alkylidene ligand, although it often contains much more information about the microstructure of the growing polymer chain.

Mixing the initiator **I**, **II**, or **III** with each monomer (10 equivalents) in C_6D_6 revealed the presence of a propagating alkylidene in the ^{1}H NMR spectra for all cases, with the results summarised in table 5.2 and illustrated in figure 5.5.

Monomer	Initiator I	Initiator II	Initiator III
exo-DL	11.54 (t*)	11.90 (m, br)	12.40 (m, br)
exo-D	11.54 (t*)	11.90 (m, br)	12.37 (m, br)
exo-L	11.54 (t*)	11.89 (m, br)	12.36 (m, br)
endo-DL	11.93 (m)	12.36 (m, br)	12.99 (m, br)
endo-D	11.92 (m)	12.35 (m, br)	12.99 (m, br)
endo-L	11.91 (m)	12.35 (m, br)	13.00 (m, br)

Table 5.2 : 400 MHz ^{1}H NMR shifts of the propagating alkylidene signal recorded in C_6D_6 at 298K (t* = pseudo-triplet ; m = multiplet ; br = broad).

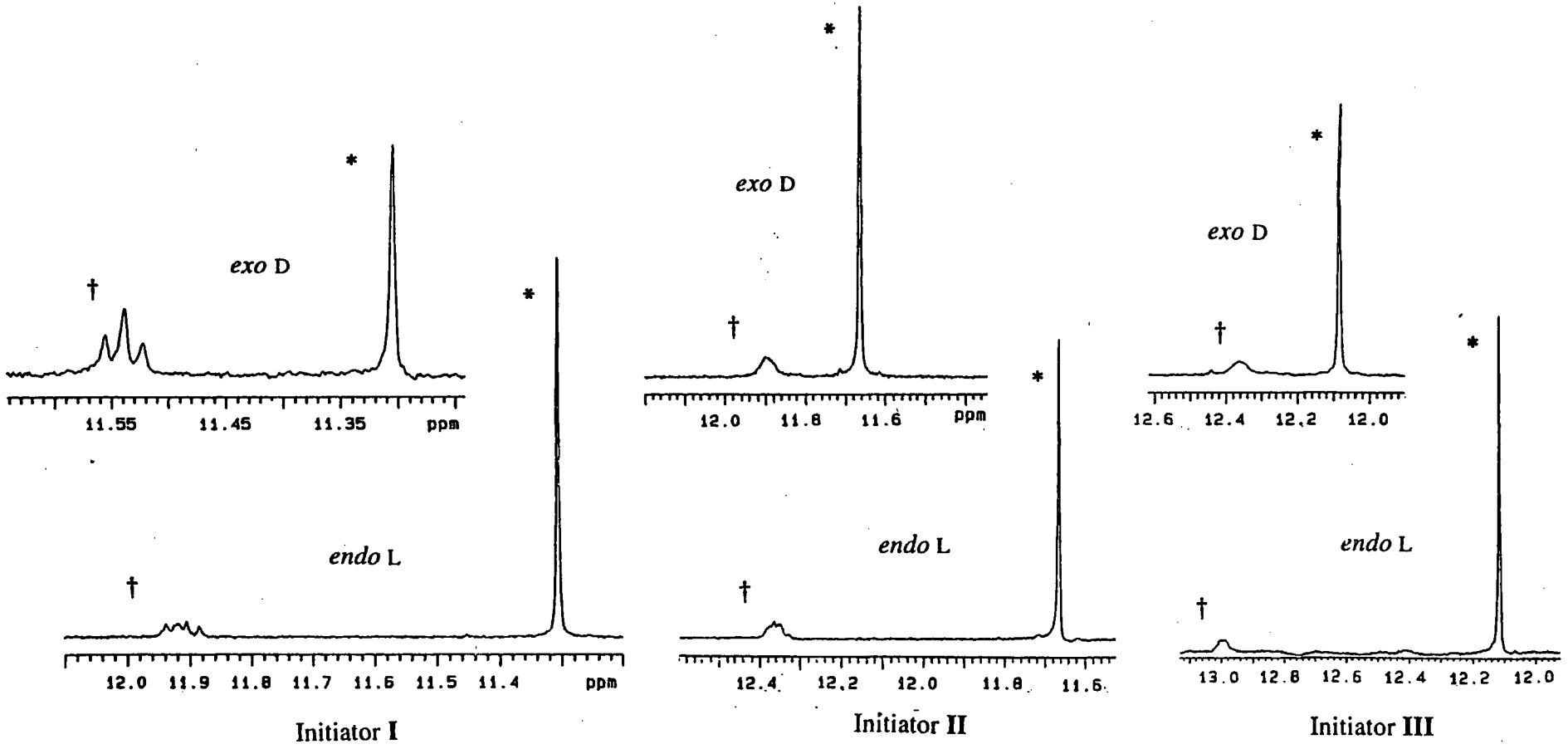

* Unreacted Initiator

† Propagating Alkylidene

Figure 5.5 Living alkylidene signals from *exo* D and *endo* L monomers with catalysts **I**, **II** and **III**.

5.3.3 Interpretation of Results.

Although no rigorous quantitative measurements were recorded allowing accurate determination of the rate constants for initiation (k_i) and propagation (k_p),[15] several deductions about the polymerisation process can be made. The ^1H NMR spectrum recorded immediately after mixing shows replacement of all the monomer signals by characteristically broad resonances attributable to the polymer, implying a rapid polymerisation process is occurring. The significant quantity of unreacted initiator remaining suggests that the rate constant for propagation is rapid compared to the rate constant for initiation (i.e. $k_p/k_i > 1$). This is expected as the alkylidene generated from the first and subsequent insertion products is significantly smaller in size than a neophylidene ligand, thus making it more accessible to incoming monomer.

Coupling of H_α to H_β in the alkylidene ligand generated from the ring-opened product should give rise to a simple doublet for the propagating alkylidene in the proton NMR. In this study, however, the signal was almost invariably an ill-defined multiplet. This may arise from the overlap of the second, third, fourth and higher insertion products,[15b,16] or may represent sensitivity of the α-proton to the cis / trans nature of at least the next double bond in the polymer chain.[15b,17] This long range effect may be further complicated by the tacticity of the polymer chain,[19b] where four possible stereochemical outcomes are possible when two monomer units are linked together (see figure 5.6).

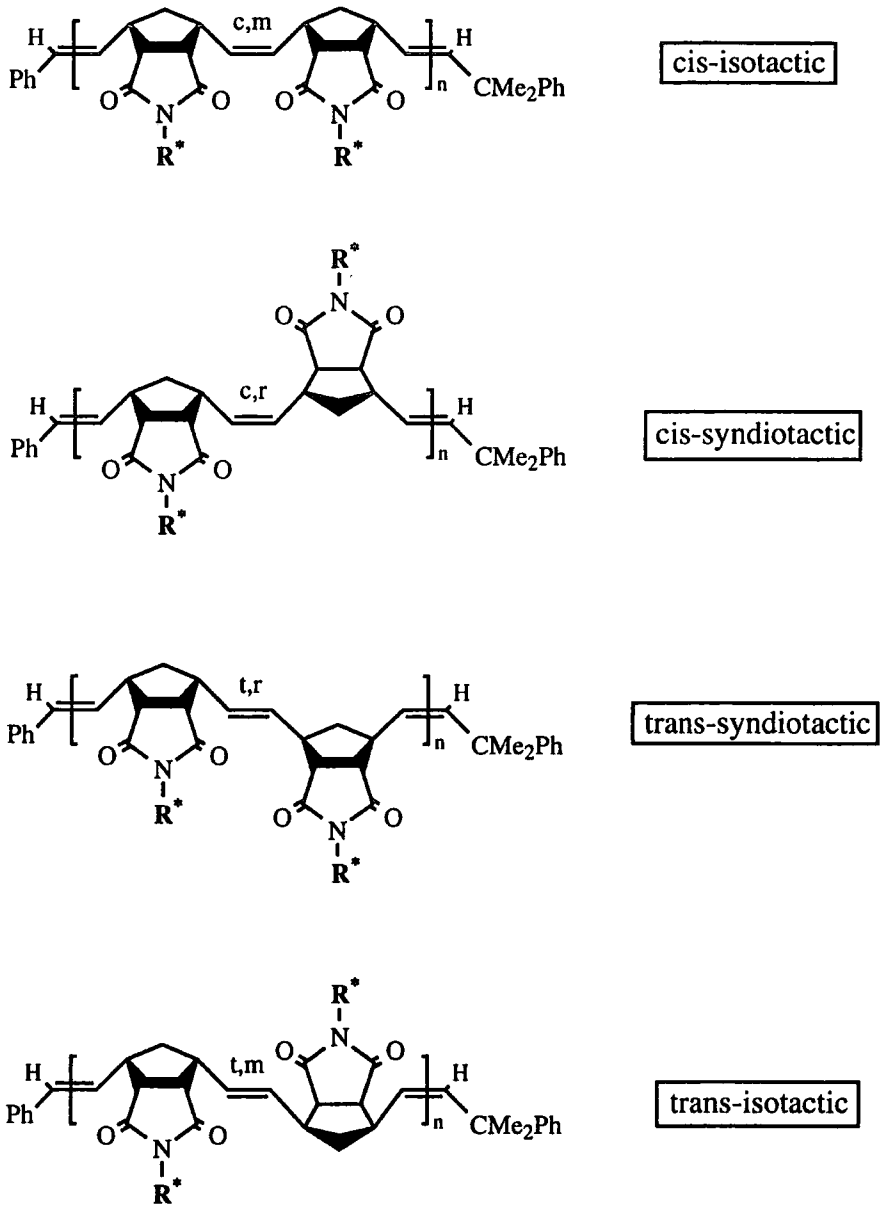

Figure 5.6 The four primary structures for poly-norbornene derivatives. (c=cis ; t=trans ; m=meso ; r=racemic -where meso and racemic refer to the relative chirality of the allylic carbons in the cyclopentane ring on each side of the double bond)

There is a significant difference in chemical shift between the propagating alkylidene signal for the *exo* and *endo* monomers with each catalyst, which must arise as a direct consequence of the orientation of the substituents and be independent of the cis / trans content. This may be due to the interaction of the growing polymer chain with the electrophilic metal centre, where the substituents from the amino acid residue in the *endo* monomers are orientated in such a way that they can bind to the

molybdenum centre from below (figure 5.7), whereas the *exo* monomer has the amino acid residue positioned where the substituents are distant from the metal centre. The position of the imido ligand also disfavours any interaction between the metal centre and the substituents attached to the *exo*-monomers.

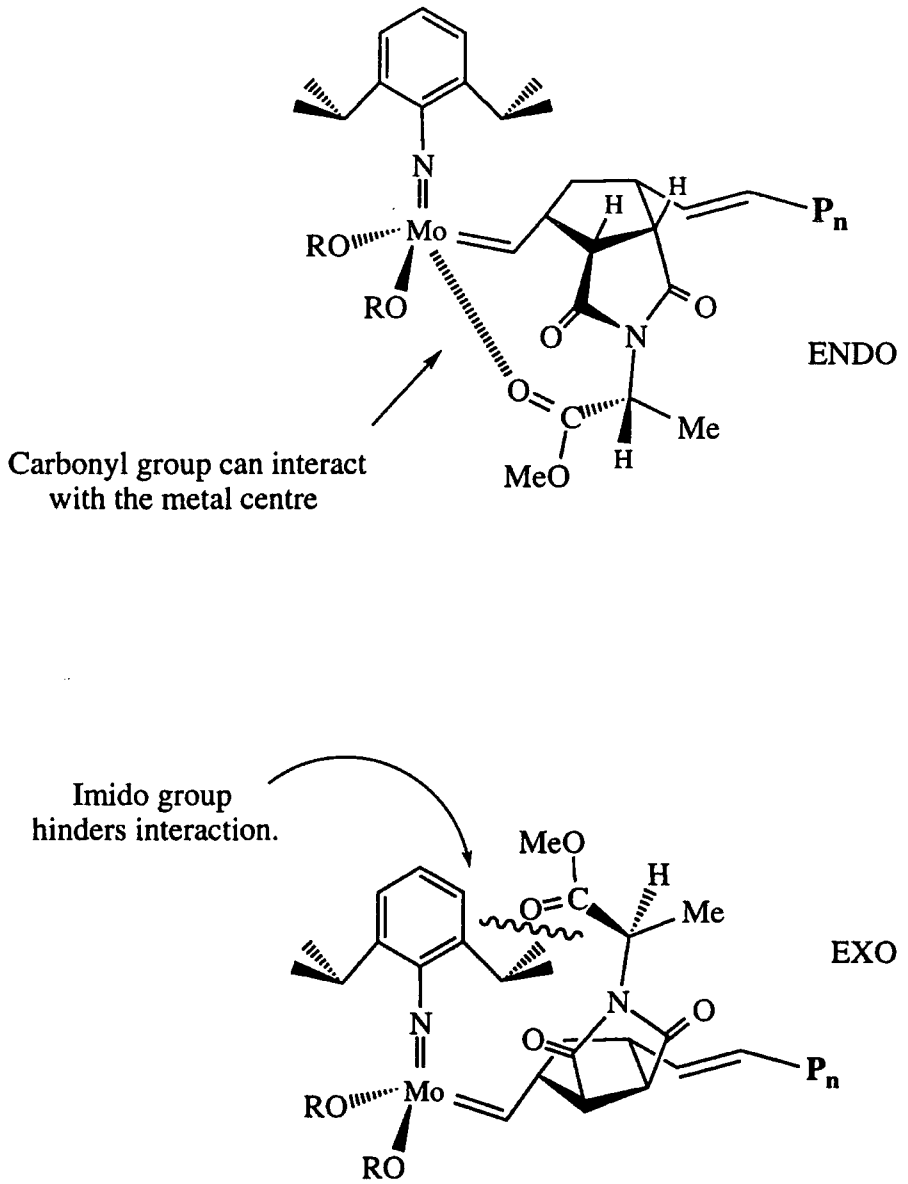

Figure 5.7 Postulated interaction of the methoxy group of an *endo* monomer with the metal centre.

5.4 The ROMP of *N*-Norbornenyl Alanine Methyl Esters with $Mo(NAr)(=CHCMe_2Ph)(OR)_2$ (R = CMe_3 ; $CMe_2(CF_3)$; $CMe(CF_3)_2$).

5.4.1 General Procedures.

All of the polymerisations were performed in an inert atmosphere glove box, typically employing 0.25 g of monomer in 3 g (3.46 cm^3) of toluene and 0.01 g of catalyst in 1 g (1.15 cm^3) of toluene. A small aliquot of monomer solution was added to the initiator solution to convert all of the initiator to the propagating ring-opened species. The remaining monomer was then added dropwise with rapid stirring and the polymerisation was allowed to proceed for a set length of time (*vide infra*) before addition of excess benzaldehyde (50 µl) to cleave the polymer from the metal centre in a 'Wittig' type reaction. The polymer was then isolated by precipitation of the toluene solution into an excess (ca 100 cm^3) of hexane, resulting in overall yield of > 90%. The resultant off-white polymers were collected by filtration and dried in a vacuum oven (full experimental details appear in section 6.5.2).

5.4.2 Variation of Solvent System.

As a measure of the ideal nature of the polymerisation, the Gel Permeation Chromatography (GPC) traces were examined. This technique records the weight average molecular weight (M_w) and the number average molecular weight (M_n), allowing the polydispersity index (PDI) to be calculated (M_w/M_n), and compared with the ideal value of 1. Initial experiments were permitted to run overnight (15-24 hours) and the results gained for the *exo*-monomers with catalysts **I** and **III** are collected in table 5.3. With initiator **I** the molecular mass distribution is reasonably narrow, but with **III** the values are much larger implying that the system is deviating from ideal behaviour.

Monomer	Catalyst	PDI
exo-DL	**I**	1.15
exo-D	**I**	1.13
exo-L	**I**	1.25
exo-DL	**III**	1.32
exo-D	**III**	1.41
exo-L	**III**	2.00

Table 5.3 Polydispersity values for *exo*-monomers with catalysts **I** and **III**.

It was noted that the polymer was not totally soluble in toluene, being observed as a gel forming around the polymerisation vessel as the reaction proceeded. If the active polymerisation site is being removed from solution, it could no longer react with monomer and is effectively 'dead'. Other active centres that were still in solution, however, could proceed with the polymerisation, thus producing chains of a higher molecular weight and causing the distribution to widen.

Polymerisations performed in a toluene / CH_2Cl_2 mixture (4:1 ratio), where the presence of the CH_2Cl_2 solubilised the forming polymer sufficiently to keep it in solution, had no effect on the PDI values suggesting the precipitation of the polymer was having no adverse effect.

5.4.3 Effect of Varying Polymerisation Time on Polymer Structure.

Another crucial factor in the ROMP of these monomers is the length of time that the reaction is permitted to run. Table 5.3 shows that generally the polymerisations employing catalyst **III** gave higher PDI values than the corresponding reaction with **I**. It is known that initiator **III** is more reactive towards olefins than **I** as a consequence of the enhanced electrophilicity at the molybdenum centre derived from the fluorinated alkoxide ligands. It is therefore probable that the greater molecular weight distribution

results from secondary metathesis, where the metal alkylidene reacts with a double bond already present within a polymer chain. If this is occurring with a double bond in the polymer chain already attached to the metal centre, low molecular weight cyclic structures will result, whereas if this process occurs with another polymer, the two chains will combine, thus increasing the molecular weight. The GPC traces for the reaction between the *exo*-L monomer and initiator **III** that were (a) allowed to run overnight (20 hours) and (b) for half an hour are shown in figure 5.8, showing a much broader distribution for the longer polymerisation time.

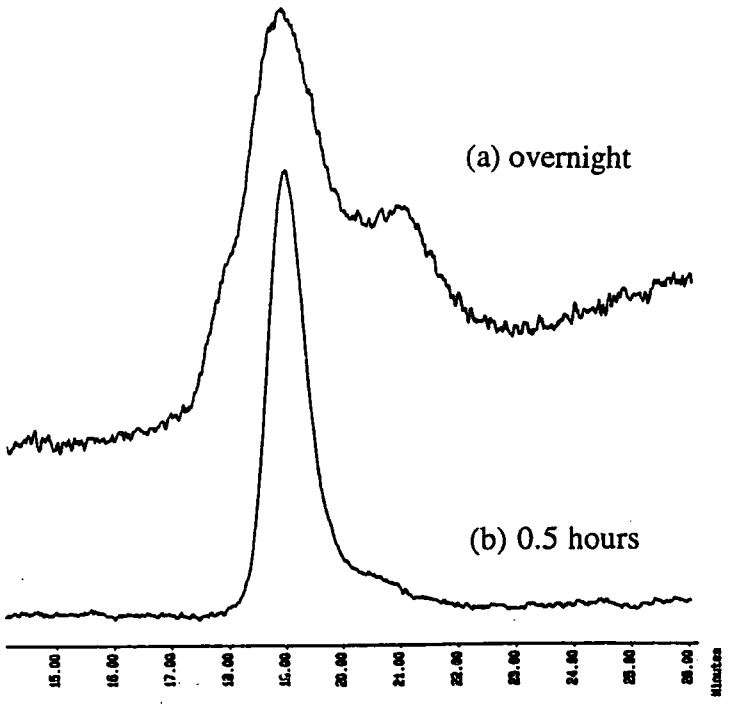

Figure 5.8 GPC trace of reaction of *exo*-L and **III** (a) overnight showing broad trace and (b) 0.5 hours showing much narrower distribution.

The time that the polymerisation was allowed to stir before the addition of benzaldehyde was reduced for reactions of *exo*-DL with **I** and **III**, and the results are displayed in table 5.4.

Monomer	Catalyst	Time	PDI
exo-DL	**I**	20 hours	1.15
exo-DL	**I**	2 hours	1.15
exo-DL	**III**	20 hour	1.32
exo-DL	**III**	0.5 hours	1.15
exo-D	**I**	20 hours	1.13
exo-D	**I**	2 hours	1.16
exo-D	**III**	20 hours	1.41
exo-D	**III**	0.5 hours	1.11
exo-L	**I**	20 hours	1.25
exo-L	**I**	2 hours	1.27
exo-L	**III**	20 hours	2.00
exo-L	**III**	0.5 hours	1.06

Table 5.4 Effect of time on PDI for *exo*-monomer with **I** and **III**.

With catalyst **I**, the reduction of time has little effect on the molecular weight distribution but we observe a drastic reduction for initiator **III** (see figure 5.8). This is consistent with the higher reactivity of **III** leading to secondary metathesis once all the monomer has been consumed.

The set of reaction conditions adopted for subsequent polymerisations was therefore to use toluene as the solvent, and permit the reaction to proceed for the time displayed in table 5.5.

Monomer Type	Catalyst	Time
exo	**I**	2 hours
endo	**I**	4 hours
exo	**II**	1 hour
endo	**II**	2 hours
exo	**III**	0.5 hours
endo	**III**	1 hour

Table 5.5 Variation of reaction time with catalyst and monomer type.

The polymerisation time for the *endo* monomers was doubled with respect to the *exo* due to the slower polymerisation predicted by steric hindrance of the ring-opened product (see section 5.2.4). This was also observed as the time taken for the polymer to reach sufficient molecular weight to precipitate from the toluene solution as a gel was noticeably greater for the *endo* monomers than for the *exo*. The complete GPC data is presented in table 5.6 showing the values obtained under the above conditions.

The variations between M_n(calculated) and M_n(observed) is a likely consequence of the differing GPC behaviour of these polymers compared with the polystyrene standards used in the calibration of the equipment.

Monomer	Catalyst	PDI	M_n (calc)	M_n (obs)	M_w
exo-DL	I	1.15	13741	22916	26354
	II	1.25	16439	19274	24052
	III	1.15	19138	23210	26722
exo-D	I	1.16	13741	20480	23816
	II	1.26	16439	19350	24460
	III	1.11	19138	18098	20020
exo-L	I	1.27	13741	27071	34277
	II	1.50	16439	19538	29388
	III	1.06	19138	20000	21282
endo-DL	I	1.29	13741	18299	23532
	II	1.60*	16439	40968	65575
	III	1.56*	19138	43822	68216
endo-D	I	1.18	13741	19581	23138
	II	1.25	16439	30602	38247
	III	1.12	19138	32986	36967
endo-L	I	1.28	13741	21380	27404
	II	1.20	16439	28569	34401
	III	1.10	19138	35238	38734

Table 5.6 Full GPC data for all polymers.

Most of these values are sufficiently low to compliment the earlier observations that the polymerisation process is living. The occasional high values (marked * in table 5.6) most probably arise due to traces of oxygen present in the system, causing two polymer chains to combine in a bimolecular termination mechanism.[20] This is corroborated by the traces where bimodal distributions are observed, with a small high molecular weight peak at ca. twice the molecular weight of the main peak.

5.4.4 Spectroscopic Characterisation of Poly (*exo*)-*N*-Norbornenyl Alanine Methyl Ester - Assignment of Polymer Microstructure.

The key feature observed for the polymers derived from the *exo* monomers is the variation of the cis / trans vinylene content when different initiators were employed as the polymerisation catalysts. This phenomenon is well documented for the case of 2,3-bis(trifluoromethyl)norbornadiene where reaction with **I** gives >98% trans content and reaction with **III** produces a polymer with >98% cis vinylene content.[21]

Initial indications that this family of monomers was following the above trend came from the IR spectra. Thin films of the polymers were cast by evaporation of a CH_2Cl_2 solution directly onto a KBr disc. After drying in a moderately warm (60°C) oven for ca. 30 minutes the spectra were recorded and appear for the *exo*-DL monomer with all three initiators in figure 5.9.

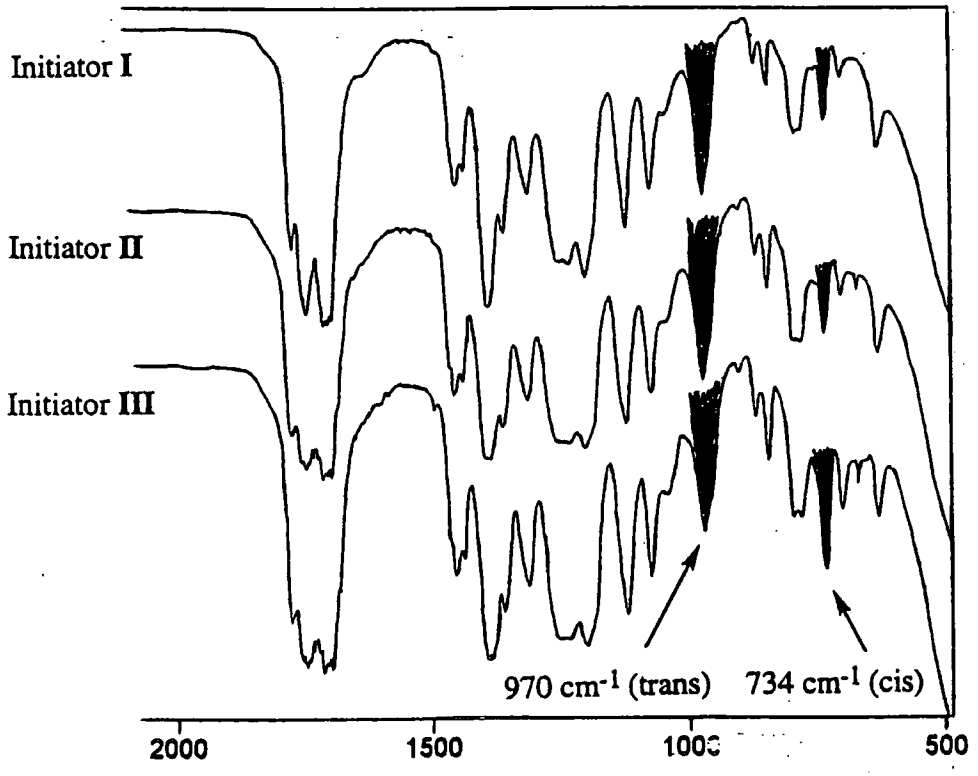

Figure 5.9 Infra-Red spectra of the polymers produced from *exo*-DL and **I, II** and **III.**

Although very similar in appearance close inspection reveals that, as we change from catalyst **I** to **III**, we observe an increase in the intensity of the band at 734 cm^{-1} (corresponding to the cis double bond stretch) and a decrease in the signal at 970 cm^{-1} from the related trans component of the polymer. This suggests an increase in σ_c (the fraction of cis-vinylene double bonds in the polymer chain) when fluorinated initiators are employed. Absolute determination of σ_c from IR spectroscopy is problematic due to the different absorbance coefficients of cis and trans double bonds, but the trend is apparent.

A more rigorous method of quantitatively assigning the cis / trans ratio is by ^1H and ^{13}C NMR spectroscopy. All of the polymers discussed in this section were found to be readily soluble in $CDCl_3$, and high field NMR spectra were recorded and assigned using a combination of HETCOR and DEPT techniques. The ^1H and ^{13}C NMR spectra of the polymers from the *exo*-DL monomer with all three catalysts appear in figure 5.11 and 5.12 respectively (labelling scheme illustrated in figure 5.10), and the data for all 9 polymers is collected in table 5.7.

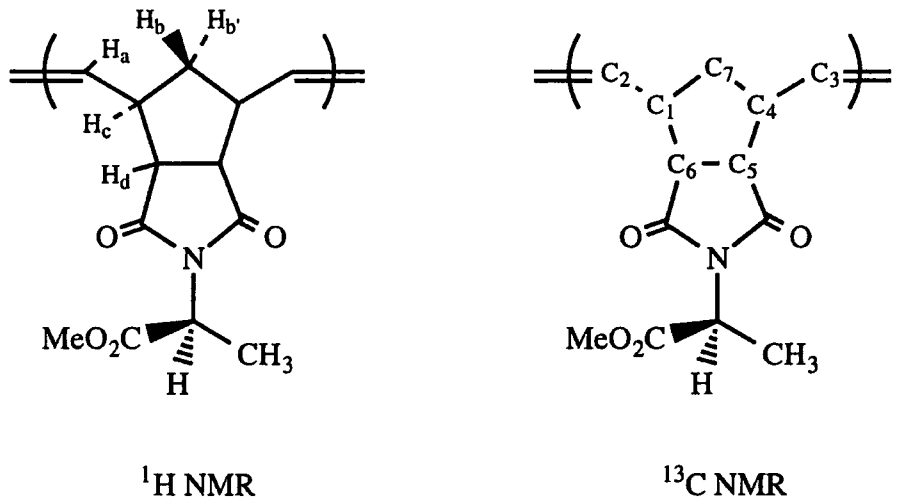

^1H NMR ^{13}C NMR

Figure 5.10 Labelling scheme adopted in NMR assignments.

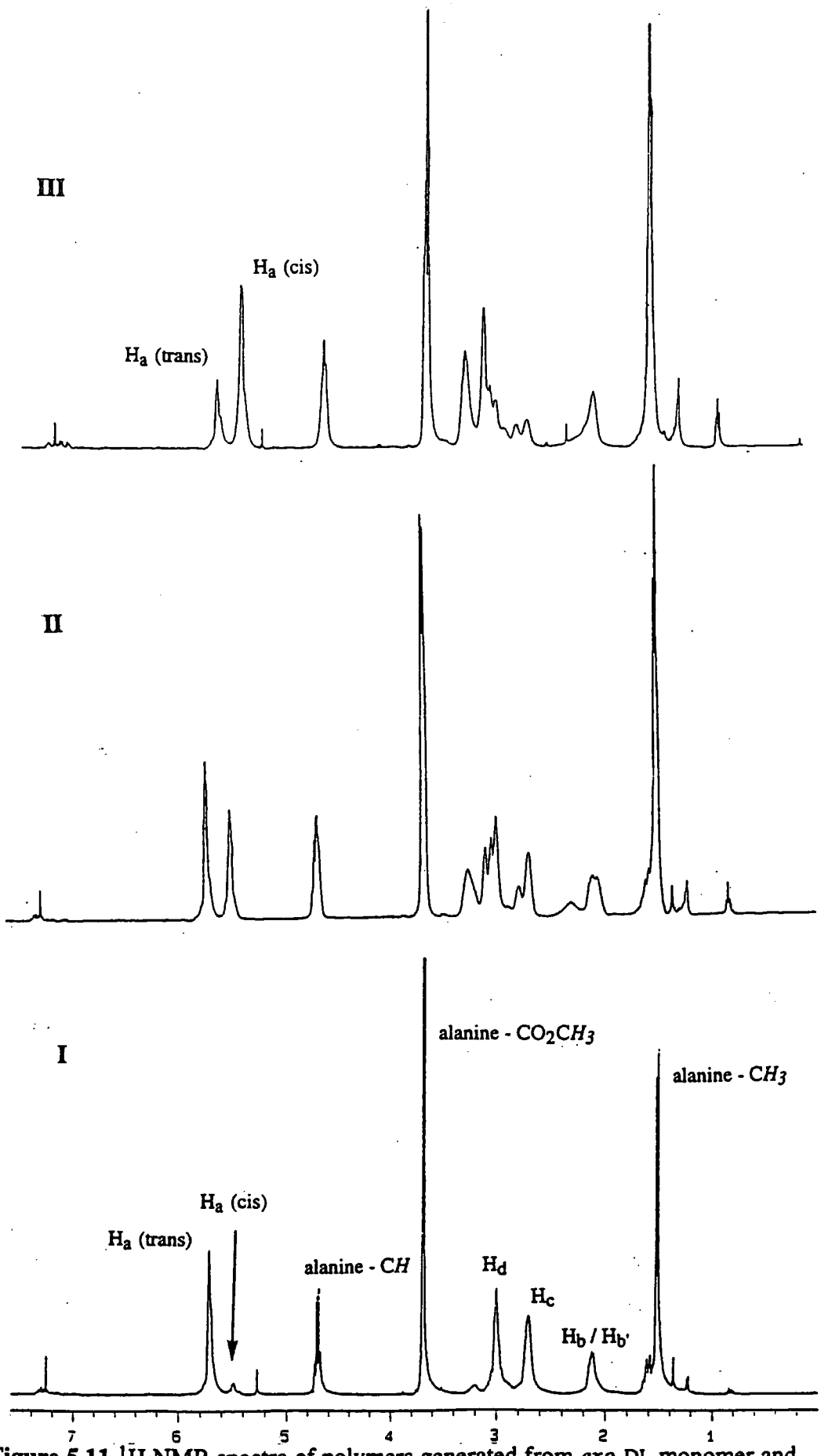

Figure 5.11 ^{1}H NMR spectra of polymers generated from *exo*-DL monomer and catalysts **I**, **II** and **III**.

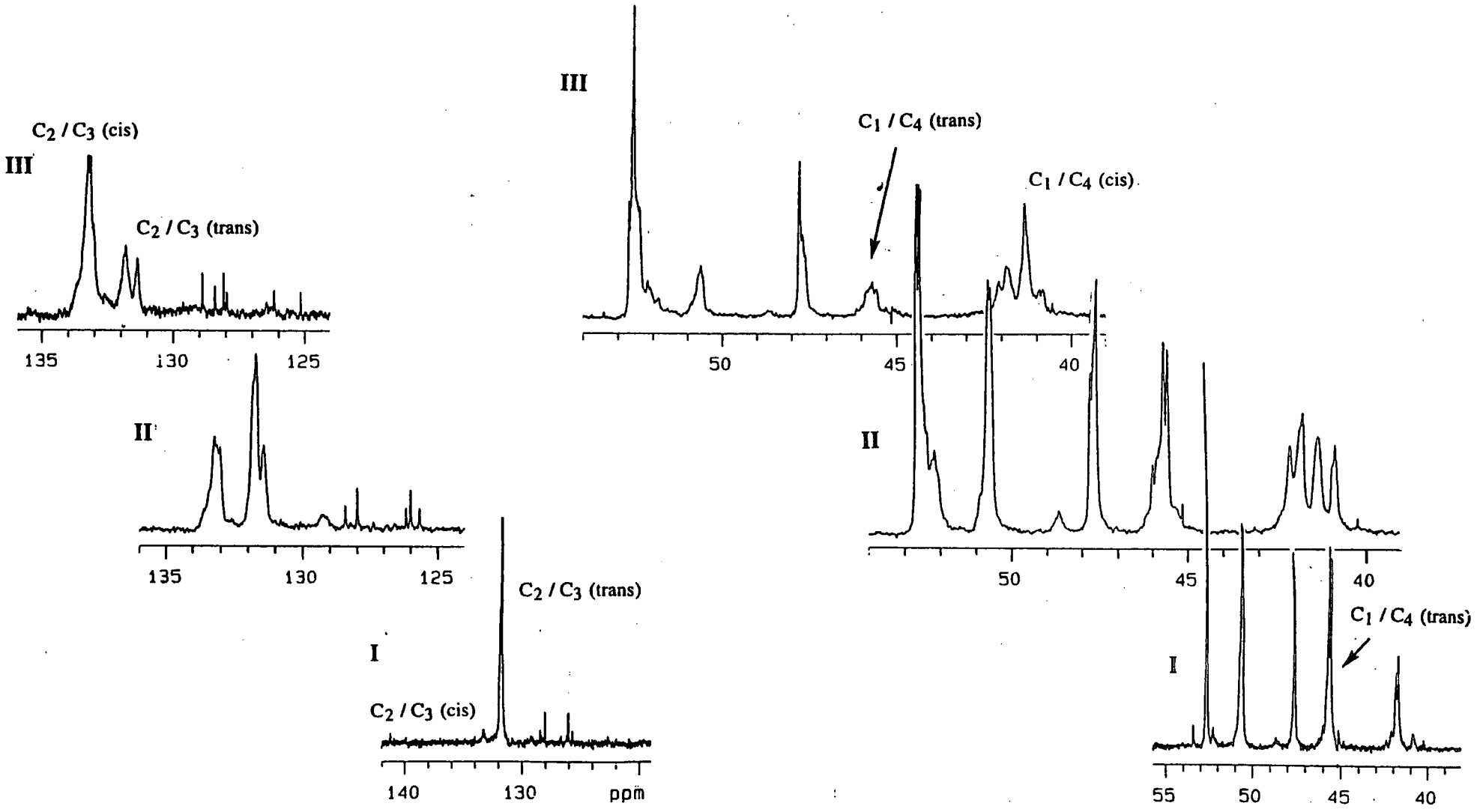

Figure 5.12 ^{13}C NMR spectra of polymers generated from *exo*-DL monomer and catalysts I, II and III.

Monomer	Initiator	σ_c *
exo-DL	I	0.09
exo-D	I	0.08
exo-L	I	0.07
exo-DL	II	0.41
exo-D	II	0.41
exo-L	II	0.43
exo-DL	III	0.71
exo-D	III	0.74
exo-L	III	0.73

* As determined by integration of the olefinic region of the ^{1}H NMR spectra.

Table 5.7 cis / trans content of polymers derived from *exo* monomers.

The increase in cis content upon changing from initiator **I** to **III** is clearly evident in the olefinic region of the ^{1}H NMR spectra, where the signal corresponding to the cis vinylene groups at 5.5 ppm gains in intensity relative to the trans signal at 5.7 ppm. Integration of these two peaks allowed σ_c to be calculated for *exo*-monomers (see figure 5.11).

The ^{13}C NMR spectra (figure 5.12) also reflect this increase in cis content as the olefinic carbon signal at 133.2 ppm (cis) grows relative to the corresponding trans peaks at 131.8 ppm. Generally in polynorbornene derived polymers, the difference in chemical shift between the cis and trans carbon atoms adjacent to the double bond (C_1 and C_4) is four to five ppm,[8] with the cis resonance appearing at higher field. This is also observed in the work presented here where the trans peak at 45.7 ppm is gradually replaced by a cis signal at 41.3 ppm, although this is slightly complicated by overlap with the C_7 bridgehead carbon resonances.

Schrock *et al* have recently unambiguously determined the tacticity in chiral polymers derived from the ROMP of 2,3-dicarboalkoxynorbornadienes and 5,6-

disubstituted norbornenes by direct (NMR) methods.[22] A similar analysis of the polymers presented in this work revealed extensive splitting of the C_1/C_4, C_5/C_6 and C_7 resonances indicating that these polymers are largely atactic, but with a slight bias towards syndiotacticity for the trans polymers.

5.4.5 Spectroscopic Characterisation of Poly (*endo*)-*N*-Norbornenyl Alanine Methyl Ester - Assignment of Polymer Microstructure.

Although polymers derived from the *endo* family of monomers may be expected to follow similar trends in cis / trans ratios to those observed for *exo* monomers, the IR spectra show almost no variation for the cis and trans C=C stretching bands at 734 and 967 cm^{-1}, suggesting the polymer microstructure is invariant to the initiator employed. ^1H NMR spectra support this observation, remaining almost constant for the polymers generated from the reaction with catalysts **I**, **II** and **III**. An unfortunate problem associated with these spectra, however, is the coincidence of the cis and trans olefinic resonances at 5.6 ppm (400MHz, $CDCl_3$), precluding accurate determination of σ_c from integration of these signals (see figure 5.13).

This peak overlap extends to the ^{13}C NMR spectra, where both the cis and trans olefinic carbon resonances lie at 129.2 ppm (see figure 5.14). The evaluation of σ_c is nevertheless possible from a quantitative ^{13}C NMR experiment through integration of the $C_1 + C_4$ peaks, where the trans signal is located at 45.3 ppm and the cis signal occurs 5 ppm upfield at 40.3 ppm. All nine polymers derived from the *endo* monomers were found to be predominantly trans, with σ_c values between 0.09 and 0.11. The splitting associated with the carbon resonances again suggest that the structure is not fully tactic.

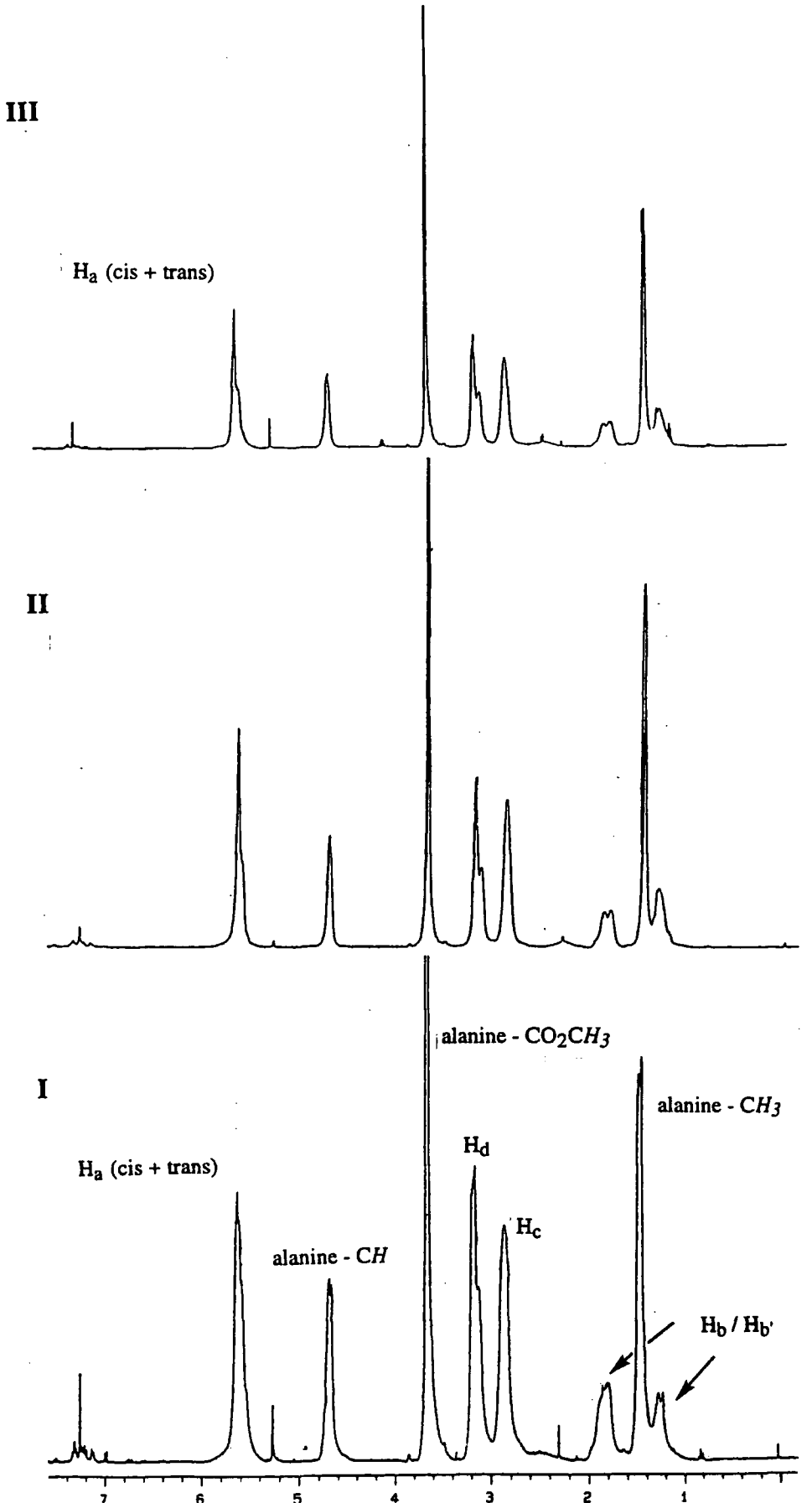

Figure 5.13 ^{1}H NMR spectra of polymers generated from *endo*-DL monomer and catalysts **I**, **II** and **III**.

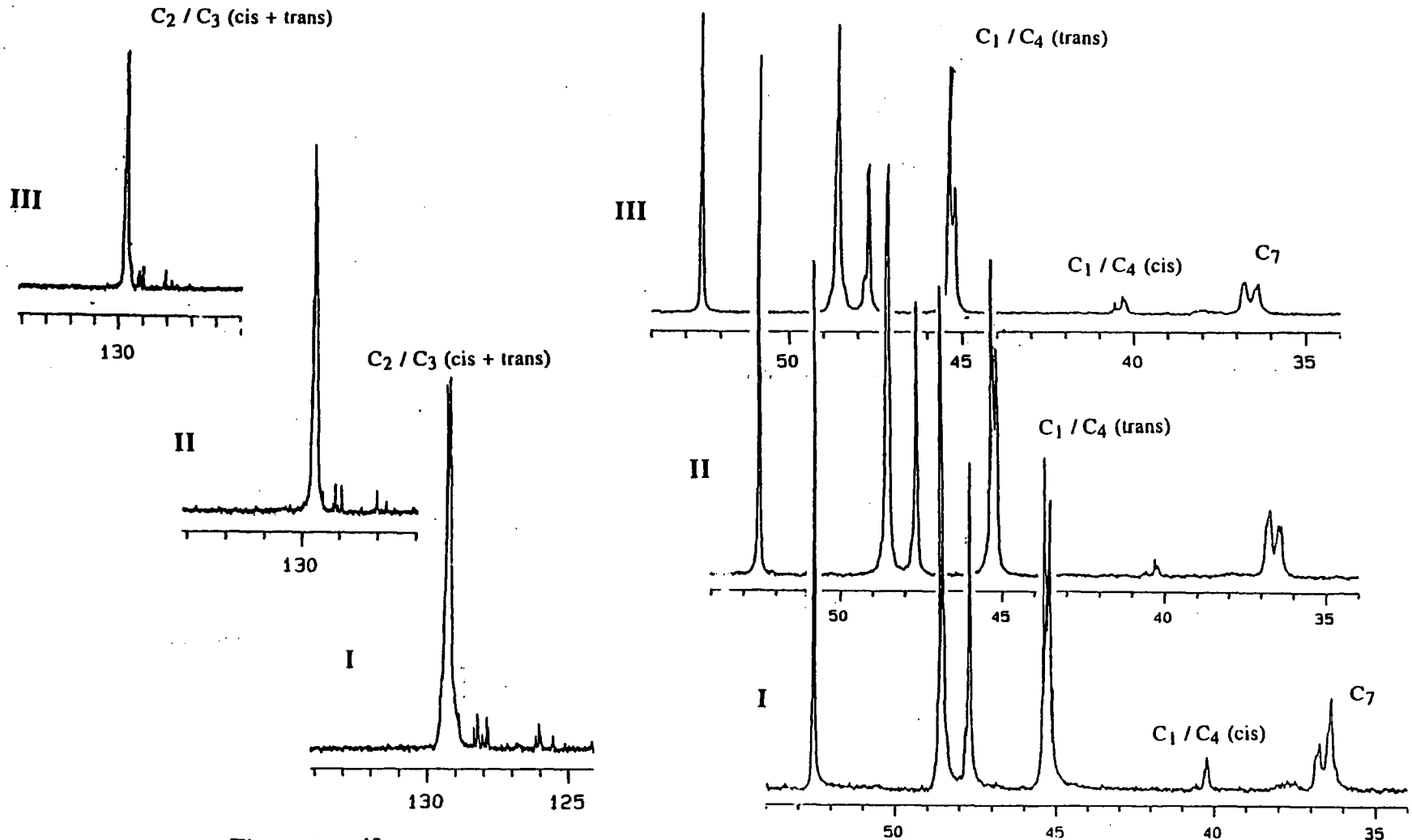

Figure 5.14 ^{13}C NMR spectra of polymers generated from *endo*-DL monomer and catalysts **I**, **II** and **III**.

5.4.6 Explanation of the Observed Polymer Microstructure.

It has been shown that a base (e.g. PMe_3) will preferentially attack a four coordinate imido alkylidene complex at the CNO face[19b] giving rise to a trigonal bipyramidal (TBP) adduct. In this TBP coordination geometry, the arylimido ring rotates into the equatorial plane which contains both the imido and alkylidene ligands. It has also been postulated that an incoming norbornene monomer will give rise to a similar arrangement of ligands about the metal centre.[19b]

The norbornene can approach the alkylidene ligand with either the bridgehead C_7 pointing towards the imido group ("7-syn" position) or away from it ("7-anti" position) as illustrated in figure 5.15.

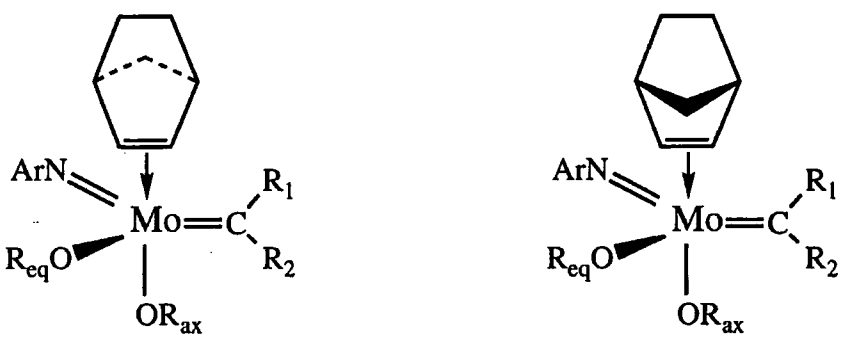

("7-syn") ("7-anti")

Figure 5.15 The two possible orientations of a norbornene ring approaching at the CNO face of a four coordinate imido alkylidene complex.

The "7-syn" orientation (i.e. with the bridging methylene pointing towards the imido ligand) is preferred on steric grounds, limiting interactions with the equatorial alkoxide OR_{eq}. The aryl ring (in the equatorial plane) will not adversely influence this orientation and possible unfavourable contacts with the alkylidene ligand are considered to be of little importance.

The formation of a pseudo triple bond between the imido nitrogen and the molybdenum centre forces the alkylidene ligand to lie with the α-H atom and β-C atom

in the N-Mo-C plane.[18] The alkylidene can thus orientate itself with the alkyl-group pointing away from the imido ligand (anti) or towards it (syn), as illustrated in figure 5.16.

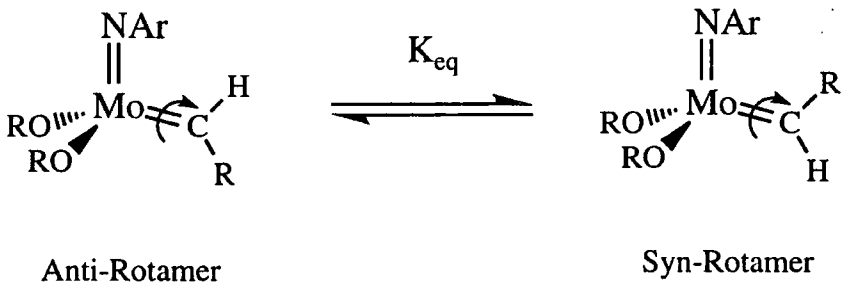

Anti-Rotamer Syn-Rotamer

Figure 5.16 Interconversion of syn and anti rotamers.

Studies have been performed on the interconversion of these two forms[19] which are both present as an equilibrium in solution. Schrock and co-workers[19b] have demonstrated that :-

1) the syn form of the initiator predominates in solution at room temperature.
2) the rate of interconversion between the two rotameric forms decreases as the alkoxide becomes more electron withdrawing.
3) the anti form is more reactive for ROMP.
4) ring opening through either rotamer generates a syn alkylidene ligand.
5) if the monomer adds in the "7-syn" position, the anti rotamer will result in exclusively trans vinylene groups and the syn form will give only cis (see figure 5.17 for an illustration with norbornene).

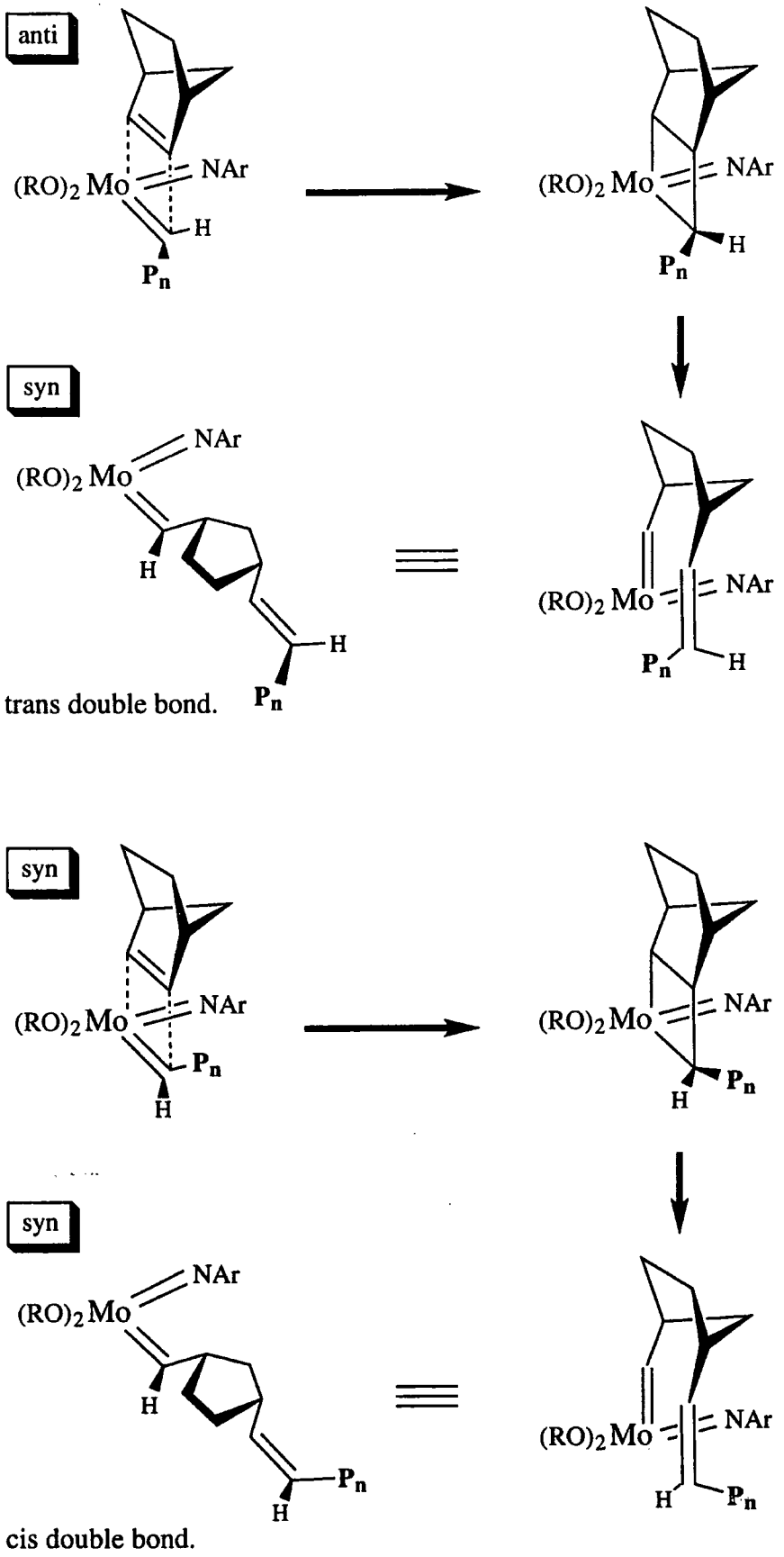

Figure 5.17 Diagrammatic illustration showing how anti rotamers give trans double bonds and syn rotamers give cis.

For the polymerisation of the *exo* monomer employing catalyst **I**, a high trans content is observed in the polymer consistent with polymerisation proceeding predominantly through the more reactive anti rotamer. This is plausible as the rate of syn-anti interconversion for this initiator is sufficiently fast to allow access to this rotamer. As the ^{t}butoxide ligands are replaced with more electron withdrawing fluorinated alkoxides (catalysts **II** and **III**) the rate of rotation about the Mo=C bond decreases sufficiently to allow the monomer to access predominantly the syn form of the catalyst giving an increased cis content as observed.

Deviations from 100% cis and trans polymers are due to either reaction through the opposite rotamer, or attack of the monomer in the "7-anti" position. The monomer that Schrock chose for his study was 2,3-bis(trifluoromethyl)norbornadiene which polymerises at a much slower rate than the *exo* monomers studied.[23] It seems the more likely explanation for the deviation from an all cis or all trans microstructure is the rapid reaction of the monomer with the less reactive syn form during polymerisations with **I**, and reaction with the trace amounts of the anti rotamer for the polymerisations with **III**.

For the case of the *endo* monomer where the polymerisation was observed to be considerably slower, the reaction is predicted to proceed primarily through the anti rotamer to give the high trans polymer isolated, even though this species is only fleetingly present for the case of catalyst **III**. This theory predicts that all polymers would be 100% trans which is not the case, suggesting that the cis-fraction of vinylene groups reflects the statistical probability of the monomer approaching in the "7-anti" position. Another possible explanation is that the polymerisation is occurring exclusively through the syn rotamer, with mainly "7-anti" approach, and the small number of cis double bonds arising from "7"-syn" approach. This is unlikely to be the case for the steric reasons outlined earlier.

5.4.7 Thermal Analysis of the Polymers.

Both Thermal Gravimetric Analysis (TGA) and Differential Scanning Calorimetry (DSC) data were recorded for all polymer samples by Mr G.M. Forrest of the IRC in polymer science and technology at Durham (see section 6.1.1 for technical description). All of the polymers were heated from room temperature to 830°C, showing no change in their mass (excluding loss of residual solvent) until a temperature of ca. 500°C is attained. The polymers then all lose ca. 80% of their total mass over a temperature range of ca. 150°C and remain at this new mass for the remainder of the experiment. A possible reason for these observations (figure 5.18) is that the polymer loses the maleimide fragment from the polymer back-bone, (73% of the overall mass), and generates a new polymeric material that is very thermally resistant. To investigate this, a sample of the polymer from the *endo*-D monomer and **I** was heated in a furnace to a temperature of 700°C under a continual flow of argon for a 3 hour period. The result was a black, shiny material similar in physical appearance to polyacetylene that proved to be insoluble in common solvents. Tests are currently being undertaken to ascertain its nature.

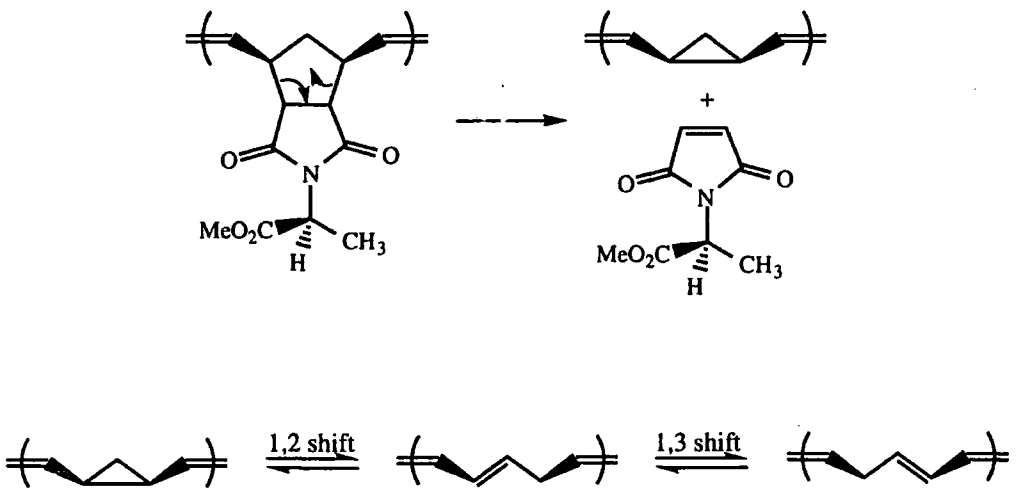

Figure 5.18 Possible thermal decomposition pathway for polymer samples.

Glass transition temperatures (T_g) for each of the polymers were obtained by Differential Scanning Calorimetry (table 5.8) and a representative trace is illustrated in figure 5.19.

Monomer	Catalyst	Glass Transition Temperature (°C)
exo-DL	I	154.4
exo-D	I	152.9
exo-L	I	153.2
endo-DL	I	192.1
endo-D	I	190.4
endo-L	I	195.1
exo-DL	II	146.2
exo-D	II	146.2
exo-L	II	147.3
endo-DL	II	192.1
endo-D	II	189.0
endo-L	II	191.3
exo-DL	III	138.2
exo-D	III	137.8
exo-L	III	136.6
endo-DL	III	192.3
endo-D	III	187.8
endo-L	III	189.1

Table 5.8 Glass transition temperatures (T_g's).

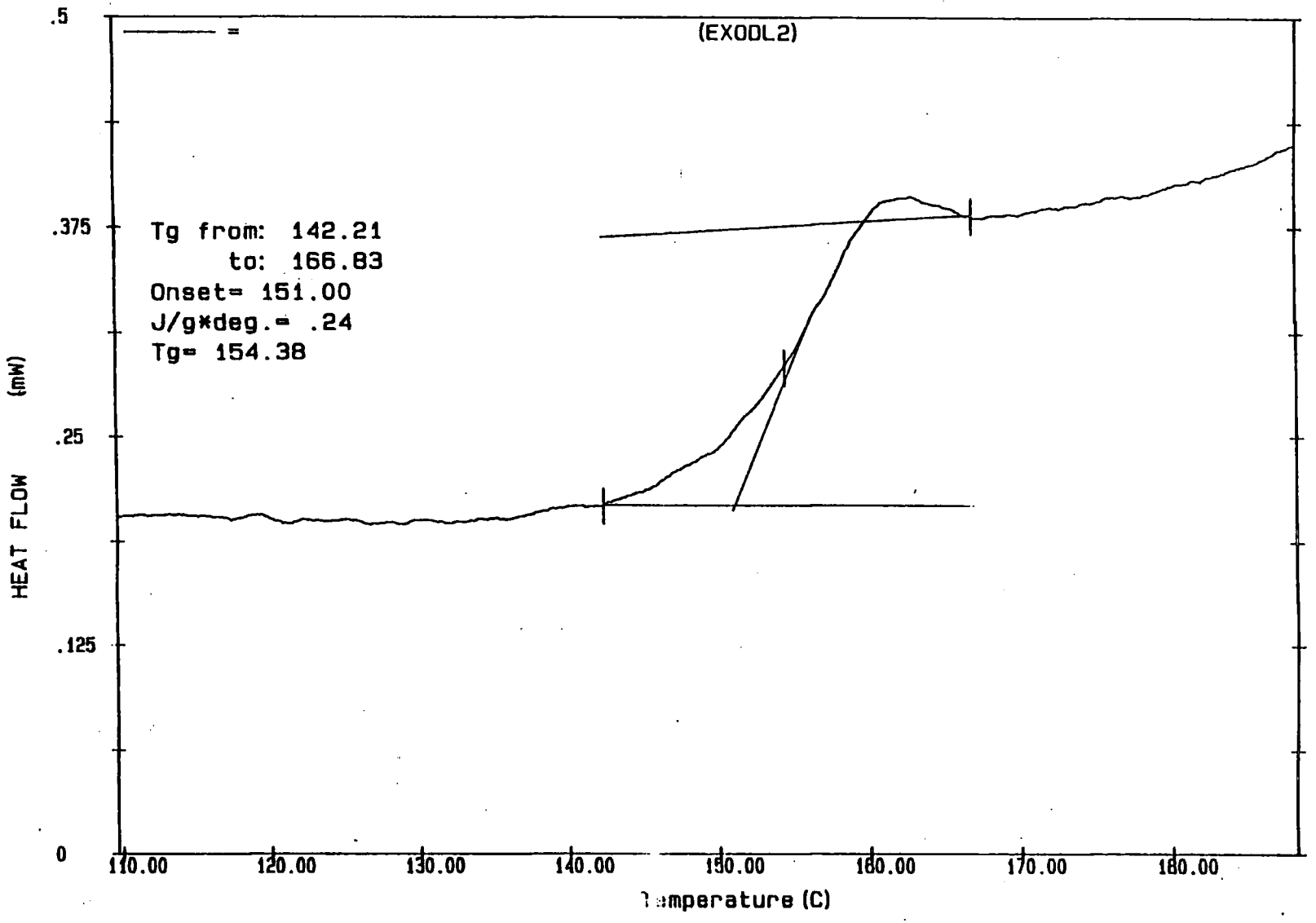

Figure 5.19 DSC trace illustrating the glass transition temperature of poly-*exo*-DL.

The glass transition point of a polymer is the temperature at which the sample ceases to exist in a glassy state and becomes soft and rubber-like. This corresponds to the polymer chains acquiring enough thermal energy to begin moving in a co-operative fashion.

The effect of increasing the cis content of the polymer chain manifests itself in the samples prepared from the *exo* derivatives as a decrease in T_g from 153.5°C (av) for **I** to 137.5°C (av) for **III**. It is proposed that the increase in σ_c causes less effective packing of the polymer chains and hence reduces the amount of thermal energy required to cause molecular motion. No such change is observed with the *endo* monomers as the T_g's are independent of the catalyst used (**I** = 192.6°C (av) ; **II** = 190.8°C (av) ; **III** = 189.7°C (av)), supporting IR and NMR data showing the invariance of σ_c to the different initiators for the *endo* monomers.

The orientation of the *N*-functionalised maleimide unit is also seen to affect the T_g of the polymers, demonstrated most clearly for the polymers generated with initiator **I**. Both the *exo* and *endo* class of monomer give rise to polymers with a similar σ_c value and yet the average difference between the T_g values is ca. 40°C. This variation in T_g must therefore arise from the substituent attached to the polymer chain influencing the inter- and intramolecular interactions present in the polymer chain. The higher T_g values for poly-*endo* samples is indicative of greater interactions being present and hence increased thermal energy is required to promote molecular motion.

5.4.8 Investigation of Optical Activity.

Optical activity in polymeric materials can be achieved in three different ways :-

1) As a result of chiral centres in the main chain of the polymer backbone.
2) From the presence of chiral residues attached to the backbone.
3) Due to overall supermolecular chirality, for example a helical conformation of the polymer chain.

Many of the polymers dealt with in this chapter were derived from optically active monomers and, through ROMP, should give rise to polymers with chiral substituents appended to the main backbone. Optical rotations were therefore determined to ascertain whether the chiral substituents behaved 'individually' or combined to give a cooperative effect, or indeed if any main chain chirality might be present. The results are presented in table 5.9 with values obtained for the monomers collected in table 5.10.

Monomer	Catalyst	[α]
exo-D	**I**	+34
	II	+38
	III	+34
exo-L	**I**	-31
	II	-35
	III	-30
endo-D	**I**	+54
	II	+50
	III	+52
endo-L	**I**	-52
	II	-50
	III	-51

Table 5.9 Optical rotation values of polymers derived from chiral monomers.

Monomer	[α]
exo-D	+43
exo-L	-43
endo-D	+22
endo-L	-25

Table 5.10 Optical rotation values for *exo* and *endo* monomers (Ref. 8).

The samples were tested at low concentrations (0.05 g in 3 cm^3 CH_2Cl_2) and then diluted by a factor of 2 in order to ascertain whether the first value calculated was a true reflection of optical activity, in which case the value of [α] would also be expected to half, according to the equation below.

$$[\alpha]_D^{20} = \frac{\alpha}{d \times l}$$

(where $[\alpha]_D^{20}$ = Specific Optical Rotation (°) ; α = Observed Reading ;

d = Density of Solution (g cm^{-3}) ; l = Path Length of Cell (dm)).

Equation 5.3 Specific optical rotation.

If the actual rotation was greater than 360° (often the case for polymers with main chain chirality), then the observed value would not decrease by half on dilution of the solution by a factor of two. For example, if the sample was rotating light 480°, a reading of 120° would be recorded (480° - 360°). If this was then diluted, the value would rise to 240° (0.5 x 480°) whereas if the value really *was* 120° then the half concentration value would be only 60°. All of the polymers tested showed that the value was reduced by half when the concentration was halved indicating the results in table 5.10 are 'true' values.

The error on [α] was calculated to be ± 5°. This value was realised by preparing five independent samples of the same polymer and taking the highest deviation from the average value. The main reason why the error is of such magnitude arises from the low concentrations of sample employed and the correspondingly small values of α recorded by the machine. This resulted in the lowest increment of the polarimeter corresponding to 1.2° and so slight variations on the recorded value gave relatively large differences in [α].

If the chirality was solely due to a macroscopic coiling of the polymer chain, we might expect to see an optical activity for the polymers prepared from the racemic monomers. No such values were observed suggesting that either the polymerisation of a racemic mixture results in both left and right handed helices being formed that cancel each other out, or the optical rotation values observed for polymers from chiral monomers is derived from another source.

In order to determine whether or not there was some cooperation between adjacent chiral centres (i.e. that the measured optical rotation might partly arise due to the macromolecular structure), two polymer samples differing in molecular weight by a factor of ten were prepared. The optical rotation values are displayed in table 5.11.

Monomer	Catalyst	M_n (calc)	M_n (obs)	n	[α]
endo-D	I	5530	5896	~22	+50
endo-D	I	51890	53928	~220	+51

(n = approx. number of repeat units in polymer chain)

Table 5.11 Comparison of chain length and optical activity.

The length of the chain can therefore be seen to have no effect on the optical activity of the polymer, as the chains vary in length by ca. 200 repeat units. This is again implying that the overall secondary structure of the polymer has little or no effect on the observed rotation value, i.e. each of the chiral centres behaves as if in dilute solution.

The apparent independence of optical activity on microstructure of the polymer is also supported by the invariance of [α] to the catalyst employed in the preparation of the sample. If the cis / trans ratio influenced the chirality, we would expect different optical rotations for the polymers from the *exo* monomers with **I**, **II** and **III**, as σ_c varies. In contrast, the change in the optical activity of polymers from 2-acycloxybicyclo[2.2.1]hept-5-enes with different catalysts is assigned to variations in double bond distribution,[24] and tacticity may also play an important role in the magnitude of [α] in a polymer sample.[25]

In conclusion, the chirality associated with the polymers presented in this study is derived from the optically active group attached to the main polymer backbone. Indications are that these groups are acting independently of each other.

5.5 Molecular Modelling Study of Idealised Polymer Fragments.

5.5.1 Introduction

In general, polymers tend to adopt coiled structures. With a view to obtaining some insight into the preferred structures adopted by the amino acid pendant polymers described here, molecular modelling studies were carried out on two idealised structural forms, namely the cis-isotactic and trans-syndiotactic polymers derived from the *endo* monomer (see figure 5.6). Polymer chains seven repeat units long were built using the program detailed in section 5.2.3 and fitted with the appropriate end groups before a minimisation was carried out.

5.5.2 *endo*-Trans Syndiotactic Polymer Chain.

An initial minimisation of 50000 iterations was performed and subsequently a further 25000 steps were carried out, giving the results below in table 5.12.

Initial Energy (kJ)	50000 Iterations (kJ)	75000 Iterations (kJ)
786.2	-34.0	-52.1

Table 5.12 Energy values for the minimisation of *endo*-trans syndiotactic polymer chain.

The energy change in the second minimisation of 25000 steps averages out as 7.24×10^{-4} kJ per iteration so the structure was deemed to have reached a stable conformation. The negative energy values indicate that the attractive interactions experienced by the molecule are greater than the repulsive ones, resulting in an arrangement that experiences an overall stabilisation.

Figure 5.20 shows the molecule in two orientations, the first being a view lengthways along the polymer back-bone (which is illustrated in a different colour to highlight its position), with the second view perpendicular to the first. Immediately apparent is an overall helical conformation of the polymer back-bone, with approximately six repeat units per turn. The chiral groups from the amino-acid residues can be seen to be located on the periphery of this secondary structure.

5.5.3 *endo*-Cis Isotactic Polymer Chain.

An identical procedure to that carried out in the preceding section was followed for a seven repeat unit cis isotactic polymer chain. The following energy values are obtained.

Initial Energy (kJ)	50000 Iterations (kJ)	75000 Iterations (kJ)
1.26×10^7	298.6	263.5

Table 5.13 Energy values for the minimisation of *endo*-cis isotactic polymer chain.

The energy values are much greater for this section of polymer chain compared to the previous example, with the destabilising repulsive terms predominating over the attractive ones giving a *net* destabilising effect. On a simplistic level this can be seen to derive in part from the relatively large side groups of the polymer chain being forced into a close environment, causing unfavourable steric interactions. The molecule is displayed in similar orientations to that of the trans syndiotactic example in figure 5.20.

Again a coiling of the polymer back-bone is observed, but a much tighter helix is generated (ca. 3 repeat units per turn). The amino acid chiral groups radiate out from this helix approximately perpendicular to the direction of the polymer back-bone.

5.5.4 Discussion.

Although both of the molecules are seen to adopt an overall helical conformation, the type and extent of coiling differs markedly. It is important to remember that the two structures are only representative fragments of the polymer chain each containing only one tacticity. In the prepared samples, both cis and trans double bonds are found and a range of tacticities is suspected. The above structures are not accurate representations of the whole polymer sample, but indicate how certain sections of that chain may be orientated. In reality the polymer sample is also not static but undergoing molecular motion. The following section deals with a very brief look at the dynamics of a small polymer fragment as a function of time

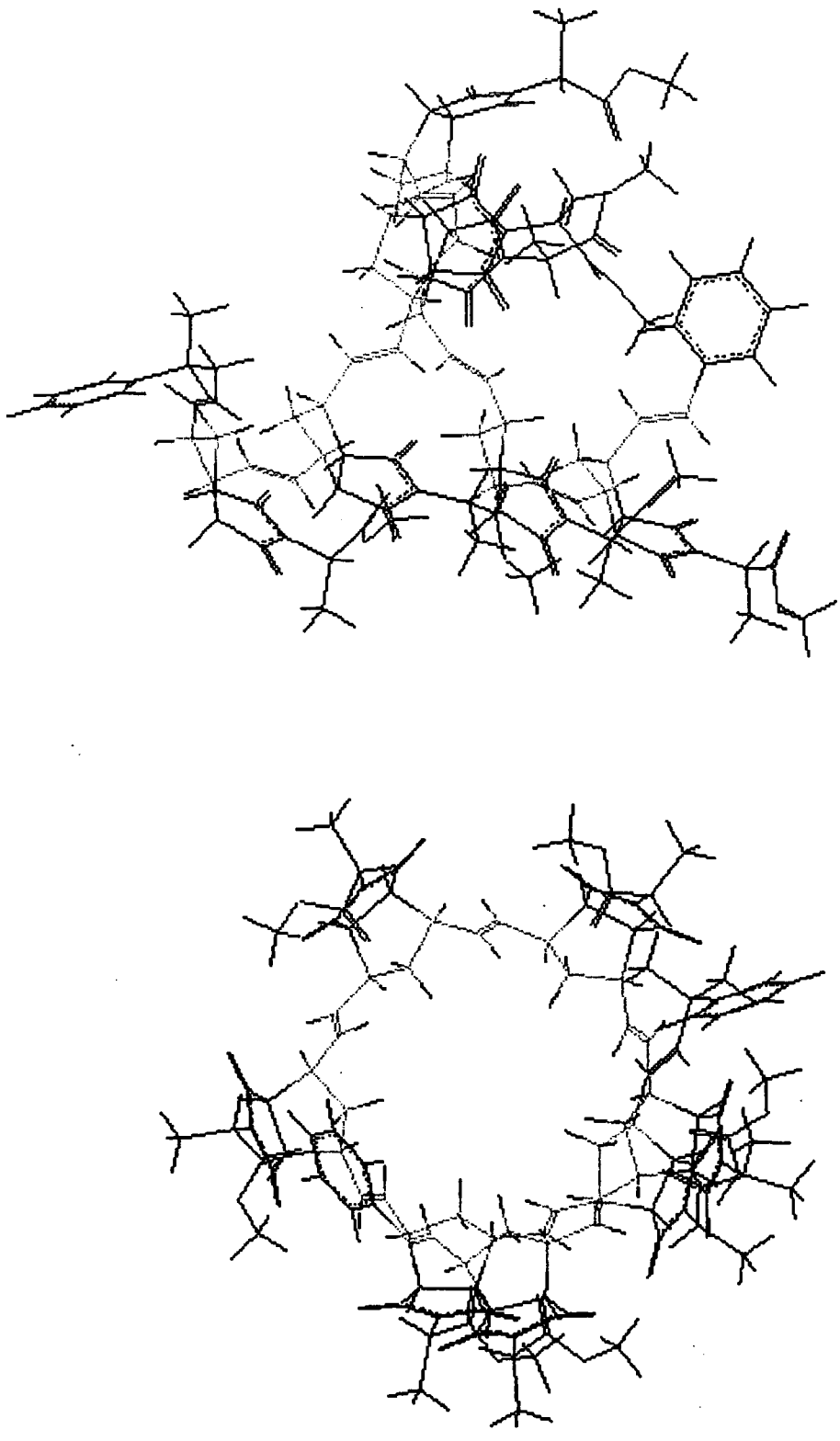

Figure 5.20 Two orientations of a seven repeat-unit trans syndiotactic polymer chain.

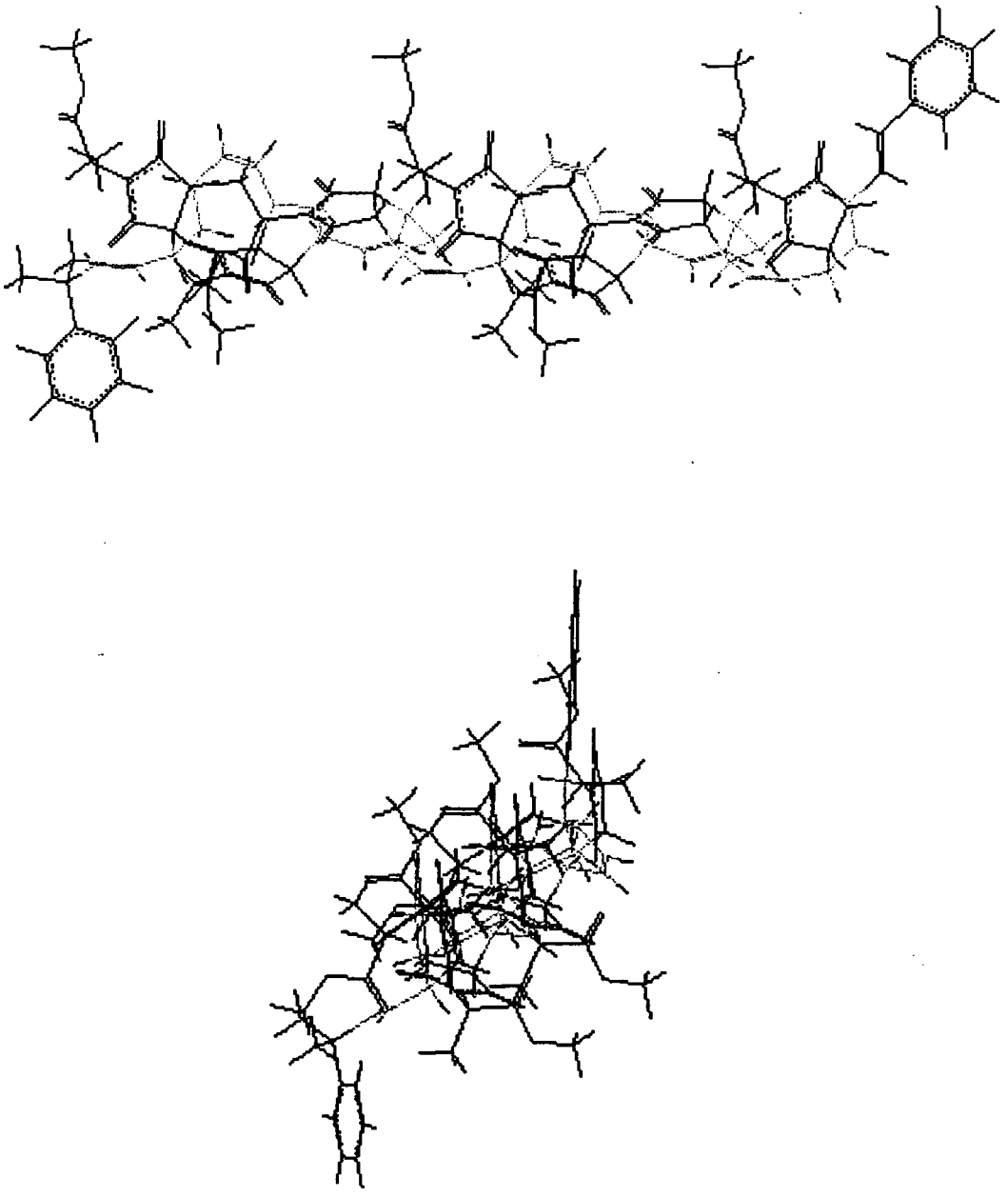

Figure 5.21 Two orientations of a seven repeat-unit cis isotactic polymer chain.

5.5.5 Molecular Dynamics of a Twenty Five Unit Sample of *endo*-Trans Syndiotactic Polymer.

In order to overcome the localised minimum problem associated with the minimisation of a molecule (see section 5.2.2 and figure 5.1), a molecular dynamics package is employed. This technique considers not only the potential energy of a system, but incorporates solutions of the equations of motion for the given configuration (i.e. the kinetic energy of the molecule is considered, derived directly from Newton's equation for motion, F = ma).

Since the force is the negative derivative of the potential energy, and the acceleration is simply the second derivative with respect to time of the atomic positions, the equation of motion can be integrated to give the trajectories of each atom as a function of time.[26] Thus the force is computed from the potential energy and atomic coordinates generated from a minimised structure, over a very small time interval (in the order 10^{-15} seconds). At this point in the process, the molecule is again minimised with respect to the internal coordinates, and the process is repeated, allowing the molecule to cross maxima and explore other stable conformations.

The main disadvantage of molecular dynamics using currently available hardware is the time-scale associated with the trajectory. Simulations are at present limited to only tens of nanoseconds or less, where actual transitions of molecules, particularly in the case of large structures such as polymers, may occur on the millisecond to second time-frame.

In the brief example shown here as an illustration of this technique, a twenty-five unit polymer chain was built from the *endo* monomer, being linked in the trans syndiotactic microstructure. The ends were capped and a minimisation of 2000 iterations performed, reducing the energy form 4.56×10^{3} kJ to 0.29×10^{-3} kJ and recording the atomic coordinates of the final structure. A molecular dynamics program was then performed over 50000 steps, recording every 500^{th} step. This actually corresponds to only 52 pico-seconds of 'real' time and hence, investigation of a plot of energy versus time reveals a much higher energy for these structures than that achieved

through minimisation alone (see figure 5.22). Theoretically, if the dynamics program was allowed to run for an indefinite length of time, the actual global minimum would be realised. In practical terms, however, this is not possible due to the massive data files that would be produced, and the computational time involved.

Figure 5.23 shows two sample configurations taken from this dynamic projection to illustrate the differences in configuration that this theoretical molecule experiences in only 52 pico-seconds. In the first structure the chain is extended with respect to the original minimised structure and experiences a total energy of 5614.6 kJ, while in the second a more compact structure is explored, with total energy of 5266.1 kJ.

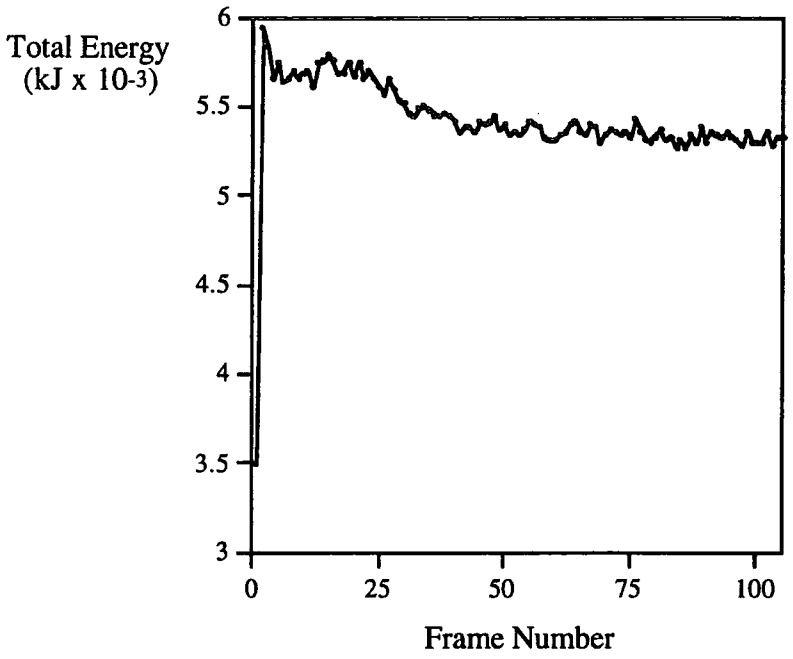

Figure 5.22 Graph of total energy versus time.

This study highlights the limitations that are encountered with molecular modelling and dynamics programs. Although these studies provide valuable insight into possible orientations, it must be remembered that in a true polymer sample, many microstructures are present and thus any rationalisations for observed physical measurements that are implied from these structures are very limited.

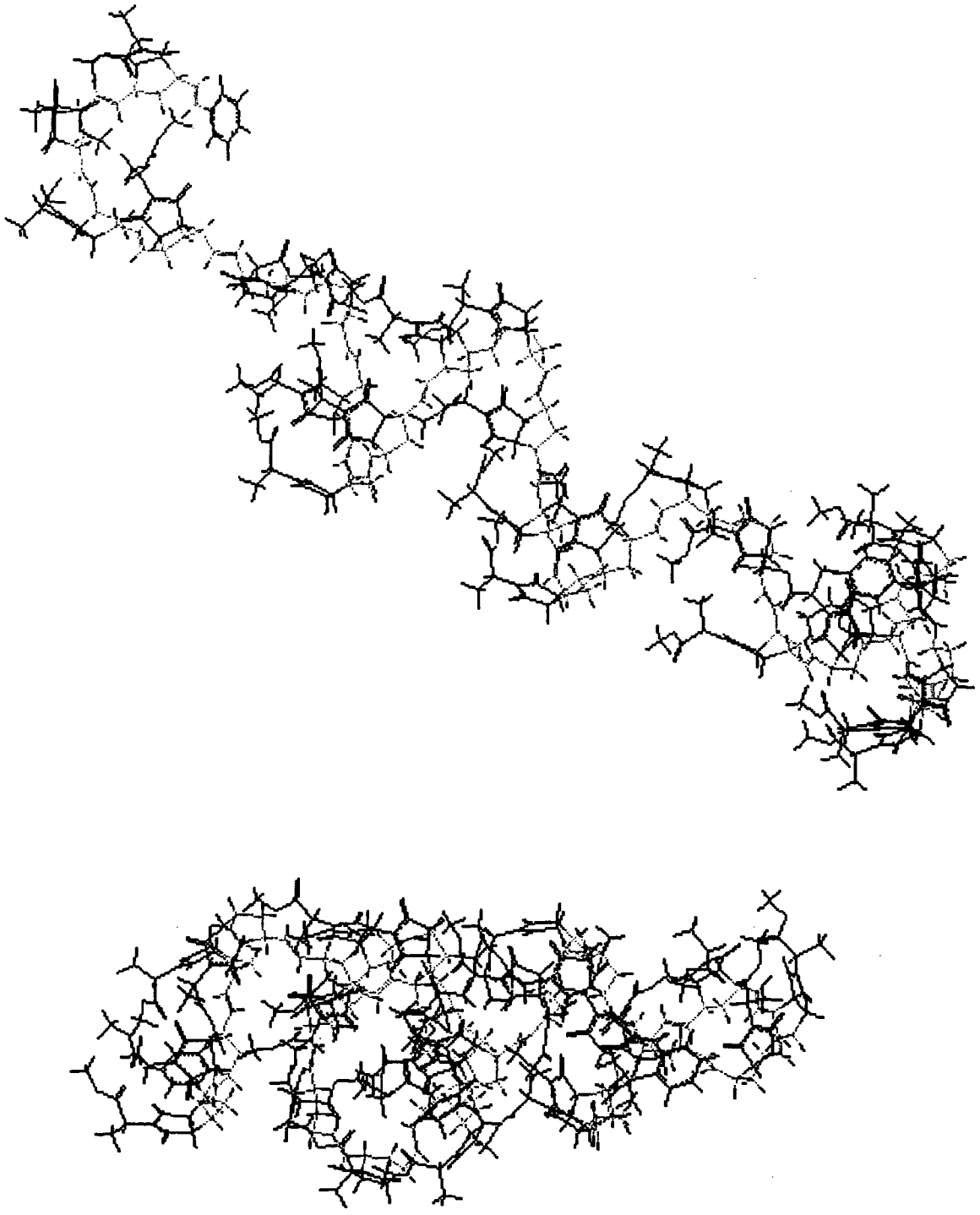

Figure 5.28 Different conformations of a twenty five unit polymer chain explored during a molecular dynamics program.

5.6 Summary

It has been demonstrated that the ring-opening metathesis polymerisation of a family of norbornene monomers proceeds in a living fashion, allowing fine control over the molecular weight and microstructure of the resulting polymers. Chiral monomers give rise to polymers in which optical activity is retained. These studies represent the first step in a search for biologically active polymers *via* ROMP.

5.7 References.

1. R.R. Schrock, G.C. Bazan, M.DiMare, J.S. Murdzek and M. O'Regan, *J. Am. Chem. Soc.*, **1990**, *112*, 3875.

2. (a) R.R. Schrock, J. Feldman, L.F. Cannizzo and R.H. Grubbs, *Macromolecules*, **1987**, *20*, 1169. (b) F. Quignard, M. Lecoute and J.-M. Basset, *J. Chem. Soc., Chem. Commun.*, **1985**, 1816.

3. R.R. Schrock and J.S. Murdzek, *Macromolecules*, **1987**, *20*, 2640 ; R.R. Schrock, W.J. Feast, V.C. Gibson, G.C. Bazan and E. Khosravi, *Polymer Commun.*, **1990**, *30*, 258.

4. S.C.G. Biagini, S.M. Bush, V.C. Gibson, L. Mazzariol, M. North, W.G. Teasdale, C.M. Williams, G. Zagotto and D. Zamuner, *Tetrahedron*, **1995**, *51(26)*, 7247.

5. M. North and S.C.G. Biagini, private communication.

6. N. Seehof, S. Grutke and W. Risse, *Macromolecules*, **1993**, *26*, 695.

7. (a) R.E. Rosenfield Jnr. and J.D. Dunitz, *Helv. Chim. Acta.*, **1976**, *61*, 2176. (b) M. Pitkanen, I. Pitkanen, H.-E. Eriksson and P. Autio, *Tetrahedron*, **1988**, *44*, 261. (c) N. Rodier, N.T. Xuong and P. Reynaud, *Acta Crystallogr., Sect. C*, **1989**, *45*, 1199. (d) W. Kwiatkowski, J. Karolak-Wojciechowska, *Acta Crystallogr., Sect. C*, **1992**, *48*, 206.

8. K.J. Ivin, *"Olefin Metathesis"*, Academic Press, London, 1983.

9. M Yamada, T. Iguchi, A. Hirao, S. Nakahama and J. Watanabe, *Macromolecules*, **1995**, *28*, 50.

10. K. Matyjaszewski, *J. Polym. Sci., Sect. A: Polymer Chemistry*, **1993**, *31*, 995.

11. K. Matyjaszewski, S. Gaynor, D. Greszta, D. Mardare and T. Shigemoto, *J. Phys. Org. Chem.*, **1995**, *8*, 306.

12. (a) R.R. Schrock, K.B. Yap, D.C. Yang, H. Sitzmann, L.R. Sita and G.C. Bazan, *Macromolecules*, **1989**, *22*, 3191. (b) W. Risse, D.R. Wheeler, L.F. Cannizzo and R.H. Grubbs, *Macromolecules*, **1989**, *22*, 3205.

13. K. Mashima, S. Fujikawa, Y. Tanaka, H. Urata, T. Oshiki, E. Tanaka and A. Nakamura, *Organometallics*, **1995**, *14*, 2633.

14. R.P. Quirk and B. Lee, *Polymer International*, **1992**, *27*, 359.

15. (a) L. Gold, *J. Chem. Phys.*, **1958**, *28*, 91. (b) G.C. Bazan, E. Khosravi, R.R. Schrock, W.J. Feast, V.C. Gibson, M.B. O'Regan, J.K. Thomas and W.M. Davis, *J. Am. Chem. Soc.*, **1990**, *112*, 8378.

16. G.C. Bazan, R.R. Schrock, E. Khosravi, W.J. Feast and V.C. Gibson, *Polymer Communications*, **1989**, *30*, 258.

17. G.C. Bazan, J.H. Oskam, H.-N. Cho, L.Y. Park and R.R. Schrock, *J. Am. Chem. Soc.*, **1991**, *113*, 6899.

18. R.R. Schrock, in *"Reactions of Coordinated Ligands"*, P.R. Braterman, Ed, Plenum, New York, 1986.

19. (a) J.H. Oskam and R.R. Schrock, *J. Am. Chem. Soc.*, **1992**, *114*, 7588. (b) J.H. Oskam and R.R. Schrock, *J. Am. Chem. Soc.*, **1993**, *115*, 11831. (c) R.R. Schrock, W.E. Crowe, G.C. Bazan, M. DiMare, M.B. O'Regan and M.H. Schofield, *Organometallics*, **1991**, *10*, 1832. (d) W.J. Feast, V.C. Gibson, K.J. Ivin, A.M. Kenwright and E. Khosravi, *J. Chem. Soc., Chem. Commun.*, **1994**, 1399.

20. W.J. Feast, V.C. Gibson, E. Khosravi, E.L.Marshall and J.P. Mitchell, *Polymer*, **1992**, *33*, 872.

21. W.J. Feast, V.C. Gibson and E.L. Marshall, *J. Chem. Soc., Chem. Commun.*, **1992**, 1157.

22. R. O'Dell, D.H. McConville, G.E. Hofmeister and R.R. Schrock, *J. Am. Chem. Soc.*, **1994**, *116*, 3414.

23. E.L. Marshall, Ph.D. Thesis, University of Durham, 1992.

24. T. Steinhäusler, F. Stelzer and E. Zenkl, *Polymer*, **1994**, *35*, 616.

25. T. Steinhäusler and F. Stelzer, *J. Mol. Catal.*, **1994**, 53.

26. R. Potenzone Jnr., *"Encyclopaedia of Polymer Science and Engineering"*, H.F. Marks, N.M. Bikales, C.G. Overberger and G. Menges Eds., **1988**, John Wiley and Sons, Volume 12, 605.

Chapter Six

Experimental Details.

6.1 General Experimental Details.

6.1.1 Experimental Techniques, Solvents and Reagents for Chapters 2-5

All manipulations of air and / or moisture sensitive compounds were performed on a conventional vacuum / inert atmosphere (nitrogen) line using standard Schlenk and cannula techniques, or in an inert (nitrogen) atmosphere filled dry box.

The following solvents were dried by prolonged reflux over a suitable drying agent, being freshly distilled and deoxygenated prior to use (drying agent in parentheses): toluene (sodium metal), pentane (lithium aluminium hydride), heptane (lithium aluminium hydride), tetrahydrofuran (sodium benzophenone ketyl), diethyl ether (lithium aluminium hydride), dichloromethane (calcium hydride) and acetonitrile (calcium hydride).

NMR solvents were dried by vacuum distillation from phosphorus (V) oxide unless otherwise stated, and stored under nitrogen or vacuum prior to use: D_6-benzene, D_8-toluene, D-chloroform, D_2-dichloromethane, D_8-THF (potassium benzophenone ketyl) and D_{12}-cyclohexane.

Elemental Analyses were performed by the microanalytical services of this department and Medac analytical laboratories.

Infrared Spectra were recorded on Perkin-Elmer 1600 series FTIR running GRAMS analyst 1600 software, and 577 grating spectrophotometers using CsI windows unless otherwise stated. Absorptions abbreviated as: vs (very strong), s (strong), m (medium), w (weak), br (broad), sp (sharp), sh (shoulder).

Mass Spectra were recorded on a VG 7070E Organic Mass Spectrometer [70eV (*ca.* 1.12 x 10^{17} J), 100 μA emission]

NMR Spectra were recorded on the following machines, at the frequencies listed, unless otherwise stated: Varian VXR400, ^{1}H (399.95 MHz), ^{13}C (100.58 MHz), ^{31}P (161.90 MHz); Brüker AC250, ^{1}H (250.13 MHz), ^{13}C (62.90 MHz), ^{31}P (101.26 MHz); Varian Gemini 200, ^{1}H (199.98 MHz), ^{13}C (50.29 MHz); Varian XL 200, ^{1}H (200.06 MHz). The following abbreviations have been used for band multiplicities: s (singlet), d (doublet), t (triplet), q (quartet), quin (quintet), sept (septet), m (multiplet). Chemical shifts are quoted as δ in ppm with respect to the following unless otherwise stated: ^{31}P (dilute aq. H_3PO_4, 0 ppm); ^{13}C (C_6D_6, 128.0 ppm; $CDCl_3$, 77.0 ppm; C_7D_8, 125.2 ppm; D_8-THF, 67.4 and 25.2 ppm); ^{1}H (C_6D_6, 7.15 ppm; $CDCl_3$, 7.26 ppm; C_7D_8, 6.98 ppm; CD_2Cl_2, 5.25 ppm; D_8-THF, 3.58 and 1.73 ppm; C_6D_{12}, 1.38 ppm).

Optical Rotations were recorded on an Optical Activity AA-10 Automatic Polarimeter using a cell of path length 5 cm (0.5 dm).

GPC traces were recorded on a Waters differential refractometer R401 fitted with a Knauer HPLC pump 64 and three PL Gel 5 μm mixed columns (100 Å – 10^4 Å). $CHCl_3$, filtered and degassed, was used as the elutant with a flow rate 1 cm^3 / minute. Samples (0.1 - 0.3 % m/v) were filtered through a Millex SR 0.5 mm filter before injection in order to remove any particulates. The columns were calibrated using commercially available polystyrene standards (Polymer Laboratories Ltd.) ranging from 162 to 7.7 x 10^5 amu. Data was analysed using PL GPC Software version 6.0.

TGA traces were recorded on a Stanton Redcroft TG 760 Series using nitrogen as the purge gas. The temperature range 20 – 830°C was employed, with a heating rate of 10°C min^{-1} and a chart recorder of 10 mm min^{-1}.

DSC traces were recorded on a Perkin Elmer DSC7 machine using nitrogen as the purge and cooling gas. Samples were weighed using a Perkin Elmer AD-4 Autobalance and a scanning rate of 10°C min^{-1} was used. The machine was calibrated with Indium (Mpt (onset) = 429.75K, ΔH_f = 28.45 J g^{-1}) and Zinc (Mpt (onset) = 692.62K, ΔH_f = 108.4 J g^{-1}) and the data was analysed using Perkin Elmer DSC7 Multitasking Software, version 3.2.

The following chemicals were prepared by previously published procedures or modifications thereof:

$V(NR)Cl_3$[1], RNH(TMS) (R = ^tBu, Ad),[2] PMe_3,[3] $[Ph_3C][B(C_6F_5)_4]$,[4] $[PhNMe_2H][B(C_6F_5)_4]$,[5] Me_2PhCCH_2MgCl,[6] Me_3CCH_2MgCl,[6] 2,4,6-$Me_3C_6H_2MgBr$,[6] LiNHAr,[7] $Mo(NAr)(=CHCMe_2Ph)(OR)_2$ (R = CMe_3, $CMe_2(CF_3)$, $CMe(CF_3)_2$).[2]

The following chemicals were obtained commercially and used as received unless stated otherwise : chromyl chloride (Aldrich), boron trichloride (1.0M solution in heptane, Aldrich), diethyl aluminium chloride (1.8M solution in toluene, Aldrich), benzyl magnesium chloride (1.0M solution in Et_2O, Aldrich), pyridine (distilled, Aldrich), $ArNH_2$ (Ar = 2,6-$^iPr_2C_6H_3$) (distilled twice, Aldrich), $Ar'NH_2$ (Ar' = 2,4,6-$^tBu_3C_6H_2$) (recrystallised from Et_2O, Aldrich), triethylamine (distilled, Aldrich), dimethylphenyl phosphine (distilled and stored over molecular sieves, Aldrich), ethylene (Air Products, passed through drying column prior to use), propene (BOC), diphenylacetlyene (Aldrich), ethylmagnesium chloride (3.4M solution in Et_2O, Aldrich), ^{n}propylmagnesium chloride (2.0M solution in Et_2O, Aldrich), methylmagnesium bromide (3.0M solution in Et_2O, Aldrich), sodium molybdate (anhydrous, Aldrich), chlorotrimethyl silane (Aldrich), 2-trifluoromethyl-2-propanol (distilled, Fluorochem) and 2,2 bis(trifluoromethyl)-2-propanol (distilled, Fluorochem).

6.2 Experimental Details to Chapter 2.

6.2.1 Ambient Temperature / Pressure Polymerisation Procedure using Diethylaluminium Chloride (DEAC) as Co-Catalyst.

Ethylene was dried by being passed through a column of $CaCl_2$, molecular sieves and P_2O_5 each separated with glass wool to ensure efficient mixing of the gas with each reagent. Further drying was achieved by passing through a bubbler containing silicone oil (30 cm^3) to which 2 cm^3 of a 1.8M solution of DEAC in toluene had been added. The system was flushed with N_2 for at least 1 hour before introduction of the species under test.

In a typical polymerisation procedure, DEAC (20 equivalents) was added *via* syringe to a stirring solution of the catalyst (50 mg) in toluene (ca. 75 cm^3), and the mixture was left to stir for 10 minutes. The catalyst solution was then purged with ethylene for 1 hour, after which time the polymerisation was terminated by purging with N_2. Any polymer formed was isolated, washed with MeOH, dil. HCl / MeOH (ca. 1:10) and toluene and dried *in vacuo*.

6.2.2 Polymerisation Procedure Using the Polyethylene Screening Rig at Sunbury.

(Described for reaction with DEAC or MAO).

The rig consists of a 3 litre stainless steel autoclave with a water-fed temperature regulation system, gas feed lines, an overhead stirrer and a liquid injection system. Pressure and temperature sensors allow specific conditions to be maintained throughout the test and a mass flow controller monitors the flow of ethylene into the autoclave, ensuring that the required pressure of ethylene is maintained.

After cleaning from the previous test, the reassembled autoclave is pressure tested with 10 bar of N_2 for 10 minutes. The autoclave is then dried by raising the temperature of the water jacket to 95°C and purging with a flow of 1 litre min^{-1} of N_2

for at least 1 hour. The temperature of the water is then set to that required for the experiment and the jacket allowed to cool. 50% of the required co-catalyst and ca. 1.5 litres of *iso*-butane (IC4) is introduced to the autoclave *via* the liquid injection system to further dry the interior. This is then stirred while the catalyst solution is prepared.

The catalyst is pre-weighed into a Schlenk tube and dissolved in ca. 50 cm^3 toluene, and the remaining 50% of co-catalyst is added. The autoclave is then pressurised with (typically) 10 bar of ethylene and allowed to reach equilibrium, and the data collection system is activated. The catalyst / co-catalyst system is passed via syringe into the injection system and then injected into the autoclave using an over pressure of N_2. After the desired time period (typically 1 hour) the polymerisation is terminated by closing the ethylene supply and venting the autoclave to the atmosphere causing the IC4 to boil off.

The polymer formed is scraped from the sides of the vessel and washed with MeOH / dil. HCl and MeOH / toluene before being dried under vacuum.

6.2.3 Ambient Temperature / Pressure Polymerisation Procedure using Methylaluminoxane (MAO) as Co-Catalyst.

MAO was kindly donated by Mr M.C.W. Chan, and was synthesised from aluminium sulphate hydrate and trimethylaluminium in toluene. Typically, 48 cm^3 (12 mmol) of the resultant toluene solution was syringed into a 500 cm^3 round bottom ampoule and a further 50 cm^3 of toluene added. This was degassed and purged with ethene (dried as above).

A solution of the catalyst precursor (0.002 - 0.01 g) in ca. 30 cm^3 of toluene was then added to the stirring M.A.O. solution, and allowed to react with the ethylene for 1 hour. Termination by purging with N_2 and isolation of the polymer was carried out as above.

6.2.4 Reaction of $Cr(N^tBu)_2Cl_2$ with $PhCH_2MgCl$:

Preparation of $Cr(N^tBu)_2(CH_2Ph)_2$ (1).

$Cr(N^tBu)_2Cl_2$ (0.25g, 094 mmol) was dissolved in ca. 80 cm^3 of Et_2O and the resulting solution cooled to -78°C in an acetone / CO_2 slush bath. Two equivalents of $PhCH_2MgCl$ (1.88 cm^3 of a 1.0M solution, 1.88 mmol) were added dropwise *via* syringe to give a translucent red solution. After warming to room temperature a white precipitate was in evidence. This mixture was stirred at room temperature for a further 18 hours. Filtration, followed by removal of the volatile components *in vacuo* gave a red solid, which was further extracted with pentane to ensure complete removal of $MgCl_2$. Recrystallisation from the minimal amount of pentane or acetonitrile at -30°C afforded pure $Cr(N^tBu)_2(CH_2Ph)_2$. Yield 0.27g (76%).

Elemental Analysis for $C_{22}H_{32}N_2Cr$, calculated (found) :- %C 70.18 (70.49), %H 8.57 (8.66), %N 7.44 (7.42).

Infra-Red data :- (Nujol mull, CsI, cm^{-1}) 1593 (m), 1352 (m, s), 1260 (w), 1223 (s, br), 1173 (w), 1092 (m ,br), 1019 (m, br), 888 (w), 806 (s), 759 (m, sp), 690 (vs), 597 (w), 534 (m, sp), 513 (m, sp), 466 (m).

Mass Spectral data :- (CI^+, *m/z*, ^{35}Cl) 377 $[M + H]^+$, 303 [M - N^tBu - 2H], 286 [M - CH_2Ph + H].

^{1}H NMR data :- (400MHz, C_6D_6, 298K) δ 6.99 (m, 10H, CH_2Ph) ; δ 2.49 (s, 4H, CH_2Ph) ; δ 1.20 (s, 18H, $C(CH_3)_3$).

^{13}C NMR data :- (100MHz, C_6D_6, 298K) δ 140.34 (s, C_6H_5-C_{ipso}) ; δ 131.60 (d, $^1J_{CH}$=157.11Hz, C_6H_5-C_{ortho}) ; δ 128.94 (d*, C_6H_5-C_{meta}) ; δ 125.65 (d, $^1J_{CH}$=160.53Hz, C_6H_5-C_{para}) ; δ 71.97 (s, $C(CH_3)_3$) ; δ 44.50 (t, $^1J_{CH}$=141.92Hz, CH_2Ph) ; δ 31.63 (q, $^1J_{CH}$=127.04Hz, $C(CH_3)_3$).

(* $^1J_{CH}$ value obscured by overlap with solvent resonance)

6.2.5 Reaction of $Cr(N^tBu)_2(CH_2Ph)_2$ (1) with $[Ph_3C][B(C_6F_5)_4]$:

Formation of $[Cr(N^tBu)_2(CH_2Ph)][B(C_6F_5)_4]$ (2).

$Cr(N^tBu)_2(CH_2Ph)_2$ (0.02 g, 0.05 mmol) and $[Ph_3C][B(C_6F_5)_4]$ (0.05 g, 0.05 mmol) were mixed as solids in an NMR tube. $CD_2Cl_2$was condensed onto the mixture and the ^{1}H NMR spectrum recorded immediately.

^{1}H NMR data :- (250MHz, CD_2Cl_2, 298K) δ 7.90 - 6.67 (m, 25H, $C_2H_2Ph_4$ + CH_2Ph) ; δ 4.22 (s, 2H, CH_2Ph) ; δ 4.00 (s, 2H, $C_2H_2Ph_4$) ; δ 1.59 (s, 18H, $C(CH_3)_3$).

^{13}C NMR data :- (100MHz, CD_2Cl_2, 298K) δ 129.70 (d*, CH_2Ph-$C_{ortho\ /\ meta}$) ; δ 128.78 (s, CH_2Ph-C_{ipso}) ; δ 128.65 (d, $^1J_{CH}$=159.9Hz, CH_2Ph-$C_{ortho\ /\ meta}$) ; δ 126.65 (d, $^1J_{CH}$=161.9Hz, CH_2Ph-C_{para}) ; δ 79.56 (s, $C(CH_3)_3$) ; δ 59.34 (t, $^1J_{CH}$=160.9Hz, CH_2Ph) ; δ 31.07 (q, $^1J_{CH}$=128.8Hz, $C(CH_3)_3$).

(* $^1J_{CH}$ coupling obscured by overlap with 1,1,1,2-tetraphenylethane signals).

6.2.6 Reaction of $Cr(N^tBu)_2(CH_2Ph)_2$ (1) with $[PhNMe_2H][B(C_6F_5)_4]$:

Formation of $[Cr(N^tBu)_2(CH_2Ph)(NMe_2Ph)][B(C_6F_5)_4]$ (3).

The reaction was prepared in an analogous manner to 6.2.5, using 0.02 g $Cr(N^tBu)_2(CH_2Ph)_2$ (0.05 mmol) and 0.043 g $[PhNMe_2H][B(C_6F_5)_4]$ (0.05 mmol).

^{1}H NMR data :- (250MHz, CD_2Cl_2, 298K) δ 7.39 - 6.87 (m, aryl H) ; δ 3.84 (s, 2H, CH_2Ph) ; δ 2.88 (s, 6H, $PhNMe_2$) ; δ 1.67 (s, 18H, $C(CH_3)_3$.

6.2.7 Reaction of $[Cr(N^tBu)_2(CH_2Ph)][B(C_6F_5)_4]$ (2) with PMe_3 :

Formation of $[Cr(N^tBu)_2(CH_2Ph)(PMe_3)][B(C_6F_5)_4]$ (4).

A sample of $[Cr(N^tBu)_2(CH_2Ph)][B(C_6F_5)_4]$ (**2**), formed as detailed in 6.2.5 was admitted to a fresh NMR tube as a CD_2Cl_2 solution. This solution was frozen in liquid nitrogen and one equivalent of PMe_3 was added *via* gas bulb. The tube was sealed and the NMR spectra recorded immediately.

^{1}H NMR data :- (400MHz, CD_2Cl_2, 298K) δ 7.39 – 6.87 (m, 25H, C_2H_2*Ph*$_4$ + CH_2*Ph*) ; δ 3.94 (d, $^3J_{PH}$=2.0Hz, 2H, CH_2Ph) ; δ 1.51 (s, 18H, C(*CH*$_3$)$_3$) ; δ 1.28 (d, $^2J_{PH}$=10.4Hz, 9H, P*Me*$_3$).

^{13}C NMR data :- (100MHz, CD_2Cl_2, 298K) δ 129.69 (d*, CH_2Ph-*C*$_{ortho\ /\ meta}$) ; δ 128.77 (s, CH_2Ph-*C*$_{ipso}$) ; δ 128.64 (d, $^1J_{CH}$=160.9Hz, CH_2Ph-*C*$_{ortho\ /\ meta}$) ; δ 126.63 (d, $^1J_{CH}$=161.0Hz, CH_2Ph-*C*$_{para}$) ; δ 76.96 (d, $^3J_{CP}$=2.3Hz, *C*(CH$_3$)$_3$) ; δ 52.86 (td, $^1J_{CH}$=159.1Hz, $^2J_{CP}$=4.2Hz, *C*H$_2$Ph) ; δ 31.45 (q, $^1J_{CH}$=128.4Hz, C(*C*H$_3$)$_3$) ; δ 17.53 (qd, $^1J_{CP}$=29.8Hz, $^1J_{CH}$=131.6Hz, P*Me*$_3$).

(* $^1J_{CH}$ value obscured by overlap with solvent resonance)

^{31}P NMR data :- (162MHz, CD_2Cl_2, 298K) δ 12.40 (s, *P*Me$_3$).

6.2.8 Reaction of CrO_2Cl_2 with AdNH(TMS) :

Preparation of Cr(NAd)$_2$(OTMS)$_2$ (5).

A solution of CrO_2Cl_2 (2.30 cm^3, 28.37 mmol) in heptane (30 cm^3) at -30°C was added dropwise over 10 minutes to a stirred solution of AdNH(TMS) (25.36 g, 113.5 mmol) also in heptane (200 cm^3) at -30°C. A brown-red precipitate was immediately observed. The mixture was allowed to warm to room temperature and stirred for 3 hours. Subsequent heating of the mixture to 60°C for 15 hours resulted in the formation of a deep red solution and an orange-red precipitate. After cooling, the

supernatant solution was filtered from the residue and the volatile components were removed under reduced pressure to give a brown solid. Extraction with toluene (3 x 50 cm^3) followed by concentration and cooling of the filtrate to -30°C afforded $Cr(NAd)_2(OTMS)_2$. Yield 3.90 g (26%).

Elemental Analysis for $C_{26}H_{48}N_2CrO_2Si_2$, calculated (found) :- %C 59.05 (59.55), %H 9.15 (9.37), %N 5.30 (5.26).

Infra-Red data :- (Nujol mull, CsI, cm^{-1}) 1340 (m, sp), 1295 (m), 1243 (s, sp), 1179 (m), 1169 (m), 1098 (m, sp), 1028 (w), 917 (vs, br), 832 (s, sh), 744 (m), 680 (w), 634 (w), 594 (w, sp), 556 (m), 504 (w, br), 455(w), 413 (m).

Mass Spectral data :- (EI+, *m/z*, ^{35}Cl) 528 [M^+], 513 [$M^+ - CH_3$], 438 [$M^+ - OSiMe_3$].

^{1}H NMR data :- (400MHz, C_6D_6, 298K) δ 2.15 (d (br), $^3J_{HH}$=2.80Hz, 12H, Ad-*Hβ*) ; δ 1.91 (s (br), 6H, Ad-*Hγ*) ; δ 1.43 (q, $^2J_{HH}$=12.80Hz, 12H, Ad-*Hδ*) ; δ 0.36 (s, 18H, OSi*Me*$_3$).

^{13}C NMR data :- (100MHz, C_6D_6, 298K) δ 80.13 (s, Ad-*Cα*) ; δ 44.86 (t, $^1J_{CH}$=129.85Hz, Ad-*Cβ*) ; δ 36.05 (t, $^1J_{CH}$=125.68Hz, Ad-*Cδ*) ; δ 29.97 (d, $^1J_{CH}$=133.17Hz, Ad-*Cγ*) ; δ 2.77 (q, $^1J_{CH}$=117.75Hz, OSi*Me*$_3$).

6.2.9 Reaction of $Cr(NAd)_2(OTMS)_2$ (5) with BCl_3 :

Preparation of $Cr(NAd)_2Cl_2$ (6).

Boron trichloride (1.0 cm^3, 1M solution in heptane) was added dropwise *via* syringe to an ice-cooled solution of $Cr(NAd)_2(OTMS)_2$ (1.50 g, 2.84 mmol) in CH_2Cl_2 (50 cm^3). The mixture was allowed to warm to room temperature and stirred for a further 2 hours. The volatile components were then removed under reduced pressure to give an purple solid which was extracted with toluene (3 x 15 cm^3). Removal of the

solvent under reduced pressure affords $Cr(NAd)Cl_2$ of sufficient purity to be used in subsequent reactions. Yield 0.98 g (82%). Analytically pure samples of the dichloride can be obtained as a microcrystalline, light purple solid by recrystallisation from saturated toluene solutions at -30°C.

Elemental Analysis for $C_{20}H_{30}N_2Cl_2Cr$, calculated (found) :- %C 57.01 (57.07), %H 7.18 (7.02), %N 6.65 (6.54).

Infra-Red data :- (Nujol mull, CsI, cm^{-1}) 1340 (m, sp), 1294 (s), 1261 (w, sh), 1159 (m, sh), 1095 (s), 1020 (m), 971 (w, br), 929 (w), 821 (m, sp), 809 (m), 594 (m, sp), 543 (s, sp), 479 (w), 444 (m), 413 (vs, sh), 372 (m), 320 (w), 232 (vs, sh).

Mass Spectral data :- (CI^+ and EI^+, *m/z*, ^{35}Cl) 774 $[Cr(NAd)_2(\mu\text{-}Cl)]_2$, 422 $[Cr(NAd)_2Cl_2 + H]$.

^{1}H NMR data :- (400MHz, C_6D_6, 298K) δ 2.02 (d (br), $^3J_{HH}$=3.20Hz, 12H, Ad-H_β) ; δ 1.78 (s (br), 6H, Ad-H_γ) ; δ 1.29 (s (br), 12H, Ad-H_δ).

^{13}C NMR data :- (100MHz, C_6D_6, 298K) δ 85.37 (s, Ad-C_α) ; δ 43.51 (t, $^1J_{CH}$=131.41Hz, Ad-C_β) ; δ 35.50 (t, $^1J_{CH}$=127.39Hz, Ad-C_δ) ; δ 29.62 (d, $^1J_{CH}$=133.87Hz, Ad-C_γ).

6.2.10 Reaction of $Cr(NAd)_2Cl_2$ (6) with PMe_3 :

Preparation of $Cr(NAd)_2Cl_2(PMe_3)$ (7).

A solution of $Cr(NAd)_2Cl_2$ (0.25 g, 0.59 mmol) in toluene (ca. 30 cm^3) was frozen in liquid nitrogen, and 1 equivalent of PMe_3 was condensed on to it. Upon warming to room temperature the solution changed colour from purple to yellow orange and a precipitate was observed. The mixture was stirred for 2 hours after which time the solid was isolated by filtration. Washing with heptane followed by recrystallisation

from a concentrated THF solution afforded analytically pure $Cr(NAd)_2Cl_2(PMe_3)$. Yield 0.38g (65%).

Elemental Analysis for $C_{23}H_{39}N_2Cl_2CrP$, calculated (found) :- %C 55.53 (55.28), %H 7.90 (7.46), %N 5.63 (5.60).

Infra-Red data :- (Nujol mull, CsI, cm^{-1}) 1298 (m), 1282 (m, sp), 1260 (m, sh), 1163 (m), 1097 (s, br), 1019 (m, br), 959 (s, br), 854 (w), 810 (m, br), 722 (m, br), 672 (w), 590 (w), 450 (w, br), 362 (m), 287 (w, br), 215 (s).

^{1}H NMR data :- (400MHz, $CDCl_3$, 298K) δ 2.11 (s (br), 6H, Ad-H_γ) ; δ 2.08 (s (br), 12H, Ad-H_β) ; δ 1.76 (d, $^2J_{PH}$=12.0Hz, 9H, PMe_3) ; δ 1.60 (s, 12H, Ad-H_δ).

^{13}C NMR data :- (100MHz, $CDCl_3$ 298K) δ 82.15 (s, Ad-C_α) ; δ 43.49 (t, $^1J_{CH}$=130.45Hz, Ad-C_β) ; δ 35.53 (t, $^1J_{CH}$=126.48Hz, Ad-C_δ) ; δ 29.19 (d, $^1J_{CH}$=132.77Hz, Ad-C_γ) ; δ 19.70 (d, $^1J_{PC}$=30.48Hz, PMe_3).

^{31}P NMR data :- (162MHz, $CDCl_3$, 298K) δ 33.03 (s, PMe_3).

6.2.11 Reaction of $Cr(NAd)_2Cl_2$ (6) with Pyridine :

Preparation of $Cr(NAd)_2Cl_2$(pyridine) (8).

A toluene (30 cm^3) solution of $Cr(NAd)_2Cl_2$ (0.25g, 0.59 mmol) was cooled to -78°C in an acetone / CO_2 slush bath. Excess pyridine (2 equivalents, 1.2 mmol, 0.1 cm^3) was added as a toluene solution (5 cm^3) to give an orange-red solution. After warming to room temperature the mixture was stirred for 2.5 hours during which time an orange precipitate was in evidence. Removal of the volatile component *in vacuo* and recrystallisation from toluene afforded pure $Cr(NAd)_2Cl_2$(pyridine). Yield 0.21g (72%).

Elemental Analysis for $C_{25}H_{35}N_3Cl_2Cr$, calculated (found) :- %C 60.00 (59.67), %H 7.05 (7.38), %N 8.40 (8.12).

Infra-Red data :- (Nujol mull, CsI, cm^{-1}) 2724 (w), 2673 (w, br), 1603 (m), 1342 (m), 1243 (w), 1215 (w), 1156 (s, sh), 1096 (s), 1069 (s), 1017 (m), 971 (w, br), 929 (w, sh), 815 (s), 774 (s), 766 (vs), 700 (s), 645 (m), 588 (s), 475 (w), 443 (w, sh), 403 (m), 364 (s), 339 (s), 310 (m, br), 232 (s), 215 (vs).

^{1}H NMR data :- (400MHz, $CDCl_3$, 298K) δ 8.94 (s (br), 2H, pyridine-H_{ortho}) ; δ 7.82 (s (br), 1H, pyridine-H_{para}) ; δ 7.43 (s (br), 2H, pyridine-H_{meta}) ; δ 2.27 (s (br), 6H, Ad-H_γ) ; δ 2.22 (s (br), 12H, Ad-H_β) ; δ 1.70 (s, 12H, Ad-H_∂).

^{13}C NMR data :- (100MHz, $CDCl_3$ 298K) δ 150.75 (d §, pyridine-C_{ortho}) ; δ 137.63 (d, $^1J_{CH}$=163.2Hz, pyridine-C_{para}) ; δ 124.41 (d, $^1J_{CH}$=167.1Hz, pyridine-C_{meta}) ; δ 83.92 (s, Ad-C_α) ; δ 42.85 (t, $^1J_{CH}$=131.6Hz, Ad-C_β) ; δ 35.65 (t, $^1J_{CH}$=127.6Hz, Ad-C_∂) ; δ 29.26 (d, $^1J_{CH}$=134.3Hz, Ad-C_γ).
(§ resolution insufficient to allow $^1J_{CH}$ to be calculated).

6.2.12 Reaction of $Cr(NAd)_2Cl_2$ (6) with $PhCH_2MgCl$:

Preparation of $Cr(NAd)_2(CH_2Ph)_2$ (9).

To a suspension of $Cr(NAd)_2Cl_2$ (0.50 g, 1.19 mmol) in diethyl ether (40 cm^3) at -50°C was added dropwise via syringe a solution of $PhCH_2MgCl$ in diethyl ether (2.4 cm^3 of a 1.0 M solution; 2.4 mmol). The mixture was allowed to warm slowly to room temperature and stirred for 15 hours to give a red solution and a small amount of $MgCl_2$ residue. The solvent was removed under reduced pressure and the product was extracted with pentane (3 x 20 cm^3). Concentration of this solution and cooling to -30°C gave red prismatic crystals of $Cr(NAd)_2(CH_2Ph)_2$. Yield 0.41 g (64%).

Elemental Analysis for $C_{34}H_{44}N_2Cr$, calculated (found) :- %C 76.65 (76.39), %H 8.33 (8.60), %N 5.26 (5.00).

Infra-Red data :- (Nujol mull, CsI, cm^{-1}) 1591 (m), 1340 (m), 1299 (s), 1213 (s, sh), 1175 (m, sh), 1096 (m, br), 1027 (w), 973 (w, br), 830 (w), 811 (w), 690 (vs, sp), 547 (w), 513 (m), 478 (w).

Mass Spectral data :- (CI^+, *m/z*, ^{35}Cl) 380 [M^+ - CH_2Ph - 3H], 290 [M^+ - CH_2Ph - NAd - 2H].

^{1}H NMR data :- (400MHz, C_6D_6, 298K) δ 7.05 (m, 10H, CH_2Ph) ; δ 2.57 (s, 4H, CH_2Ph) ; δ 1.93 (d (br), $^3J_{HH}$=2.40Hz, 12H, Ad-$H\beta$) ; δ 1.91 (s, 6H, Ad-$H\gamma$).; δ 1.50 (q (br), $^2J_{HH}$=12.40Hz, 12H, Ad-$H\delta$).

^{13}C NMR data :- (100MHz, C_6D_6, 298K) δ 140.60 (s, CH_2Ph-C_{ipso}) ; δ 131.47 (d, $^1J_{CH}$=157.51Hz, CH_2Ph-C_{ortho}) ; δ 128.67 (d*, CH_2Ph-C_{meta}) ; δ 125.31 (d, $^1J_{CH}$=160.23Hz, CH_2Ph-C_{para}) ; δ 72.84 (s, Ad-$C\alpha$) ; δ 44.48 (t, $^1J_{CH}$=128.95Hz, Ad-$C\beta$) ; δ 43.22 (t, $^1J_{CH}$=141.52Hz, CH_2Ph) ; δ 35.94 (t, $^1J_{CH}$=126.28Hz, Ad-$C\delta$) ; δ 29.47 (d, $^1J_{CH}$=131.96Hz, Ad-$C\gamma$).

(* Overlap with solvent peak prevents $^1J_{CH}$ to be calculated).

6.2.13 Reaction of $Cr(NAd)_2Cl_2$ (6) with $PhMe_2CCH_2MgCl$:

Preparation of $Cr(NAd)_2(CH_2CMe_2Ph)_2$ (10).

The procedure was analogous to that described above for $Cr(NAd)_2(CH_2Ph)_2$, using $Cr(NAd)_2Cl_2$ (0.31 g, 0.73 mmol) and $PhMe_2CCH_2MgCl$ solution (1.5 cm^3 of a 0.95 M solution in diethyl ether; 1.46 mmol). Recrystallisation from pentane at -30°C afforded red crystals of $Cr(NAd)_2(CH_2CMe_2Ph)_2$. Yield 0.34 g (76%).

Elemental Analysis for $C_{40}H_{56}N_2Cr$, calculated (found) :- %C 77.88 (77.53), %H 9.15 (9.67), %N 4.54 (4.37).

Infra-Red data :- (Nujol mull, CsI, cm^{-1}) 1934 (w, br), 1864 (w), 1788 (w), 1606 (m), 1494 (s, sp), 1341 (s, sp), 1298 (vs), 1229 (s), 1206 (vs, sh), 1097 (s), 1081 (m), 1045 (s), 1027 (s), 966 (m), 833 (s), 814 (m), 759 (vs), 694 (vs), 592 (m), 556 (m, br), 486 (m, sp), 416 (m, br).

^{1}H NMR data :- (400MHz, C_6D_6, 298K) δ 7.45 (d, $^3J_{HH}$=7.20Hz, 4H, Ph-H_{ortho}) ; δ 7.24 (t, $^3J_{HH}$=7.60Hz, 4H, Ph-H_{meta}) ; δ 7.08 (t, $^3J_{HH}$=7.40Hz, 2H, Ph-H_{para}) ; δ 2.20 (s, 4H, CH_2CMe_2Ph) ; δ 1.93 (s (br), 18H, Ad-$H\beta$ + Ad-$H\gamma$) ; δ 1.61 (s, 12H, CH_2CMe_2Ph) ; δ 1.51 (q (br), $^2J_{HH}$=12.40Hz, 12H, Ad-$H\delta$).

^{13}C NMR data :- (100MHz, C_6D_6, 298K) δ 152.67 (s, Ph-C_{ipso}) ; δ 126.37 (d, $^1J_{CH}$=156.30Hz, Ph-C_{meta}) ; δ 125.36 (d, $^1J_{CH}$=160.23Hz, Ph-C_{para}) ; δ 85.47 (t, $^1J_{CH}$=123.41Hz, CH_2CMe_2Ph) ; δ 73.34 (s, Ad-$C\alpha$) ; δ 45.21 (t, $^1J_{CH}$=129.35Hz, Ad-$C\beta$) ; δ 40.88 (s, CH_2CMe_2Ph) ; δ 36.38 (t, $^1J_{CH}$=125.93Hz, Ad-$C\delta$) ; δ 33.26 (q, $^1J_{CH}$=125.48Hz, CH_2CMe_2Ph) ; δ 30.05 (d, $^1J_{CH}$=133.57Hz, Ad-$C\gamma$).

6.2.14 Reaction of $Cr(NAd)_2Cl_2$ (6) with Me_3CCH_2MgCl :

Preparation of $Cr(NAd)_2(CH_2CMe_3)_2$ (11).

The procedure was analogous to that described above for $Cr(NAd)_2(CH_2Ph)_2$, using from $Cr(NAd)_2Cl_2$ (0.35 g, 0.83 mmol) and Me_3CCH_2MgCl solution (2.0 cm^3 of a 0.82 M solution in diethyl ether; 1.66 mmol). Recrystallisation from pentane at -30°C afforded red microcrystalline $Cr(NAd)_2(CH_2CMe_3)_2$. Yield 0.23 g (55%).

Elemental Analysis for $C_{30}H_{52}N_2Cr$, calculated (found) :- %C 73.12 (73.04), %H 10.64 (10.21), %N 5.69 (5.63).

Infra-Red data :- (Nujol mull, CsI, cm^{-1}) 1459 (vs), 1353 (s), 1343 (s), 1300 (s, sh), 1232 (s), 1214 (s, sp), 1099 (m), 1085 (m), 1058 (m), 1000 (w), 975 (m, sh), 931 (w, br), 834 (m), 811 (w), 722 (m, br), 591 (w), 483 (w, br), 421 (w).

^{1}H NMR data :- (400MHz, C_6D_6, 298K) δ 2.19 (s, 4H, CH_2CMe_3) ; δ 2.15 (d (br), $^3J_{HH}$=2.40Hz, 12H, Ad-H_β) ; δ 1.97 (s (br), 6H, Ad-H_γ) ; δ 1.53 (q (br), $^2J_{HH}$=12.40Hz, 12H, Ad-H_δ) ; δ 1.31 (s, 18H, CH_2CMe_3).

^{13}C NMR data :- (100MHz, C_6D_6, 298K) δ 87.04 (t, $^1J_{CH}$=121.70Hz, CH_2CMe_3) ; δ 73.14 (s, Ad-C_α) ; δ 45.72 (t, $^1J_{CH}$=129.15Hz, Ad-C_β) ; δ 36.46 (t, $^1J_{CH}$=127.19Hz, Ad-C_δ) ; δ 34.27 (s, CH_2CMe_3) ; δ 33.68 (q, $^1J_{CH}$=125.48Hz, CH_2CMe_3) ; δ 30.11 (d, $^1J_{CH}$=133.57Hz, Ad-C_γ).

6.3 Experimental Details to Chapter 3.

6.3.1 Reaction of $Cr(N^tBu)_2Cl_2$ with $ArNH_2$:

Preparation of $Cr(NAr)_2(NH^tBu)Cl$ (12).

A solution of $ArNH_2$ (356μl, 1.89 mmol) in pentane (20 cm^3) was added dropwise over 10 minutes to a stirred solution of $Cr(N^tBu)_2Cl_2$ (0.25 g, 0.94 mmol) in pentane (70 cm^3) at -78°C. The mixture was allowed to warm to room temperature during which the colour gradually changed from black to red. The mixture was stirred at ambient temperature for a further 18 hours, after which time the volatile components were removed under reduced pressure. Extraction of the resultant red oily residue with pentane (50 cm^3) followed by concentration and cooling of the filtrate to ca. -30°C afforded dark red crystals of $Cr(NAr)_2(NH^tBu)Cl$. Yield 0.289 g (3 crops) (60%).

Elemental Analysis for $C_{28}H_{44}N_3ClCr$, calculated (found) :- %C 65.93 (66.00), %H 8.69 (9.02), %N 8.24 (7.96).

Infra-Red data :- (Nujol mull, CsI, cm^{-1}) 3225 (m), 1579 (w), 1260 (s), 1198 (m, br), 1096 (s, br), 1056 (m), 1018 (s,br), 983 (m), 932 (w), 795 (s), 760 (m), 749 (s), 703 (m), 636 (w), 526 (w), 250 (s), 230 (m).

Mass Spectral data :- (EI^+, *m/z*, ^{35}Cl) 509 [M^+], 437 [M-NH^{t}Bu+H].

^{1}H NMR data :- (400MHz, C_6D_6, 298K) δ 11.84 (s (br), 1H, N*H*^{t}Bu) ; δ 6.88 (m, 6H, C_6H_3) ; δ 3.97 (sept (br), 2H, C*H*$(CH_3)_2$) ; δ 3.81 (sept (br), 2H, C*H*$(CH_3)_2$) ; δ 1.28 (s, 9H, NH^t*Bu*) ; δ 1.22 - 0.99 (m, 12H, CH(C*H*$_3)_2$).

^{13}C NMR data :- (100MHz, C_6D_6, 298K) δ 161.02, 160.01 (C_6H_3-C_{ipso}) ; δ 146.48, 145.36 (C_6H_3-C_{ortho}) ; δ 123.10 (d, $^1J_{CH}$=154.90Hz, C_6H_3-C_{meta}) ; δ 122.76 (d, $^1J_{CH}$=155.60Hz, C_6H_3-C_{meta}) ; * ; δ 64.50 (s, NH*C*$(CH_3)_3$) ; δ 32.37 (q, $^1J_{CH}$=126.40Hz, NHC(*C*$H_3)_3$) ; δ 29.33 (d, $^1J_{CH}$=125.12Hz, *C*H$(CH_3)_2$) ; δ 28.43(d, $^1J_{CH}$=127.44Hz, *C*H$(CH_3)_2$) ; δ 24.74, 23.75, 23.23, 23.11 (overlapping quartet resonances, CH(*C*$H_3)_2$).

(* C_6H_3-C_{para} resonances obscured by C_6D_6 signal).

6.3.2 Reaction of $Cr(N^tBu)_2Cl_2$ with LiNHAr :

Preparation of Cr(NAr)$_2$(NH^{t}Bu)Cl (12).

$Cr(N^tBu)_2Cl_2$ (0.25 g, 0.94 mmol) was dissolved in diethyl ether (30 cm^3) and cooled in a dry-ice/acetone slush bath to -78°C. This solution was then added dropwise over 10 minutes to a cold (-78°C) solution of LiNHAr (0.346 g, 2.08 mmol) in diethyl ether (30 cm^3). The mixture was allowed to warm to room temperature and stirred for 18 hours. The resultant red solution was filtered from the white precipitate and the volatile components were removed under reduced pressure to give a red oily solid. Extraction with pentane (50 cm^3) followed by concentration and cooling of the filtrate to ca. -30°C afforded $Cr(NAr)_2(NH^tBu)Cl$. Yield 0.125 g (26%).

6.3.3 Reaction of $Cr(N^tBu)_2Cl_2$ with $Ar'NH_2$ (Ar' = 2,4,6-^{t}Bu$_3$-C_6H_2) :

Preparation of $Cr(N^tBu)(N\text{-}C_6H_2\text{-}2,4,6\text{-}^tBu_3)Cl_2$ (13)

$Cr(N^tBu)_2Cl_2$ (1.0 g, 3.77 mmol) and 2,4,6-^{t}Bu$_3$-$C_6H_2NH_2$ (0.88 g, 3.77 mmol) were mixed in an ampoule and ca. 75 cm^3 of heptane was added. The mixture was heated to 60°C for 5 days and then filtered whilst still hot. The solution was concentrated and placed at -30°C, affording fine red needles of $Cr(N^tBu)(N\text{-}2,4,6\text{-}^tBu_3\text{-}C_6H_2)Cl_2$. Yield 0.98 g (57%).

Elemental Analysis for $C_{22}H_{38}N_2CrCl_2$, calculated (found) :- %C 58.27 (58.81), %H 8.44 (8.69), %N 6.18 (6.16).

Infra-Red data :- (Nujol mull, CsI, cm^{-1}) 2726 (m), 1586 (s, sp), 1254 (w), 1197 (s, sh), 1137 (m), 1032 (w), 930 (w), 881 (m, sp), 792 (w), 764 (m, sp), 658 (w), 576 (m), 529 (m), 494 (w), 459 (m), 416 (m), 230 (m).

Mass Spectral data :- (EI$^+$, *m/z*, ^{35}Cl) 452 $[M]^+$, 417 [M - Cl], 382 [M - N^{t}Bu].

^{1}H NMR data :- (400MHz, C_6D_6, 298K) δ 7.35 (s, 2H, 2,4,6-^{t}Bu$_3$-C_6H_2) ; δ 1.52 (s, 18H, 2,4,6-^{t}*Bu*-C_6H_2) ; δ 1.16 (s, 9H, $NC(CH_3)_3$) ; δ 1.03 (s, 9H, 2,4,6-^{t}*Bu*-C_6H_2).

^{13}C NMR data :- (100MHz, C_6D_6, 298K) δ 159.99 (s, C_6H_2-C_{ipso}) ; δ 153.64 (s, C_6H_2-C_{para}) ; δ 145.23 (s, C_6H_2-C_{ortho}) ; δ 122.05 (d, $^1J_{CH}$=155.6Hz, C_6H_2-C_{meta}) ; δ 89.41 (s, $NC(CH_3)_3$) ; δ 37.22 (s, $C(CH_3)_3$-4 position) ; δ 35.21 (s, $C(CH_3)_3$-2,6 positions) ; δ 32.57 (q, $^1J_{CH}$=126.27Hz, $C(CH_3)_3$-2,6 positions) ; δ 31.03 (q, $^1J_{CH}$=125.90Hz, $NC(CH_3)_3$) ; δ 29.01 (q, $^1J_{CH}$=129.18Hz, $C(CH_3)_3$-4 position).

6.3.4 Reaction of $Cr(NAr)_2(NH^tBu)Cl$ (12) with BCl_3 :

Preparation of $Cr(NAr)_2Cl_2$ (14).

Boron trichloride (1.0 cm^3, 1M solution in heptane) was added dropwise *via* syringe to an ice-cooled solution of $Cr(NAr)_2(NH^tBu)Cl$ (0.43 g, 0.84 mmol) in CH_2Cl_2 (50 cm^3). The mixture was allowed to warm to room temperature and stirred for a further 3 hours. The volatile components were then removed under reduced pressure to give a red oily solid which was washed with cold pentane (2 x 5 cm^3) dried *in vacuo*. The solid was sublimed at 80°C (5 x 10^{-2} Torr) onto a dry-ice/acetone probe to give analytically pure $Cr(NAr)_2Cl_2$. Alternatively, pure $Cr(NAr)_2Cl_2$ can be obtained by recrystallisation at -30°C from a saturated pentane solution. Yield 0.30 g (75%).

Elemental Analysis for $C_{24}H_{34}N_2Cl_2Cr$, calculated (found) :- %C 60.89 (60.54), %H 7.24 (7.38), %N 5.92 (5.92).

Infra-Red data :- (Nujol mull, CsI, cm^{-1}) 2360 (w), 1579 (m), 1342 (m), 1259 (s), 1222(w), 1179 (w), 1142 (w), 1096 (m, br), 1057 (m), 1019 (m, br), 931 (w), 799 (s), 753 (m), 600 (w), 523 (w), 427 (m), 250 (s), 220 (s).

Mass Spectral data :- (EI^+, *m/z*, ^{35}Cl) 473 $[M]^+$, 437 $[M\text{-}Cl]^+$, 402 $[M\text{-}2Cl]^+$.

^{1}H NMR data :- (400MHz, C_6D_6, 298K) δ 6.75 (m, 6H, C_6H_3), δ 3.81 (sept, $^3J_{HH}$=6.70Hz, 4H, $CH(CH_3)_2$) ; δ 1.03 (d, $^3J_{HH}$=7.20Hz, 24H, $CH(CH_3)_2$).

^{13}C NMR data :- (100MHz, C_6D_6, 298K) δ 162.89 (s, C_6H_3-C_{ipso}) ; δ 149.07 (s, C_6H_3-C_{ortho}) ; δ 132.24 (d, $^1J_{CH}$=161.74Hz, C_6H_3-C_{para}) ; δ 123.20 (d, $^1J_{CH}$=160.93Hz, C_6H_3-C_{meta}) ; δ 29.43 (d, $^1J_{CH}$=128.54Hz, $CH(CH_3)_2$) ; δ 23.76 (q, $^1J_{CH}$=126.63Hz, $CH(CH_3)_2$).

6.3.5 Reaction of $Cr(NAr)_2Cl_2$ (14) with pyridine :

Preparation of $Cr(NAr)_2Cl_2$(pyridine) (15).

Excess pyridine (2 equivalents, 1.06 mmol, 0.08 cm^3) was added to a solution of $Cr(NAr)_2Cl_2$ (0.25g, 0.53 mmol) in ca. 30 cm^3 of pentane at room temperature. An immediate purple precipitate was observed, and the suspension was left stirring for 16 hours. Removal of the volatile component *in vacuo* afforded $Cr(NAr)_2Cl_2$(pyridine) as a purple microcrystalline solid, which could be obtained pure by recrystallisation from a concentrated CH_2Cl_2 solution at -78°C. Yield 0.23g (79%).

Elemental Analysis for $C_{29}H_{39}N_3Cl_2Cr$, calculated (found) :- %C 63.04 (63.22), %H 7.11 (7.11), %N 7.60 (7.68).

Infra-Red data :- (Nujol mull, CsI, cm^{-1}) 1603 (w), 1577 (m), 1461 (vs, br), 1260 (m), 1215 (m), 1173 (w), 1154 (w), 1093 (m, br), 1073 (m), 1015 (m), 932 (w), 799 (s), 760 (s, sp), 723 (s), 692 (s, sp), 637 (m), 533 (w).

Mass Spectral data :- (EI^+, *m/z*, ^{35}Cl) 472 $[M\text{-}py]^+$, 437 $[M\text{-}py\text{-}Cl]^+$.

^{1}H NMR data :- (400MHz, $CDCl_3$, 298K) δ 8.97 (s (br), 2H, pyridine-H_{ortho}) ; δ 7.89 (t (br), 1H, pyridine-H_{para}) ; δ 7.50 (t (br), 2H, pyridine-H_{meta}) ; δ 7.19 - 7.12 (m, 6H, C_6H_3) ; δ 3.73 (sept, $^3J_{HH}$=6.80Hz, 4H, $CH(CH_3)_2$) ; δ 1.12 (d, $^3J_{HH}$=6.80Hz, 24H, $CH(CH_3)_2$).

^{13}C NMR data :- (100MHz, $CDCl_3$, 298K) δ 162.13 (s, C_6H_3-C_{ipso}) ; δ 149.49 (d, $^1J_{CH}$=181.55Hz, pyridine-C_{ortho}) ; δ 149.17 (s, C_6H_3-C_{ortho}) ; δ 138.00 (d, $^1J_{CH}$=166.36Hz, pyridine-C_{para}) ; δ 132.10 (d, $^1J_{CH}$=161.33Hz, C_6H_3-C_{para}) ; δ 124.69 (d, $^1J_{CH}$=165.86Hz, pyridine-C_{meta}) ; δ 122.83 (d, $^1J_{CH}$=159.12Hz, C_6H_3-C_{meta}) ; δ 29.05 (d, $^1J_{CH}$=130.05Hz, $CH(CH_3)_2$) ; δ 23.91 (q, $^1J_{CH}$=126.53Hz, $CH(CH_3)_2$).

6.3.6 Reaction of $Cr(NAr)_2Cl_2$ (14) with PMe_3 :

Formation of $Cr(NAr)_2Cl_2(PMe_3)$ (16).

One equivalent of PMe_3 (0.04 mmol.) was condensed *via* a gas bulb onto a frozen C_6D_6 (0.8 cm^3) solution of $Cr(NAr)_2Cl_2$ (0.02 g, 0.04 mmol.) at -196°C. On warming to room temperature no visible change occurred. The ^1H NMR spectrum however was consistent with the formation of $Cr(NAr)_2(Cl)_2(PMe_3)$.

^{1}H NMR data :- (400MHz, C_6D_6, 298K) δ 6.95 - 6.85 (m, 6H, C_6H_3) ; δ 4.03 (sept, $^3J_{HH}$=6.60Hz, 4H, $CH(CH_3)_2$) ; δ 1.53 (d, $^2J_{PH}$=10.80Hz, PMe_3) δ 1.12 (d, $^3J_{HH}$=6.40Hz, 24H, $CH(CH_3)_2$).

^{13}C NMR data :- (100MHz, C_6D_6, 298K) δ 161.39 (s, C_6H_3-C_{ipso}) ; δ 148.20 (s, C_6H_3-C_{ortho}) ; δ 131.62 (d, $^1J_{CH}$=160.63Hz, C_6H_3-C_{para}) ; δ 122.95 (d, $^1J_{CH}$=157.61Hz, C_6H_3-C_{meta}) ; δ 29.17 (d, $^1J_{CH}$=130.86Hz, $CH(CH_3)_2$) ; δ 24.22 (q, $^1J_{CH}$=126.03Hz, $CH(CH_3)_2$) ; δ 14.15 (d, $^1J_{PC}$=20.92Hz, PMe_3).

^{31}P NMR data :- (162MHz, C_6D_6, 298K) δ 8.12 (s, PMe_3).

6.3.7 Reaction of $Cr(NAr)_2Cl_2$ (14) with LiNHAr :

Preparation of $Cr(NAr)_2(NHAr)Cl$ (17).

$Cr(NAr)_2Cl_2$ (1.0g, 2.12 mmol) was dissolved in THF and cooled to -78°C in an acetone / CO_2 slush bath. This was added to a solution of one equivalent of LiNHAr (0.39g 2.12 mmol) also dissolved in THF at -78°C, and the mixture was slowly allowed to attain room temperature. Subsequent stirring for 18 hours resulted in the formation of a purple-red solution that afforded an oily solid when the volatile component was removed *in vacuo*. Extraction from LiCl with pentane and cooling to -30°C results in isolation of pure $Cr(NAr)_2(NHAr)Cl$ as a purple crystalline material. Yield (3 crops) 0.78g (60%).

Elemental Analysis for $C_{36}H_{52}N_3ClCr$, calculated (found) :- %C 70.39 (70.02), %H 8.53 (9.08), %N 6.84 (6.46).

Infra-Red data :- (Nujol mull, CsI, cm^{-1}) 3345 (m), 1581 (w), 1262 (m, br), 1224 (w), 1177 (m, sp), 1095 (m, br), 983 (w), 933 (m), 801 (s, sh), 759 (vs), 753 (vs), 663 (w), 618 (m), 589 (w), 428 (m), 252 (s, sp), 236 (vs, sp).

Mass Spectral data :- (EI^+, *m/z*, ^{35}Cl) 614 $[M]^+$, 438 $[M\text{-}NAr]^+$.

^{1}H NMR data :- (400MHz, C_6D_6, 298K) δ 12.22 (s (br), 1H, N*H*Ar) ; δ 7.03 (m, 3H, NHAr-C_6H_3) ; δ 6.85 (m, 6H, NAr-C_6H_3) ; δ 4.00 (sept, $^3J_{HH}$=6.80Hz, 4H, C*H*$(CH_3)_2$) ; δ 1.23 (d, $^3J_{HH}$=6.80Hz, 12H, CH(C*H*$_3)_2$) ; δ 1.06 (d, $^3J_{HH}$=6.80Hz, 24H, CH(C*H*$_3)_2$).

^{13}C NMR data :- (100MHz, C_6D_6, 298K) δ 160.80 (s, C_6H_3-*C*$_{ipso}$) {δ 160.89 ; δ 160.45} ; δ 153.76 (s, C_6H_3-*C*$_{ipso}$) ; δ 146.63 (s, C_6H_3-*C*$_{ortho}$) {δ 146.53 ; δ 146.21} ; δ 141.15 (s, C_6H_3-*C*$_{ortho}$) ; δ 129.17 (d*, C_6H_3-*C*$_{para}$) ; δ 123.67 (d, $^1J_{CH}$=156.82Hz, C_6H_3-*C*$_{meta}$) ; δ 122.93 (d, $^1J_{CH}$=158.33Hz, C_6H_3-*C*$_{meta}$) ; δ 28.99 (d, $^1J_{CH}$=129.26Hz, *C*H$(CH_3)_2$) ; δ 28.91 (q*, *C*H$(CH_3)_2$) ; {δ 25.62 ; δ 24.81 ; δ 23.73 ; δ 22.90, q*, CH(*C*H$_3)_2$}

(* Splitting obscured by solvent peak or other signals ; Values in { } from the spectrum recorded at -80°C in D_8-toluene).

6.3.8 Reaction of $Cr(NAr)_2Cl_2$ (14) with Mg in the presence of PMe_3 :

Preparation of $Cr(NAr)_2(PMe_3)_2$ (18).

Trimethylphosphine (0.22 cm^3, 2.11 mmol), was condensed onto a solution of $Cr(NAr)_2Cl_2$, (0.25 g, 0.53 mmol), and activated magnesium turnings (0.014 g, 0.58 mmol), in THF (50 cm^3) cooled at -196°C. The solution was stirred for 30 minutes at -78°C before being allowed to warm to room temperature, at which time 1 atmosphere of nitrogen was introduced to the vessel. Upon reaching room temperature an orange

brown colouration became apparent, slowly changing to a yellow green after 1 hour. Volatiles were removed by vacuum after 16 hours. A green pentane solution was extracted by filtration, leaving white magnesium chloride. Recrystallisation from a saturated pentane solution at -30°C afforded a dark green crystals. Yield, 0.14 g (46%).

Elemental Analysis for $C_{30}H_{52}N_2CrP_2$, calculated (found) :- %C 64.96 (64.71), %H 9.45 (9.14), %N 5.05 (4.86).

Infra-Red data :- (Nujol mull, CsI, cm^{-1}) 1918 (w), 1583 (w, sp), 1559 (w), 1417 (m), 1357 (w), 1325 (s, sh), 1275 (s, sh), 1156 (w), 1100 (m, br), 1057 (w), 980 (s, sp), 938 (vs, br), 841 (m), 800 (s), 724 (s), 714 (m), 664(s), 474 (w, br), 440 (w, br).

^{1}H NMR data :- (400MHz, C_6D_6, 298K) δ 7.16 - 7.10 (m, 6H, C_6H_3) ; δ 4.23 (sept $^3J_{HH}$=6.80Hz, $CH(CH_3)_2$) ; δ 1.27 (d, $^3J_{HH}$=6.80Hz, $CH(CH_3)_2$) ; δ 1.09 (d, $^2J_{PH}$=6.80Hz, PMe_3).

^{13}C NMR data :- (100MHz, C_6D_6, 298K) δ 159.61 (s, C_6H_3-C_{ipso}) ; δ 142.48 (s, C_6H_3-C_{ortho}) ; δ 122.71 (d, $^1J_{CH}$=154.14Hz, C_6H_3-C_{meta}) ; δ 122.06 (d, $^1J_{CH}$=159.12Hz, C_6H_3-C_{para}) ; δ 27.90 (d, $^1J_{CH}$=128.34Hz, $CH(CH_3)_2$) ; δ 24.00 (q, $^1J_{CH}$=125.39Hz, $CH(CH_3)_2$) ; δ 21.42 (m‡, $^1J_{PC}$=21.32Hz, PMe_3).
(m‡ denotes the X part of an ABX splitting pattern).

^{31}P NMR data :- (162MHz, C_6D_6, 298K) δ 53.71 (s, PMe_3).

6.3.9 Reaction of $Cr(NAr)_2Cl_2$ (14) with Mg in the presence of PMe_2Ph :

Preparation of $Cr(NAr)_2(PMe_2Ph)_2$ (19).

$Cr(NAr)_2Cl_2$ (0.4 g, 0.85 mmol) and excess activated magnesium turnings (0.023 g, 0.93 mmol, 1.1 equivalents) were introduced to an ampoule and ca. 50 cm^3 THF added. This was cooled to -78°C and a THF solution of PMe_2Ph (0.24 cm^3, 1.69

mmol) also at -78°C was added slowly *via* cannula. The solution was allowed to warm slowly to room temperature and left to stir for 24 hours, after which time the initially red solution had acquired a yellow green colour. The volatiles were removed *in vacuo* and the product was extracted from $MgCl_2$ as a pentane solution. Concentration and cooling to -30°C afforded $Cr(NAr)_2(PMe_2Ph)_2$ as green crystals. Yield 0.23 g (40%).

Elemental Analysis for $C_{40}H_{56}N_2CrP_2$, calculated (found) :- %C 70.77 (70.47), %H 8.32 (8.19), %N 4.13 (3.68).

Infra-Red data :- (Nujol mull, CsI, cm^{-1}) 1582 (m, sh), 1415 (s), 1355 (m), 1273 (s), 1223 (s, sh), 1174 (w), 1156 (w), 1096 (s), 1058 (m, sp), 1044 (m), 981 (s, sp), 938 (s), 895 (s, br), 829 (m, sp), 796 (s, sp), 753 (s), 741 (vs), 696 (s), 674 (s), 603 (w, br), 560 (w), 489 (s), 421 (vs).

^{1}H NMR data :- (400MHz, C_6D_6, 298K) δ 7.55 - 6.97 (m (br), 16H, C_6H_3 + PMe_2Ph) ; δ 4.23 (sept (br), 4H, $^3J_{HH}$=6.80Hz, $CH(CH_3)_2$) ; δ 1.35 (d, $^2J_{PH}$=6.00Hz, PMe_2Ph) ; δ 1.15 (d, $^3J_{HH}$=6.40Hz, $CH(CH_3)_2$).

^{13}C NMR data :- (100MHz, C_6D_6, 298K) δ 158.90 (s, C_6H_3-C_{ipso}) ; δ 142.53 (s, C_6H_3-C_{ortho}) ; δ 140.21 (d, $^1J_{PC}$=33.40Hz, PMe_2Ph-C_{ipso}) ; δ 130.71 (m, $^2J_{PC}$=6.14Hz, PMe_2Ph-C_{ortho}) ; δ 128.69 (d*, C_6H_3-C_{para}) ; δ 122.39 (d, $^1J_{CH}$=159.02Hz, C_6H_3-C_{meta}) ; δ 122.14 (d, $^1J_{CH}$=154.49Hz, PMe_2Ph-C_{para}) ; δ 27.45 (d, $^1J_{CH}$=120.48Hz, $CH(CH_3)_2$) ; δ 23.53 (d, $^1J_{CH}$=125.40Hz, $CH(CH_3)_2$) ; δ 19.72 (m‡, $^1J_{PC}$=22.13Hz, PMe_2Ph).

(* splitting obscured by overlap with solvent peak ; m‡ denotes the X part of an ABX splitting pattern).

^{31}P NMR data :- (162MHz, C_6D_6, 298K) δ 68.09 (s, PMe_2Ph).

6.3.10 Reaction of $Cr(NAr)_2(PMe_3)_2$ (18) with C_2H_4.

Excess ethylene (5 equivalents) was condensed into an NMR tube containing $Cr(NAr)_2(PMe_3)_2$ (0.03 g, 0.05 mmol) in ca. 400 µl C_6D_6. The ^1H NMR spectrum was recorded immediately showing that a rapid reaction had occurred, generating an unknown species.

^1H NMR data :- (400MHz, C_6D_6, 298K) δ 7.01 (m, 6H, C_6H_3) ; δ 3.95 (sept 4H, $^3J_{HH}$=6.60Hz, $CH(CH_3)_2$) ; δ 2.91 (s (br), 1.5H) ; δ 2.13 (s (br), 1.5H) ; δ 1.22 (d, $^3J_{HH}$=6.40Hz, $CH(CH_3)_2$) ; δ 1.08 (s (br), 9H, PMe_3).

6.3.11 Reaction of $Cr(NAr)_2(PMe_3)_2$ (18) with C_3H_6.

One equivalent of propene was admitted to an NMR tube containing a solution of $Cr(NAr)_2(PMe_3)_2$ (0.03 g, 0.05 mmol.) in C_6D_6 (400 µl) at -196°C. Despite prolonged warming to 60°C the ^1H NMR spectrum did not change from that of the starting materials.

6.3.12 Reaction of $Cr(NAr)_2(PMe_3)_2$ (18) with Diphenylacetylene.

An NMR tube containing 0.03 g of $Cr(NAr)_2(PMe_3)_2$ (0.05 mmol) was charged with one equivalent of diphenylacetylene (0.008 g). C_6D_6 was added *via* vacuum transfer and the ^1H NMR recorded, indicating no reaction had occurred. The tube was therefore introduced to an oil bath at 60°C (± 0.5°C) and maintained at this temperature overnight. Subsequent NMR spectra indicated that reaction had occurred.

^1H NMR data :- (400MHz, C_6D_6, 298K) δ 7.89 (d, $^3J_{HH}$=7.20Hz, 2H, Ph-H_{ortho}) ; δ 7.36 (d, $^3J_{HH}$=7.20Hz, 2H, *Ph*) ; δ 7.25 (t, $^3J_{HH}$=7.20Hz, 2H, Ph-H_{para}) ; δ 7.04 - 6.96 (m, C_6H_3) ; δ 4.09 (sept, $^3J_{HH}$=6.70Hz, $CHCH_3)_2$) ; δ 1.18 / 1.14 / 1.12 (overlapping doublets, $CH(CH_3)_2$ + PMe_3).

^{13}C NMR data :- (100MHz, C_6D_6, 298K) δ 157.66 (d, $^3J_{PC}$=3.82Hz, C_6H_3-C_{ipso}) ; δ 149.91 (d, $^3J_{PC}$=4.53Hz, Ph-C_{ipso}) ; δ 145.16 (d, $^2J_{PC}$=5.33Hz, Ph_2C_2) ; δ 144.44 (d, $^4J_{PC}$=3.82Hz, C_6H_3-C_{ortho}) ; δ 135.04 (d, J_{PC}=3.12Hz, *Ph*) ; δ 131.66 (d, $^1J_{CH}$=159.82Hz, *Ph*) ; δ 128.81 (d*, *Ph*) ; δ 127.40 (d*, *Ph*) ; δ 125.54 (d*, *Ph*) ; δ 125.15 (d, $^1J_{CH}$=159.42Hz, *Ph*) ; δ 122.61 (d, $^1J_{CH}$=152.58Hz, C_6H_3-C_{meta}) ; δ 27.92 (d, $^1J_{CH}$=125.93Hz, $CH(CH_3)_2$) ; δ 24.06 (q, $^1J_{CH}$=125.53Hz, $CH(CH_3)_2$) ; δ 17.39 (d, $^1J_{PC}$=25.55Hz, P*Me*$_3$).

(* splitting obscured by overlap with solvent resonance)

^{31}P NMR data :- (162MHz, C_6D_6, 298K) δ 30.89 (s, PMe_3).

6.4 Experimental Details to Chapter 4.

6.4.1 Reaction of $Cr(NAr)_2Cl_2$ (14) with 2,4,6-$Me_3C_6H_2MgBr$:

Preparation of $Cr(NAr)_2(2,4,6\text{-}Me_3C_6H_2)_2$ (20).

To a solution of $Cr(NAr)_2Cl_2$ (0.40 g, 0.84 mmol) in diethyl ether (40 cm^3) at -50°C was added dropwise *via* syringe a solution of 2,4,6-$Me_3C_6H_2MgBr$ in diethyl ether (1.02 cm^3 of a 1.72 M solution; 1.76 mmol). The mixture was allowed to warm slowly to room temperature, during which time the initially red solution had acquired a green colour. This was stirred for 15 hours after which time a small amount of $MgCl_2$ residue was observed. The solvent was removed under reduced pressure and the product was then extracted with pentane (3 x 20 cm^3). Concentration of this solution and cooling to -30°C gave red-green crystals of $Cr(NAr)_2(2,4,6\text{-}Me_3C_6H_2)_2$. Yield 0.40 g (74%).

Elemental Analysis for $C_{42}H_{56}N_2Cr$, calculated (found) :- %C 78.71 (78.25), %H 8.81 (8.73), %N 4.37 (4.28).

Infra-Red data :- (Nujol mull, CsI, cm^{-1}) 2724 (w), 2669 (w, br), 1585 (m, sp), 1315 (m), 1277 (s, sp), 1263 (s), 1221 (m), 1174 (m, sh), 1103 (m, sh), 1054 (m), 1027 (m), 980 (m, sh), 931 (m), 847 (s, sp), 797 (s), 753 (vs), 701 (m, sp), 606 (w), 583 (m), 540 (w, sh), 437 (w), 404 (w).

Mass Spectral data :- (EI^+, *m/z*, ^{35}Cl) 521 [M - 2,4,6-$Me_3C_6H_2$],

^{1}H NMR data :- (400MHz, C_6D_6, 298K) δ 6.89 (s, 6H, C_6H_3) ; δ 6.75 (s, 4H, 2,4,6-$Me_3C_6H_2$) ; δ 3.92 (sept, $^3J_{HH}$=6.60Hz, 4H, $CH(CH_3)_2$) ; δ 2.97 (s, 12H, *2,4,6*-$Me_3C_6H_2$) ; δ 2.08 (s, 6H, 2,*4*,6-$Me_3C_6H_2$) ; δ 0.91 (d, $^3J_{HH}$=6.80Hz, 24H, $CH(CH_3)_2$).

^{13}C NMR data :- (100MHz, C_6D_6, 298K) δ 202.91 (s, C_6H_2-*Cipso*) ; δ 159.60 (s, C_6H_3-*Cipso*) ; δ 145.61 (s, C_6H_3-*Cortho*) ; δ 140.48 (s, C_6H_2-*Cortho*) ; δ 139.52 (s, C_6H_2-*Cpara*) ; δ 123.85 (d, $^1J_{CH}$=156.61Hz, C_6H_3-*Cmeta*) ; δ 27.97 (q, $^1J_{CH}$=133.17Hz, 2,*4*,6-$Me_3C_6H_2$) ; δ 27.57 (d, $^1J_{CH}$=131.56Hz, $CH(CH_3)_2$) ; δ 24.21 (q, $^1J_{CH}$=126.03Hz, $CH(CH_3)_2$) ; δ 21.30 (q, $^1J_{CH}$=126.03Hz, *2,4,6*-$Me_3C_6H_2$).

6.4.2 Reaction of $Cr(NAr)_2Cl_2$ (14) with $PhCH_2MgCl$:

Preparation of $Cr(NAr)_2(CH_2Ph)_2$ (21).

The procedure was analogous to that described above for $Cr(NAr)_2$(2,4,6-$Me_3C_6H_2)_2$, using $Cr(NAr)_2Cl_2$ (0.25 g, 0.53 mmol) and a $PhCH_2MgCl$ solution (1.06 cm^3 of a 1.0 M solution in diethyl ether; 1.06 mmol). Recrystallisation from pentane at -30°C afforded green crystals of $Cr(NAr)_2(CH_2Ph)_2$. Yield 0.18 g (69%).

Elemental Analysis for $C_{38}H_{48}N_2Cr$, calculated (found) :- %C 78.05 (78.12), %H 8.27 (8.39), %N 4.79 (4.46).

Infra-Red data :- (Nujol mull, CsI, cm^{-1}) 1590 (w), 1318 (m, br), 1266 (m, sh), 1175 (w), 1099 (w, br), 1058 (w), 1026 (m), 984 (w), 933 (w, sp), 796 (s), 753 (vs, sp), 722 (s), 692 (s), 530 (w), 475 (m), 452 (m).

^{1}H nmr data :- (400MHz, C_6D_6, 298K) δ 7.17 - 6.88 (m, 16H, C_6H_3 and CH_2Ph) ; δ 3.85 (sept, $^3J_{HH}$=6.60Hz, 4H, $CH(CH_3)_2$) ; δ 3.41 (s, 4H, CH_2Ph) ; δ 1.12 (d, $^3J_{HH}$=7.20Hz, 24H, $CH(CH_3)_2$).

^{13}C nmr data :- (125MHz, C_6D_6, 298K) δ 158.00 (s, C_6H_3-*C_{ipso}*) ; δ 146.03 (s, C_6H_3-*C_{ortho}*) ; δ 140.15 (s, CH_2Ph-*C_{ipso}*) ; δ 132.69 (d, $^1J_{CH}$=158.32Hz, CH_2Ph-*C_{ortho}*) ; δ 128.78 (d*, CH_2Ph-*C_{meta}*) ; δ 127.12 (d*, C_6H_3-*C_{para}*) ; δ 126.24 (d, $^1J_{CH}$=160.23Hz, CH_2Ph-*C_{para}*) ; δ 122.79 (d, $^1J_{CH}$=156.41Hz, C_6H_3-*C_{meta}*) ; δ 59.88 (t, $^1J_{CH}$=139.61Hz, CH_2Ph) ; δ 28.48 (d, $^1J_{CH}$=129.35Hz, $CH(CH_3)_2$) ; δ 23.87 (q, $^1J_{CH}$=125.90Hz, $CH(CH_3)_2$).

(*Overlap with solvent peak prevents $^1J_{CH}$ to be calculated).

6.4.3 Reaction of $Cr(NAr)_2Cl_2$ (14) with MeMgBr :

Preparation of $Cr(NAr)_2(CH_3)_2$ (22).

The procedure was analogous to that described above for $Cr(NAr)_2$(2,4,6-$Me_3C_6H_2)_2$, using $Cr(NAr)_2Cl_2$ (0.390 g, 0.83 mmol) and a MeMgBr solution (0.58 cm^3 of a 3 M solution in diethyl ether; 1.65 mmol). The product was too soluble to allow recrystallisation from pentane, however green microcrystalline $Cr(NAr)_2(CH_3)_2$ was isolated from a concentrated acetonitrile solution at -30°C. Yield 0.18 g (51%).

Elemental Analysis for $C_{26}H_{40}N_2Cr$, calculated (found) :- %C 72.19 (71.70), %H 9.32 (9.24), %N 6.48 (6.49).

Infra-Red data :- (Nujol mull, CsI, cm^{-1}) 1919 (w), 1583 (w), 1271 (m), 1157 (w, br), 1110 (m, sh), 1058 (w), 994 (w, sp), 933 (w), 795 (m, sp), 722 (s, sp), 515 (m, sh), 446 (w, br).

Mass Spectral data :- (CI$^+$, *m/z*, ^{35}Cl) 433 $[M]^+$, 418 $[M\text{-}CH_3]^+$, 402 $[M\text{-}2CH_3]^+$.

^{1}H NMR data :- (400MHz, C_6D_6, 298K) δ 6.91 (m, 6H, C_6H_3) ; δ 3.73 (sept, $^3J_{HH}$=6.90Hz, 4H, $CH(CH_3)_2$) ; δ 1.83 (s, 6H, *Me*) ; δ1.12 (d, $^3J_{HH}$=6.80Hz, 24H, $CH(CH_3)_2$).

^{13}C NMR data :- (100MHz, C_6D_6, 298K) δ 157.81 (s, C_6H_3-C_{ipso}) ; δ 145.24 (s, C_6H_3-C_{ortho}) ; δ 127.60 (d*, C_6H_3-C_{para}) ; δ 122.74 (d, $^1J_{CH}$=156.41Hz, C_6H_3-C_{meta}) ; δ 49.73 (q, $^1J_{CH}$=130.45Hz, CH_3) ; δ 28.80 (d, $^1J_{CH}$=125.12Hz, $CH(CH_3)_2$) ; δ 23.52 (q, $^1J_{CH}$=126.03, $CH(CH_3)_2$).
(* Splitting obscured by C_6D_6 peak).

6.4.4 Reaction of $Cr(NAr)_2Cl_2$ (14) with $PhMe_2CCH_2MgCl$:

Preparation of $Cr(NAr)_2(CH_2CMe_2Ph)_2$ (23).

The procedure was analogous to that described above for $Cr(NAr)_2(2,4,6\text{-}Me_3C_6H_2)_2$, using $Cr(NAr)_2Cl_2$ (0.40 g, 0.84 mmol) and a $PhMe_2CCH_2MgCl$ solution (1.78 cm^3 of a 0.95 M solution in diethyl ether; 1.69 mmol). Recrystallisation from pentane at -30°C afforded green crystals of $Cr(NAr)_2(CH_2CMe_2Ph)_2$. Yield 0.41 g (72%).

Elemental Analysis for $C_{44}H_{60}N_2Cr$, calculated (found) :- %C 78.99 (78.73), %H 9.04 (9.49), %N 4.19 (4.20).

Infra-Red data :- (Nujol mull, CsI, cm^{-1}) 1597 (w), 1494 (m, sp), 1317 (m), 1260 (vs), 1185 (m, sh), 1095 (vs, br), 1020 (vs, br), 930 (w), 864 (w, br), 797 (vs), 763 (s, sp), 752 (s, sp), 697 (s, sp), 625 (w), 554 (m), 454 (w, br).

^{1}H NMR data :- (400MHz, C_6D_6, 298K) δ 7.43 (d, $^3J_{HH}$=7.60Hz, 4H, C_6H_5-*H_{ortho}*) ; δ 7.22 (m, 4H, C_6H_5-*H_{meta}*) ; δ 7.06 (m, 2H, C_6H_5-*H_{para}*) ; δ 6.90 (m, 6H, C_6H_3) ; δ 3.71 (sept, $^3J_{HH}$=6.80Hz, 4H, $CH(CH_3)_2$) ; δ 2.15 (s, 4H, CH_2CMe_2Ph) ; δ 1.60 (s, 12H, CH_2CMe_2Ph) ; δ 1.08 (d, $^3J_{HH}$=6.80Hz, 24H, $CH(CH_3)_2$).

^{13}C NMR data :- (100MHz, C_6D_6, 298K) δ 157.78 (s, C_6H_3-*C_{ipso}*) ; δ 151.25 (s, Ph-*C_{ipso}*) ; δ 145.33 (s, C_6H_3-*C_{ortho}*) ; δ 128.33, 127.37, 126.67, 125.88 and 123.27 (overlapping doublets due to C_6H_3-*C_{meta}* , *C_{para}* and Ph-*C_{ortho}* , *C_{meta}* and *C_{para}*) ; δ 96.23 (t, $^1J_{CH}$=125.88Hz, CH_2CMe_2Ph) ; δ 41.61 (s, CH_2CMe_2Ph) ; δ 32.24 (q, $^1J_{CH}$=124.22Hz, CH_2CMe_2Ph) ; δ 28.32 (d, $^1J_{CH}$=129.35Hz, $CH(CH_3)_2$) ; δ 24.07 (q, $^1J_{CH}$=125.90Hz, $CH(CH_3)_2$).

6.4.5 Reaction of $Cr(NAr)_2Cl_2$ (14) with Me_3CCH_2MgCl :

Preparation of $Cr(NAr)_2(CH_2CMe_3)_2$ (24).

The procedure was analogous to that described above for $Cr(NAr)_2(2,4,6\text{-}Me_3C_6H_2)_2$, using $Cr(NAr)_2Cl_2$ (0.472 g, 1.00 mmol) and a Me_3CCH_2MgCl solution (2.43 cm^3 of a 0.82 M solution in diethyl ether; 2.00 mmol). Recrystallisation from pentane at -30°C afforded green crystals of $Cr(NAr)_2(CH_2CMe_3)_2$. Yield 0.42 g (77%).

Elemental Analysis for $C_{34}H_{56}N_2Cr$, calculated (found) :- %C 74.95 (75.20), %H 10.36 (10.69), %N 5.14 (4.84).

Infra-Red data :- (Nujol mull, CsI, cm^{-1}) 1584 (w), 1560 (w), 1356 (m), 1319 (w), 1275 (m), 1259 (m), 1229 (s), 1177 (w), 1096 (m), 1079 (s), 1067 (s, sh), 984 (m), 930 (w, br), 897 (w), 798 (vs), 755 (vs, sp), 723 (m), 621 (m, br), 535 (w), 457 (w), 432 (w).

^{1}H NMR data :- (400MHz, C_6D_6, 298K) δ 6.90 (m, 6H, C_6H_3) ; δ 3.80 (sept, $^3J_{HH}$=6.8Hz, 4H, $CH(CH_3)_2$) ; δ 2.52 (s, 4H, CH_2CMe_3) ; δ 1.33 (s, 18H, CH_2CMe_3) ; δ 1.12 (d, $^3J_{HH}$=6.00Hz, 24H, $CH(CH_3)_2$).

^{13}C NMR data :- (100MHz, C_6D_6, 298K) δ 157.86 (s, C_6H_3-C_{ipso}) ; δ 145.24 (s, C_6H_3-C_{ortho}) ; δ 127.33 (d, $^1J_{CH}$=157.91Hz, C_6H_3-C_{para}) ; δ 123.14 (d, $^1J_{CH}$=157.51Hz, C_6H_3-C_{meta}) ; δ 94.93 (t, $^1J_{CH}$=123.21Hz, CH_2CMe_3) ; δ 34.99 (s, CH_2CMe_3) ; δ 33.43(q, $^1J_{CH}$=124.49Hz, CH_2CMe_3) ; δ 28.51 (d, $^1J_{CH}$=128.54Hz, $CH(CH_3)_2$) ; δ 23.91 (q, $^1J_{CH}$=125.90Hz, $CH(CH_3)_2$).

6.4.6 Reaction of $Cr(NAr)_2(CH_2CMe_3)_2$ (24) with C_6D_6 :

Formation of $Cr(NAr)_2(CHDCMe_3)(C_6D_5)$ (25).

$Cr(NAr)_2(CH_2CMe_3)_2$ (0.01 - 0.02 g) was introduced into an NMR tube and C_6D_6 (ca. 400 µl) was condensed on to it. The tube was sealed and the spectra were recorded monitoring the change from **24** to **25**.

^{1}H NMR data :- (400MHz, C_6D_6, 298K) δ 6.93 (m, 6H, C_6H_3) ; δ 3.94 (sept, $^3J_{HH}$=6.80Hz, 4H, $CH(CH_3)_2$) ; δ 1.83 (s (br), 0.3H, $CHDCMe_3$) ; δ 1.29 (s, 9H, CMe_3) ; δ 1.12 (d, $^3J_{HH}$=6.80Hz, 12H, $CH(CH_3)_2$) ; δ 1.09 (d, $^3J_{HH}$=7.20Hz, 12H, $CH(CH_3)_2$) ; δ 0.90 (s, 12H, CMe_4).

^{13}C NMR data :- (100MHz, C_6D_6, 298K) δ 192.17 (t, $^2J_{CD}$=16.20Hz, C_6D_5-C_{ipso}) ; δ 157.91 (s, C_6H_3-C_{ipso}) ; δ 145.76 (s, C_6H_3-C_{ortho}) ; δ 136.04 (d, $^1J_{CH}$=159.23Hz, C_6H_3-C_{para}) ; δ 135.74 (t, $^1J_{CD}$=24.75Hz, C_6D_5) ; δ 123.11 (d, $^1J_{CH}$=156.32Hz, C_6H_3-C_{meta}) ; δ 97.98 (t, $^1J_{CD}$=19.56Hz, $CHDCMe_3$) ; δ 35.78 (s, CMe_3) ; δ 35.65 (s, CMe_4)

; δ 33.13 (q, $^1J_{CH}$=124.73Hz, C*Me*$_3$) ; δ 31.58 (q, $^1J_{CH}$=123.93Hz, C*Me*$_4$) ; δ 28.59 (d, $^1J_{CH}$=129.36Hz, *C*H(CH$_3$)$_2$) ; δ 24.15 (q, $^1J_{CH}$=125.94Hz, CH(*C*H$_3$)$_2$) ; δ 23.71 (q, $^1J_{CH}$=125.94Hz, CH(*C*H$_3$)$_2$).

6.4.7 Kinetic Study of the Conversion of Cr(NAr)$_2$(CH$_2$CMe$_3$)$_2$ (24) to Cr(NAr)$_2$(CHDCMe$_3$)(C$_6$D$_5$) (25).

The concentration of **24** was calculated by monitoring the reduction in the integral of the methylene signal C*H*$_2$CMe$_3$ at 2.52 ppm in comparison with an internal constant. The constant chosen was the integral of the aryl peaks of the imido ligand as, assuming no decomposition of the imido groups (no evidence from NMR) integration of the peaks at δ 6.90 (for **24**) and δ 6.93 (for **25**) will remain constant throughout the reaction. Other signals in the spectra were complicated by overlap but the aryl resonances were found to be sufficiently separated from the signal of the protio impurity in the deuterated solvent to allow accurate measurement of the integral. Three separate determinations of the integral were recorded and errors were estimated from the deviation of these values from the average of the three recordings.

In a typical experiment, 0.01 - 0.02g of **24** was dissolved in C$_6$D$_6$ (ca. 400μl) and the initial spectrum recorded. The NMR tube was then maintained at a steady temperature (± 0.5°C) by complete submergence in an oil bath. At regular intervals, the samples were removed from the oil bath and the ^{1}H NMR spectra recorded immediately, with a typical acquisition time of 1.5 - 2 minutes.

6.4.8 Reaction of Cr(NAr)$_2$(CH$_2$CMe$_3$)$_2$ (24) with D$_8$-THF :

Formation of Cr(NAr)$_2$(=CHCMe$_3$)(THF) (26).

The reaction was carried out employing an analogous method to that described for the reaction of Cr(NAr)$_2$(CH$_2$CMe$_3$)$_2$ with C$_6$D$_6$ (section 6.4.6).

^{1}H NMR data :- (400MHz, D_8-THF, 298K) δ 14.62 (s, 1H, =C*H*CMe$_3$) ; δ 7.00-6.77 (m, 6H, C_6H_3) ; δ 4.07 (sept, $^3J_{HH}$=6.70Hz, 2H, C*H*(CH$_3$)$_2$) ; δ 3.54 (sept, $^3J_{HH}$=6.40Hz, 2H, C*H*(CH$_3$)$_2$) ; δ 1.31 (s, 9H, =CHC*Me$_3$*) ; δ 1.24 (d, $^3J_{HH}$=7.00Hz, 6H, CH(C*H$_3$*)$_2$) ; δ 1.21 (d, $^3J_{HH}$=6.80Hz, 6H, CH(C*H$_3$*)$_2$) ; δ 1.05 (d, $^3J_{HH}$=6.80Hz, 6H, CH(C*H$_3$*)$_2$) ; δ 0.88 (d, $^3J_{HH}$=6.80Hz, 6H, CH(C*H$_3$*)$_2$) ; δ 0.94 (s, 12H, C*Me$_4$*).

^{13}C NMR data :- (100MHz, D_8-THF, 298K) δ 328.00 (d, $^1J_{CH}$=*****Hz, =*C*HCMe$_3$) ; δ 160.91 (s, C_6H_3-*C$_{ipso}$*) ; δ 158.82 (s, C_6H_3-*C$_{ipso}$*) ; δ 142.77 (s, C_6H_3-*C$_{ortho}$*) ; δ 142.18 (s, C_6H_3-*C$_{ortho}$*) ; δ 124.46 (d, $^1J_{CH}$=159.84Hz, C_6H_3-*C$_{para}$*) ; δ 123.60 (d, $^1J_{CH}$=159.44Hz, C_6H_3-*C$_{para}$*) ; δ 122.63 (d, $^1J_{CH}$=154.71Hz, C_6H_3-*C$_{meta}$*) ; δ 122.32 (d, $^1J_{CH}$=155.21Hz, C_6H_3-*C$_{meta}$*) ; δ 80.77 (quin, $^1J_{CD}$=23.14Hz, THF (bound)) ; δ 49.30 (s, *C*Me$_3$) ; δ 32.95 (q, C*Me$_4$*) ; δ 31.84 (s, C*Me$_3$*) ; δ 29.09 (d, $^1J_{CH}$=128.86Hz, *C*H(CH$_3$)$_2$) ; δ 28.39 (d, $^1J_{CH}$=128.45Hz, *C*H(CH$_3$)$_2$) ; δ 24.20 ; δ 24.10 ; δ 23.57 (q*, CH(C*H$_3$*)$_2$).

(* overlapping quartets).

6.4.9 Reaction of Cr(NAr)$_2$(=CHCMe$_3$)(THF) (26) with PMe$_3$:

Preparation of Cr(NAr)$_2$(=CHCMe$_3$)(PMe$_3$) (27).

Cr(NAr)$_2$(CH$_2$CMe$_3$)$_2$ (0.31g, 0.58 mmol) was dissolved in THF and allowed to stir for 1 week to completely convert to the alkylidene THF adduct Cr(NAr)$_2$(=CHCMe$_3$)(THF) (**26**), which was not isolated. The solution was then cooled to -196°C in liquid nitrogen and evacuated before 1 equivalent of PMe$_3$ was condensed onto it. This was allowed to warm to room temperature before introducing an atmosphere of nitrogen. After 30 minutes, the volatile component was removed *in vacuo* and the complex was redissolved in THF. This solvent did not yield a solid material after repeated concentration and so the solvent was removed and the product was isolated as a bright red amorphous solid from recrystallisation of a concentrated heptane solution at -30°C. Yield 0.28g (88%).

Elemental Analysis for $C_{32}H_{53}N_2CrP$, calculated (found) :- %C 70.04 (70.24), %H 9.73 (9.89), %N 5.10 (5.61).

Infra-Red data :- (Nujol mull, CsI, cm^{-1}) 1583 (w), 1558 (w), 1415 (m), 1357 (m), 1322 (s, sh), 1281 (s), 1255 (m), 1233 (w), 1175 (w), 1157 (w), 1105 (w), 1094 (m), 1058 (w), 1045 (w), 989 (m, sp), 947 (s, br), 847 (m), 799 (m, sh), 769 (m), 759 (m), 749 (s), 736 (m), 670 (m), 589 (w), 457 (w).

^{1}H NMR data :- (400MHz, D_8-THF, 298K) δ 14.79 (d, $^3J_{PH}$=6.40Hz, =C*H*CMe$_3$) ; δ 7.08 (m, C_6H_3) ; δ 4.31 (sept, 2H, C*H*(CH$_3$)$_2$) ; δ 4.01 (sept, 2H, C*H*(CH$_3$)$_2$) ; δ 1.55 (d, $^2J_{PH}$=9.60Hz, 9H, P*Me$_3$*) ; δ 1.29 (s, 9H, =CHC*Me$_3$*) ; δ 1.22 (d, $^3J_{HH}$=7.20Hz, 6H, CH(C*H$_3$*)$_2$) ; δ 1.17 (d, $^3J_{HH}$=7.20Hz, 6H, CH(C*H$_3$*)$_2$) ; δ 1.13 (d, $^3J_{HH}$=6.80Hz, 6H, CH(C*H$_3$*)$_2$) ; δ 1.11 (d, $^3J_{HH}$=6.80Hz, 6H, CH(C*H$_3$*)$_2$).

^{13}C NMR data :- (100MHz, C_6D_6, 298K) δ 339.93 (d, $^2J_{PH}$=26.25Hz, =*C*HCMe$_3$) ; δ 156.99 (s, C_6H_3-*C$_{ipso}$*) ; δ 153.18 (s, C_6H_3-*C$_{ipso}$*) ; δ 144.65 (s, C_6H_3-*C$_{ortho}$*) ; δ 141.27 (s, C_6H_3-*C$_{ortho}$*) ; δ 122.45 (d, $^1J_{CH}$=159.23Hz, C_6H_3-*C$_{para}$*) ; δ 123.02 (d, $^1J_{CH}$=159.94Hz, C_6H_3-*C$_{para}$*) ; δ 122.45 (d, $^1J_{CH}$=159.23Hz, C_6H_3-*C$_{meta}$*) ; δ 122.42 (d, $^1J_{CH}$=159.23Hz, C_6H_3-*C$_{meta}$*) ; δ 48.99 (s, =CH*C*Me$_3$) ; δ 31.80 (q, $^1J_{CH}$=125.13Hz, =CHC*Me$_3$*) ; δ 28.63 (d, $^1J_{CH}$=128.76Hz, *C*H(CH$_3$)$_2$) ; δ 28.00 (d, $^1J_{CH}$=128.45Hz, *C*H(CH$_3$)$_2$) ; δ 23.76 (q, $^1J_{CH}$=121.61Hz, P*Me$_3$*) ; δ 19.49 (q, $^1J_{CH}$=129.79Hz, CH(*C*H$_3$)$_2$) ; δ 19.22 (q, $^1J_{CH}$=129.79Hz, CH(*C*H$_3$)$_2$).

^{31}P NMR data :- (162MHz, D_8-THF, 298K) δ 21.62 (s, *P*Me$_3$).

6.5 Experimental Details to Chapter 5.

6.5.1 General NMR Scale Reactions between *N*-Norbornenyl Alanine Methyl Ester and Mo(NAr)(=CHCMe$_2$Ph)(OR)$_2$.

The following account outlines the general procedure for the ring-opening metathesis polymerisation of each of the monomers studied on this scale. Typically, 0.01 g of catalyst **I**, **II** or **III** was weighed out into a sample vial within an inert atmosphere glove-box, and sufficient C_6D_6 was added to allow a solution to form (ca. 100 µl). Ten equivalents of the monomer under investigation (0.045, 0.038 and 0.013 g for catalyst **I**, **II**, and **III** respectively) were dissolved in a similar fashion using ca. 300 µl of C_6D_6, and added to the rapidly stirring catalyst solution. This was left for 5 minutes after which time the mixture was transferred to a 5 mm NMR tube and sealed under N_2. The tube was kept frozen until the spectrum was recorded.

6.5.2 General Preparative Scale Reactions between *N*-Norbornenyl Alanine Methyl Ester and Mo(NAr)(=CHCMe$_2$Ph)(OR)$_2$.

All of the polymerisations were performed in an inert atmosphere glove box. Typically 0.25 g of monomer was dissolved in 3 g (3.46 cm^3) of toluene that had been freshly distilled, degassed and passed through a column of activated alumina prior to use. A small aliquot of this solution (2-3 drops from a pipette) was added to a rapidly stirring solution of 0.01 g of **I**, **II** or **III** in 1 g (1.15 cm^3) of toluene and the mixture allowed to stir for ca. 1 minute before the rest of the monomer solution was added dropwise over 5 minutes.

The polymerisation was allowed to proceed for set length of time before addition of excess benzaldehyde (50 µl) to cap the polymer in a 'Wittig' type reaction. The polymer was then isolated by precipitation of the toluene solution into an excess (ca 100 cm^3) of hexane. Any remaining polymer that had precipitated from the toluene solution was redissolved in CH_2Cl_2 and added to the hexane solution, resulting overall

yields of 90 - 100%. The off-white polymer was collected by filtration and dried in a vacuum oven at 65°C for 16 hours.

6.5.3 Spectroscopic Assignments for ROMP Polymers.

(using labelling scheme outlined in section 5.4.4).

a) Polymers from *exo*-Monomers.

Infra-Red data :- (thin film cast from CH_2Cl_2, KBr, cm^{-1}) 3466 (w), 2952 (m), 2864 (w), 1747 (vs), 1707 (vs), 1450 (m), 1387 (vs), 1311 (m), 1230 (s, sh), 1199 (s), 1120 (m, sp), 1070 (m), 967 (m), 734 (m), 627 (m).

^{1}H NMR data :- (400MHz, $CDCl_3$, 298K) δ 5.72 (m (br), H_a-trans) ; δ 5.52 (m (br), H_a-cis) ; δ 4.74 (q, $^1J_{CH}$=7.20Hz, alanine C-*H*) ; δ 3.71 (s, alanine CO_2CH_3) ; δ 3.29 (s (br), H_d-cis) ; δ 3.11 (s (br), H_c-cis) ; δ 3.00 (s (br), H_d-trans) ; δ 2.71 (s (br), H_c-trans) ; δ 2.07 and δ 1.60 (s (br), H_b and $H_{b'}$) ; δ 1.51 (s, alanine CH_3).

^{13}C NMR data :- (100MHz, $CDCl_3$, 298K) δ 177.4 (*C*=O) ; δ 169.7 (alanine CO_2CH_3) ; δ 133.1 (C_2 and C_3-cis) ; δ 131.7 (C_2 and C_3-trans) ; δ 52.7 (alanine CO_2CH_3) ; δ 50.6 (C_5 and C_6) ; δ 47.6 (alanine *C*H) ; δ 45.7 (C_1 and C_4-trans) ; δ 41.3 (C_1 and C_4-cis) ; δ 42.1 / 41.7 / 40.8 (C_7 bridgehead) ; δ 14.2 (alanine CH_3).

b) Polymers from *endo*-Monomers.

Infra-Red data :- (thin film cast from CH_2Cl_2, KBr, cm^{-1}) 3459 (w), 2996 (m), 2952 (m), 1749 (vs), 1703 (vs), 1452 (m), 1389 (vs), 1320 (m), 1230 (s, sh), 1202 (s), 1123 (m, sp), 1080 (m), 967 (m), 734 (m), 627 (m).

^{1}H NMR data :- (400MHz, $CDCl_3$, 298K) δ 5.63 (m (br), H_a-trans + H_a-cis) ; δ 4.68 (q (br), alanine C-*H*) ; δ 3.67 (s, alanine CO_2CH_3) ; δ 3.20 (s (br), H_d-trans + H_d-cis) ; δ

2.87 (s (br), H_c + and H_c-cis) ; δ 1.84 and δ 1.36 (s (br), H_b and $H_{b'}$) ; δ 1.50 (s, alanine CH_3).

^{13}C NMR data :- (100MHz, $CDCl_3$, 298K) δ 175.6 (*C*=O) ; δ 169.5 (alanine CO_2CH_3) ; δ 129.2 (C_2 and C_3-cis and trans) ; δ 52.5 (alanine CO_2CH_3) ; δ 48.6 (C_5 and C_6) ; δ 47.7 (alanine *C*H) ; δ 45.3 (C_1 and C_4-trans) ; δ 40.3 (C_1 and C_4-cis) ; δ 36.8 / 36.3 (C_7 bridgehead) ; δ 14.2 (alanine CH_3).

6.5.4 Details of the Molecular Modelling Program used in Chapter 5.

The molecular simulation program *Discover* was used in all the molecular modelling experiments, running within Biosym's graphical molecular modelling interface Insight II (version 2.3.0).

6.6 References.

1. D.D. Devore, J.D. Lichtenhan, F. Takusagawa and E.A. Maatta, *J. Am. Chem. Soc.*, **1987**, *109*, 7408.

2. R.R. Schrock, J.S. Murdzek, G.C. Bazan, M. DiMare, J. Robbins and M. O'Regan, *J. Am. Chem. Soc.*, **1990**, *112*, 3875.

3. PMe_3 kindly donated by Mr M.C.W. Chan and Miss L.J. Sequiera.

4. J.C.W. Chien, W.M. Tsai and M.D. Rausch, *J. Am. Chem. Soc.*, **1991**, *113*, 8570.

5. E.B. Tjaden, D.C. Swenson, R.F. Jordan and J.L. Petersen, *Organometallics*, **1995**,

6. Grignard reagents made by slow addition of the relevant chloro or bromo compound to activated magnesium in ether, followed by reflux overnight. The reaction was filtered and titrated prior to use.

7. LiNHAr was prepared by treatment of $^{n}BuLi$ with $ArNH_2$.

Appendices

APPENDIX 1.

Appendix 1A: **Crystal Data for $Cr(N^tBu)_2(CH_2Ph)_2$ (1).**

$C_{22}H_{32}CrN_2$:	376.50
Crystal System:	Orthorhombic
Space Group:	$P2_12_12_1$
Cell Dimensions:	a = 9.785(8) Å
	b = 14.72(2) Å
	c = 14.794(10) Å
	$\alpha = 90°$
	$\beta = 90°$
	$\gamma = 90°$
	U = 2135(3) $Å^3$
	Z = 4
	$D_c = 1.171$ g cm^{-3}.
Final R indices [$I>2\sigma(I)$]	0.0259 (wR2 = 0.0658)

Appendix 1B: **Crystal Data for $Cr(NAd)_2(CH_2CMe_2Ph)_2$ (10).**

$C_{40}H_{56}CrN_2$:	616.87
Crystal System:	Triclinic
Space Group:	$P\bar{1}$
Cell Dimensions:	a = 12.229(2) Å
	b = 12.902(2) Å
	c = 13.454(2) Å
	$\alpha = 70.566(2)°$
	$\beta = 64.689(3)°$
	$\gamma = 62.846(2)°$
	U = 1682.4(3) $Å^3$
	Z = 2
	$D_c = 1.218$ g cm^{-3}.
Final R indices [$I>2\sigma(I)$]	0.0435 (wR2 = 0.1041)

Appendix 1C: **Crystal Data for $Cr(NAr)_2(NH^tBu)Cl$ (12). (Ar=2,6-^{i}Pr$_2$-C_6H_3).**

$C_{28}H_{44}ClCrN_3$:	510.11
Crystal System:	Triclinic
Space Group:	$P\bar{1}$
Cell Dimensions:	a = 11.483(6) Å
	b = 11.634(6) Å
	c = 12.426(6) Å
	α = 81.91(3)°
	β = 71.16(2)°
	γ = 68.16(2)°
	U = 1458.0(13) Å^3
	Z = 2
	D_c = 1.162 g cm^{-3}.
Final R indices [I>2σ(I)]	0.0430 (wR2 = 0.1075)

Appendix 1D(i): **Crystal Data for $Cr(NAr)_2Cl_2$(pyridine) (15).**

$C_{29}H_{39}Cl_2CrN_3$:	552.53
Crystal System:	Monoclinic
Space Group:	$P2_1/c$
Cell Dimensions:	a = 10.465(3) Å
	b = 8.896(2) Å
	c = 31.961(8) Å
	α = 90°
	β = 98.45(3)°
	γ = 90°
	U = 2943.2(13) Å^3
	Z = 4
	D_c = 1.247 g cm^{-3}.
Final R indices [I>2σ(I)]	0.0438 (wR2 = 0.0900)

Appendix 1D(ii): **Crystal Data for $Cr(NAr)_2Cl_2$(pyridine) (15).**

$C_{29}H_{39}Cl_2CrN_3$:	552.53
Crystal System:	Triclinic
Space Group:	$P\bar{1}$
Cell Dimensions:	a = 9.5275(8) Å
	b = 10.7197(10) Å
	c = 15.5038(14) Å
	α = 97.572(2)°
	β =105.819(5)°
	γ = 104.820(2)°
	U = 1437.8(2) $Å^3$
	Z = 2
	D_c = 1.276 g cm^{-3}.
Final R indices [I>2σ(I)]	0.0447 (wR2 = 0.1068)

Cr–N(2)	1.660(2)	Cr–N(1)	1.679(2)
Cr–N(3)	2.159(2)	Cr–Cl(1)	2.2893(7)
Cr–Cl(2)	2.3035(7)	N(1)–C(1)	1.384(3)
C(1)–C(2)	1.429(3)	C(1)–C(6)	1.413(3)
C(2)–C(3)	1.387(3)	C(3)–C(4)	1.384(4)
C(4)–C(5)	1.389(4)	C(5)–C(6)	1.393(3)
N(2)–C(13)	1.356(3)	C(13)–C(18)	1.424(3)
C(13)–C(14)	1.430(3)	C(14)–C(15)	1.377(4)
C(15)–C(16)	1.384(5)	C(16)–C(17)	1.390(4)
C(17)–C(18)	1.384(4)	N(3)–C(29)	1.334(3)
N(3)–C(25)	1.335(3)	C(25)–C(26)	1.381(4)
C(26)–C(27)	1.380(4)	C(27)–C(28)	1.370(5)
C(28)–C(29)	1.384(4)		

(C-C Distances of *iso*-propyl groups in the range 1.497(4)–1.533(3)Å)

N(2)–Cr–N(1)	109.36(9)	N(2)–Cr–N(3)	154.44(8)
N(1)–Cr–N(3)	96.10(8)	N(2)–Cr–Cl(1)	90.50(6)
N(1)–Cr–Cl(1)	107.81(7)	N(3)–Cr–Cl(1)	83.51(6)
N(2)–Cr–Cl(2)	89.16(6)	N(1)–Cr–Cl(2)	106.94(7)
N(3)–Cr–Cl(2)	81.20(6)	Cl(1)–Cr–Cl(2)	143.22(3)
C(1)–N(1)–Cr	147.8(2)	N(1)–C(1)–C(2)	119.6(2)
N(1)–C(1)–C(6)	118.3(2)	C(2)–C(1)–C(6)	121.9(2)
C(3)–C(2)–C(1)	116.8(2)	C(3)–C(2)–C(7)	123.0(2)
C(1)–C(2)–C(7)	120.1(2)	C(4)–C(3)–C(2)	122.0(2)
C(5)–C(4)–C(3)	120.5(2)	C(4)–C(5)–C(6)	120.8(2)
C(5)–C(6)–C(1)	118.0(2)	C(5)–C(6)–C(10)	120.7(2)
C(1)–C(6)–C(10)	121.3(2)	C(13)–N(2)–Cr	169.1(2)
N(2)–C(13)–C(18)	119.2(2)	N(2)–C(13)–C(14)	119.4(2)
C(18)–C(13)–C(14)	121.4(2)	C(15)–C(14)–C(13)	118.0(2)
C(15)–C(14)–C(19)	121.4(2)	C(13)–C(14)–C(19)	120.6(2)
C(14)–C(15)–C(16)	120.9(3)	C(17)–C(16)–C(15)	121.0(3)
C(16)–C(17)–C(18)	121.1(3)	C(17)–C(18)–C(13)	117.5(2)
C(17)–C(18)–C(22)	121.2(2)	C(13)–C(18)–C(22)	121.3(2)
C(29)–N(3)–C(25)	117.4(2)	C(29)–N(3)–Cr	121.2(2)
C(25)–N(3)–Cr	121.3(2)	N(3)–C(25)–C(26)	122.9(3)
C(27)–C(26)–C(25)	119.3(2)	C(26)–C(27)–C(28)	118.1(3)
C(27)–C(28)–C(29)	119.4(3)	N(3)–C(29)–C(28)	122.9(3)

(Angles within *iso*-propyl groups in the range 109.9(2)–113.7(2)°)

Appendix 1E: **Crystal Data for $Cr(NAr)_2(NHAr)Cl$ (17).**

$C_{36}H_{52}ClCrN_3$:	614.26
Crystal System:	Monoclinic
Space Group:	$P2_1/n$
Cell Dimensions:	a = 10.4714(11) Å
	b = 15.411(2) Å
	c = 21.493(2) Å
	$\alpha = 90°$
	$\beta = 94.707(2)°$
	$\gamma = 90°$
	U = 3456.7(6) $Å^3$
	Z = 4
	$D_c = 1.180$ g cm^{-3}.
Final R indices [$I>2\sigma(I)$]	0.0588 (wR2 = 0.1177)

Appendix 1G: **Crystal Data for $Cr(NAr)_2(CH_2Ph)_2$ (21).**

$C_{38}H_{48}CrN_2$:	584.78
Crystal System:	Orthorhombic
Space Group:	$P2_12_12_1$
Cell Dimensions:	a = 9.8995(5) Å
	b = 17.6771(8) Å
	c = 19.1110(9) Å
	$\alpha = 90°$
	$\beta = 90°$
	$\gamma = 90°$
	U = 3344.3(3) $Å^3$
	Z = 4
	$D_c = 1.161$ g cm^{-3}.
Final R indices [$I>2\sigma(I)$]	0.0546 (wR2 = 0.1051)

Appendix 1F: **Crystal Data for $Cr(NAr)_2(CH_2CMe_2Ph)_2$ (23).**

$C_{44}H_{60}CrN_2$:	668.94
Crystal System:	Monoclinic
Space Group:	$P2_1/c$
Cell Dimensions:	a = 22.568(4) Å
	b = 19.356(4) Å
	c = 19.611(3) Å
	$\alpha = 90°$
	$\beta = 114.383(11)°$
	$\gamma = 90°$
	U = 7802(2) $Å^3$
	Z = 8
	$D_c = 1.139$ g cm^{-3}.
Final R indices [$I>2\sigma(I)$]	0.0923 (wR2 = 0.15.64)

Appendix 1H:	**Crystal Data for $Cr(NAr)_2(CH_2CMe_3)_2$ (24).**
$C_{34}H_{56}CrN_2$:	544.81
Crystal System:	Monoclinic
Space Group:	$P2_1/n$
Cell Dimensions:	a = 10.6808(10) Å
	b = 17.081(2) Å
	c = 18.494(2) Å
	$\alpha = 90°$
	$\beta = 101.869(2)°$
	$\gamma = 90°$
	U = 3301.9(6) $Å^3$
	Z = 4
	$D_c = 1.096$ g cm^{-3}.
Final R indices [$I>2\sigma(I)$]	0.0408 (wR2 = 0.1095)

APPENDIX 2.

2.1 First Year Induction Courses: October 1992.

The course consists of a series of one hour lectures on the services available in the department.

1. Departmental Safety
2. Safety Matters
3. Electrical Appliances and Infrared Spectroscopy
4. Chromatography and Microanalysis
5. Atomic Absorption and Inorganic Analysis
6. Library Facilities
7. Mass Spectroscopy
8. Nuclear Magnetic Resonance
9. Glass Blowing Techniques

2.2 Examined Lecture Courses: October 1992-April 1993

Three courses were attended consisting of 6 one hour lectures followed by a written examination in each.

"Synthetic Methodology in Organometallic and Coordination Chemistry", 3 lectures Prof. V.C. Gibson and 3 lectures Prof D. Parker.

"Diffraction Techniques", 4 lectures Prof. J.A.K. Howard and 2 lectures Prof. R.W. Richards.

"Synthetic Polymers", 6 lectures Prof. W.J. Feast.

2.3 Research Colloquia, Seminars and Lectures Organised by the Department of Chemistry.

(* - Indicates Colloquia attended by the author).

During the Period 1992 - 1993.

15th October	Dr. M. Glazer and Dr. S. Tarling, Oxford University and Birbeck College, London, "It pays to be British!- The Chemists Role as an Expert Witness in Patent Litigation."
20th October	Dr. H.E. Bryndza, Du Pont Central Research, "Synthesis, Reactions and Thermochemistry of Metal (Alkyl) Cyanide Complexes and Their Impact on Olefin Hydrocyanation Catalysis."
22nd October	Prof. A. Davies, University College London, The *Ingold-Albert Lecture* "The Behaviour of Hydrogen as a Pseudometal."
28th October	* Dr. J.K. Cockcroft, University of Durham, "Recent Developments in Powder Diffraction."
29th October	* Dr. J. Emsley, Imperial College, London, "The Shocking History of Phosphorus."
4th November	* Dr. T.P. Kee, University of Leeds, "Synthesis and Co-ordination Chemistry of Silylated Phosphites."
5th November	* Dr. C.J. Ludman, University of Durham, "Explosions, A Demonstration Lecture."
11th November	Prof. D. Robins, Glasgow University, "Pyrrolizidine Alkaloids: Biological Activity, Biosynthesis and Benefits."
12th November	Prof. M.R. Truter, University College, London, "Luck and Logic in Host-Guest Chemistry."
18th November	* Dr. R. Nix, Queen Mary College, London, "Characterisation of Heterogeneous Catalysts."
25th November	Prof. Y. Vallee, University of Caen, "Reactive Thiocarbonyl Compounds."
25th November	Prof. L.D. Quin, University of Massachusetts, Amerherst, "Fragmentation of Phosphorus Heterocycles as a Route to Phosphoryl Species with Uncommon Bonding."
26th November	* Dr. D. Humber, Glaxo, Greenford, "AIDS- The Development of a Novel Series of Inhibitors of HIV."
2nd December	Prof. A.F.. Hegarty, University College, Dublin, "Highly Reactive Enols Stabilised by Steric Protection."
2nd December	Dr. R.A. Aitken, University of St. Andrews, "The Versatile Cycloaddition Chemistry of $Bu_3P.CS_2$."

3rd December	Prof. P. Edwards, Birmingham University, *The SCI Lecture*, "What is Metal?"
9th December	Dr. A.N. Burgess, ICI Runcorn, "The Structure of Perfluorinated Ionomer Membranes."
1993.	
20th January	Dr. D.C. Clary, University of Cambridge, "Energy Flow in Chemical Reactions."
21st January	Prof. L. Hall, Cambridge, "NMR- Window to the Body."
27th January	* Dr. W. Kerr, University of Strathclyde, "Development of the Pauson-Khand Annulation Reaction: Organocobalt Mediated Synthesis of Natural and Unnatural Products."
28th January	Prof. J. Mann, University of Reading, "Murder, Magic and Medicine."
3rd February	Prof. S.M. Roberts, University of Exeter, "Enzymes in Organic Synthesis."
10th February	Dr. D. Gillies, University of Surrey, "NMR and Molecular Motion in Solution."
11th February	* Prof. S. Knox, Bristol University, *The Tilden Lecture*, "Organic Chemistry at Polynuclear Metal Centres."
17th February	Dr. R.W. Kemmitt, University of Leicester, "Oxatrimethylenemethane Metal Complexes."
18th February	Dr. I. Fraser, ICI Wilton, "Reactive Processing of Composite Materials."
22nd February	Prof. D.M. Grant, University of Utah, "Single Crystals, Molecular Structure, and Chemical Shift Anisotropy."
24th February	Prof. C.J.M. Stirling, University of Sheffield, "Chemistry of Flat-Reactivity of Ordered Systems."
10th March	* Dr. P.K. Baker, University College of North Wales, Bangor, "Chemistry of Highly Versatile 7-Coordinate Complexes."
11th March	Dr. R.A.Y. Jones, University of East Anglia, "The Chemistry of Wine Making."
17th March	Dr. R.J.K. Taylor, University of East Anglia, "Adventures in Natural Product Synthesis."
24th March	Prof I.O. Sutherland, University of Liverpool, "Chromogenic Reagents for Cations."
13th May	* Prof. J.A. Pople, Carnegie-Mellon University, Pittsburgh, USA, *The Boys-Rahman Lecture*, "Applications of Molecular Orbital Theory."

21st May	* Prof. L. Weber, University of Bielefeld, "Metallo-phospha Alkenes as Synthons in Organometallic Chemistry."
1st June	Prof. J.P. Konopelski, University of California, Santa Cruz, "Synthetic Adventures with Enantiomerically Pure Acetals."
2nd June	* Prof. P. Ciardelli, University of Pisa, "Chiral Discrimination in the Stereospecific Polymerisation of Alpha Olefins."
7th June	Prof. R.S. Stein, University of Massachusetts, "Scattering Studies of Crystalline and Liquid Crystalline Polymers."
16th June	Prof. A.K. Covington, University of Newcastle, "Use of Ion Selective Electrodes as Detectors in Ion Chromatography."
17th June	Prof. O.F. Nielson, H.C. Ørsted Institute, University of Copenhagen, "Low-Frequency IR and Raman Studies of Hydrogen Bonded Liquids."

During the Period 1993 - 1994.

13th September	* Prof. Dr. A.D. Schlüter, Freie Univerisität Berlin, Germany, "Synthesis and Characterisation of Molecular Rods and Ribbons."
13th September	* Dr. K.J. Wynne, Office of Naval Research, Washington, USA, "Polymer Surface Design for Minimal Adhesion."
14th September	* Prof. J.M. DeSimone, University of North Carolina, Chapel Hill, USA, "Homogeneous and Heterogeneous Polymerisations in Environmentally Responsible Carbon Dioxide."
28th September	Prof. H. Ila, North Eastern Hill University, India, "Synthetic Strategies for Cyclopenanoids *via* Oxoketene Dithioacetals."
4th October	* Prof. F.J. Feher, University of California, Irvine, USA, "Bridging the Gap between Surfaces and Solution with Sessilquioxanes."
14th October	Dr. P. Hubberstey, University of Nottingham, "Alkali Metals: Alchemist's Nightmare, Biochemist's Puzzle and Technologist's Dream."
20th October	* Dr. P. Quale, University of Manchester, "Aspects of Aqueous ROMP Chemistry."
21st October	Prof. R. Adams, University of South Carolina, USA, "Chemistry of Metal Carbonyl Cluster Complexes: Development of Cluster Based Alkyne Hydrogenation Catalysis."
27th October	Dr. R.A.L. Jones, Cavendish Laboratory, Cambridge, "Perambulating Polymers."

10th November	Prof. M.N.R. Ashfold, University of Bristol, "High Resolution Photofragment Translational Spectroscopy: A New Way to Watch Photodissociation."
17th November	Dr. A. Parker, Rutherford Appleton Laboratory, Didcot, "Applications of Time Resolved Resonace Raman Spectroscopy to Chemical and Biochemical Problems."
24th November	* Dr. P.G. Bruce, University of St. Andrews, "Structure and Properties of Inorganic Solids and Polymers."
25th November	Dr. R.P. Wayne, University of Oxford, "The Origin and Evolution of the Atmosphere."
1st December	Prof. M.A. McKervey, Queen's University, Belfast, "Synthesis and Applications of Chemically Modified Calixarines."
8th December	Prof. O. Meth-Cohn, University of Sunderland, "Friedel's Folly Revisited - A Super Way to Fused Pyridines."
16th December	Prof. R.F. Hudson, University of Kent, "Close Encounters of the Second Kind."
<u>1994.</u>	
26th January	* Prof. J. Evans, University of Southampton, "Shining Light on Catalysts."
2nd February	Dr. A. Masters, University of Manchester, "Modelling Water Without Using Pair Potentials."
9th February	Prof. D. Young, University of Sussex, "Chemical and Biological Studies on the Coenzyme Tetrahydrofolic Acid."
16th Feburary	* Prof. K.H. Theopold, University of Delaware, USA, "Paramagnetic Chromium Alkyls: Synthesis and Reactivity."
23rd February	Prof. P.M. Maitlis, University of Sheffield, "Across the Border: From Homogeneous to Heterogeneous Catalysis."
2nd March	Dr. C. Hunter, University of Sheffield, "Noncovalent Interactions between Aromatic Molecules."
9th March	Prof. F. Wilkinson, Loughborough University of Technology, "Nanosecond and Picosecond LaserFlash Photolysis."
10th March	Prof. S.V. Ley, University of Cambridge, "New Methods for Organic Synthesis."
25th March	* Dr. D.J. Dilworth, University of Essex, "Technetium and Rhenium Compounds with Applications as Imaging Agents."
28th April	Prof. R.J. Gillespie, McMaster University, Canada, "The Molecular Structure of some Metal Fluorides and Oxofluorides: Apparent Exceptions to the VSEPR Model."

12th May	Prof. D.A. Humphreys, McMaster University, Canada, "Bringing Knowledge to Life."

During the Period 1994 - 1995.

5th October	Prof. N.L. Owen, Brigham Young University, Utah, USA, "Determining Molecular Structure - the INADEQUATE NMR way"
19th October	* Prof. N. Bartlett, University of California, "Some Aspects of Ag(II) and Ag(III) Chemistry."
2nd November	* Dr. P.G. Edwards, University of Wales, Cardiff, "The Manipulation of Electronic and Structural Diversity in Metal Complexes - New Ligands."
3rd November	Prof. B.F.G. Johnson, Edinburgh Universitry, "Arene-Metal Clusters."
9th November	Dr. G. Hogarth, University College, London, "New Vistas in Metal Imido Chemistry."
10th November	Dr. M. Block, Zeneca Pharmaceuticals, Macclesfield, "Large-scale Manufacture of ZD 1542, a Thromboxane Antagonist Synthase Inhibitor."
16th November	Prof. M. Page, University of Huddersfield, "Four-Membered Rings and β-Lactamase."
23rd November	Dr. J.M.J. Williams, University of Loughborough, "New Approaches to Asymmetric Catalysis."
7th December	Prof. D. Briggs, ICI and University of Durham, "Surface Mass Spectrometry."

1995.

11th January	Prof. P. Parsons, University of Reading, "Applications of Tandem Reactions in Organic Synthesis."
18th January	Dr. G. Rumbles, Imperial College, London, "Real or Imaginary Third Order Non-Linear Optical Materials."
25th January	Dr. D.A. Roberts, Zeneca Pharmaceuticals, "The Design and Synthesis of Inhibitors of the Renin-Angiotensin System."
1st February	* Dr. T. Cosgrove, University of Bristol, "Polymer do it at Interfaces"
8th February	* Dr. D. O'Hare, University of Oxford, "Synthesis and Solid State Properties of Poly-, Oligo- and Multidecker Metallocenes."
22nd February	Prof. E. Schaumann, University of Clausthal, "Silicon and Sulphur Mediated Ring Opening Reactions of Epoxide."

1st March	Dr. M. Rosseinsky, University of Oxford, "Fullerene Intercalation Chemistry."
22nd March	* Dr. M. Taylor, University of Auckland, New Zealand, "Structural Methods in Main Group Chemistry."
26th April	Dr. M. Schroder, University of Edinburgh, "Redox-Active Macrocyclic Complexes: Rings, Stacks and Liquid Crystals."
3rd May	Prof. E.W. Randall, Queen Mary and Westfield College, "New Perspectives in NMR Imaging."
4th May	Prof. A.J. Kresge, University of Toronto, USA, *The Ingold Lecture,* "Reactive Intermediates: Carboxylic-acid Enols and Other Unstable Species."

2.4 Conferences and Symposia Attended.

(* denotes poster presentation).

1.* *"Meeting of the Innovative Polymer Synthesis Panel"*
University of Durham, July 1993.

2. *"The Sixth Firth Symposium"*
University of Sheffield, April 1994.

3.* *"XVIth International Conference of Organometallic Chemistry"*
University of Sussex, July 1994.

4. *"New Chemistry with Alkoxide and Imide Ligands"*
Burlington Place, London, February 1995.

5.* *"11th International Symposium on Olefin Metathesis and Related Chemistry (ISOM 11)"*
University of Durham, July 1995.

2.5 Publications.

J. CHEM. SOC., CHEM. COMMUN., 1994 2505

Amino Acid derived Homochiral Polymers *via* Ring-opening Metathesis Polymerisation

Martyn P. Coles,[a] Vernon C. Gibson,*[a] Luisa Mazzariol,[b] Michael North,*[b] William G. Teasdale,[b] Carol M. Williams[b] and Dora Zamuner[b]

[a] Department of Chemistry, University of Durham, South Road, Durham, UK DH1 3LE
[b] Department of Chemistry, University of Wales, Bangor, Gwynedd, UK LL57 2UW

Homochiral norbornene monomers derived from amino acids undergo ring-opening metathesis polymerisation with $[Mo(=CHCMe_2Ph)(=NC_6H_3Pr^i_2\text{-}2,6)(OBu^t)_2]$ to give homochiral polymers with narrow molecular mass distributions.

Naturally occurring polymers such as proteins and nucleic acids occur with very well defined primary, secondary and tertiary structures, and these are of fundamental importance in determining the biological and chemical properties of the polymer. There is growing academic and commercial interest in synthetic biopolymers, whose structure–activity relationships are also likely to be closely dependent upon all aspects of their molecular architecture. It is therefore vital to obtain the maximum possible level of control over the assembly of such macromolecules. Ring-opening metathesis polymerisation (ROMP) of strained cyclic alkenes using well-defined metal alkylidene initiators[1] allows control over many aspects of the polymer assembly, including its molecular mass and molecular mass distribution,[2] alkene backbone configuration[3] and tacticity.[4] The application of ROMP methodology to highly functionalised biopolymers has not previously been addressed. Therefore, we have initiated a project aimed at the synthesis and ROMP of amino acid and peptide derived norbornenes, with the ultimate aim of utilising the chirality and molecular recognition capacity of the amino acid or peptide to control the architecture of synthetic polymers. Here, we describe the synthesis of homochiral polymers derived from norbornenes functionalised with optically pure alanine ester residues.

Each optical isomer of the *exo*- and *endo*-norbornene monomers† **3a,b** were synthesised by treatment of L-, D- or DL-alanine methyl ester **2** with either the *exo* **1a** or *endo* **1b** anhydrides according to Scheme 1. That no racemisation occurred during this monomer synthesis was shown by the additional preparation of monomers derived from both DL- and L-isoleucine. Commercially available DL-isoleucine is actually a racemic mixture of both diastereomers, so the norbornene derivatives derived from the racemic isoleucine show two sets of peaks in both the ^1H and ^{13}C NMR spectra. The monomers derived from L-isoleucine, however, gave a single set of peaks, indicating that no epimerisation of the α-centre had occurred within the detection limits of NMR spectroscopy.

The polymerisation was initially investigated on an NMR scale by adding 10 equiv. of the monomer to initiator **4** in deuteriated benzene. In all cases, a ^1H NMR signal was observed in the range δ 11–12 attributable to the propagating metal alkylidene hydrogen of a living polymer chain[2] (Scheme 2). The polymerisations were then carried out on a preparative scale, the monomer being added to a rapidly stirring solution of the initiator **4** in toluene. After 15–24 h, the living polymers were quenched by the addition of benzaldehyde and the resultant polymer was isolated by precipitation from hexane.† GPC data, *cis*/*trans* content and specific rotations are collected in Table 1. In all cases, the molecular mass distribution is reasonably narrow and the vinylene linkages in the polymer backbone are predominantly *trans* (77–91%), as expected for the *tert*-butoxide initiator.[3,4] The polymers derived from the optically active monomers D- and L-**3a** and D- and L-**3b** are

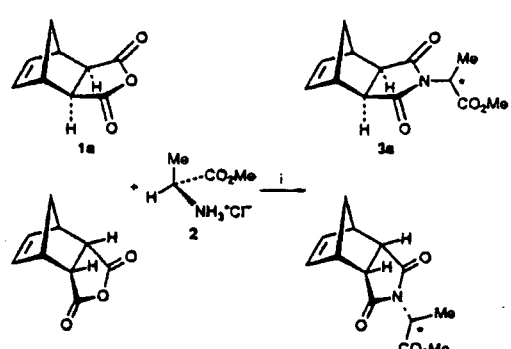

Scheme 1 *Reagents and conditions*: i, Et_3N, toluene, heat

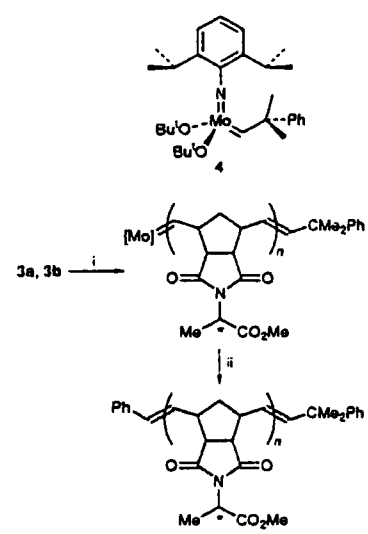

Scheme 2 *Reagents and conditions*: i, **4**, toluene, room temp.; ii, PhCHO, room temp.

Table 1 Physical parameters of the polymers derived from **3a** and **3b** using initiator **4**

Monomer (equivalents)	σ_c[a]	$[\alpha]_D^{20}$	M_n(found)[b]	M_n(calc.)	PDI (M_w/M_n)
L-**3a** (21)	0.08	−31	9065	5316	1.25
D-**3a** (54)	0.09	+34	10199	13349	1.13
DL-**3a** (85)	0.10	—	43030	21063	1.15
L-**3b** (46)	0.22	−52	21379	11608	1.28
D-**3b** (54)	0.20	+54	19581	13472	1.18
DL-**3b** (60)	0.23	—	18298	15027	1.29

[a] σ_c = %*cis*/100. [b] M_n and M_w were determined by gel permeation chromatography recorded on 0.1–0.3% m/v samples using a Waters differential refractometer R401 fitted with a Waters 590 pump and 3 PLgel 5 mm mixed columns previously calibrated using commercially available polystyrene standards (Polymer Laboratories) in the molecular mass range 162 to 1.03×10^6 ($CHCl_3$ flow rate = 1 $cm^3\ min^{-1}$).

themselves optically active, and they can be considered as artificial peptides in which the amide backbone has been replaced by an all carbon system.

In summary, we have shown that it is possible to prepare optically pure norbornenes derived from amino acids, and to use them as monomers for ROMP. The resulting polymers are optically active, have narrow molecular mass distributions, and the geometry of the alkenes can be controlled. Our studies in this area are currently being extended to the use of other amino acids and peptides within the norbornene monomers, and will be reported in due course.

The authors thank the EPSRC Innovative Polymer Synthesis Initiative for a studentship to M. P. C., the Interdisciplinary Research Centre in Polymer Science and Technology for polymer characterisation services, and the EEC-Erasmus scheme for grants to L. M. and D. Z.

Received, 8th September 1994; Com. 4/05476H

Footnote

† All new compounds gave satisfactory spectral and analytical data

References

1 R. H. Grubbs and W. Tumas, *Science*, 1989, 243, 907; R. R. Schrock, *Acc. Chem. Res.*, 1990, 23, 158; W. J. Feast and V. C. Gibson, Olefin Metathesis, in *Chemistry of the Metal-Carbon Bond*, ed. F. R. Hartley, Wiley, New York, 1989, vol. 5.

2 G. C. Bazan, R. R. Schrock, E. Khosravi, W. J. Feast, V. C. Gibson, M. B. O'Regan, J. K. Thomas and W. M. Davis, *J. Am. Chem. Soc.*, 1990, 112, 8378; G. C. Bazan, R. R. Schrock, H.-N. Cho and V. C. Gibson, *Macromolecules*, 1991, 24, 4495.

3 W. J. Feast, V. C. Gibson and E. L. Marshall, *J. Chem. Soc., Chem. Commun.*, 1992, 1157.

4 D. H. McConville, J. R. Wolf and R. R. Schrock, *J. Am. Chem. Soc.*, 1993, 115, 4413; J. H. Oskam and R. R. Schrock, *J. Am. Chem. Soc.*, 1993, 115, 11831.

Polymer Bulletin 33, 529–533 (1994)

Polymer Bulletin

New homogeneous ethylene polymerization catalysts derived from transition metal imido precursors

Martyn P. Coles and Vernon C. Gibson*

Department of Chemistry, University Science Laboratories, South Road, Durham DH1 3LE, UK

SUMMARY

New ethylene polymerization catalysts based on half-sandwich imido complexes of the Group 5 metals and bis(imido) complexes of the Group 6 metals are described.

INTRODUCTION

The discovery in the early 1980's that methylalumoxane (MAO) dramatically enhances the activity and longevity of Group 4 metallocene-based olefin polymerization catalysts (1), and the subsequent advances that have been made towards well-defined, single-component systems (2), have stimulated intense academic and industrial interest in metallocene-based polymerization technology. An important challenge lies in extending this type of chemistry to other transition metal systems, where modified activities and selectivities, particularly with regard to co-monomer incorporation and increased tolerance of heteroatom functionalities, may result.

The substitution of a mono-anionic cyclopentadienyl (Cp) ring in a Group 4 metallocene for appropriate di-anionic ligands as the transition series is transcended from left to right (Scheme 1a) offers a systematic approach to the development of new molecular systems with the potential for "metallocene-like" reactivity. This relationship derives from the similar $1\sigma,2\pi$ bonding characteristics of certain mono- and di-anionic ligands which give rise to [CpML] and [ML_2] fragments with closely related frontier orbital characteristics: the basis of this 'isolobal' relationship has been outlined elsewhere (3).

* Corresponding author

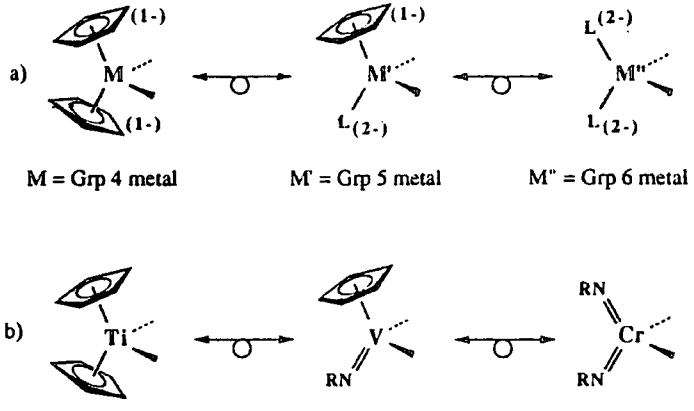

Scheme 1

Our approach has been to exchange Cp groups for organoimido (NR) ligands (3, 4), illustrated for the Ti→V→Cr series in Scheme 1(b). Here, we report on the ethylene polymerization activity of the Group 5 half-sandwich imido and Group 6 bis(imido) systems as conventional, dual-component catalysts derived from the transition metal dichlorides and Et_2AlCl (DEAC) or MAO as co-catalysts.

RESULTS AND DISCUSSION

The results of the polymerization runs, carried out under a flow of ethylene at 25°C in toluene solution, are collected in Table 1. Two points are worthy of note: first, the catalysts derived from the first row transition metal complexes $CpV(Ntol)Cl_2$ and $Cr(NBu^t)_2Cl_2$ are considerably more active than their second row counterparts, and secondly the vanadium-derived catalysts are more active than the chromium systems.

100 MHz ^{13}C NMR spectra recorded on polyethylene (PE) samples obtained from typical runs employing the vanadium and chromium catalysts showed that for both systems the resultant PE is of high molecular weight with little evidence of branching (< 1 per 5000 carbons). For the polymer derived from the vanadium catalyst, integration of the chain-end resonances versus the main-chain methylene carbons shows *ca.* 0.7 end-groups per 1000 carbons, compared with *ca.* 0.5 per 1000 carbons for the chromium derived sample; these correspond to number average molecular weights (M_n) of *ca.* 40,000 and 60,000 respectively. However, difficulties in completely solubilising the

samples indicate that these values underestimate the actual molecular weight of the polymer, a view supported by GPC analyses which reveal main peak M_w's of 2.1×10^5 and 1.2×10^6 respectively.

In summary, half-sandwich imido dihalide complexes of the Group 5 metals and bis(imido) dihalides of the Group 6 metals, in conjunction with DEAC or MAO as co-catalysts, are active catalysts for ethylene polymerization affording high molecular weight polyethylene with little branching.

Catalyst Precursor (mmol)	Activator (mmol/equiv.)	Yield Polyethylene (g)	Activity ($gmmol^{-1}hr^{-1}$)
$CpV(Ntol)Cl_2$ (0.175)	Et_2AlCl (3.50/20)	0.44	15.1
$CpV(Ntol)Cl_2$ (0.007)	MAO (12/1715)	0.19	27.1
$Cr(NBu^t)_2Cl_2$ (0.193)	Et_2AlCl (3.86/20)	1.73	9.0
$Cr(NBu^t)_2Cl_2$ (0.040)	MAO (12/300)	0.19	4.4
$CpNb(NAr)Cl_2$ (0.120)	Et_2AlCl (3.60/30)	0.06	0.6
$Mo(NBu^t)_2Cl_2$ (0.160)	Et_2AlCl (3.20/20)	< 0.03	< 0.2

Table 1. Conditions: C_2H_4 (1 bar), 25°C, toluene solution. tol = tolyl; Ar = 2-$Bu^tC_6H_4$.

EXPERIMENTAL

GENERAL

$CpV(Ntol)Cl_2$ (5), $Cr(NBu^t)_2Cl_2$ (6), $Mo(NBu^t)_2Cl_2$ (7) were prepared by previously reported procedures. $CpNb(N\text{-}2\text{-}Bu^tC_6H_4)Cl_2$ was prepared by an analogous procedure to that described for $CpNb(N\text{-}2,6\text{-}Pr^i_2C_6H_3)Cl_2$ (3). Methylalumoxane (MAO) was prepared by the partial hydrolysis of trimethylaluminum using aluminum sulphate hydrate according to the procedure of Kaminsky (1). Et_2AlCl (1.8 M solution in toluene) was purchased from Aldrich Chemical Co. and used as received.

^{13}C NMR spectra were recorded in $C_2D_4Cl_2$/1,2,4-trichlorobenzene on a JEOL GX400 spectrometer operating at 100 MHz. GPC data were recorded on 0.02% w/v samples in trichlorobenzene solvent using a Waters 150 CV chromatograph fitted with Shodex 10^7 Å linear 10^4 Å columns, previously calibrated against polystyrene standards.

POLYMERIZATION RUNS

The polymerizations were carried out in a glass Schlenk vessel at 25°C in toluene solvent (75 mL). The ethylene gas was purified by passing through a column of $CaCl_2$, 4Å molecular sieves and P_2O_5, each separated by glass wool, followed by bubbling through a silicone oil bubbler (30 cm^3) to which 2 cm^3 of Et_2AlCl solution had been added. In a typical procedure, a toluene solution of Et_2AlCl was added *via* syringe to a stirred solution of the transition metal dihalide (0.05 g) in toluene (75 mL). The mixture was stirred for 10 min after which the solution was purged with a continuous stream of ethylene. After 1hr, the ethylene flow was stopped and the polymerization quenched by addition of a small amount of methanol. The resultant polymer was then isolated by filtration, washed sequentially with acidified methanol, methanol and toluene, and dried *in vacuo* overnight. For runs using MAO as co-catalyst, the MAO solution was first syringed into the reactor vessel followed by a toluene solution of the metal dihalide.

ACKNOWLEDGEMENTS

The Engineering and Physical Sciences Research Council, UK, is gratefully acknowledged for a studentship to MPC. BP Chemicals are thanked for financial support and for ^{13}C NMR and GPC measurements on the polyethylene samples. Mr. M.C.W. Chan is thanked for conveying the result of the $CpNb(NAr)Cl_2$ polymerization run.

REFERENCES

1. Sinn, H.; Kaminsky, W.; Vollmer, H-J.; Woldt, R. (1980) Angew. Chem., Int. Ed. Engl., 19: 390. Kaminsky, W.; Miri, M.; Sinn, H.; Woldt, R. (1983) Makromol. Chem. Rapid Commun. 4: 417. Kaminsky, W.; Luker, H. (1984) Makromol. Chem. Rapid Commun., 5: 225.
2. Jordan, R.F.; Dasher, W.E.; Echols, S. F. (1986) J. Am. Chem. Soc., 108: 1718. Jordan, R.F.; Bajgur, C.S.; Willett, R.; Scott, B. (1986) J. Am. Chem. Soc., 108: 7410. Jordan, R.F.; LaPointe, R.E.; Bajgur, C.S.; Echols, S.F.; Willett, R. (1987) J. Am. Chem. Soc., 109: 4111. Hlatky, G.G.; Turner, H.W.; Eckman, R.R. (1989) J. Am. Chem. Soc., 111: 2728. Borkowsky, S.L.; Jordan, R.F.; Hinch, G.D. (1991) Organometallics, 10: 1268. Bochmann, M.; Jaggar, A.J.; Nicholls, J.C. (1990) Angew. Chem., Int. Ed. Engl., 29: 780. Bochmann, M.; Jaggar, A.J. (1992) J. Organomet. Chem., 424: C5. Bochmann, M.; Lancaster, S.J. (1993) Organometallics, 12: 633. Yang, X.; Stern, C.L.; Marks, T.J. (1991) J. Am. Chem. Soc., 113: 3623.

3. Williams, D.N; Mitchell, J.P.; Poole, A.D.; Siemeling, U.; Clegg, W.; Hockless, D.C.R.; O'Neil, P.A.; Gibson, V.C. (1992) J. Chem. Soc., Dalton Trans., 739. Williams, D.S.; Schofield, M.H.; Schrock, R.R. (1993) Organometallics, 12: 4560.
4. Cockcoft, J.K.; Gibson, V.C.; Howard, J.A.K.; Poole, A.D.; Siemeling, U.; Wilson, C. (1992) J. Chem. Soc. Chem. Commun., 1668. Siemeling, U.; Gibson, V.C. (1992) J. Organomet. Chem., 426: C25. Dyer, P.W.; Gibson, V.C.; Howard, J.A.K.; Whittle, B.; Wilson, C. (1992) J. Chem. Soc. Chem. Commun., 1666.
5. Devore, D.D.; Lichtenhan, J.D.; Takusagawa, F.; Maatta, E.A. (1987) J. Am. Chem. Soc., 109: 7408.
6. Danopoulos, A.A.; Leung, W-H.; Wilkinson, G.: Hussain-Bates, B.; Hursthouse, M.B. (1990) Polyhedron, 9: 2625.
7. Schoettel, G.; Kress, J.; Osborn, J.A. (1989) J. Chem. Soc. Chem. Commun., 1062.

Received: 15 August 1994/Accepted: 18 August 1994

J. CHEM. SOC., CHEM. COMMUN., 1995

Well-defined Ethylene Polymerisation Catalysts derived from Bis(imido) Chromium(VI) Precursors

Martyn P. Coles,[a] Christopher I. Dalby,[a] Vernon C. Gibson,*[a] William Clegg[b] and Mark R. J. Elsegood[b]

[a] *Department of Chemistry, University Science Laboratories, South Road, Durham, UK DH1 3LE*
[b] *Department of Chemistry, University of Newcastle, Newcastle upon Tyne, UK NE1 7RU*

Well-defined, cationic alkyl chromium polymerisation catalysts are generated upon treatment of the chromium(VI) dialkyl complexes $Cr(NR)_2(CH_2R')_2$ (R = Bu^t, R' = Ph; R = 2,6-Pr$^i_2$C$_6$H$_3$, R' = Ph, H) with the borate salts $[Ph_3C][B(C_6F_5)_4]$ or $[PhNMe_2H][B(C_6F_5)_4]$.

In recent years there has been a resurgence of interest in group 4 metallocene compounds as homogeneous alkene polymerisation catalysts (i) due to the spectacular rate enhancements afforded by methylaluminoxane (MAO) as a co-catalyst[1] and (ii) due to the subsequent development of well-defined, cationic alkyl derivatives[2] that have allowed unprecedented levels of control over the polymerisation process and much insight into how such catalysts function.

We have been exploring the isolobal relationship between η^5-C_5H_5 and imido ligands with a view to developing new reagents for organic synthesis and polymerisation catalysis.[3] The bis(imido)chromium system is of particular relevance to polymerisation catalysis since chromium catalysts play a central role in the worldwide production of polyolefins. The commercial catalyst formulations are heterogeneous, the Union Carbide 'Unipol' family of catalysts being prepared by treatment of silica with low-valent organometallic compounds such as chromocene,[4] while the Philips catalyst system involves the deposition of CrO_3 on silica, followed by reductive activation.[5] With the exception of Theopold's half-sandwich Cr^{III} system,[6] examples of homogeneous chromium polymerisation catalysts remain rare. Here, we describe the synthesis and characterisation† of some novel well-defined cationic alkyl chromium complexes that are surprisingly efficient homogeneous ethylene polymerisation catalysts.

The catalysts are derived from the chromium(VI) dialkyl compounds $Cr(NR)_2(CH_2R')_2$ [1 R = Bu^t, R' = Ph; 2: R = 2,6-Pr$^i_2$C$_6$H$_3$, R' = Ph; 3 R = 2,6-Pr$^i_2$C$_6$H$_3$, R' = H] which may be synthesised in good yield according to Scheme 1. Schaverien[7] has previously found that the dialkyl derivatives of bis(*tert*-butylimido)chromium are invariably oils which presents considerable difficulties in their handling and purification. We have found, however, that the previously unreported dibenzyl derivative may be isolated as a deep-red crystalline solid. We have also recently described the first bis(arylimido)chromium complexes[8] and find that the 2,6-diisopropylphenylimido group affords a beneficial effect on crystallinity; for example, not only the dibenzyl complex 2 but also the dimethyl derivative 3 bearing 2,6-diisopropylphenylimido ligands may be isolated as crystalline green solids. Due to the close isolobal relationship of compounds 1–3 with metallocene dialkyl species that are commonly used as precursors to cationic metallocene alkyl catalysts, a crystal structure of a chromium precursor was of considerable interest. X-Ray quality crystals of 1 were grown from a saturated pentane solution at −30 °C and the molecular structure is shown in Fig. 1.‡

The most striking feature of the structure is the presence of η^1- and η^2-benzyl ligand coordination modes. The bond parameters for the η^2 ligand, a C(9)–C(10) bond length of 1.443(3) Å, a Cr–C(9)–C(10) angle of 82.16(11)° and elongated C_{ipso}–C_{ortho} distances [1.409(3) Å (av) *cf.* 1.395(3) Å (av.) for the η^1 CH_2Ph group] are within the ranges found for other η^2-benzyl ligands.[9] The interaction of the *ipso* carbon with the metal centre lies between the Cr–C(9) and Cr–C(16) bonds and is approximately in the plane defined by C(9)–Cr–C(16) (deviation 4.8°) consistent with the metallocene-like frontier orbitals of the $[Cr(NR)]_2$ fragment. The N–Cr–N angle of 116.09(8)° is comparable with the value found in $Cr(NBu^t)_2(2,4,6\text{-}Me_3C_6H_2)_2$ [114.5(3)°][10] as are the Cr=N distances of 1.625(2) and 1.632(2) Å.

The presence of the η^2-benzyl ligand is not clearly evident in room temperature solution NMR spectra due to rapid averaging of the η^1- and η^2-environments, and furthermore a frozen structure is not observed to −80 °C in CD_2Cl_2. A solid state ^{13}C NMR spectrum, however, clearly shows the two coordination modes, with distinguishing shifts for the *ipso*-phenyl carbon atoms at δ 157.9 (η^1) and 124.4 (η^2).

Treatment of 1 with $[Ph_3C][B(C_6F_5)_4]$ in CH_2Cl_2 affords Ph_3CCH_2Ph and the red cationic mono-benzyl complex 4 which forms an immiscible oil in hydrocarbon solvents but is completely miscible in CH_2Cl_2. NMR data for 4 indicate that the remaining benzyl ligand is bound in η^2-fashion; for example, the *ipso* carbon resonance occurs at δ 128.8 with a small $^2J_{CH}$ coupling of 5.3 Hz to the benzyl methylene hydrogens (confirmed by selective decoupling of the methylene

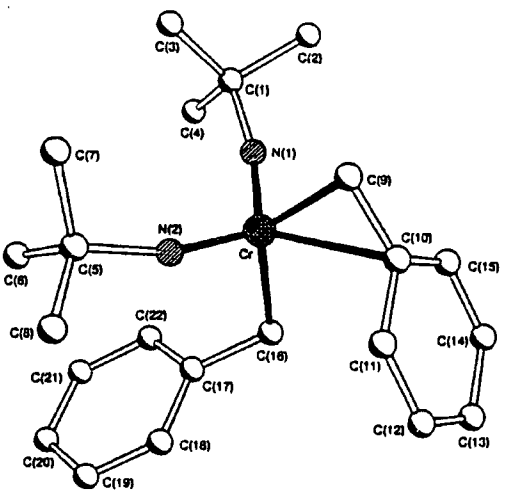

Fig. 1 Molecular structure of 1, without H atoms and with atom labels. Selected dimensions (Å and °): Cr–N(1) 1.625(2), Cr–N(2) 1.632(2), Cr–C(9) 2.071(2), Cr–C(10) 2.357(2), Cr–C(16) 2.096(3), C(9)–C(10) 1.443(3), C(10)–C(11) 1.411(3), C(10)–C(15) 1.406(3), other C–C in this ligand in range 1.371(3)–1.384(3), C(16)–C(17) 1.475(3), other C–C in this ligand in range 1.375(3)–1.402(3); N(1)–Cr–N(2) 116.09(8), C(9)–Cr–C(10) 37.32(8), C(9)–Cr–C(16) 131.93(8), C(10)–Cr–C(16) 94.86(7), Cr–N(1)–C(1) 166.07(13), Cr–N(2)–C(5) 160.60(13), Cr–C(9)–C(10) 82.16(11), Cr–C(16)–C(17) 114.73(13).

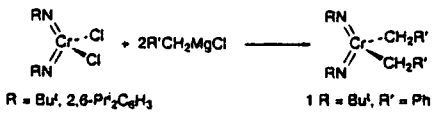

R = Bu^t, 2,6-Pr$^i_2$C$_6$H$_3$

1 R = Bu^t, R' = Ph
2 R = 2,6-Pr$^i_2$C$_6$H$_3$, R' = Ph
3 R = 2,6-Pr$^i_2$C$_6$H$_3$, R' = H

Scheme 1

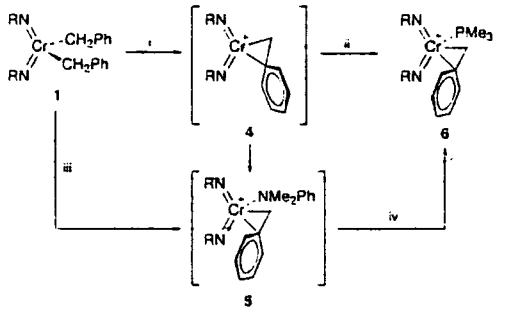

Scheme 2 *Reagents and conditions*: i, $[Ph_3C][B(C_6F_5)_4]$ (1 equiv.), CH_2Cl_2, room temp. 30 min; ii, PMe_3 (1 equiv.), CH_2Cl_2, room temp. 10 min; iii, $[PhNMe_2H][B(C_6F_5)_4]$, CH_2Cl_2, room temp. 30 min; iv, PMe_3 (1 equiv.), CH_2Cl_2, room temp. 10 min

protons in the ^{13}C NMR spectrum); the methylene carbon resonance appears at δ 59.3. It has not proved possible to establish the precise structure of 4, for example by X-ray crystallography, due to its oily nature; a higher nuclearity species is a possibility, though a single resonance for the *tert*-butylimido methyl groups appears to rule out a static structure involving both bridging and terminal imido groups. Treatment of 4 with trimethylphosphine gives a PMe_3 adduct 6 whose NMR data are consistent with the four coordinate, pseudo-tetrahedral structure shown in Scheme 2. The methylene hydrogens of the η^2-benzyl ligand show a coupling of 2 Hz to the adjacent phosphorus, while the methylene carbon appears as a doublet resonance at δ 52.9 ($^2J_{CP}$ = 4.5 Hz) in the proton decoupled spectrum. The *ipso* carbon resonance at δ 128.8, by contrast, shows no coupling to phosphorus, though a small triplet splitting (5.3 Hz) due to the methylenic hydrogens is observable in the proton coupled spectrum. These observations are consistent with the benzyl methylene group lying adjacent to the PMe_3 ligand by comparison with the spectral features of other $[M(NBu^t)_2(L)(PMe_3)]$ complexes,[11] where L is an alkene or alkyne. The reaction of 1 with $[PhNMe_2H][B(C_6F_5)_4]$ gives a more complicated product mixture that contains both bound and free $PhNMe_2$, plus an additional minor species that remains unidentified. The spectral features of the major component are consistent with the mono-amine adduct 5. This same mixture results upon treatment of the base-free cation 4 with 1 equiv. of $PhNMe_2$, while the mixture containing 5 is cleanly converted to 6 upon treatment with PMe_3.

Solutions of both 4 and 5 in either CH_2Cl_2 or toluene are highly active for the polymerisation of ethylene, with figures of merit considerably higher than for conventional dual component systems of the type $Cr(NBu^t)_2Cl_2$–Et_2AlCl and $Cr(NBu^t)_2Cl_2$–MAO.[12] For example, exposure of the solutions of 4 or 5 to 10 bar of ethylene for 60 min periods produces polyethylene§ with activities in the range 25 000 to 66 000 $gmol^{-1}\ h^{-1}\ bar^{-1}$.

BP Chemicals and the EPSRC are gratefully acknowledged for financial support. Professor R. K. Harris and Mr T. V. Thompson are thanked for measuring the solid state ^{13}C NMR spectrum of 1.

Received, 23rd May 1995; Com. 5/03297K

Footnotes

† *Crystal data* for 1: $C_{22}H_{32}CrN_2$, M = 376.5, orthorhombic, space group $P2_12_12_1$, a = 9.785(8), b = 14.75(2), c = 14.794(10) Å, U = 2135(3) Å^3, Z = 4, D_c = 1.171 g cm^{-3}, $F(000)$ = 808. 11 235 reflections were measured on a Stoe-Siemens diffractometer using graphite-monochromated Mo-Kα radiation (λ = 0.71073 Å, 2θ < 50°, μ = 0.542 mm^{-1}) with ω/θ scans and on-line profile fitting.[13] Data were corrected for absorption by a semi-empirical method from Ψ-scan data.[14] Structure solution was by direct methods,[14] refinement by full-matrix least-squares analysis on F^2 for all 3769 independent reflections (R_{int} = 0.0571).[14] $Rw = \{\Sigma[w(F_o^2 - F_c^2)^2]/\Sigma[w(F_o^2)^2]\}^{1/2}$ = 0.0678 for all data, conventional R [on F values of 3651 reflections with $F_o^2 > 2\sigma(F_o^2)$] = 0.0259, goodness of fit S = 1.062 on F^2 for 246 refined parameters. All non-H atoms were refined with anisotropic displacement parameters, H-atoms were constrained. Refinement of an enantiopole parameter indicates probable racemic twinning.[15] Atomic coordinates, bond lengths and angles, and thermal parameters have been deposited at the Cambridge Crystallographic Data Centre. See Information for Authors, Issue No. 1.

‡ *Selected spectroscopic data* for 1: ^1H NMR (C_6D_6, 400 MHz, 298 K): δ 6.99 (m, 10 H, C_6H_5), 2.49 (s, 4 H, CH_2Ph) and 1.20 [s, 18 H, $NC(CH_3)_3$]. ^{13}C NMR (C_6D_6, 100.6 MHz, 298 K): δ 140.34 (s, C_6H_5–C_{ipso}), 131.60 (d, $^1J_{CH}$ 157.1 Hz, C_6H_5–C_{ortho}), 128.94 (d*, C_6H_5–C_{meta}), 125.65 (d, $^1J_{CH}$ 160.5 Hz, C_6H_5–C_{para}), 71.97 [s, $C(CH_3)_3$], 44.50 (t, $^1J_{CH}$ 141.9 Hz, CH_2Ph), 31.63 [q, $^1J_{CH}$ 127.0 Hz, $C(CH_3)_3$]. For 2: ^1H NMR (C_6D_6, 400 MHz, 298 K): δ 7.17–6.88 (m, 16 H, CH_2Ph and C_6H_5), 3.85 (sept, $^3J_{HH}$ 6.6 Hz, 4 H, $CHMe_2$), 3.41 (s, 4 H, CH_2Ph), and 1.12 (d, $^3J_{HH}$ 7.2 Hz, 24 H, $CHMe_2$). ^{13}C NMR (C_6D_6, 125 MHz, 298 K): δ 158.00 (s, C_6H_5–C_{ipso}), 146.03 (s, C_6H_5–C_{ortho}), 140.15 (s, C_6H_5–C_{ipso}), 132.69 (d, $^1J_{CH}$ 158.3 Hz, C_6H_5–C_{ortho}), 128.78 (d*, C_6H_5–C_{meta}), 127.12 (d*, C_6H_5–C_{para}), 126.24 (d, $^1J_{CH}$ 160.2 Hz, C_6H_5–C_{para}), 122.79 (d, $^1J_{CH}$ 156.4 Hz, C_6H_5–C_{meta}), 59.88 (t, $^1J_{CH}$ 139.6 Hz, CH_2Ph), 28.48 (d, $^1J_{CH}$ 129.3 Hz, $CHMe_2$), 23.37 (q, $^1J_{CH}$ 125.9 Hz, $CHMe_2$). For 3: ^1H NMR (C_6D_6, 400 MHz, 298 K): δ 6.91 (m, 6 H, C_6H_5), 3.73 (sept, $^3J_{HH}$ 6.9 Hz, 4 H, $CHMe_2$), 1.83 (s, 6 H, CH_3) and 1.12 (d, $^3J_{HH}$ 6.8 Hz, 6 H, $CHMe_2$). ^{13}C NMR (C_6D_6, 100.6 MHz, 298 K): δ 157.81 (s, C_6H_5–C_{ipso}), 145.24 (s, C_6H_5–C_{ortho}), 127.60 (d*, C_6H_5–C_{para}), 122.74 (d, $^1J_{CH}$ 156.4 Hz, C_6H_5–C_{meta}), 49.73 (q, $^1J_{CH}$ 130.5 Hz, CH_3), 28.80 (d, $^1J_{CH}$ 128.9 Hz, $CHMe_2$), 23.52 (q, $^1J_{CH}$ 126.0 Hz, $CHMe_2$). (* $^1J_{CH}$ value obscured by overlap with solvent resonance.)

For 4: ^1H NMR (CD_2Cl_2, 250 MHz, 298 K): δ 6.67–7.90 (m, 25 H, $C_2H_2Ph_4$ and CH_2Ph), 4.22 (s, 2 H, $CH_2C_6H_5$), 4.00 (s, 2 H, $C_2H_2Ph_4$) and 1.59 (s, 18 H, CMe_3). ^{13}C NMR (CD_2Cl_2, 100.6 MHz, 298 K): δ 128.65 (d, $^1J_{CH}$ 159.9 Hz, $CH_2C_6H_5$–C_{otm}), 129.70 (d*, $CH_2C_6H_5$–C_{otm}), 128.78 (t, $^2J_{CH}$ 5.3 Hz, $CH_2C_6H_5$–C_{ipso}), 126.65 (d, $^1J_{CH}$ 161.9 Hz, $CH_2C_6H_5$–C_{para}), 79.56 (s, CMe_3), 59.34 (t, $^1J_{CH}$ 160.9 Hz, $CH_2C_6H_5$) and 31.07 [q, $^1J_{CH}$ 128.8 Hz, $C(CH_3)_3$]. (* $^1J_{CH}$ value obscured by overlap with 1,1,1,2-tetraphenylethane resonances.) For 5: ^1H NMR (CD_2Cl_2, 250 MHz, 298 K): δ 6.87–7.39 (m, aryl H), 3.84 (s, 2 H, $CH_2C_6H_5$), 2.88 (s, 6 H, $C_6H_5NMe_2$), 1.67 (s, 18 H, CMe_3). For 6: ^1H NMR (CD_2Cl_2, 400 MHz, 298 K): δ 6.67–7.90 (m, aryl H), 3.94 (d, $^3J_{PH}$ 2.0 Hz, 2 H, $CH_2C_6H_5$), 1.51 (s, 18 H, CMe_3) and 1.28 (d, $^2J_{PH}$ 10.4 Hz, 9 H, PMe_3). ^{13}C NMR (CD_2Cl_2, 100.6 MHz, 298 K): δ 128.64 (d, $^1J_{CH}$ 160.9 Hz, CH_2C_6H–C_{otm}), 129.69 (d*, $CH_2C_6H_5$–C_{otm}), 128.77 (t, $^2J_{CH}$ 5.3 Hz, $CH_2C_6H_5$–C_{ipso}), 126.63 (d, $^1J_{CH}$ 161.0 Hz, $CH_2C_6H_5$–C_{para}), 76.96 (d, $^3J_{CP}$ 2.3 Hz, CMe_3), 52.86 (td, $^1J_{CH}$ 159.1 Hz, $^2J_{CP}$ 4.5 Hz, $CH_2C_6H_5$), 31.45 (q, $^1J_{CH}$ 128.4 Hz, CMe_3) and 17.53 (qd, $^1J_{CP}$ 29.8 Hz, $^1J_{CH}$ 131.6 Hz, PMe_3). (* $^1J_{CH}$ value obscured by overlap with 1,1,1,2-tetraphenylethane resonances.) ^{31}P NMR (CD_2Cl_2, 101.26 MHz, 298 K): δ 12.4 (s, PMe_3). Satisfactory analyses has been obtained for compounds 1–3.

§ Details of the polyethylene products will be published at a later date.

References

1 H. Sinn, W. Kaminsky, H-J. Vollmer and R. Woldt, *Angew. Chem., Int. Ed. Engl.*, 1980, 19, 390; W. Kaminsky, M. Miri, H. Sinn and R. Woldt, *Makromol. Chem. Rapid Commun.*, 1983, 4, 417; W. Kaminsky and H. Luker, *Makromol. Chem. Rapid Commun.*, 1984, 5, 225.

2 R. F. Jordan, W. E. Dasher and S. F. Echols, *J. Am. Chem. Soc.*, 1986, 108, 1718; R. F. Jordan, C. S. Bajgur, R. Willett and B. Scott, *J. Am. Chem. Soc.*, 1986, 108, 7410; R. F. Jordan, R. E. LaPointe, C. S. Bajgur, S. F. Echols and R. Willett, *J. Am. Chem. Soc.*, 1987, 109, 4111; G. G. Hlatky, H. W. Turner and R. R. Eckman, *J. Am. Chem. Soc.*, 1989, 111, 2728; S. L. Borkowsky, R. F. Jordan and G. D. Hinch, *Organometallics*, 1991, 10, 1268; M. Bochmann, A. J. Jaggar and J. C. Nicholls, *Angew. Chem., Int. Ed. Engl.*, 1990, 29, 780; M. Bochmann and A. J. Jaggar, *J. Organomet. Chem.*, 1992, 424, C5; M. Bochmann and S. J. Lancaster, *Organometallics*, 1993, 12, 633; X. Yang, C. L. Stern and T. J. Marks, *J. Am. Chem. Soc.*, 1991, 113, 3623.

3 D. N. Williams, J. P. Mitchell, A. D. Poole, U. Siemeling, W. Clegg, D. C. R. Hockless, P. A. O'Neil and V. C. Gibson, *J. Chem. Soc., Dalton Trans.*, 1992, 739; J. K. Cockcroft, V. C. Gibson, J. A. K. Howard, A. D. Poole, U. Siemeling and C. Wilson, *J. Chem. Soc., Chem. Commun.*,

1992, 1668; U. Siemeling and V. C. Gibson, *J. Organomet. Chem.*, 1992, 426, C25; P. W. Dyer, V. C. Gibson, J. A. K. Howard, B. Whittle and C. Wilson, *J. Chem. Soc., Chem. Commun.*, 1992, 1666.
4 F. J. Karol, G. L. Karapinka, C. Wu, A. W. Dow, R. N. Johnson and W. L. Carrick, *J. Polm. Sci., Polym. Chem. Ed.*, 1972, 10, 2621; F. J. Karol, G. L. Brown and J. M. Davison, *J. Polym. Sci., Polym. Chem. Ed.*, 1973, 11, 413.
5 A. Clark, *Catal. Rev.*, 1969, 3, 145.
6 B. J. Thomas and K. H. Theopold, *J. Am. Chem. Soc.*, 1988, 110, 5902; B. J. Thomas, S.-K. Noh, G. K. Schulte, S. C. Sendlinger and K. H. Theopold, *J. Am. Chem. Soc.*, 1991, 113, 893; G. Bhandari, Y. Kim, J. M. McFarland, A. L. Rheingold and K. H. Theopold, *Organometallics*, 1995, 14, 738; K. H. Theopold, R. A. Heintz S. K. Noh and B. J. Thomas, Homogeneous Chromium Catalysts for Olefin Polymerisation, in *Homogeneous Transition Metal Catalysed Reactions*, ed. W. R. Moser and D. Slocum, ACS, Washington, DC, 1992, p. 591.
7 N. Meijboom, C. J. Schavarien and A. G. Orpen, *Organometallics*, 1990, 9, 774.
8 M. P. Coles, C. I. Dalby, V. C. Gibson, M. R. J. Elsegood and W. Clegg, *Polyhedron*, 1995, in press.
9 R. F. Jordan, R. E. LaPointe, N. Baenziger and G. D. Hinch, *Organometallics*, 1990, 9, 1539, and references cited therein.
10 A. C. Sullivan, G. Wilkinson, M. Motevalli and M. B. Hursthouse, *J. Chem. Soc., Dalton Trans.*, 1988, 53.
11 P. W. Dyer, V. C. Gibson, J. A. K. Howard, B. Whittle and C. Wilson, *Polyhedron*, 1995, 14, 103.
12 M. P. Coles and V. C. Gibson, *Polymer Bulletin*, 1994, 33, 529.
13 W. Clegg, *Acta Crystallogr., Sect. A*, 1981, 37, 22.
14 G. M. Sheldrick, SHELXTL Manual, Siemens Analytical X-ray Instruments Inc., Madison, WI, USA, 1990; SHELXL-93, program for crystal structure refinement, University of Göttingen, 1993.
15 H. D. Flack, *Acta Crystallogr., Sect. A*, 1983, 39, 876.

Pergamon

Polyhedron Vol. 14, No. 17–18, pp. 2455–2559, 1995

0277–5387/95 $9.50+0.00

0277–5387(95)00058–5

BIS(ARYLIMIDO) COMPLEXES OF CHROMIUM(VI)*

MARTYN P. COLES, CHRISTOPHER I. DALBY and VERNON C. GIBSON†

Department of Chemistry, University Science Laboratories, South Road, Durham, DH1 3LE, U.K.

and

WILLIAM CLEGG and MARK R. J. ELSEGOOD

Department of Chemistry, University of Newcastle, Newcastle upon Tyne, NE1 7RU, U.K.

(*Received* 13 *December* 1994; *accepted* 17 *January* 1995)

Abstract—A synthetic entry into bis(arylimido) chromium(VI) chemistry is described. $Cr(NAr)_2(NHBu^t)Cl$ (1; Ar = 2,6-$Pr^i_2C_6H_3$) may be obtained (1) by treatment of $Cr(NBu^t)_2Cl_2$ with two equivalents of 2,6-diisopropylaniline in pentane, or (2) via the reaction of $Cr(NBu^t)_2Cl_2$ with two equivalents of LiNHAr in Et_2O. An X-ray structure determination on 1 reveals a pseudo-tetrahedral coordination geometry with Cr—N distances of 1.643(3) and 1.654(4) Å for the imido groups and 1.813(3) Å for the tert-butylamido ligand; the substituents of the amide are orientated perpendicular to the Cl—Cr—N(amido) plane. Compound 1 is readily converted to $Cr(NAr)_2Cl_2$(2) by treatment with excess BCl_3 in dichloromethane.

The synthetic entry into bis(imido) chromium(VI) chemistry established by Nugent and Harlow[1] involves the treatment of CrO_2Cl_2 with $Bu^tNHSiMe_3$ to give $Cr(NBu^t)_2(OSiMe_3)_2$ [eq. (1)], a reaction that to date has proved specific to the tert-butylimido system.[2] Wilkinson and co-workers[3] subsequently showed that $Cr(NBu^t)_2(OSiMe_3)_2$ can be converted to $Cr(NBu^t)_2Cl_2$ by reaction with BCl_3 [eq. (2)], and the dichloride has been used to access several bis(tert-butylimido) chromium derivatives.

$$CrO_2Cl_2 + 4Bu^tNHSiMe_3 \xrightarrow[\text{heptane}]{60^\circ C} Cr(NBu^t)_2(OSiMe_3)_2 + 2[Bu^tNH_2SiMe_3]Cl \quad (1)$$

$$Cr(NBu^t)_2(OSiMe_3)_2 + 2BCl_3 \xrightarrow[2\,h]{CH_2Cl_2} Cr(NBu^t)_2Cl_2 + B(OSiMe_3)_2Cl \quad (2)$$

Schaverien and co-workers[2] have employed the five-coordinate pyridine adduct, $Cr(NBu^t)_2Br_2(py)$, to prepare a number of alkyl derivatives of the type $Cr(NBu^t)_2R_2$, where $R = CH_2CMe_3$, CH_2SiMe_3, CH_2CMe_2Ph, and $R_2 = o\text{-}(CH_2SiMe_3)_2C_6H_4$. With few exceptions, the dialkyls are oils, which leads to difficulties with their handling and manipulation.

In general, arylimido ligands often lend favourable solubility and crystallinity characteristics to imido complexes and in some cases may confer enhanced stability on their derivatives. The development of a synthetic entry into the bis(arylimido) chromium system remained, therefore, an important objective. A potential entry using chromate as a starting material, analogous to the route employed for the synthesis of bis(imido) molybdenum complexes, affords reduced chromium

*Author to whom correspondence should be addressed.

†First presented at the XVI International Conference on Organometallic Chemistry, University of Sussex, 10–15 July 1994.

products that do not contain imido ligands.[4] In recent work on bis(imido) molybdenum systems, we have exploited proton transfer between a free aniline and tert-butylimido ligands to access arylimido derivatives.[5,6] Here, we take advantage of this proton transfer methodology to prepare bis(arylimido) chromium(VI) complexes on a useful scale, thereby opening up the bis(arylimido) chromium system to development.

RESULTS AND DISCUSSION

Treatment of $Cr(NBu^t)_2Cl_2$ with two equivalents of 2,6-diisopropylaniline proceeds smoothly to afford the bis(arylimido) complex, $Cr(NAr)_2(NHBu^t)Cl$ (**1**; Ar = 2,6-$Pr^i_2C_6H_3$), in 60% isolated yield. ^1H and ^{13}C NMR spectra reveal resonances attributable to inequivalent imido ligands, a consequence of the local C_1 symmetry arising from the amido hydrogen and Bu^t substituents orientating towards the imido groups. A characteristic high frequency signal is found at δ 11.84 for the nitrogen-bound proton of the tert-butylamido ligand. A plausible mechanism for the formation of **1**, involving intermediate five-coordinate aniline adducts and amido species, is shown in Scheme 1. Whilst there is good precedent for the viability of these intermediates, it should be recognized that we have not been able to observe them directly, and therefore a pathway involving direct proton transfer from the aniline to the imido nitrogen cannot be excluded. Bu^tNH_3Cl is, however, the sole by-product of the reaction. We have also found that **1** can be accessed, albeit in lower yield, by treatment of $Cr(NBu^t)_2Cl_2$ with two equivalents of LiNHAr in diethyl ether.

Crystals of **1** suitable for an X-ray structure determination were grown from a saturated pentane solution at −30°C. The molecular structure is shown in Fig. 1 and selected bond lengths and angles are collected in Table 1. The molecule is pseudo-tetrahedral with inter-ligand angles in the range 106–112°. The ArN═Cr═NAr angle of 109.3(2)° is somewhat smaller than for bis(tert-butylimido) analogues (114–116°),[3,7] a reflection of the greater steric flexibility of the aryl substituent. The Cr═N—Ar angles of 157.0(3)° and 159.4(3)° lie at the low end of the range typically observed for bis(imido) complexes containing quasi-linear imido ligands[6] and the Cr═NAr bond lengths of 1.643(3) and 1.654(4) Å are longer than for tert-butylimido derivatives (1.58–1.63 Å),[7] a consequence of π-bonding between the imido nitrogen and the *ipso*-carbon of the aryl substituent which leads to a reduction in the M—N π-bond order. The Cr—N(amide) distance of 1.813(3) Å compares with values for molybdenum and tungsten tert-butylamides of 1.93–2.05 Å.[1,8,9] The shorter distance in the chromium complex is not fully compensated by the smaller ionic radius for chromium (0.52 Å) compared with molybdenum and tungsten (0.62 Å) and therefore may also reflect stronger π-bonding between the amido nitrogen and the chromium centre.

A convenient way of illustrating the orientation of the amide ligand in a pseudo-tetrahedral complex is using a representation[10] of the type shown in Fig. 2, in which the molecule is viewed along the amide–metal axis with the two imido ligands and chloride defining a plane beneath the metal. The orientation of the amido substituent is such as to allow the donor *p*-orbital of the amide ligand to lie in the Cr—N(1)—Cl plane; this is consistent with the two imido ligands dominating the π-donor bonding to the metal[10] and is related to the orientational constraints seen in bent metallocene compounds.

The mono-amido complex **1** may be converted to $Cr(NAr)_2Cl_2$ (**2**) via a procedure analogous to that described for the conversion of $Cr(NBu^t)_2(OSiMe_3)_2$ to $Cr(NBu^t)_2Cl_2$.[3] We have also found that it is possible to synthesize **2** in a "one-pot" reaction from $Cr(NBu^t)_2Cl_2$ without isolation of the intermediate **1**.

The synthetic procedures described herein allow a convenient entry point for developing the derivative chemistry of the bis(2,6-diisopropylphenylimido)chromium system, procedures that should be extendable to other arylimido derivatives.

EXPERIMENTAL

General

All manipulations were carried out under dry nitrogen using standard Schlenk and cannula techniques or in a conventional nitrogen-filled glovebox. Solvents were refluxed over an appropriate drying agent, and distilled and degassed prior to use. Elemental analyses were performed by the microanalytical services of the Department of Chemistry at Durham. NMR spectra were recorded on a Varian VXR 400 S spectrometer at 400.0 MHz (^1H) and 100.6 MHz (^{13}C); chemical shifts are referenced to the residual protio impurity of the deuterated solvent; IR spectra (Nujol mulls, CsI windows), Perkin–Elmer 577 and 457 grating spectrophotometers; mass spectra, VG 7070E [70 eV (*ca* 1.12×10^{17} J), 100 μA emission]. $Cr(NBu^t)_2Cl_2$ was synthesized via the procedure described by Wil-

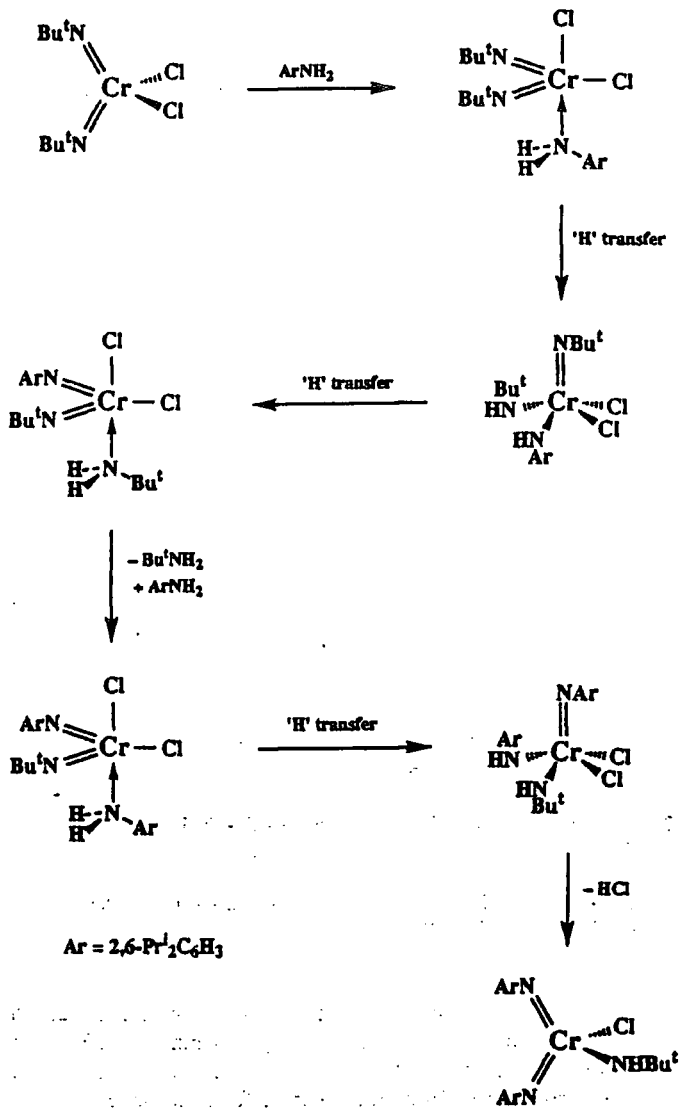

Scheme 1. A plausible mechanism for the formation of 1.

kinson and co-workers,[3] but employing heptane as solvent. CrO_2Cl_2, BCl_3 (1.0 M solution in heptane) and 2,6-diisopropylaniline were purchased from Aldrich Chemical Co.; the aniline was distilled under dinitrogen prior to use. All other chemicals were obtained commercially and used as received unless stated otherwise.

Preparation of $Cr(N\text{-}2,6\text{-}Pr^i_2C_6H_3)_2(NHBu^t)Cl$

Procedure A. A solution of $H_2N\text{-}2,6\text{-}Pr^i_2C_6H_3$ (356 μl, 1.89 mmol) in pentane (20 cm^3) was added dropwise over 10 min to a stirred solution of $Cr(NBu^t)_2Cl_2$ (0.25 g, 0.94 mmol) in pentane (70 cm^3) at −78°C. The mixture was allowed to warm to room temperature, during which the colour gradually changed from black to red. The mixture was stirred at ambient temperature for a further 18 h, after which the volatile components were removed under reduced pressure. Extraction of the resultant red oily residue with pentane (50 cm^3) followed by concentration and cooling of the filtrate to *ca* −30°C afforded dark red crystals of $Cr(N\text{-}2,6\text{-}Pr^i_2C_6H_3)_2(NHBu^t)Cl$. Yield 0.288 g (60%).

Procedure B. $Cr(NBu^t)_2Cl_2$ (0.25 g, 0.94 mmol) was dissolved in diethyl ether (30 cm^3) and cooled in a dry-ice/acetone slush bath. This solution was then added dropwise over 10 min to a cold (−78°C)

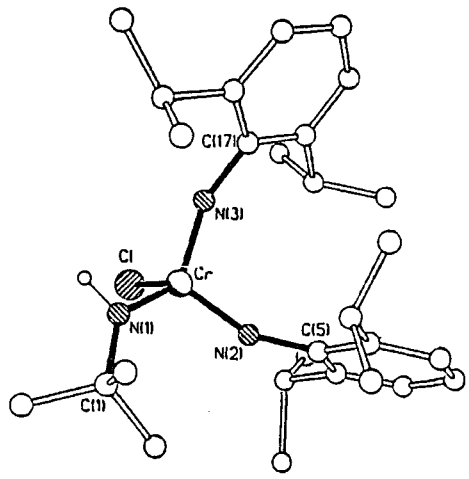

Fig. 1. Molecular structure of 1 without hydrogen atoms and disorder, and with key atoms labelled.

(m, 6H, C_6H_3), 3.97 [sept (br), 2H, $CHMe_2$], 3.81 [sept (br), 2H, $CHMe_2$], 1.28 (s, 9H, CMe_3), 1.22–0.99 (m, 12H, $CHMe_2$). ^{13}C NMR (100 MHz, C_6D_6): δ 161.0, 160.0 (*ipso*-C_6H_3), 146.5, 145.4 (*o*-C_6H_3), 123.1 (d, $^1J_{CH}$ = 154.0 Hz, *m*-C_6H_3), 122.8 (d, $^1J_{CH}$ = 154.7 Hz, *m*-C_6H_3),* 64.5 (CMe_3), 32.4 (q, $^1J_{CH}$ = 125.7 Hz, CMe_3), 29.3 (d, $^1J_{CH}$ = 124.4 Hz, $CHMe_2$), 28.4 (d, $^1J_{CH}$ = 126.7 Hz, $CHMe_2$), 24.7, 23.8, 23.3, 23.1 (overlapping quartet resonances, $CHMe_2$). *p-C_6H_3 resonances obscured by C_6D_6 signal. MS (EI$^+$, *m/z*, ^{35}Cl): 509 [M]$^+$, 437 [M − NHBu^t + H], 262 [Cr(NAr)Cl]$^+$. IR (Nujol, CsI, cm^{-1}): 3225w, 1579w, 1260s, 1198m(br), 1096s(br), 1056m, 1018s(br), 983m, 932w, 795s, 760m, 749s, 703m, 636w, 526w, 250s, 230m.

Table 1. Selected bond lengths (Å) and angles (°) for 1

Cr—N(2)	1.643(3)	Cr—N(3)	1.654(4)
Cr—N(1)	1.813(3)	Cr—Cl	2.247(2)
N(1)—C(1)	1.479(6)	N(2)—C(5)	1.392(5)
N(3)—C(17)	1.380(5)		
N(2)—Cr—N(3)	109.3(2)	N(2)—Cr—N(1)	110.1(2)
N(3)—Cr—N(1)	110.6(2)	N(2)—Cr—Cl	108.63(13)
N(3)—Cr—Cl	106.18(13)	N(1)—Cr—Cl	111.96(13)
C(1)—N(1)—Cr	136.7(3)	C(5)—N(2)—Cr	157.0(3)
C(17)—N(3)—Cr	159.4(3)		

solution of LiNH-2,6-$Pr^i_2C_6H_3$ (0.346 g, 2.08 mmol) in diethyl ether (30 cm^3). The mixture was allowed to warm to room temperature and stirred for 18 h. The resultant red solution was filtered from the white precipitate and the volatile components were removed under reduced pressure to give a red oily solid. Extraction with pentane (50 cm^3) followed by concentration and cooling of the filtrate to *ca* −30°C afforded Cr(N-2,6-$Pr^i_2C_6H_3)_2$(NHBu^t)Cl. Yield 0.125 g (26%).

Found: C, 66.0; H, 9.0; N, 8.0. Calc. for $C_{28}H_{44}N_3ClCr$: C, 65.9; H, 8.7; N, 8.2%. ^1H NMR (400 MHz, C_6D_6): δ, 11.84 (s, 1H, N*H*Bu^t), 6.88

Preparation of Cr(N-2,6-$Pr^i_2C_6H_3)_2Cl_2$

Boron trichloride (1.0 cm^3, 1 M solution in heptane) was added dropwise via syringe to an ice-cooled solution of Cr(N-2,6-$Pr^i_2C_6H_3)_2$(NHBu^t)Cl (0.43 g, 0.84 mmol) in CH_2Cl_2 (50 cm^3). The mixture was allowed to warm to room temperature and stirred for a further 3 h. The volatile components were then removed under reduced pressure to give a red oily solid which was washed with cold pentane (2 × 5 cm^3) and dried *in vacuo*. The solid was sublimed at 80°C (5×10^{-2} Torr) on to a dry-ice/acetone probe to give analytically pure Cr(N-2,6-$Pr^i_2C_6H_3)_2Cl_2$. Yield 0.30 g (75%).

Cr(N-2,6-$Pr^i_2C_6H_3)_2Cl_2$ can also be prepared in a "one-pot" reaction by direct treatment of the oily residue obtained from the preparation of 1 with

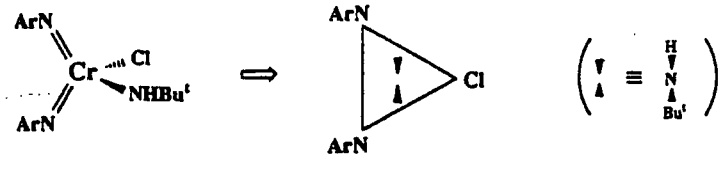

Fig. 2. A triad representation of 1.

BCl_3 according to the procedure outlined above. Found: C, 60.5; H, 7.4; N, 5.9. Calc. for $C_{24}H_{34}N_2Cl_2Cr$: C, 60.9; H, 7.2; N, 5.9%. ^{1}H NMR (400 MHz, C_6D_6): δ 6.75 (m, 6H, C_6H_3), 3.81 (sept, $^3J_{HH}$ = 6.7 Hz, 4H, $CHMe_2$), 1.02 (d, $^3J_{HH}$ = 6.7 Hz, 24H, $CHMe_2$). ^{13}C NMR (100 MHz, C_6D_6): δ 162.9 (s, *ipso*-C_6H_3), 149.1 (s, *o*-C_6H_3), 132.2 (d, $^1J_{CH}$ = 160.8 Hz, *p*-C_6H_3), 123.2 (d, $^1J_{CH}$ = 160.0 Hz, *m*-C_6H_3), 29.4 (d, $^1J_{CH}$ = 127.8 Hz, $CHMe_2$), 23.8 (q, $^1J_{CH}$ = 125.9 Hz, $CHMe_2$). MS (EI$^+$, *m/z*, ^{35}Cl): 473 $[M]^+$, 437 $[M-Cl]^+$, 402 $[M-2Cl]^+$, 262 $[Cr(NAr)Cl]^+$. IR (Nujol, CsI, cm^{-1}): 2360w, 1579m, 1342m, 1259s, 1222w, 1179w, 1142w, 1096m(br), 1057m, 1019m(br), 931w, 799s, 753m, 600w, 523w, 427m, 250s, 220s.

X-ray crystallography for **1**

Crystal data. $C_{28}H_{44}ClCrN_3$, M = 510.11, triclinic, space group $P\bar{1}$, a = 11.483 (6), b = 11.634 (6), c = 12.426 (6) Å, α = 81.91, β = 71.16, γ = 68.16 (2)°, U = 1458.0 (13) Å^3 at 160 K (Mo-K_α radiation, λ = 0.71073 Å), Z = 2, D_c = 1.162 g cm^{-3}, μ = 0.503 mm^{-1}, $F(000)$ = 548.

Data collection and processing: crystal size 0.31 × 0.16 × 0.12 mm, Stoe–Siemens diffractometer with Cryostream cooler,[11] cell parameters from 2θ values (17–22°) of 40 reflections measured at $\pm\omega$, intensities from ω–θ scans, 2θ range 5–45°, index ranges h–11 to 12, k–12 to 12, l–10 to 13, together with some Friedel opposites; corrections for 16% intensity decay of five standard reflections, semi-empirical absorption corrections,[12] transmission 0.876–0.983; 4448 measured reflections, 3793 unique data, R_{int} = 0.086 on F^2.

Structure solution and refinement:[12] Patterson and difference syntheses, hydrogen atoms riding with U(H) = 1.2U_{eq}(C); full-matrix least-squares refinement on F^2 for all unique data, with weighting $w^{-1} = \sigma^2(F_0^2) + (0.0653P)^2$, where $P = (F_0^2 + 2F_c^2)/3$, anisotropic displacement parameters for all non-hydrogen atoms; extinction effects negligible; two-fold disorder for one isopropyl group with refined occupancy factors 0.47:0.53(3); all shifts <0.001 times corresponding parameter e.s.d.; final difference map between +0.700 and −0.469 e Å^{-3}. For 322 parameters, $R_w2 = [\Sigma w(F_0^2 - F_c^2)^2]/\Sigma w(F_0^2)^2]^{1/2}$ = 0.1333 for all data, conventional R = 0.0430 for unweighted F values of 2318 reflections having $F_0^2 > 2\sigma(F_0^2)$, goodness of fit = 1.018 on F^2.

Atomic coordinates, complete bond lengths and angles, and displacement parameters have been deposited as supplementary material at the Cambridge Crystallographic Data Centre.

Acknowledgements—BP Chemicals and the Engineering and Physical Sciences Research Council are thanked for financial support.

REFERENCES

1. W. A. Nugent and R. L. Harlow, *Inorg. Chem.* 1980, **19**, 777.
2. N. Meijboom, C. J. Schaverien and G. A. Orpen, *Organometallics* 1990, **9**, 774.
3. A. A. Danopoulos, Wa-Hung Leung, G. Wilkinson, B. Hussain-Bates and M. B. Hursthouse, *Polyhedron* 1990, **21**, 2625.
4. P. W. Dyer, V. C. Gibson and J. C. Jeffrey, *Polyhedron*, submitted.
5. M. Jolly, J. P. Mitchell and V. C. Gibson, *J. Chem. Soc., Dalton Trans.* 1992, 1329.
6. A. Bell, W. Clegg, P. W. Dyer, M. R. J. Elsegood, V. C. Gibson and E. L. Marshall, *J. Chem. Soc., Chem Commun.* 1994, 2247, 2547.
7. (a) M. B. Hursthouse, M. Motevalli, A. C. Sullivan and G. Wilkinson, *J. Chem. Soc., Chem. Commun.* 1986, 1398; (b) M. B. Hursthouse, M. Motevalli, A. C. Sullivan and G. Wilkinson, *J. Chem. Soc., Dalton Trans.* 1988, 53; (c) Wa-Heung Leung, A. A. Danopoulos, G. Wilkinson, B. Hussain-Bates and M. B. Hursthouse, *J. Chem. Soc., Dalton Trans.* 1991, 2051; (d) Hon-Wah Lam, G. Wilkinson, B. Hussain-Bates and M. B. Hursthouse, *J. Chem. Soc., Dalton Trans.* 1993, 1477.
8. D. M.-T. Chan, W. C. Fultz, W. A. Nugent, D. C. Roe and T. H. Tulip, *J. Am. Chem. Soc.* 1985, **107**, 251; P. Legzdins, S. J. Rettig and K. J. Ross, *Organometallics* 1993, **12**, 2103.
9. N. Bryson, M.-T. Youinou and J. A. Osborn, *Organometallics* 1991, **10**, 3389.
10. V. C. Gibson, *J. Chem. Soc., Dalton Trans.* 1994, 1607; V. C. Gibson, *Angew. Chem.* 1994, **106**, 1640.
11. J. Cosier and A. M. Glazer, *J. Appl. Cryst.* 1986, **19**, 105.
12. G. M. Sheldrick, SHELXTL/PC Manual, Siemens Analytical X-ray Instruments Inc., Madison, U.S.A. (1990); SHELXL-93, Program for Crystal Structure Refinement, University of Göttingen, Germany (1993).